COMPUTATION ASSISTED *DE NOVO* DESIGN AND DEVELOPMENT OF COMBINATORIAL FLUOROPHORE LIBRARY FOR THERANOSTICS

A Thesis submitted

in partial fulfillment for the Degree of

Doctor of Philosophy

by

RAKESH R

Department of Chemistry

INDIAN INSTITUTE OF SPACE SCIENCE AND TECHNOLOGY

THIRUVANANTHAPURAM

JUNE, 2018

CERTIFICATE

This is to certify that the thesis entitled **Computation Assisted *De Novo* Design and Development of Combinatorial Fluorophore Library for Theranostics** submitted by **Rakesh R** to the Indian Institute of Space Science and Technology, Thiruvananthapuram, in partial fulfillment for the award of the degree of **Doctor of Philosophy** is a *bona fide* record of research work carried out by him under my supervision. The contents of this thesis, in full or in parts, have not been submitted to any other Institution or University for the award of any degree or diploma.

Dr. K. G. Sreejalekshmi
Supervisor
Department of Chemistry

Thiruvananthapuram
June, 2018

Counter signature of HOD with seal

DECLARATION

I declare that this thesis entitled **Computation Assisted *De Novo* Design and Development of Combinatorial Fluorophore Library for Theranostics** submitted in partial fulfillment of the degree of **Doctor of Philosophy** is a record of original work carried out by me under the supervision of Dr. K. G. Sreejalekshmi, and has not formed the basis for the award of any other degree or diploma, in this or any other Institution or University. In keeping with the ethical practice in reporting scientific information, due acknowledgements have been made wherever the findings of others have been cited.

Rakesh R
SC12D017

Thiruvananthapuram – 695547
25/06/2018

ACKNOWLEDGEMENTS

I take this opportunity to express my sincere appreciation towards each one for their support in fulfilling this long intellectual journey.

First and foremost, I would like to thank my beloved supervisor Dr. K. G. Sreejalekshmi for her support and guidance throughout the course of my work. She was always there for me when I needed assistance and encourage through her dynamic and positive attitude. She endlessly mentored, inspired, and encouraged me since I joined the group. She gave me tremendous opportunities and freedom in research and showed extreme patience. Her firm belief in my abilities gave me the confidence and courage to tackle each new challenge. She taught me to grow as a better human being by keeping ethics in scientific research and values in personal life. I appreciate your caring, enthusiastic, considerate and optimistic approach to issues that gave me an opportunity to tap the best concepts from you. Thank you for dedicating your time and energy for moulding me through our countless discussions. Also I appreciate your patience and dedications in correcting my thesis. You are more than a guide to me and one could not wish for a better supervisor than you.

I would like to thank IIST for the financial assistance and Director, IIST for providing me the facilities to carry out the work. I would like to thank all the faculty members of Department of Chemistry for their support extended to me during this period. I'm sincerely indebted to my doctoral committee members Dr. K.M. Sureshan, IISER- Thiruvananthapuram, Dr. Pradeepkumar P. I., IIT-Bombay, Dr. K.V. Radhakrishnan, CSIR-NIIST, Thiruvananthapuram, Dr. Deepak T.G. and Dr. Nirmala R. James from IIST, Thiruvananthapuram for the constant monitoring and reviewing of my research work. I express my deep sense of gratitude to all the staff members of Department of Chemistry and a talented group of fellow research scholars for their help.

My heartfelt gratitude to Dr. Sarah Titus, my senior, fellow researcher for guiding me in the first steps in the group and for teaching me a good lab culture. I'm

grateful for your support throughout my work and for all the constructive criticisms, discussions and motivational words. Thank you for considering me as your younger brother and for your love and care. I would also like to thank my friendly group members past and present - Swathi, Mrudul, and Manjinder for their support. I would also like to thank my internship students especially Desna, Dona, Saina, Lakshmi, and Parvathi for giving a nice company to me.

I am forever indebted to my friends in IIST especially Swagat, Abhishek, Sujith, Najeeb, Sabu, and Sarath with whom I began and shared this incredible journey for their companionship, encouragement, criticism, advice, and for all the precious memories.

I also like to extend my gratitude to various institutes such as NIIST, IISER, SCTIMST Thiruvananthapuram, SAIF-IIT Madras, STIC-CUSAT, and ACTREC-Mumbai for all the facilities extended. I take this opportunity to thank my friends in these institutes for their timely help.

I cannot forget to express appreciation to all my teachers without whom I could not have succeed in my life. Thanking all the amazing people in my life those who directly or indirectly helped me for the completion of this work.

Words are inadequate to express my gratitude towards my wonderful parents, my amazing brother Renjish and sister Chithra. Your infinite love and care, unconditional support and patience while I pursued my intellectual goals has given me the courage and inner strength to expand my knowledge to the fullest. This work would never have been possible without the support and encouragement of my family.

Last but not the least, I would like to thank the ‘The God Almighty’ who gave me strength, confidence and success to accomplish this work.

Rakesh R

ABSTRACT

The synergism between therapy and diagnostics is considered as a new innovation to the treatment techniques. Thus theranostics, the combination of therapeutics and imaging capabilities into a single package, has emerged as a powerful tool towards personalized medicine and is anticipated to revolutionize modern treatment modalities. Transformation of the idea of theranostics from the lab to the clinic is possible only by the advancements in individual components. Moreover, rather than depending on the strength of individual components, a single molecule possessing the desired attributes may contribute significantly to the realization of the concept. The development of trackable therapeutics will allow the real-time monitoring of drug release and its pharmacokinetics and thereby increase the treatment efficacy. The advancements in the field of single molecule based theranostics are possible only by accelerating the development of novel core scaffolds. The symbiosis of computational and synthetic chemistries may open new vistas in the theranostic field, which is rarely explored. In this regard, we formulated our research problem to design novel core molecules by exploring the hidden potential of computational and classical chemistry aimed towards contributing significantly to the growing field of theranostics.

In our search for novel organic functional molecules, we hypothesized the combination of diverse heterocycle fragments through molecular hybridisation, a widely adopted technique in drug discovery for the design of core skeleton for the envisaged theranostic platform. Our longstanding interest in 1,3-thiazole, coupled with its extensive pharmaceutical relevance and untapped potential as fluorophore core prompted us to choose this member of azole family as the anchoring unit. A computer aided fluorophore design strategy was adopted by placing donor-acceptor fragments as end groups, utilizing the intramolecular charge transfer phenomena resulting in a novel 5-(hetero-2-yl)-1,3-thiazole core. Molecular engineering around the thiazole core utilizing its *C2*, *C4* and *C5* positions afforded a library of multi-directional charge transfer molecules. The preliminary structure property study carried out with the aid of DFT and TD-DFT methods revealed that *C5* position of thiazole was critical in imparting colour tunability. The calculations also helped to identify the potential of *C4* position to emerge as an orthogonal handle.

Motivated by the rational design of novel molecules based on bi(heteroyl) thiazole-het core, we further proceeded with the retrosynthetic design and development of facile routes to generate the combinatorial library of fluorophores. Using the untapped potential of classical chemistry, we identified a classical [4+1] thiazole ring route where carbonyl compounds, secondary amines and halo methyl heterocycles served as building blocks for the modular synthesis of multi-heterocyclic D-A systems. The versatility of the developed method was validated by the synthesis of a 70 member library built on 5-(thiophene-2-yl)-1,3-thiazole and 5-(furan-2-yl)-1,3-thiazole cores, and out of which 35 members were fully

characterized. We also attempted to adapt our synthetic strategy to suit green chemistry protocols and successfully developed a one-pot multi-component mechanochemical method to synthesize these thiazoles. Compared to the existing literature methods, utilizing highly expensive transition metal catalysts for constructing bi(hetero)aryl core, our method is simple, highly versatile, economical, having a high atom economy and synthesised using readily available reagents.

In order to validate the theranostic potential of the synthetically achieved systems, we next proceeded with the systematic exploration of their therapeutic and diagnostic properties. For the validation of the therapeutic potential, both *in vitro* and *in silico* methods were employed. The preliminary *in vitro* studies using selected members of the synthesized library confirmed that one of the molecules of the 5-(thiophene-2-yl)-1,3-thiazole family was active against HL-60 (leukemia) cell line whereas the same molecule exhibited promising results in MCF-7 (breast cancer) and HT-29 (colon cancer). Inspired by these findings, and considering the synthetic feasibility and availability of reagents, we generated a 43200 member virtual library by diversity amplification around the core. The computation of pharmaceutically relevant descriptors using ADME predicting tool indicated that 97.5% molecules in the designed library were within the range of properties recommended for 95% of drugs in the market and hence the druggable nature of the core scaffold was confirmed. Further *in silico* analysis were carried out in three different families of cancer biomarker proteins viz- human estrogen receptor, aurora kinase, and cyclin dependent kinase using the in-house virtual library. The results from docking studies were compared with those of respective classes of protein inhibitors and known anticancer drugs and it was found that the molecules retained most of the crucial binding interactions with the proteins. Among the studied cores, molecules built on 5-(furan-2-yl)-1,3-thiazole core was found to have a better binding affinity for the active site of proteins. Specifically, N-containing heterocycles viz; 3-pyridyl, 2-substituted quinoxalines and pyrazines played vital roles in ATP competitive binding in aurora kinase proteins. Thus the designed scaffold holds the promise for developing potent drug molecules.

Excited by the vast potential of these cores in therapeutics, we next attempted to evaluate their photophysical properties for the development of druggable fluorophore molecules for applications in the field of theranostics. The photophysical properties of developed fluorophores were studied in six different solvents of varying polarity. The study of structure photophysical relationship shed light on the importance and influence of different fragments on the photophysical properties of 5-(hetero-2-yl)-1,3-thiazoles. The significance of *C5* position in developing colour tunable fluorophore was further confirmed by experiments. The *C4* position can be used a gateway for a second charge transfer channel by choosing appropriate donor and acceptor fragments. All the molecules exhibited solvent dependant photophysical properties and showed positive solvatochromism with large Stokes shift values which are desirable attributes for imaging applications. Additionally, the molecules displayed very high quantum yield values up to 87%, especially in non polar solvents. These molecules are further capable of exhibiting colour tunable solid state emission and are thus among one of the smallest family

of organic molecules capable of exhibiting solid state red emission. The crystal structure analysis revealed the molecular rigidity obtained by the multiple short interactions to be responsible for the solid state emission. The preliminary evaluation of theranostic property in HeLa and L929 cell lines identified that the molecules were potential candidates for the development of theranostic platforms.

We further performed computational calculations to understand the fundamental nature of the core molecules. A benchmark study using twelve different functionals identified the hybrid functional PBE0 as the best functional to describe the vertical absorption energy with a mean absolute error less than 0.3 eV. This result would help in designing molecules with tailored wavelength of interest in future research. The solvent effect on the photophysical properties was also verified by computational calculations using polarizable continuum model. The intramolecular charge transfer was verified by the partial density of states calculation by identifying the percentage contribution of various fragments to HOMO and LUMO and the information was used to design the multidirectional charge transfer compounds. The computational calculations assisted in identifying the existence of charge separated quinoid state in polar solvents and gave insights on the conformational preference of the molecules.

After achieving the main objectives of the thesis, we also investigated the potential of the multi-heterocyclic 1,3-thiazole core in multi-functional material development by expanding the prospects of thiazole chemistry from drug discovery to advanced functional materials. The molecules with a nitro substituent at *C5* of thiophene behaved as static functional molecules whereas the aldehyde derivatives hold promise as dynamic functional systems. The study also revealed the potential of the core to exhibit the aggregation induced emission phenomena and the molecular dynamics study confirmed the time dependent formation of aggregates. The sensitivity of the molecules towards the HCl vapours were detected and a naked eye sensor for acid vapours was developed. The sensor behaviour was then rationalised by computational studies. Further, the observed mechanoresponsive fluorescence behaviour of the aldehyde substituted molecules widens their scope as advanced functional materials.

It is noteworthy that the present study has successfully and significantly contributed to the emerging area of theranostics through the development of trackable therapeutics. The salient features of the work include the combined approach by utilizing the prospectives of computational chemistry and classical chemistry to design and develop novel single small organic molecule based fluorescent therapeutic agents. Further, the concept of molecular hybridisation of heterocycles was used for the development of a novel 5-(hetero-2-yl)-1,3-thiazole core scaffold capable of accommodating panoply of substituents around the core. A simple, economical and highly versatile synthetic route was developed by using commercially available building blocks. *In vitro* and *in silico* methods were used to reveal the therapeutic potential of the systems and detailed photophysical studies unveiled the probable imaging capabilities. Further computational calculations helped us to identify the fundamental nature of the core scaffold. Finally, the

potential of the bi(hetero)aryl core from medicinal chemistry to materials chemistry transformations for multi-functional material development was illustrated. The research has opened new avenues in heterocyclic chemistry research, especially in thiazole chemistry, by identifying novel molecular systems with a broad spectrum of tunable properties and is expected to realise its goal of single molecule based trackable therapeutics for applications in personal medicine in the future.

TABLE OF CONTENTS

LIST OF TABLES

LIST OF FIGURES

LIST OF SCHEMES

ABBREVIATIONS

3D	Three dimensional
A	Acceptor
ACN	Acetonitrile
ACQ	Aggregation caused quenching
ADME	Absorption, distribution, metabolism and excretion
AIE	Aggregation induced emission
ALA	Aminolevulinic acid
AM1	Austin model 1
APC	Anaphase-promoting complex
ATP	Adenosine triphosphate
AURK	Aurora kinase
B3LYP	Becke, three-parameter, Lee-Yang-Parr
BBB	Blood brain barrier
BODIPY	Boron-dipyrromethane
CADD	Computer-aided drug design
CAFD	Computer aided fluorophore design
CAM-B3LYP	Coulomb-attenuating method B3LYP
CAS-SCF	Complete active space self-consistent field
CC	Coupled cluster
CCDC	Cambridge crystallographic data centre
$CDCl_3$	Chloroform-d
CDK	Cyclin-dependent kinase
CIS	Configuration interaction singles
CNS	Central nervous system
CT	Charge transfer
D	Donor
DCM	Dichloromethane
DFG	Asp-Phe-Gly
DFT	Density functional theory

DMEM	Dulbecos modified eagles medium
DMF	N,N-dimethylformamide
DMSO	Dimethyl sulphoxide
DNA	Deoxyribonucleic acid
DOS	Diversity-oriented synthesis
DSC	Differential scanning calorimetry
EGFR	Epidermal growth factor receptor
ER	Estrogen receptor
ES	Excited state
ESI-MS	Electron spray ionization-mass spectrometry
Et_3N	Triethylamine
EWG	Electron withdrawing group
FDA	Food and drug administration
FET	Field effect transistors
FMO	Frontier molecular orbital
FT	Furanylthiazole
FU	Fluorouracil
GGA	Generalized gradient approximation
GI	Growth inhibition
GPCR	G-protein coupled receptors
GS	Ground state
HBr	Hydrogen bromide
HCl	Hydrochloric acid
HF	Hartree Fock
HOMO	Highest occupied molecular orbital
HR-MS	High resolution mass spectrometry
HTS	High-throughput screening
ICG	Indocyanine green
ICT	Intramolecular charge transfer
IEFPCM	Integral equation formalism of polarized continuum model
IUPAC	International union of pure and applied chemistry
KSCN	Potassium thiocyanate

LBD	Ligand binding domain
LBDD	Ligand-based drug design
LC-BLYP	Long-range-corrected- Becke, Lee-Yang-Parr
LD	Lethal dosage
LUMO	Lowest unoccupied molecular orbital
m.p.	Melting point
MAE	Mean absolute error
MCR	Multi-component reactions
MD	Molecular dynamics
MDCK	Madin-Darby canine kidney epithelial
MeOH	Methanol
MICT	Multidirectional intramolecular charge transfer
MR-CI	Multi-reference configuration interaction
MTT	(3-(4,5-dimethylthiazol-2-yl)-2,5-diphenyltetrazolium bromide)
NBO	Natural bonding orbital
NBS	N-bromosuccinimide
NCCS	National centre for cell sciences
NCI	National cancer institute
NDDO	Neglect of non-bonded differential overlap
NH_3	Ammonia
NIR	Near infrared
NMR	Nuclear magnetic resonance
OLED	Organic light emitting diode
OPLS	Optimized potential for liquid simulations
ORTEP	Oak ridge thermal-ellipsoid plot
PBE	Perdew–Burke-Ernzerhof
PDB	Protein data bank
PDOS	Partial density of states
PDT	Photodynamic therapy
PM	Parameterized model
Ppm	Parts per million
PPP	Pariser-Parr-Pople

PSA	Polar surface area
PT	Perturbation theory
QSAR	Quantitative structure activity relationship
QY	Quantum yield
RDF	Radial distribution function
RIM	Restriction of intramolecular motion
RNA	Ribonucleic acid
RO5	Rule of five
RPA	Random phase approximations
RSH	Range separated hybrid
SBDD	Structure based drug design
SERM	Selective estrogen receptor modulators
SPPS	Structure photophysical property relationship
SRB	Sulforhodamine B
SS	Stokes shift
TD-DFT	Time dependant density functional theory
TGI	Total growth inhibition
THF	Tetrahydrofuran
TICT	Twisted intramolecular charge transfer
TLC	Thin layer chromatography
TMS	Trimethylsilane
TT	Thienylthiazole
UV	Ultraviolet
WHO	World health organization
XRD	X-ray diffraction
ZINDO	Zerner's intermediate neglect of differential overlap

NOTATIONS

α	Alpha
Å	Angstrom
β	Beta
cal	Calorie
Da	Dalton
º	Degree
ºC	Degree Centigrade
δ	Delta
eV	Electron volt
ε	Epsilon
fs	Femtosecond
γ	Gamma
g	Gram
Hz	Hertz
h	Hour
K	Kelvin
λ	Lamda
µg	Microgram
µL	Microlitre
mg	Milligram
mL	Millilitre
mm	Millimetre
mmol	Millimole
min	Minutes
nm	Nanometre
ns	Nanosecond
ν	Nu
ω	Omega
%	Percentage
ϕ	Phi
π	Pi
ρ	Rho
σ	Sigma
θ	Theta
V	Volume
W	Watt

CHAPTER 1

INTRODUCTION

The increasing statistics of occurrence of various diseases urge the development of novel and effective diagnostic and treatment techniques which typically involves simultaneous improvements in both drug design and diagnostics parts. Although potent drugs are often discovered for the existing and new diseases, the population demographics would demand a substantial improvement in research on the prevention, diagnosis and therapy of various life threatening diseases. According to WHO report, ischaemic heart disease and stroke are the biggest killers followed by lung cancer with 1.7 million deaths (WHO, 2015). Cancer, characterized by the uncontrolled cell proliferation and metastasis (Vogelstein and Kinzler, 2004), is one of the leading public health problems in the world and the second largest cause of death in USA (Siegel *et al.*, 2016). From the third largest death cause in 1990, cancer occupied a second position among largest death causing diseases in 2013 (Global, 2015). Therefore, there is no surprise that research on cancer diagnosis and therapy remains topical for both developed and developing countries.

Focusing further on cancer, which is a heterogeneous and adaptable disease, it is very essential to diagnose early and decide on various types of treatments depending upon patients' characteristics and disease progression. Among surgery, radiotherapy and chemotherapy, latter is widely used to treat various kinds of cancer. Conventional chemotherapeutics are based on cytotoxic agents which kill all the dividing cells and thereby causing severe side effects to patients (Lu and Mahato, 2009). However, improvements in the molecular understanding of the malignant progression of cancer led to the development of targeted drugs which are molecules capable of inhibiting, stimulating or modulating

the activity of the target (Landry and Gies, 2008) and thereby having a profound effect in controlling cancer. Such *molecularly targeted drugs* including imatinib, gefitinib, bortezomib, rituximab, trastuzumab among others (Table 1.1) have proved their vital roles in the successful treatment of cancer (Huang *et al.*, 2014; Narang and Varia, 2011). Considering these success stories, it would be worthy to think about molecular targeted drugs with diagnostic capabilities to address diagnosis and therapy utilizing a single platform. Research along similar lines spurred the idea of theranostics which is discussed now, with an emphasis on anticancer studies.

Table 1.1 Selected molecular targeted drugs

Drugs	**Targets**
Imatinib	Bcr-Abl
Dasatinib	Multiple tyrosine kinases
Gefitinib	Epidermal growth factor receptor (EGFR)
Erlotinib	EGFR
Sorafenib	Multiple tyrosine kinases
Trastuzumab	HER2 receptor
Rituximab	CD20

1.1. Theranostics

It is a known fact that because of the heterogeneous nature of the tumor, it is often difficult to visualize and treat it properly. The different areas of therapeutics and imaging techniques have shown tremendous improvement in these years but were not sufficient to improve the quality of life of the patients. The integrated method of combining the individual strength of both therapeutics and diagnostics was not familiar to the scientific community until Funkhouser introduced the term *theranostics* in 2002 (Funkhouser, 2002). According to him, theranostics is "a material that combines the modalities of therapy and diagnostic imaging". Theranostics has the potential to revolutionize the field of medicine from the conventional traditional approach to a *one drug fits all* approach (Rai *et al.*, 2010). It allows therapy and imaging simultaneously with the same dosage of the material.

Compared to the conventional approach where the individual items are injected independently, this *single package* has the potential to overcome the undesirable biodistribution and has much better selectivity (Kelkar and Reineke, 2011). Theranostics enables the diagnostics of a disease, treatment planning, dosimetry, pre- and post-treatment assessment and moreover is considered to be a giant leap towards personalized medicine (Amir-Aslani and Mangematin, 2010; Crawley *et al.*, 2014). This precision therapy allows the effective and economical clinical output for individual persons with reduced time and cost. The area of theranostics is still in its infancy and a lot more improvements are needed for its translation into the clinic. The significant advances in the areas of chemistry, biology, biotechnology, medicine and imaging technologies contribute remarkably to the progress of theranostics. The different therapeutical and imaging modalities that can be used for theranostics are listed in table 1.2 (Bardhan *et al.*, 2011). Theranostics has currently developed into two separate classes (Zhang *et al.*, 2016) where biomaterials are developed by- (i) incorporating complexes from the assemblies of therapeutic and diagnostic units or (ii) covalent conjugation of molecules combining different chemotherapeutic agents, imaging agents, and targeting ligands using suitable covalent linkers.

Table 1.2. List of various therapeutical and imaging modalities

	Modality	**Agent**
Therapeutics	Chemotherapy	Anticancer drugs (doxorubicin, paclitaxel etc)
	Radiation therapy	X-rays and radio nucleotides
	Photodynamic therapy	Photosensitizer
	Gene therapy	siRNA, DNA
	Photothermal therapy	Nanoscale materials
	Magnetic hyperthermia	Magnetic nanoparticles
Imaging	Magnetic resonance imaging	Manganese, iron oxide, gadolinium agents etc.

	Computed tomography	Iodine, barium and other contrasting agents
	Fluorescence	Organic fluorophores, quantum dots, and nano particles
	Positron emission tomography	Radioisotopes
	Ultrasound	Nanoparticles

Currently, there is a growing interest in nanotheranostics where different drug molecules, targeting ligands, and imaging probes were linked to a common nanoplatform as evident from the boom in its literature (Chen *et al.*, 2011; Doane and Burda, 2012; Lim *et al.*, 2014; Ma *et al.*, 2016; Mura and Couvreur, 2012). Nanoplatforms are important components towards nanotheranostics which include a wide variety of systems ranging from organic structures like liposomes, polymeric micelles, and dendrimers to inorganic nanoparticles such as silica nanoparticles, graphene materials and various core/shell nanoparticles (Ma *et al.*, 2016).

The therapeutic property can be imparted using various strategies. Most important and widely explored one is the attachment of known chemotherapeutic drug using covalent and/or non-covalent interactions. The literature is rich enough with theranostic formulations using chemotherapeutic agents (Li *et al.*, 2016) like doxorubicin, paclitaxel, and methotrexate in nanocarriers like liposomes (Huang *et al.*, 2016), polymeric micelles (Panja *et al.*, 2016), and inorganic nanoparticles (Ding *et al.*, 2016). Whereas combinations of these drugs are also widely employed (Yang *et al.*, 2007). Therapeutic outputs are achieved by photothermal therapy using nanoparticles, magnetic hyperthermia therapy using iron oxide nanoparticles, photodynamic therapy (PDT) using photosensitizer, gene therapy using siRNA and DNA, and photoacoustic therapy using carbon nanotubes (Bardhan *et al.*, 2011).

Different targeting ligands are also frequently employed to improve the selectivity and specificity of the systems. For example, folic acid for recognizing folate receptors (Maeng *et al.*, 2010; Y. Zhang *et al.*, 2017), various peptides, (Jo *et al.*, 2016), antibodies (Conde *et al.*, 2014; Lim *et al.*, 2011; Scarberry *et al.*, 2008;

B. Zhang *et al.*, 2017), and aptamers (Das *et al.*, 2015; Lyu *et al.*, 2016; Yu *et al.*, 2011) are widely used as targeting agents in nanotheranostics. These targeting nanocarriers have enhanced uptake by cancer cell lines, localized selectively to the affected area and hence show much better diagnostics and therapy.

Diagnostics can be performed using several contrasting agents (Bardhan *et al.*, 2011; Wu *et al.*, 2014). It includes optical imaging using various agents like organic fluorophores (Zheng *et al.*, 2014), inorganic nanoparticles (Luo *et al.*, 2012; Lv *et al.*, 2015; Muthu *et al.*, 2015) like quantum dots and carbon dots, magnetic resonance imaging using manganese, iron oxide and gadolinium nanoparticles (Y. Chen *et al.*, 2015b; Zhang *et al.*, 2015), computed tomography using gold and iodine nanoparticles (Liu *et al.*, 2014), positron emission tomography using various radioisotopes (F. Chen *et al.*, 2015a; Lopez-Rodriguez *et al.*, 2015), and ultra sound imaging (Min *et al.*, 2015; Wang *et al.*, 2014).

A multimodal therapy was also developed in which two or more diagnostic capabilities were introduced into a single platform (Bardhan *et al.*, 2009; Fan *et al.*, 2014; Song *et al.*, 2015). It is based on the exploitation of individual advantages of each imaging modality and hence is expected to deliver better theranostic efficiency.

1.2. Single Molecule Based Theranostic Agents

The idea of integrating all the features required for theranostics into a single molecule holds a great potential in the future. Even though the idea is still in its infancy, and a lot more hurdles have to be crossed for the successful implementation in clinical practices, attempts along these lines have reported promising results. A number of targeted near-infrared (NIR) fluorophores are under preclinical studies and till now, approved for clinical use in humans is awaited (R. R. Zhang *et al.*, 2017). The following sections present the state-of-the-art and promising developments towards single molecule based theranostics.

1.2.1. PDT in theranostics

PDT is a widely accepted non-invasive treatment modality in which light, a photosensitizer and molecular oxygen are the major components (Dolmans *et al.*, 2003). Compared to the current cancer treatments, PDT has an inherent selectivity feature in which visible or NIR light is directed to the localized photosensitizer. The photosensitizer is considered to be nontoxic in dark and in the presence of light, will get excited and transfer energy to molecular oxygen, to produce very reactive short life singlet oxygen which will destroy the tumor lesions. PDT also has several shortcomings - the ideal photosensitizer should absorb in the therapeutic window (650-900 nm), light penetration is limited to a few millimeters and most importantly, in hypoxia conditions, PDT is ineffective which limit its use in certain kinds of tumors. Sufficient improvements in photosensitizer and light irradiation setups have to be made for enjoying all the potential offered by PDT. Photosensitizers with targeting groups and development of activatable photosensitizers have led to third generation photosensitizers with improved selectivity and specificity (Bugaj, 2011).

Photosensitizers with inherent fluorescence can be used for imaging and hence locating diseases. The manifestation of the required attributes into a sensitizer will be rather challenging due to the demand for proper balancing between fluorescence and triplet state quantum yields and these properties are often contradictory to each other. Pandey and co-workers conjugated a HPPH (2-[1-hexyloxyethyl]-2-devinyl pyropheophorbide), now in Phase II clinical trials, with cyanine dye and the conjugate exhibited remarkable photocytotoxicity and imaging capabilities (Ethirajan *et al.*, 2011). Multi-functional photosensitizer molecule was developed by conjugating with suitable imaging agents for their use in different imaging modalities like magnetic resonance imaging, computed tomography, positron emission tomography, and fluorescence imaging. Hydroporphyrin derivatives like chlorins have shown potential in imaging and PDT (Singh *et al.*, 2015). Celli *et al.* reviewed the plausible applications of imaging and PDT agents,

along with their dosimetry status by monitoring the dose response to various tissues (Celli *et al.*, 2010). Fluorescence imaging-guided resection and PDT was successfully used for treating lung cancers (Josefsen and Boyle, 2012). *N*-(2-hydroxypropyl) methacrylamide copolymer-conjugated zinc protoporphyrin systems developed by Fang and co-workers caused necrosis and 70% of the tumors were treated successfully using different tumor models. They further confirmed the tumor imaging using breast and colon cancer models (Fang *et al.*, 2015). Recently, thio-heterocyclic fused naphthalimide was reported as a novel core for theranostics by Zhang and co-workers (Zhang *et al.*, 2016). They performed *in vitro* and *in vivo* analyses and confirmed effective PDT and imaging potentials which may be considered as a positive step towards the goal of small single molecule theranostic agents. Ideally, the synergetic imaging and PDT capabilities in a molecule added a new dimension in cancer treatment. Such a system offers multiple competencies like diagnostics, therapy guidance, monitoring of lesions, treatment assessment and understanding the mechanism of cell action (Celli *et al.*, 2010).

1.2.2. Trackable therapeutics

The idea of trackable therapeutics has recently emerged as a novel concept spurring much research interest among the scientific community (Bertrand *et al.*, 2016). Administration of a single molecule for therapy and diagnostics will lead to the development of multi-functional theranostic agents. The straightforward approaches would be either to integrate imaging capabilities into an existing drug or adding therapeutic property to dye molecules. However, conjugation strategy using a polymer or other carrier molecules would make the systems more complex and further these higher molecular weight systems would also have poor cell penetration ability.

In the past few years, research on targeted fluorophores showed tremendous improvement and a number of molecules reached the preclinical stage.

For example, Cetuximab-800CW was the first tumor targeted fluorophore to reach clinical trials (Rosenthal *et al.*, 2015). NCT01508572 and NCT01987375 are cancer biomarker targeted NIR fluorophores used for fluorescence guided surgery to reach clinical trials (R. R. Zhang *et al.*, 2017).

Indocyanine green (ICG) was the first and the only NIR fluorescent dye to get approval in clinical trials (Frangioni, 2003). Following that, heptamethine indocyanine NIR fluorescent dyes with cancer selectivity were developed, among which IR-808 selectively accumulated in the mitochondria of cancer cells and exhibited potential cytotoxicity (Tan *et al.*, 2012). The same system also could act as a PDT agent with imaging and targeting capabilities. Among several other derivatives of IR-808 which were later developed, IR-808DB showed tumor inhibition potential greater than that for the therapeutic drug cyclophosphamide along with NIR imaging competence (Luo *et al.*, 2013). Other fluorophores with inherent targeting properties that were developed include IR-783 which showed uptake in prostate, bladder, renal and pancreatic cancers, IR-780, and MHI-148 (Henary *et al.*, 2012; Lee *et al.*, 2011; Tan *et al.*, 2012).

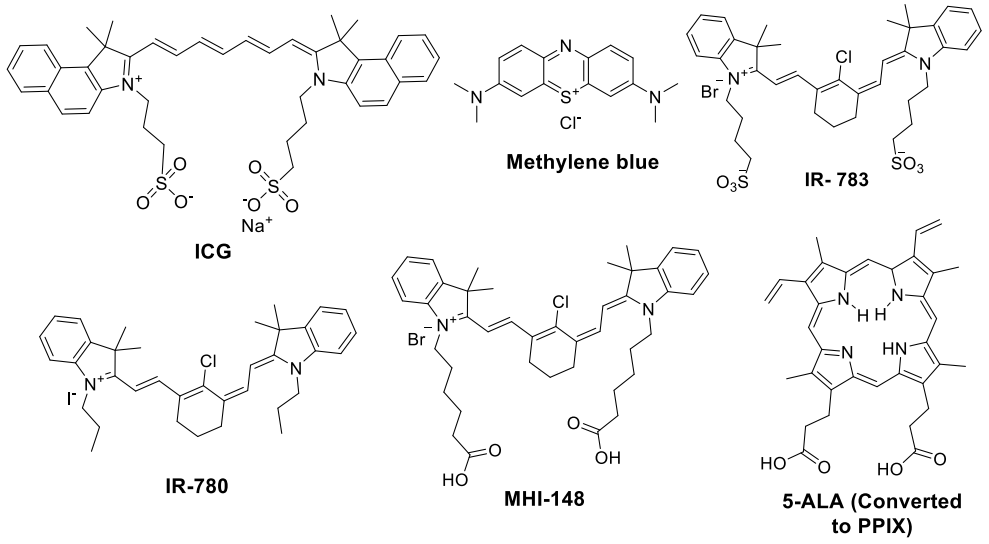

Figure 1.1. Chemical structures of fluorophores used for cancer detection

Recently a new analogue of ICG, IR-DBI was developed by Tan *et al.* capable of exhibiting multimodal therapeutic properties including mitochondrial targeting, NIR emission, PDT, photothermal and chemotherapeutic effects (Tan *et al.*, 2017). Figure 1.1 lists the clinically approved fluorophores for cancer detection among which methylene blue and 5-aminolevulinic acid (5-ALA) have poor targeting ability and table 1.3 summarises ICG dyes and their tumor targeting areas.

Table 1.3.Tumor targeting of indocyanine dyes

Dye	**$\lambda_{abs/em}$(nm)**	**Tumor type targeted**
ICG	780/812	-
IR-780	777/823	Breast, lung, cervical
IR-783	766/782	Prostate, cervical, breast, lung
MHI-148	785/808	Prostate, leukemia, breast

Among the wide variety of porphyrin dyes, only very few display cancer selectivity. For instance, porphyrazine derivative Pz 247 is an NIR emissive fluorophore with selective accumulation in lysosomes of tumor cells and MDA-MB-231 in breast tumor cells (Trivedi, *et al.*, 2010a). Later naphtha-pz derivative was synthesized with enhanced photophysical properties (Trivedi, Lee*, et al.*, 2010b). Some gadolinium conjugates of porphyrazine also exhibited improved uptake by tumor cells (Song *et al.*, 2010).

Another important class of single molecule based theranostic agents comprises of the complexes of transition metals, mainly of ruthenium (Ru). Compounds such as NAMI-A, KP1019 and KP1339 (Gao *et al.*, 2017; Modjtahedi and Dean, 1994) displayed very good therapeutical and photophysical properties in which NAMI-A and KP1339 have already entered the clinical trials (Bratsos *et al.*, 2007). Farrell *et al.* reported another set of Ru complexes having good cytotoxicity and localization in cytoplasm and nucleus on fluorescence imaging (Cardoso *et al.*, 2014). Cyclometalated iridium(III) complexes displayed excellent cytotoxicity greater than cisplatin with mitochondria targeting and are considered as a promising candidates towards theranostics (Yi Li *et al.*, 2015).

1.3. Computer Aided Design of Theranostic Agents

It is evident from the previous discussion that there is a growing interest in the area of single molecules based theranostic agents for the last few years. But, most of the systems are developed around fewer core structures leading to a serious crunch in the number of novel cores exhibiting theranostic properties. Further advancement in single molecule based theranostic agents can gain momentum and lead to breakthroughs with the development of efficient molecules. This demands novel cores systems with therapeutic potential along with excellent photophysical properties to be designed and developed. In this context, considering the significance and challenges associated with a *de novo* core design, it is highly reasonable to rely on computer aided strategies which can guide and accelerate the design process. Though the computer aided drug design (CADD) strategy is much familiar in the development of therapeutics, to the best of our knowledge, these techniques are not at all exploited for the design and development of theranostic agents. Different computational techniques can be used either individually or in combined forms for the development of molecules with therapeutic properties along with very good photophysical properties.

1.3.1. Computer aided drug design

The conventional drug design is a very lengthy and time consuming process with low success rates. On an average, it takes around 12-15 years and around $500-800 million to bring a drug into the market (Rawlins, 2004). The traditional drug discovery involves the synthesis of a large collection molecules and their screening in a number of target proteins using high throughput screening (HTS) protocols. Novel potent, selective and highly specific drugs have to be developed in order to address the drawbacks associated with existing drugs. With the advancement in chemistry, biology, genomics, proteomics and instrumentation facilities, the underlying mechanism of drug action was explored and suitable target

proteins were identified (Overington *et al.*, 2006). Development of novel drug molecules with high specificity and with no or reduced side effects is the need of the hour. The CADD strategies have the potential to resolve the current problems and avoid unnecessary laboratory illness and expenses associated with the conventional drug design process. With the improvement in computational power and development of sophisticated algorithms, it is now possible to perform computational modelling calculations even in laptops or desktop systems. The figure 1.2 clearly illustrates the various processes involved in the CADD process.

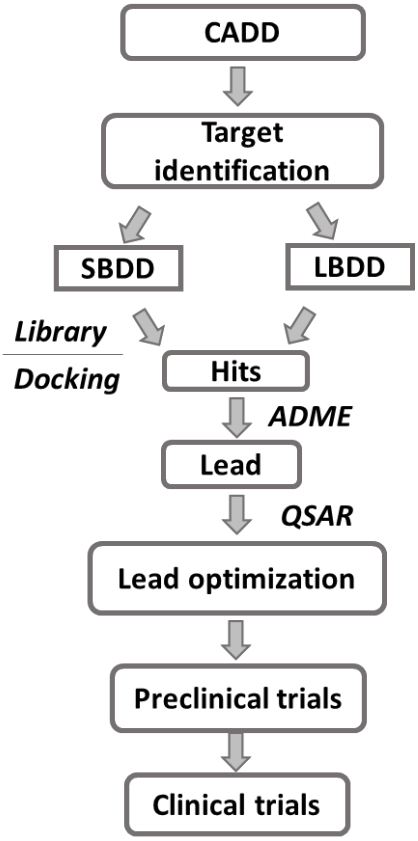

Figure 1.2. Computer aided drug design

There are many success stories linked to CADD which encouraged the researchers to use computational methods for drug discovery. For example, aggrastat, a drug used for the prevention of early myocardial infarction, is considered as the first drug candidate to originate from a pharmacophore based

virtual screening lead. A direct search of Merck Sample Collection resulted in the identification of a RGD- mimicking lead compound and was suggested as a specific inhibitor of GP IIb/IIIa mediated platelet aggregation (Hartman *et al.*, 1992). Further lead optimization through experimental and molecular modelling studies led to the drug aggrastat and was marketed in 1998 (Cook *et al.*, 1999). Similarly, PRX-00023, PRX-03140, PRX-08066 and SC12267 are some of the drugs developed using CADD program. Apart from the discovery of novel drug molecules, CADD can also be used for increasing the specificity and efficiency of known drug molecules. For example, Carraro *et al.* discovered a set of new compounds with good antiproliferative activity against human leukemia cell lines but with poor solubility (Carraro *et al.*, 2004). Later, a series of molecules with better activity and solubility was developed with the help of molecular modelling (Radi *et al.*, 2011). The remarkable improvement in CADD, allows the medicinal chemists to use this valuable tools in a variety of stages in the drug discovery process. (Xiang *et al.*, 2012).

CADD process can also be used for the early stage identification of pharmacochemical properties. The ADME (absorption, distribution, metabolism and excretion) and toxicity profiles can be used for identifying molecules with druggable character in the early stage itself thereby avoiding their later stage omission. This initial screening from the in-house library can be used to select molecules with diverse physiochemical properties. CADD can be employed either in 1) ligand based drug design (LBDD) or 2) structure based drug design (SBDD). LBDD is an indirect method and used for unknown 3-D target structure. It uses similarity searching and pharmacophore mapping. A pharmacophore can be considered as a set of structural features that are recognized at the receptor site and is responsible for its activity (Gund, 1977). The steric and electronic features required for the binding will be analysed and subsequently new molecules are designed. A quantitative structure activity relationship (QSAR) is also developed using all the experimental and computational properties to get a mathematical relationship between a set of descriptors and their activity.

On the other hand, SBDD is a direct method using the 3-D structure of the target. With the advancement of X-ray crystallography and nuclear magnetic resonance (NMR) spectroscopy, the determination of the structure of the target proteins became much easier. If these are not available, homology modelling, a reliable method to obtain the structural informations in the absence of experimental data can be performed to make the 3-D models as demonstrated in the case of G-protein coupled receptors (GPCR) (Evers and Klabunde, 2005). However, the success of model building is dependent on the sequence identity between the target and the template. If the sequence identity is above 50%, it is possible to build reliable models with RMSD falling around 1Å. There are plenty of success stories reported such as the development of first renin inhibitor drug called Aliskiren by Ciba-Geigy (now Novartis), the development of more selective benzophenone-based inhibitor drugs by Kohring et al, the discovery of new cardiovascular drug HAMI 3379 and so on (França, 2015). In SBDD, molecular docking is yet another widely accepted method for the virtual screening of compound libraries. Once the structure of the target is known, potent ligand molecules capable of binding to the active site can be determined. Using different searching and scoring algorithms, ligand molecules are ranked according to their binding energies. Several novel inhibitors were developed with improved activity using molecular docking approach (Shoichet *et al.*, 2002) whereas further improvements by sufficiently addressing the receptor flexibility is needed for the development of better and efficient systems (Yuriev and Ramsland, 2013).

1.3.2. Computational methods in materials design

Computational chemistry techniques have emerged as a versatile and fundamental tool in modern research where the power of quantum mechanical theories is utilized to accurately and completely describe a system. Various properties of interest of a molecule such as structure, spectroscopic properties, reaction mechanism, and other physical properties can be calculated using molecular mechanics, *ab initio*, semiempirical methods, density functional theory

(DFT) and molecular dynamics (MD) (Lewars, 2016). For the last two decades, computational chemistry has proven its potential in diverse fields of science including drug design, materials chemistry and nanotechnology (Dykstra *et al.*, 2011).

The emergence of DFT produced a drastic change in the use of computational chemistry techniques and now it is possible to perform routine calculations in desktop computers within few days. Compared to *ab intio* methods, DFT uses electron density based methods rather than wave function based methods, and produces accurate results within short time periods. Later, time dependent density functional theory (TD-DFT) was developed (Runge and Gross, 1984) as an extension of DFT for describing the excited state behaviour of molecules. These methods hold several advantages due to their simplicity and system independent inputs, the speed of computation with a reliable accuracy of moderate size systems, and the possibility to couple with different environmental models (Laurent *et al.*, 2014). But one has to keep in mind that the possibility of systematic improvements is limited in DFT and hence be cautious in applying it in novel molecules. The analysis of a number of benchmark studies will provide useful information in the rational design of molecules.

With the explosion of research in materials science, employing computational chemistry techniques in molecule to material transformation is getting significant attention these days. Similar to the usage of CADD in designing molecules with therapeutical potential, DFT methods can be used to address several problems in materials design. For example in dye designing process, it has been used for designing molecules having visible or NIR absorption and emission, generating colour tunable scaffolds, molecules with large Stokes shift, molecules for dye sensitized solar cells and so on (Beverina and Salice, 2010; Guillaumont and Nakamura, 2000; He *et al.*, 2008; Jacquemin *et al.*, 2008; Mishra *et al.*, 2009).

However, a perusal of literature suggested that the potential of computational methods has not been fully utilized in the area of theranostics, although it has been widely used for the design and evaluation of individual components. The rational design strategy was developed for the photosensitizers used in PDT and further experimental investigation proved the photodynamic activity which highlights the strength of these adopted theoretical methods (Alberto *et al.*, 2013; Quartarolo *et al.*, 2009). Computational methods can also be used for the fundamental understanding of the molecules and a structure property relationship can be generated which will guide in the rational design of novel compounds of interest. So these methods can be considered as green protocols and environmentally safe since they eliminate the synthesis of large number of candidates. However, computational chemistry techniques can't stand alone in developing theranostic molecules nor it can replace the experiments. The combined synergetic methods have to be developed where experiment and theory should complement each other.

1.4. Combinatorial Strategies in Materials Development

The demand for large number of diverse, yet closely related molecules, by the pharmaceutical industry led to the exploration of combinatorial libraries in the final decade of the twentieth century. Subsequently, a large number of peptides (Pinilla *et al.*, 1995) and oligonucleotides (Gold *et al.*, 1995) were initially developed for meeting the requirement of HTS. Later, a combinatorial library of small organic molecules consisting of diverse and complex structures was developed (Thompson and Ellman, 1996). A collection of diverse class of drug-like molecule were synthesized using diversity oriented synthesis (DOS) strategy (Schreiber, 2000). DOS and combinatorial approach allow the synthesis of molecular libraries in a limited period of time. Nowadays, these approaches have

been extended to the field of materials science and engineering (Koinuma and Takeuchi, 2004; Takeuchi *et al.*, 2005).

Diversity oriented fluorescence library was designed to meet the requirement of fluorescence probe development (Vendrell *et al.*, 2012). The same library may also be used in the molecular docking to identify novel structural motifs that bind on targets. Similarly, the molecules selected from the virtual screening or molecular docking protocols can be synthesized simultaneously using combinatorial methods. Hence this strategy has a huge potential in finding suitable candidates for the theranostic regime. For achieving it, the *de novo* designed library should ideally have multiple diversity multiplication sites positioned around a chosen core. Moreover, the simple synthetic procedures using readily available starting compounds will accelerate the efficiency of library design for theranostics. Further, this strategy can be extended for the development of core skeletons with multi functionality to boost their realization in varied technological applications. Considering the significance of heterocycles in the therapeutic realm along with the growing interest of heterocyclic systems in materials science, a brief discussion on the importance of these systems is now presented.

1.5. Importance of Multi-heterocyclics

Heterocycles are an elite class of compounds in the chemical space with vital role in the existence of life in nature. Majority of the natural products and molecules of biochemical importance like vitamins, amino acids, nucleic acid bases and many of the natural drugs such as papaverine, codeine, atropine, quinine and so on (Butler *et al.*, 2014; Joule and Mills, 2010) contain heterocycles. The rich chemistry possessed by the family heterocycles continues to be successfully utilized for deriving new drug molecules.

Many of the cytotoxic drugs including alkylating agents, antimetabolites, alkaloids and antitumor drugs have a heterocycle component. The availability of

diverse class of heterocycles and possibility to expand the three-dimensional space around it with different substituents using known chemistry led to the discovery of novel anticancer drugs. About 30% anticancer drugs approved by food and drug administration (FDA), contain oxygen and nitrogen heterocycles (Martins *et al.*, 2015). The heterocycles widely used in anticancer research are pyrimidine (Kamal *et al.*, 2011; Shiau and Chen, 2013), pyrrole (Gholap, 2016; Gupton, 2006), indole (Singh Sidhu *et al.*, 2016; Tunbridge *et al.*, 2013), quinolone (Afzal *et al.*, 2015; S. Chen *et al.*, 2013) and pyrazole (Lv *et al.*, 2010). Heterocyclic anticancer drugs available in the market are listed in figure 1.3 (Martins *et al.*, 2015). Hence, including relevant heterocycles in the core scaffold can be thought of as a viable strategy to increase the druggability of the molecules.

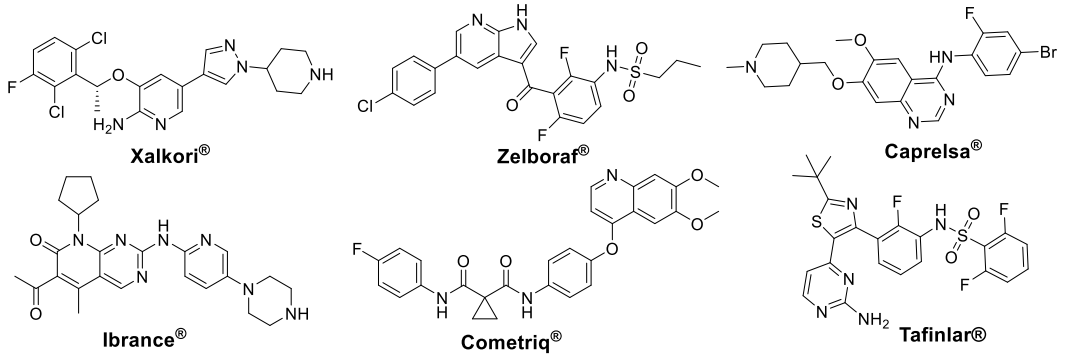

Figure 1.3. Heterocyclic antitumor drugs approved by FDA

The heterocyclic molecules also important components in plant pigments such as porphyrin and anthocyanine dyes, and naturally occurring dye indigo. Also the molecules like psoralen derivatives, porphyrins, and phthalocyanine derivatives are used for photochemotherapy and PDT (Joule and Mills, 2010). Heterocyclic fluorophores are important class of compounds in sensing applications as well. They have large photoresponses, can be used for the design of full colour tunable fluorophores, are chemically and thermally stable, and have increased polarizability (Barone *et al.*, 2015; Prampolini *et al.*, 2013). The newly designed NIR dyes for imaging cancer consist of heterocyclic organic fluorophores (Sun *et al.*, 2016; Yang *et al.*, 2017).

In addition to their therapeutic properties, heterocyclic compounds expand their horizons in the development of advanced functional materials also. They found potential applications in bulk heterocycle solar cells (Bürckstümmer *et al.*, 2011), organic semiconductors (Mishra and Bäuerle, 2012), organic photovoltaics (Roncali *et al.*, 2014), dye sensitized solar cells (Wu and Zhu, 2013), electro-optic applications (Marder *et al.*, 1997) and so on. Thus heterocycles play a crucial role in the molecule to material transformations for diverse technological applications.

1.6. Scope and Objectives

As discussed in the previous sections, the synergism between therapy and imaging capabilities has a huge impact on modern treatment modalities. Theranostics is considered to be a giant leap towards the concept of personalized medicine (Crawley *et al.*, 2014). Recently the idea of trackable therapeutics has been introduced along with the hunt for single molecule capable of exhibiting both therapeutic and imaging properties. The present work was initiated and intended to contribute to our long term goal of developing a novel heterocyclic scaffold for theranostics wherein the designed small molecule will comprise of synergistically functioning therapeutic as well as imaging units. Our focus in the present research program is on computation assisted *de novo* design and the development of a combinatorial library of fluorophores centered around 1,3-thiazole core as theranostic agents.

The literature clearly underlines the lack of sufficient core scaffolds and efficient systems to meet the need of the hour. Thus, our primary objective was to develop a novel 1,3-thiazole based core with therapeutic property and excellent photophysical properties. We attempted extending the concept of molecular hybridisation where potential fragments are hybridised to get a novel pharmacophore, currently being explored in drug discovery contexts, to the development of multi-heterocyclic theranostics. Our idea was to combine the individual strength of different approaches/methods and contribute significantly

towards an emerging field. A computer aided fluorophore design strategy was planned for the *de novo* design of novel core molecules with diverse structural features and properties. Followed by the multi-heterocyclic core design, formulation of retrosynthetic routes and accomplishing facile synthetic routes were the next objectives. Further, we performed an *in vitro* screening in cancer cell lines, followed by a detailed *in silico* binding studies on cancer biomarkers to reveal the therapeutic potential of the systems. Our next objective was to study the structure photophysical properties of the core molecules and to explore the imaging capabilities for theranostic development. We were also interested in thorough understanding of the nature of the core and its photophysical properties with the aid of computational tools. An attempt also has been made to explore the multi-functional application of the developed core molecules.

The specific objectives of the current research work are

- Computational design of *de novo* multi-heterocyclics with therapeutic and diagnostic attributes
- Formulating the synthetic routes, chemical synthesis and characterization
- Design of combinatorial libraries by diversity multiplication around the core
- Evaluation of therapeutic potential of library members by *in vitro* and *in silico* screening
- Detailed study of structure photophysical properties
- Investigation of the potential of chosen systems in imaging application
- Computation assisted detailed understanding of the developed cores

1.7. Organization of the Thesis

The entire research work is summarized in eight chapters and contents of each chapter are briefly discussed below

Chapter 1 gives the background of the work, literature and state-of-the-art of the research problem. It starts with describing the current anticancer treatment scenario and further introduces the concept and scope of theranostics. A briefing on different theranostic systems developed so far is included in this chapter. Further, the concept of single molecule based theranostics is described with available literature data. It also contains a discussion about the possibility of incorporating computer aided methods like molecular modelling and DFT methods for the development of theranostic agent. Further, the concept of combinatorial strategies in theranostic development is also included. The chapter ends with describing the scope and objective of the research work and the chapter-wise organization of the thesis.

Chapter 2 deals with the computational assisted design of *de novo* multi-heterocyclic fluorescent core. The molecular hybridisation of heterocycles along with D-A concept in designing the novel scaffold is described. The chapter also analyses the diversity multiplication sites in detail along with the tunable nature of the core using computational methods.

Chapter 3 describes the development of systematic routes to the designed core scaffold. The retrosynthetic analysis, chemical synthesis of the library of molecules along with their characterization details are also presented.

Chapter 4 deals with the evaluation of the therapeutical potential of the synthesized molecules along with the generation of a virtual library built on the core scaffold. It also includes *in silico* ADME property prediction to find out the drug-likeness of the molecules. Further, detailed binding studies of virtual library members in the active site of targets chosen from various protein families are also included.

Chapter 5 describes the photophysical properties of the developed thiazole-heterocycles. The solution and solid state fluorescence, solvatochromism and photophysical data of all the synthesized molecules along with detailed structure

photophysical relationship are included in the chapter. The results of theranostic potential evaluation are also presented in this chapter.

Chapter 6 is an attempt to understand the fundamental nature of the thiazole-heterocycle core using computational tools. The effect of different functionals, basis sets and solvent effects on absorption wavelength were analysed and described. Investigations on the multi-directional charge transfer and quinoid nature of the core are also presented in this chapter.

Chapter 7 attempts to explore the potential of the thiazole-heterocycle core in multi-functional applications. The aggregation induced emission and its validation using molecular dynamics simulation, acid sensing potential and mechanochromic behaviour of the core are also included in chapter 7.

Chapter 8 includes the conclusion and future direction of the current research work.

CHAPTER 2

DE NOVO DESIGN OF MULTI-HETEROCYCLIC FLUORESCENT CORE

2.1. Background

The hybridisation of fragments with established activity can be a useful strategy in the design of novel potential molecules for specified applications. For example, molecular hybridisation has emerged as one of the powerful tools in drug design process. Here the combination of two or more pharmacophores having well studied pharmacological and physiochemical features are used in the rational design of novel molecules with multi-functional properties. Thus designed novel molecules can be further modified with suitable functional groups for tailored and enhanced properties. These modified molecules possibly have the potential to interact with various biological targets with improved selectivity and hence, reduce the side effects. This strategy has been successfully used for the development of several new drugs. One advantage of hybridising strategy is that several pharmaceutically relevant fragments can be coupled to generate a diversity oriented combinatorial library to contribute to the medicinally relevant chemical space. Although the term molecular hybridisation is frequently used in the drug design scenario, the concept is not new to other fields of chemistry. For example, the hybridisation of known fluorescent dyes into a single molecule for the development novel fluorophore was reported by several groups (Bochkov *et al.*, 2013; Jiao *et al.*, 2011; Katori *et al.*, 2015). Yuan *et al.* developed NIR emissive fluorophores "Changsha dyes" by the combination of well-known fluorophores rhodamine and cyanine. (Yuan *et al.*, 2012).. Perusal of literature suggested that the concept of molecular hybridisation is not well explored in the theranostic regime, despite its

enormous potential. We felt it would be highly interesting to integrate biologically active fragments and fluorophore scaffolds into a single platform for the development of active molecules with imaging capabilities. Such an attempt, following a rational approach, is expected to contribute significantly for the development of novel minimal architecture theranostics which is now discussed.

2.2. Results and Discussions

2.2.1. Design of core molecules

Design of novel scaffolds with multi-faceted properties is always fascinating, but highly challenging and hence remains largely unmet. However, immense opportunities exist once the core is designed, in that it can be decorated with different fragments for improving the properties as well as selectivity. Different aspects are to be kept in mind during these designing processes. We are particularly interested in the *de novo* design of novel scaffold which is considered as a highly complex and yet exciting task. The strategy involves the development of novel core skeleton by integrating the two important components of the theranostics, 'therapeutics and imaging' into a single platform (figure 2.1) and will be described in the following sections separately.

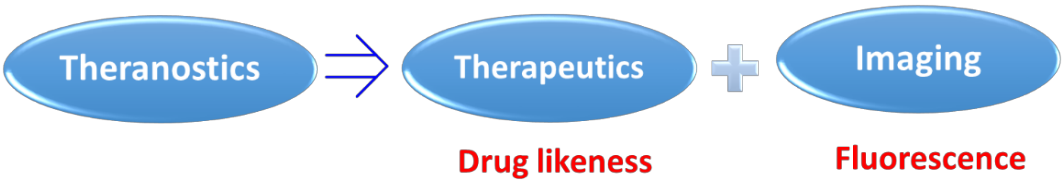

Figure 2.1. The concept of theranostics

2.2.1.1. Selection of cores with therapeutic potential

The expedition of unexplored region of chemical space has a vital role in the drug discovery process. But the selection of biologically relevant chemical

space with synthetic flexibility is rather challenging (Deng *et al.*, 2013). In this regard, exploration of small molecules possessing extraordinary properties is highly imperative. Small molecule drugs are molecules having relatively small molecular weight typically below 1000 Daltons and constitute around 90% of drugs available in the market (Lu and Atala, 2016). They can interact with numerous macromolecules and interfere in many of the metabolic pathways (Cj *et al.*, 2012), are relatively inexpensive, can be synthesized rapidly in high purity and can be appended with a variety of substituents to produce a functionally diverse library with desired biological activity (Galloway *et al.*, 2010).

In the design of drug-like molecules where the selection of core is extremely important, 1,3-thiazole skeleton is considered as an important fragment owing to its pharmaceutical interest. The presence of thiazole ring is considered significant in a multitude of other applications as well (figure 2.2).

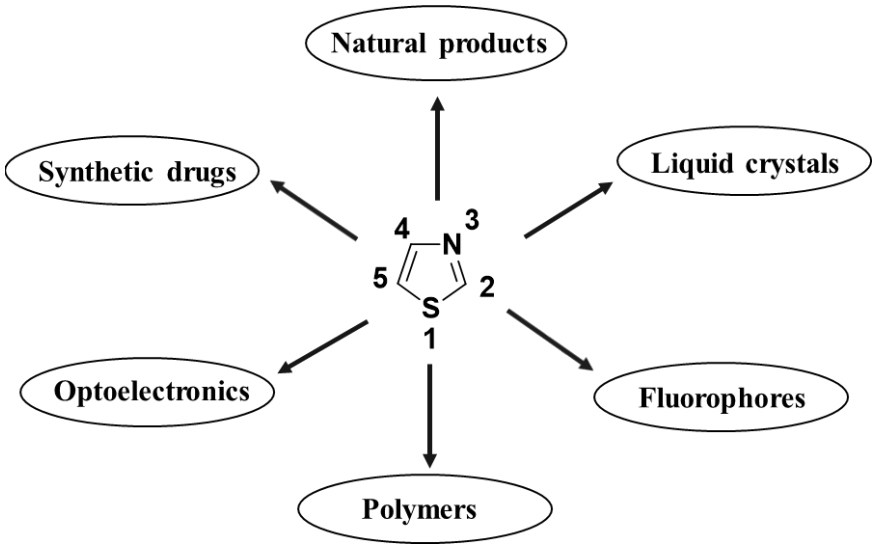

Figure 2.2. Plausible applications of thiazole containing systems

The nitrogen and sulphur heteroatoms bearing thiazole exhibit a wide spectrum of biological activities such as anticancer, antibacterial, antifungal, antiviral, anti-inflammatory, antiparkinsonian, antihypertensive, antiallergic, anti-HIV, and so on (de Souza, 2005; Kashyap *et al.*, 2012). Therefore thiazole is an

active fragment in many of the drugs such as sulphathiazole (antimicrobial), ritonavir (antiviral), talipexole (antiparkinsonian), abafungal (antifungal), and bleomycin (antineoplastic). Inspired by these excellent therapeutic properties of thiazole and our group's long-standing interest in thiazole chemistry, and its potential to exhibit multi-dimensional properties, we decided to choose thiazole as our central core in the design of novel theranostic platforms.

Considering the requirements of drug-likeness and imaging properties within the same molecular system, we felt it worth to explore the heterocyclic toolbox to select fragments for developing multi-heterocyclic core system around thiazole core. Heterocycles are considered to be *privileged medicinal scaffolds* (Bräse, 2015) and found in numerous biologically active molecules and FDA approved drugs (Ali *et al.*, 2015; Vitaku *et al.*, 2014). A plethora of heterocycles are known with well-established chemistry and reported to have interesting biological properties. Further, the chemical space around these heterocycles can be modified with suitable substituents to enhance the activity. In the present work, we discuss the systematic design of multi-heterocyclic core system starting with a simple biheteroyl core, ie; the thiazole-heterocycle (thiazole-het) core, and subsequent modifications utilising the inherent three site tunability around the thiazole core. We further aimed to attach various substituents around the core to populate the three dimensional space around it so as to generate a diversity oriented library (figure 2.3). Further core design strategy will be described in the respective sections of fluorophore design and virtual library generation.

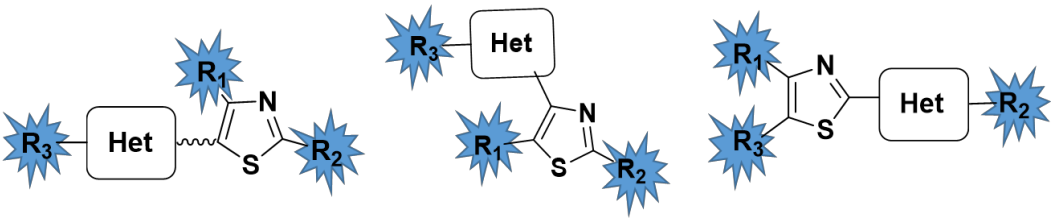

Figure 2.3. Diversity oriented library of thiazole-het core

2.2.1.2. Selection of imaging scaffolds

Because of the wide scope of molecular engineering around the core for fine tuning of the optical properties, organic fluorophores gained considerable attraction among researchers. Small organic fluorophores possess a great number of advantages as their simple structure and low molecular weight allow the synthesis in good yield and high purity with repeatability. They also hold attractive features like well-defined tunable structure, high chemical stability, good cell permeability, predictable and peculiar properties, good signal to noise ratio and so on (Terai and Nagano, 2013). In the myriad of molecules available in the chemical space, the expedition for small organic fluorophores is extremely interesting because of their potential to develop as multi-functional materials (Kowada *et al.*, 2015; Levi and Müller, 2016; Müller and Bunz, 2007; Wysocki and Lavis, 2011; Yun *et al.*, 2014). Additionally, minimal organic fluorophores achieved a significant role in biological scenario (Lace and Prandi, 2016; Ueda, 2012) as their small volumes allow them to access tiny cavities and were used as environmental sensitive fluorophores, probes for understanding protein folding mechanisms and in binding site analysis (Kim *et al.*, 2014; Kobayashi *et al.*, 2010; Li *et al.*, 2013; Terai and Nagano, 2013; Ye *et al.*, 2014).

Despite these excellent attributes and high demand for fluorophores, reports on novel core skeletons with tunable emission properties are limited in number (Kim *et al.*, 2008; Lavis and Raines, 2008). The development of new efficient fluorophore scaffolds are always challenging task because it should ideally address the critical parameters like colour tunability in both solution and solid state, high quantum yield, large Stokes shift, simple core structure with synthetic flexibility, solubility and processability. At the same time, small fluorophores with drug-likeness are also extremely important whereas remains under developed. Furthermore, new molecular skeletons coupled with a multitude of properties attuned for various applications are limited in number which could be attributed to

the challenges in the rational design of novel core with tunable properties (Cheng *et al.*, 2016; Liu *et al.*, 2015).

Because of the above mentioned difficulties and due to the complexity underlying the photophysical phenomena, most of the new fluorophore scaffolds are developed in a trial and error manner. One of the widely adopted methods for imparting useful and tunable photophysics in a scaffold is to design push pull architecture by taking advantage of intramolecular charge transfer (ICT) phenomena. Conjugated molecules with electron donor (D) and electron acceptor (A) units have received particular interest in the construction of low band gap materials for various optoelectronics applications like organic light emitting diodes (OLEDs) (Muller *et al.*, 2003), field effect transistors (FETs) (Zhou *et al.*, 2007), photovoltaic devices (Duan *et al.*, 2012), nonlinear optics (Chemla, 2012), dye senzitised solar cells (Hagfeldt *et al.*, 2010; Mishra and Bäuerle, 2012) and so on. Push pull molecules have also found widespread applications in biology, particularly in bioimaging. D-A conjugated molecules have the advantage that their electronic and optoelectronic properties can be easily modulated by selection of diverse donor and acceptor groups. These push pull molecules are known as charge transfer chromophores (Kivala and Diederich, 2008) and are generally excited using visible light when electrons get transferred to a new molecular orbital formed by the interaction of D and A groups. The common electron accepting and electron donor groups are listed in table 2.1 with their Hammett substituent constants (Hansch *et al.*, 1991) which would guide in the judicious selection of substituents for fine tuning the properties.

Table 2.1. Electron accepting and electron donating groups with their Hammett substituent constants

Donor (D) groups	σ_p	**Acceptor (A) groups**	σ_p
NO_2	0.78	NMe_2	-0.83
CN	0.66	NHMe	-0.70
CF_3	0.54	NH_2	-0.66
CHO	0.42	NHPh	-0.56
COOH	0.45	NPh_2	-0.22

COMe	0.50	OH	-0.37
COOMe	0.45	OMe	-0.27
$COCF_3$	0.80	OPh	-0.03
SO_2Me	0.72		
SO_2CN	1.26		

D-π-A systems based on heteroaromatic scaffolds have attracted considerable attention in the area of organic functional materials. As we have already decided to select thiazole as our central core considering its therapeutic potentials, imparting push pull nature to thiazole cores would expand their use as multi-functional materials. Heterocyclic chromophore scaffolds have a plethora of advantages as reviewed by Bures (Bureš, 2014) such as higher chemical and thermal robustness, ability to behave as auxiliary acceptors and donors, enhanced polarizability, improved solubility and conformational stability, acid-base chelating properties, synthetic flexibility and tunability, and wide scope of biological properties.

Thiazole building block is a promising candidate in many of the functional materials but its fluorescence properties are not much explored and limited to very few scaffolds. A bisazole molecule oxyluciferin is a naturally available thiazole fluorophore, generated during the bioluminescence of firefly (figure 2.4) with an intense luminescence emission (Naumov *et al.*, 2009) in the blue region. A few commercially available thiazole containing fluorophores such as thiazole orange and SYBR Green I which are being used as DNA labelling agents, generally are categorised under cyanine class of dyes (figure 2.5). Here the thiazole rings are part of a benzothiazole fragment whose optical properties were well explored (El-Shishtawy *et al.*, 2013; Hrobarik *et al.*, 2004; Hrobáriková *et al.*, 2010).

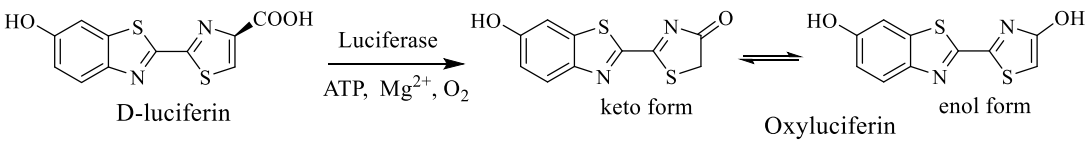

Figure 2.4. Generation of oxyluciferin in the bioluminescence of firefly

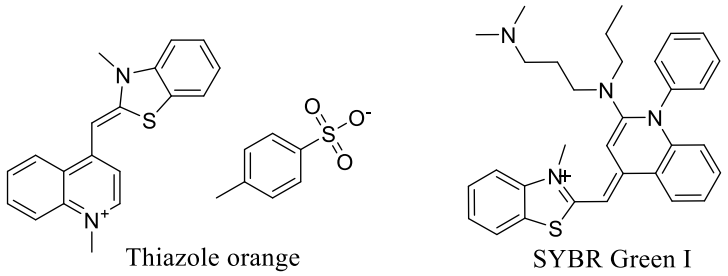

Figure 2.5. Commercially available thiazole containing fluorophores

Among the thiazole scaffolds, 4-hydroxythiazoles discovered by Beckert *et al.* was the one which has been studied extensively (Stippich *et al.*, 2009), particularly for its fluorescence properties for different applications. Sekar *et al.* reported the fluorescence properties of styryl dyes with thiazole fragment (Thorat and Sekar, 2017). Recently, a series of novel 5-N-arylaminothiazoles were reported by Yamaguchi *et al.* showing emission tunability (Yamaguchi *et al.*, 2015) from 460 to 610 nm along with a positive solvatochromism. Later, D-A thiazoles based fluorophore with aryl enamine and aryl aza-enamine side groups were synthesized and reported by Lugovik (Lugovik *et al.* 2017). These recent literature emphasize the importance of thiazole core for the development of efficient fluorophore. Therefore, inspired by the potential of thiazole core for its excellent photophysical properties, we decided to explore the chemical space around the thiazole for mutiheterocyclic core development using a D-A strategy assisted by computational chemistry and will be described in the following sections.

2.2.1.3. Computer aided fluorophore design

As discussed earlier, most of the fluorophore discoveries were either serendipitous or the result of screening of a number of compounds. However, the potential of computer aided fluorophore design (CAFD) for the development of luminogens was not well explored till recently. Few studies met with partial success in predicting the optical properties of the novel molecules (Terai and Nagano, 2013) whereas computational chemistry calculations applied in the right direction can help in accelerating these design and development process. We believe that the

coupling of computational chemistry tools with the classical approaches in understanding the structure-property relationship will tremendously improve the efficiency of fluorophore designing process.

TD-DFT is the most widely used theory in explaining the structural and optical properties of the dyes (Laurent *et al.*, 2014). Several benchmark studies were already carried out (Adamo and Jacquemin, 2013; Bousquet *et al.*; Charaf-Eddin *et al.*, 2013; Jacquemin *et al.*, 2009; Jacquemin *et al.*, 2008; Laurent and Jacquemin, 2013). Le Guennic *et al.* designed a series of novel aza-boron-dipyrromethane (Aza-BODIPY) dyes using TD-DFT approach by evaluating the effect of different functionals and basis sets (Le Guennic *et al.*, 2012). It has to be admitted that design of novel series of molecules based on the known Aza-BODIPY framework is not much challenging as compared to the *de novo* design and development of a totally unexplored scaffold.

Inspired by the potential of DFT methods in the design of dye molecules which received sparse attention, we formulated our strategy to design the luminescent molecules with the aid of computational chemistry calculations. We used Gaussian 09 software for the calculations. All the calculations constituted mainly three processes which started with the optimization of the chosen molecule using the input geometry followed by the vibrational frequency calculation to identify the minimum in the potential energy surface. Finally, the absorption wavelength was predicted using single point calculation using TD-DFT methods using appropriate theory and basis sets.

Several rationales have been used for the design of novel fluorophore scaffold (Liu *et al.*, 2013). Our design strategy envisaged the coupling of diverse heterocycles to generate donor (D)-acceptor (A) cores accommodating tunable handles around the 1,3-thiazole core guided by computational calculations and knowledge database on fluorophore design. Our choice for heterocycles stemmed from their aromatic delocalization energies (eg: thiazole = 25 kcal/mol, thiophene

= 29 kcal/mol, furan =16 kcal/mol, pyrrole = 22 kcal/mol) which are generally less than that of benzene (36 kcal/mol), which would favour ICT (Breitung *et al.*, 2000) and hence would be significant. Heteroaromatics have the added advantage that they can act as auxiliary donor and acceptor systems (Albert *et al.*, 1997). It is well known that the introduction of push-pull molecules enable the ICT phenomena which will lead to red shift in the absorption and emission maxima. Further, increasing the conjugation length along the CT direction would improve the spectral wavelength along with enhanced molar absorptivity values. Whereas, the introduction of rotatable groups would enhance the geometric relaxation and thereby increase the Stokes shift which is a vital parameter for fluorophores.

As discussed before, we particularly focused on the molecular engineering around the 1,3-thiazole core for the *de novo* design which started with analysing the electron densities on different atoms to find the anchoring sites for heterocycles and functional groups for the development of multi-heterocyclic fluorophore. The three site tunability available in the thiazole core will give the freedom to attach diverse substituents to fine tune the properties. The electron rich *C5* and electron deficient *C2* positions impart polarizability to the thiazole core (figure 2.6) and hence it can behave both as an auxiliary donor and acceptor (Breitung *et al.*, 2000).

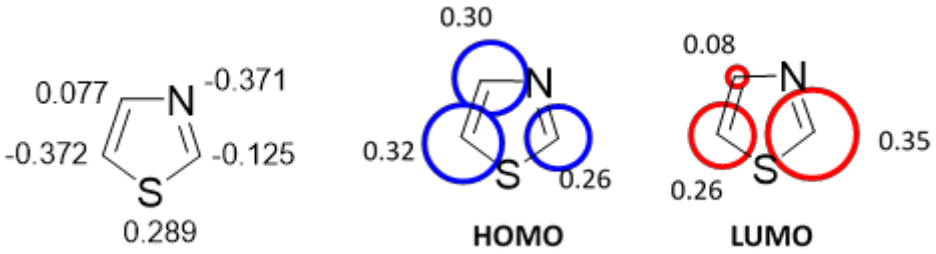

Figure 2.6. Mulliken atomic charges on thiazole ring atoms and atomic contribution to HOMO and LUMO electron densities

Hypothetically, any heterocycle can be attached to any of the three positions *C2, C4* or *C5* of the thiazole ring. We started the fluorophore design by selecting thiophene as the heterocycle and coupled it to 1,3-thiazole in order to

construct a thienylthiazole (TT) core. The construction of TT core was visualized in three orientations by inserting 2-thienyl unit on 2nd, 4th, and 5th positions of 1,3-thiazole core following which absorption maxima was predicted and found to be 299 nm, 277 nm and 295 nm respectively (figure 2.7). It is noteworthy that the attachment of thiophene at *C2* or *C5* resulted in almost similar absorption maxima. Since the coupling of heterocycle to the *C5* of thiazole is underdeveloped, we decided to focus on the design and development of 5-(heteroaryl)thiazole, with TT core as the first example, for further studies.

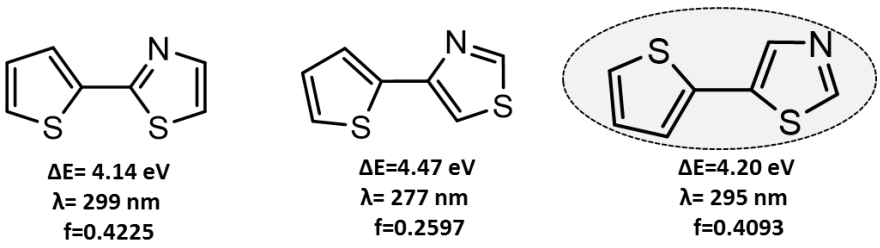

Figure 2.7. The calculated band gap and absorption wavelength of TT core

Attaching D-A fragments as end groups resulted in a push pull system and considerable change in band gap was observed as demonstrated in the figure 2.8a.

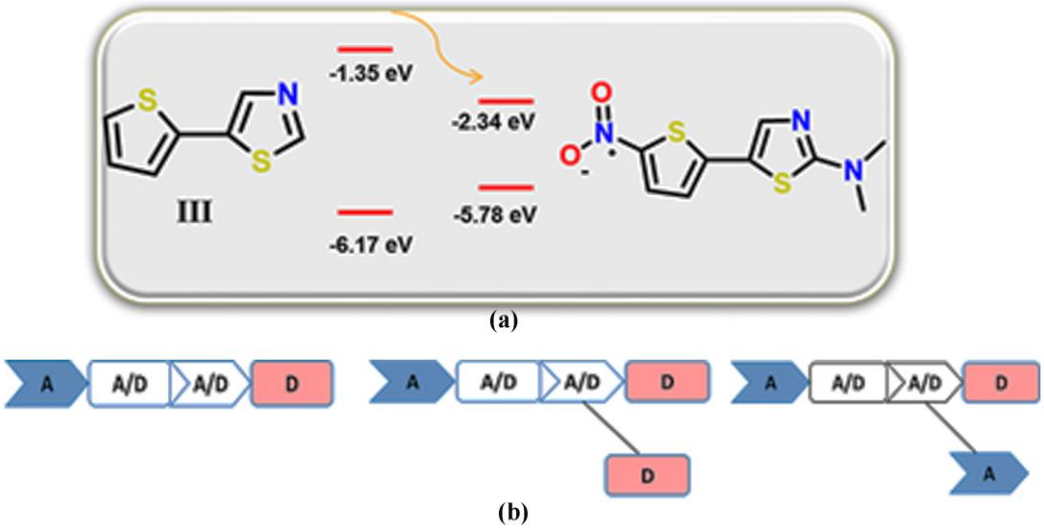

Figure 2.8: (a) Band gap tunability in TT core and (b) designer D-A systems

This opens a new avenue for the development of designer systems like D-A diad, triad, tetrad etc by using diverse heterocycles as indicated in figure 2.8b. HOMO and LUMO energy levels were modulated by the suitable substitution of D and A groups (Radhakrishnan and Sreejalekshmi, 2016a). For example, as shown in figure 2.9, when *C4* was modified with methyl and nitro groups, the resulting systems exhibited a noticeable change in the frontier molecular orbital (FMO) energy levels. Presence of nitro group at *C4* stabilized both HOMO and LUMO by 0.58 and 0.52 eV respectively whereas methyl group substitution destabilized the HOMO and LUMO by 0.11 and 0.14 eV respectively. The HOMO was delocalized all over the molecule whereas the LUMO was localized to the acceptor fragment which indicates the possible ICT phenomena in the designed molecules.

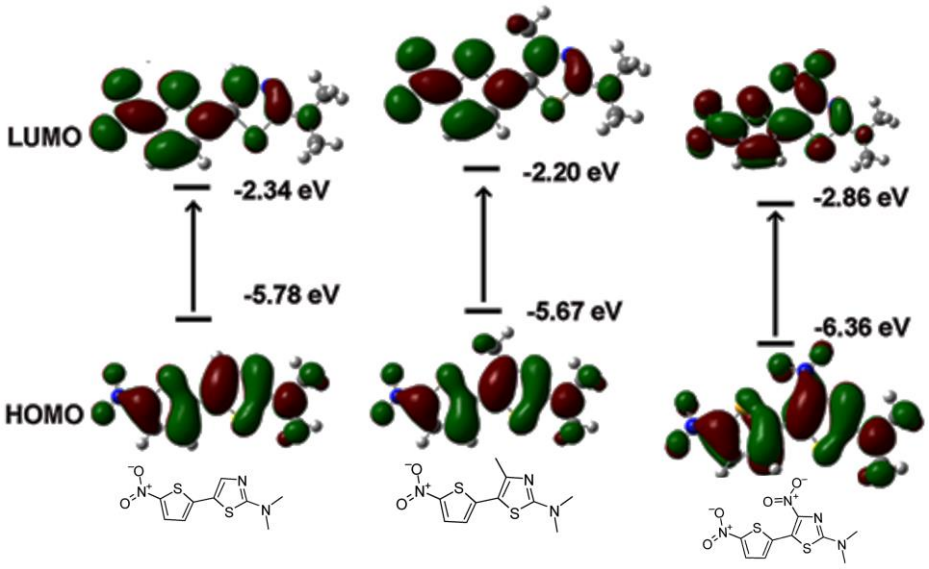

Figure 2.9. Modulation of HOMO and LUMO energies by varying substitution at *C4* of thiazole

Inspired by the preliminary analysis on the designed TT core, we further expanded the design strategy using different heterocycles. We chose diverse heterocycles around the 1,3-thiazole core, positioned at the electron rich *C5*, aiming at a novel family of band gap controllable systems. Accordingly, nine such heterocycles were chosen to generate biheteroyl systems and the resulting variations in the energy gaps were computed to draw first hand information on their

charge delocalization behaviour (figure 2.10) (Radhakrishnan and Sreejalekshmi, 2018).

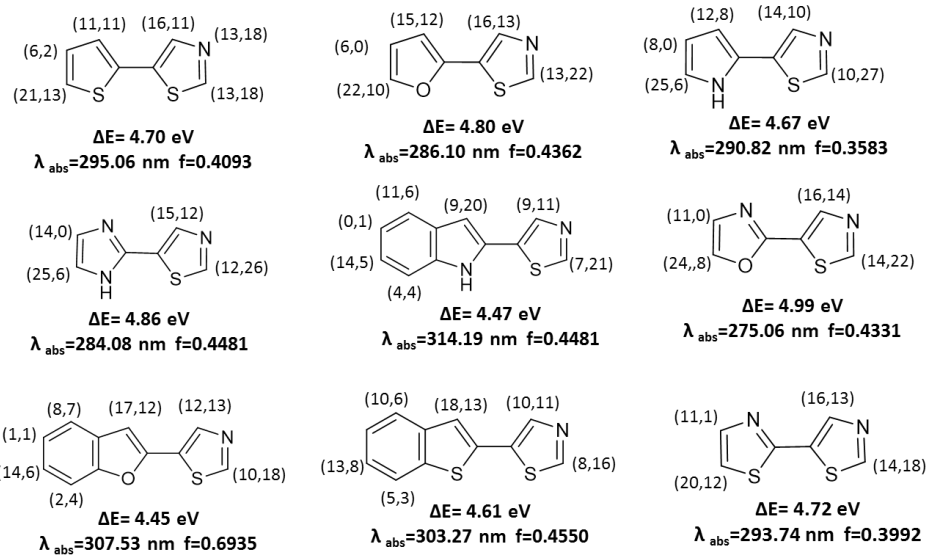

Figure 2.10. Band gap, absorption wavelength and force constant predicted in different biheteroaryl cores with percentage atomic contribution to HOMO and LUMO electron densities (in the parenthesis) using PBE0/6-31G(d,p)

From the figure, by looking at the electron densities on different atoms, it is clear that the charge delocalization behaviour can be well modulated by attaching different substituents on the heterocycle, and hence a diverse class of D-A molecules can be generated with probably interesting photophysical properties. Encouraged by these interesting observations, we appended NMe_2 at *C2* of thiazole and *C5* of the second heterocycle was decorated with NO_2, to obtain a predicted band gap variation from 3.44 - 3.75 eV and absorption tunability of 368 - 405 nm using gas phase calculation at PBE0/6-31g(d,p) (figure 2.11). It is also clear from the figure 2.12 that the percentage contribution of electron density to HOMO and LUMO was different for various heterocycles and hence a change in heterocycle itself is sufficient to perturb the electronic properties of the system (Radhakrishnan and Sreejalekshmi, 2018). Among the compounds I-IX, when contribution of *het* fragment towards the percentage electron density differences between LUMO and HOMO are considered, it follows the order 16, 6, 1, 5, 1, 11, 7, 18 and 22

respectively. Overall an 18% variation in HOMO and 28% variation in LUMO was observed for *het* fragment. So it may be possible to tune the core systems for designing molecules such as D-D-D-A, D-D-A-A, D-A-D-A and D-A-A-A by the judicious selection of fragments for desired properties.

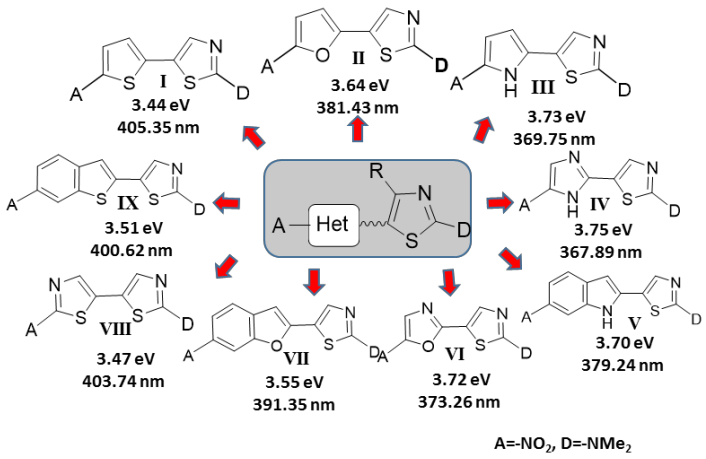

Figure 2.11. Band gap and absorption wavelength tunability in the designed multi-core systems

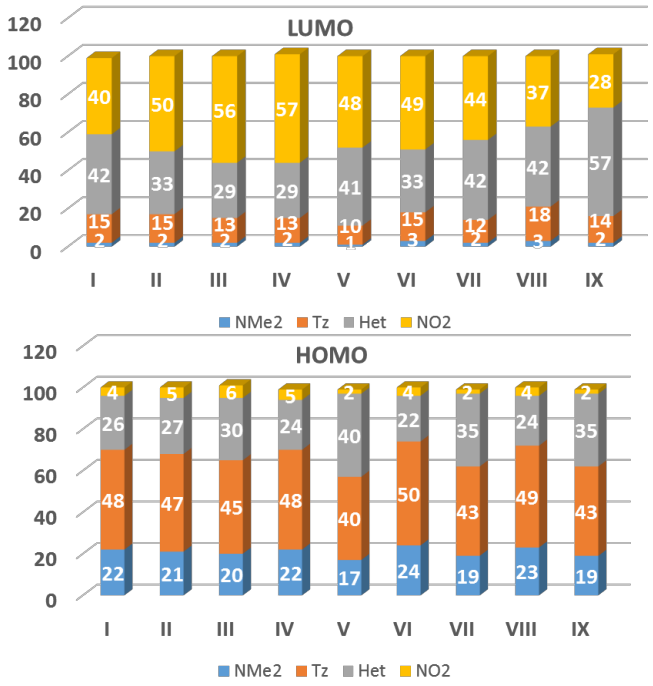

Figure 2.12. Percentage contribution of each fragment to the HOMO and LUMO

Analysing the electron densities of HOMO and LUMO (figure 2.6), there was a significant difference in lobe sizes of HOMO and LUMO noticed at *C4*. The lobe size of LUMO was found to be considerably smaller than that of HOMO, which suggested *C4* as a tunable site. To be more precise, the size differences suggested that introduction of electron donating group at *C4* of thiazole will destabilize HOMO. Hence the energy gap between HOMO and LUMO will decrease by placing electron rich substituents at *C4*. To evaluate the potential of *C4* for fine tuning the properties associated with the core, we started by substituting *C4* with a phenyl group and predicted the absorption spectra of all the 9 biheteroyl cores and is given in figure 2.13. It is obvious that the *C4* substituents also contribute significantly to electronic perturbations in the core and a red shift in absorption wavelength was observed among all the investigated cores.

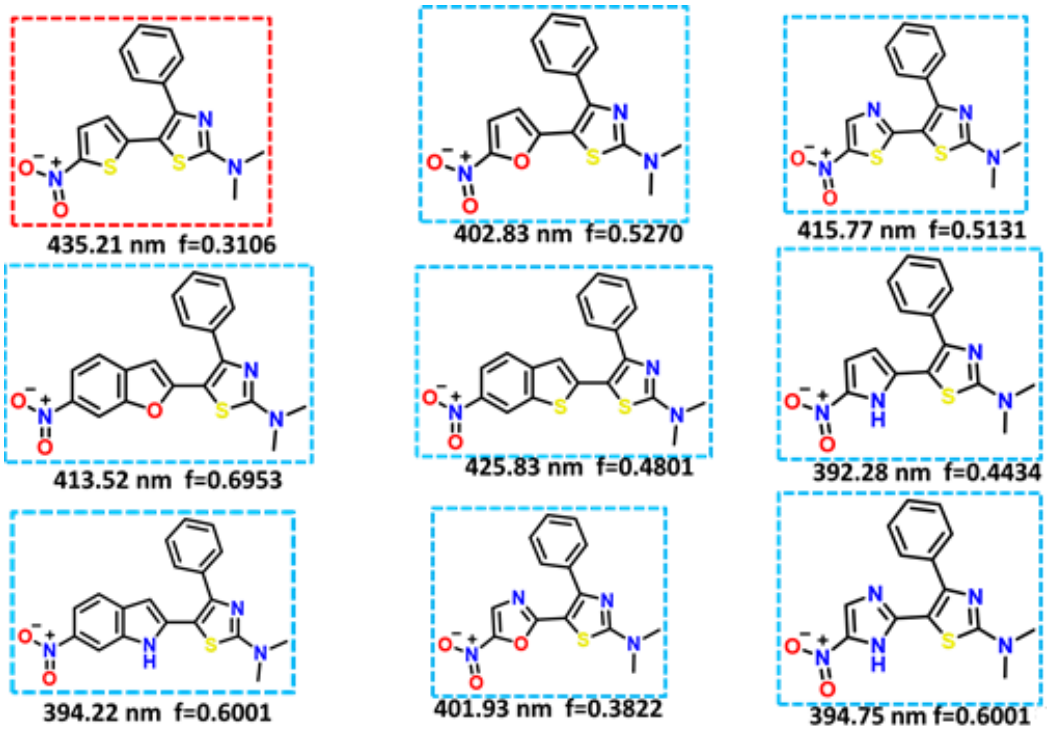

Figure 2.13. Calculated absorption wavelength among different biheteroyl core with *C4* substitution

Hence a core was designed with push pull fragments at both end and D/A group at *C4* of the thiazole (figure 2.14).

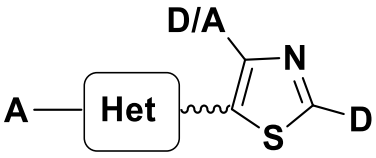

Figure 2.14. The designed multi-heterocyclic core

Next, we conducted a preliminary structure property relationship study by varying the substituents at *C2*, *C4*, and *C5* in the TT core. By simply varying the acceptor strength at *C5* of thiophene using the well-known electron accepting groups like cyano, aldehyde, or nitro and increasing the conjugation along the CT direction resulted in a substantial shift in absorption wavelength from 295 – 525 nm and band gap difference of 2.03 eV, attesting to the success of our strategy of utilizing *C2* → *C5* as the direction of ICT in the tunable core design (figure 2.15) (Radhakrishnan and Sreejalekshmi, 2018). Further, it was exciting that the force constant value which would reflect on molar extinction coefficient also varied significantly. This is in line with the general concept that attaching a substituent along the same direction as that of CT intensifies the oscillator strength to a greater extent and leads to a larger increase in the effective absorption area (Pavlopoulos, 1973).

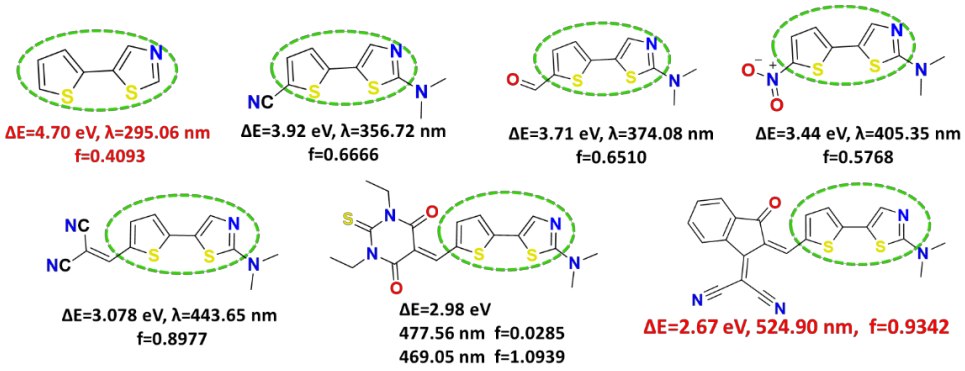

Figure 2.15. Calculated absorption wavelength with *C5* variation

Next, we studied the effect of different functional groups at *C4* of thiazole by modifying *C4* with commercially available building blocks while keeping *C2* and *C5* substituents intact (table 2.2). Effect of *C4* was not that much pronounced as compared to that of *C5*, but a 95 nm difference in absorption wavelength was

observed. As discussed earlier, substitution of electron donating groups gave the more red shifted absorption among the studied compounds. Also, increasing the conjugation along *C4* had a noticeable effect on the absorption wavelength and band gap.

Table 2.2. Effect of substituents at *C4* on the electronic properties

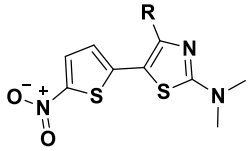

R	HOMO (eV)	LUMO (eV)	Band gap (eV)	Excitation energy (nm)
				Gas
CH_3	-5.67	-2.21	3.46	401.64 nm
-NO_2	-6.36	-2.86	3.50	412.21 nm
-t-Bu	-5.83	-2.35	3.48	445.27 nm
-NMe_2	-5.42	-2.03	3.39	421.16 nm
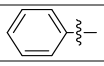	-5.70	-2.30	3.40	435.21 nm
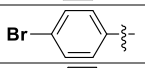	-5.83	-2.41	3.42	439.35 nm
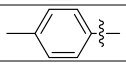	-5.64	-2.27	3.37	441.93 nm
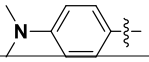	-5.16	-2.11	3.05	496.85 nm
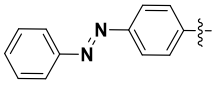	-5.74	-2.45	3.29	490.46 nm
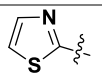	-5.88	-2.42	3.46	417.97 nm

Finally, we studied the effect of different amine donors at *C2* on the electronic properties of the molecule by keeping *C4* and *C5* intact (table 2.3). However, the variation in absorption wavelength and band gap tunability at *C2* were not much significant as compared to that achieved by *C4* and *C5* modulations. Then also a 71 nm variation in absorption and 0.51 eV difference in band gap could be achieved by a simple change of donor group from 1,8-naphthalimide to diphenylamine.

Table 2.3. Effect of substituent at *C2* on the electronic properties

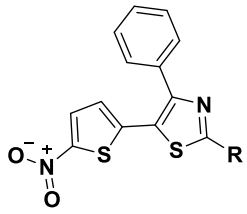

R	HOMO (eV)	LUMO (eV)	Band gap (eV)	Excitation energy (nm)
				Gas
	-5.70	-2.30	3.40	435.21 f*=0.3106
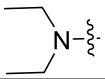	-5.64	-2.28	3.36	439.95 f=0.3214
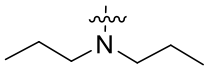	-5.64	-2.27	3.37	438.45 f=0.3351
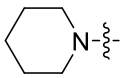	-5.66	-2.28	3.38	440.90 f=0.3183
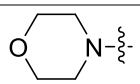	-5.79	-2.36	3.43	433.87 f=0.3064
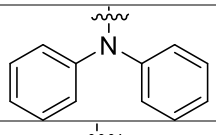	-5.63	-2.36	3.37	458.45 f=0.3037
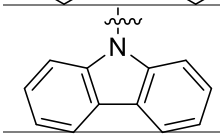	-5.95	-2.56	3.39	435.47 f=0.3647
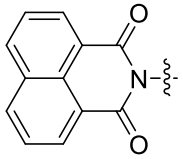	-6.39	-2.64	3.75	387.27 f=0.1905
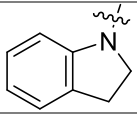	-5.61	-2.37	3.24	455.99 f=0.3832
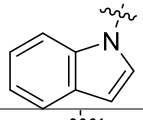	6.01	-2.60	3.41	433.95 f=0.3346
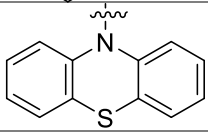	-5.74	-2.40	3.34	447.25 f=0.2888

**=force constant*

With the help of computational chemistry calculations, we have developed a novel 5-(hetero-2-yl)-1,3-thiazole core having three site tunability at *C2*, *C4* and *C5* of thiazole (figure 2.16). Further by attaching various heterocycles at *C2* and *C4*, a multi-heterocyclic core can be developed. DFT calculation revealed the potential space for further expanding the molecular library. Using the inherent three site tunability around thiazole core and judicious selection of substituents, there is considerable room for molecular engineering for designer systems.

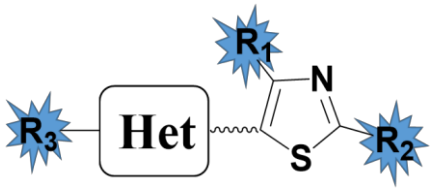

Figure 2.16: The designed multi-heterocyclic core

2.3. Experimental Details

2.3.1. Computational details

DFT calculations were performed using Gaussian 09, Rev. B.01 version (Frisch *et al.*, 2009). The geometry optimization and vibrational frequency calculations of the selected molecules in the ground state were performed using hybrid functional PBE0 and Pople's 6-31G(d,p) basis set. Vibrational frequency calculations confirmed that the molecules were minimum in the potential energy surface (no imaginary frequency was present). For predicting the absorption spectrum, single point energy calculations were carried out with TD–DFT calculations using the same level of theory and absorption spectra were computed for the first ten excited states. Solvent effects were taken into consideration using integral equation formalism of polarizable continuum model (IEFPCM). Partial density of states (PDOS) calculations were performed using GaussSum 3.0 software (O'boyle *et al.*, 2008). The molecular orbitals were visualized using GaussView 5.0 (Gaussian Inc.).

2.4. Conclusion

Aiming towards the development of a novel scaffold for theranostics, we designed a multi-heterocyclic core with the aid of computational tools. Because of the pharmacophoric potential of thiazole scaffold, we kept it as the central core and the multitude of therapeutic properties of diverse heterocycles prompted us to couple them to the thiazole fragment. In order to impart fluorescence property to the designed biheteroyl core, we adopted the D-A strategy by exploiting the ICT phenomena. The change in heterocycle at the *C5* of thiazole itself produced a remarkable effect on the electronic property of the systems. *C2* and *C5* positions of thiazole were utilized to channelize CT in the molecules. *C4* was identified as a tunable handle, which demonstrated the potential to fine tune the properties for multi-functional applications. It can behave as an orthogonal handle, can be used to customize a second ICT channel, can influence the orientations of the molecule such as planarity and cis-trans conformations and so on. The preliminary structure property study using DFT and TD-DFT suggested that the *C5* position was the crucial one in the development of colour tunable fluorophore. By utilizing the inherent three site tunability of thiazole, a combinatorial library of diverse multi-heterocyclic molecules can be generated. The success of computational assisted library design can be claimed in totality only with the design and development of suitable synthetic methods to access the virtual molecules and further experimental studies to substantiate the predictions. This will be the next hurdle to overcome and is addressed in the forthcoming chapter.

Computational studies- Summary

Theory- *DFT/ PBE0/6-31g(d,p)*		
No	**Job**	**No of molecules**
1	Optimizations	58
2	Frequency calculations	58
3	TD-DFT single point calculations	56

CHAPTER 3

DESIGN OF SYNTHETIC ROUTE AND SYNTHESIS OF 1,3-THIAZOLE BASED MULTI-HETEROCYCLIC CORE

3.1. Background

The high and increasing demand for functional molecules always possess challenges to synthetic organic chemists to constantly improve and innovate new synthetic methodologies (De Moliner *et al.*, 2017). The DOS, with its immense potential to generate molecular diversity from simple and readily available starting compounds, has the considerable scope of expanding unexplored regions of chemical space of small molecules for diverse applications (Burke and Schreiber, 2004). The diversity can be achieved through appendage or building block diversity, functional group diversity, stereo chemical diversity and skeletal (scaffold) diversity (Galloway *et al.*, 2010). Combinatorial chemistry emerged as a powerful tool in the synthesis of diverse chemical libraries by the judicious combination of different starting materials (Balkenhohl *et al.*, 1996). Compared to classical methods, modern synthetic strategies like multi-component reactions (MCRs), transition metal catalysed reactions, and cycloaddition reactions are also widely exploited (De Moliner *et al.*, 2017).

When it comes to the synthesis of designed molecules, simplicity, efficiency, versatility, cost-effectiveness and sustainable routes are highly preferred. As discussed in the previous chapter, the improvement in computational chemistry helps the rational design of virtual molecules with desired properties much easier. Along similar lines, synthetic chemistry should also be matured enough to handle these hurdles. In this context, the design of functional molecules

with simple architecture and desired properties would be highly appreciable and preferred over those with highly complex structures and limited synthetic feasibility. Hence our efforts, as discussed in this chapter, were focussed on the design of a simple, yet versatile synthetic route to the newly designed fluorophore core with minimum number of steps using readily available reagents.

3.2. Results and Discussions

3.2.1. Development of synthetic route to bi(hetero)aryl systems

As detailed in the previous chapter, with the aid of computational chemistry techniques, we have designed a *de novo* fluorophore core based on 5-(hetero-2-yl)-1,3-thiazole. Now, in order to prove and validate the success of design strategy, synthesis of the designed molecular systems and their property evaluations need to be carried out. The designed scaffold being built on a bi(hetero)aryl core, we analysed literature for existing routes to related systems. Bi(hetero)aryl cores are reported to be generally synthesized using a C-C formation by coupling two heterocycles of interest (Nishihara, 2012). Transition metal catalyzed cross couplings like C-X/C-M widely used for achieving the systems have some limitations like the requirement of prefunctionalization of the coupling partners, and preactivations of the substrates which are associated with tedious synthetic steps (Yang *et al.*, 2017). Later, transition metal catalyzed direct oxidative C-H/C-H cross coupling were developed (Wencel-Delord and Glorius, 2013). Although transition metal catalyzed reactions are one of the most powerful tools in chemist's arsenal, they have some serious drawbacks associated with them. Most of the transition metal catalysts are highly expensive. Further, they are toxic and hence their removal from biological samples is highly demanded, which again adds to their cost. Their sensitivity to moisture and oxygen impose strict manipulation of reactions conditions; sometimes special additives and co-catalysts are needed for improving the selectivity and efficiency of the reactions. Finally, the large usage (in

terms of frequency of usage) of transition metals are not in line with sustainable chemistry concepts (Sun and Shi, 2014). Because of these reasons, we decided to explore transition metal free reactions for the synthesis of the designed systems.

For the synthesis of 5-(hetero-2-yl)-1,3-thiazole, we first focussed on the synthesis of thienylthiazole (TT) core. Almost all the literature on thienylthiazole synthesis employed transition metal catalyzed coupling reactions (Chen *et al.*, 2014; Wakamiya *et al.*, 2006), organo lithium/magnesium reagents (Jenkins and Pickup, 1993; Tao *et al.*, 2013), and Lawesson's reagent (Kumar *et al.*, 2013; Ozturk *et al.*, 2007) (figure 3.1). Another method which caught our attention was the one employed for thiazole ring formation using (substituted) thioureas and α-halocarbonylthiophenes. Due to our long-standing interest in thiazole synthesis (Sreejalekshmi *et al.*, 2006; Titus and Sreejalekshmi, 2014), we decided to explore the latter route which if successful, would be far less expensive in terms of reagents, catalysts and even reaction conditions. Particularly, since the chemistry of thioureas is sufficiently developed, a wide choice of reactants would be available to play with. The reaction of N-acylthioureas with Z-CH_2Br, (where Z is a methylene activating group) was felt interesting because the final products are largely decided by the substitution pattern in the thioureas. The reaction of benzoylthioureas with α-bromo compounds sparked controversy in that they form thiazolidene-2-imines (Singh *et al.*, 2006) rather than imidazole-2-thiones (Zeng *et al.*, 2003). Furthermore, N-acylthioureas afford thiazoles only when N is disubstituted (Rajappa *et al.*, 1979) as demonstrated by Ried in the synthesis of morpholinothiazoles (Ried and Kaiser, 1976). Whereas α-halocarbonyl compounds are generally employed in [4+1] thiazole ring condensation (Rajasekharan *et al.*, 1986), other groups that can activate the methylene group for cyclization can also be useful as exemplified by the synthesis of 2-amino-5-heterylthiazoles (Rajappa *et al.*, 1982). The chemistry of 5-(2-thienylthiazole) seemed to be underdeveloped and hence we were excited to explore the untapped potential of classical chemistry approach due the following reasons- i) [4+1] reaction of 1-(acyl/aroyl)-3,3-(disubstituted)-thioureas with methylene activated thiophene is not known and ii) once such a synthesis is

accomplished without use of any transition metal reagents, we may end up with the envisaged core with minimal architecture which can be decorated with suitable substituents to make designer systems.

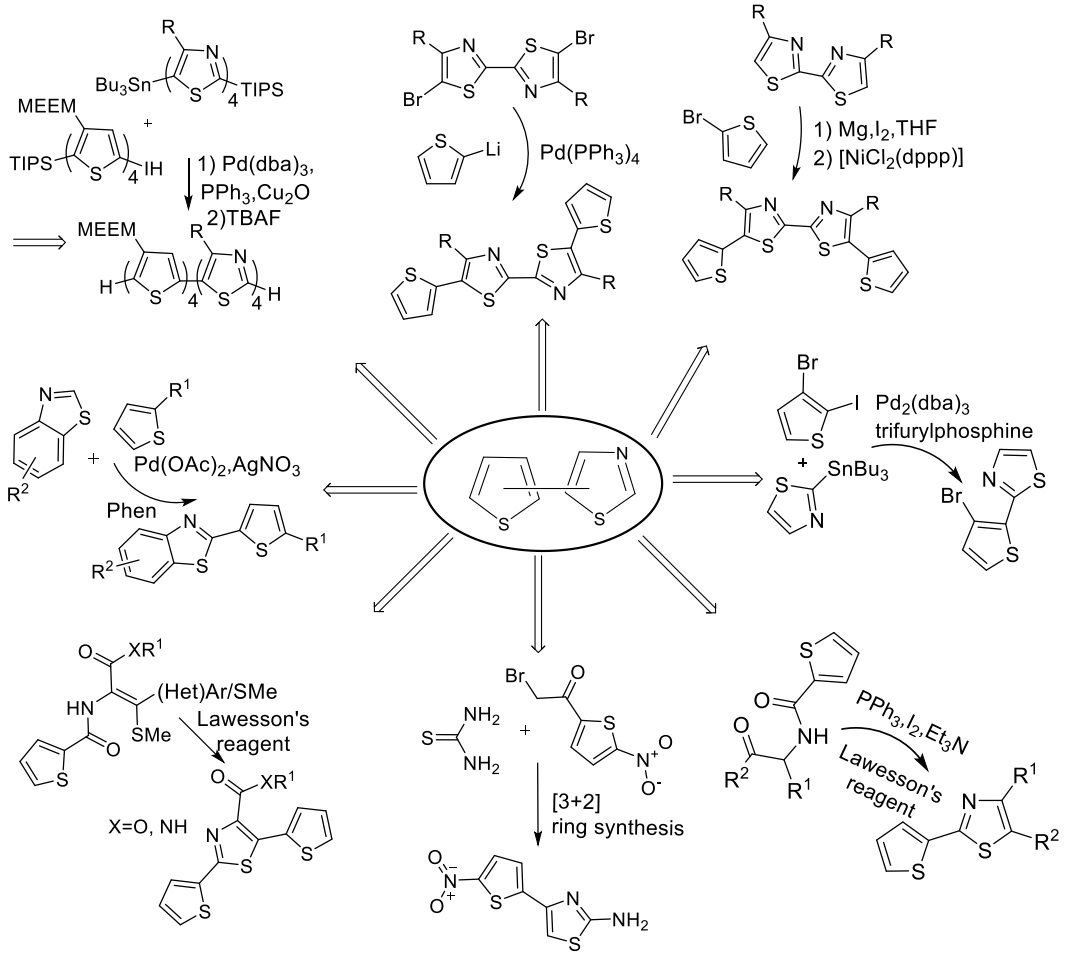

Figure 3.1. General synthetic routes reported for the synthesis of TT core

3.2.2. Retrosynthetic analysis of bi(hetero)aryl scaffold

From the retrosynthetic analysis, TT could result from the reaction of 1-(acyl/aroyl)-3,3-(disubstituted)thioureas with thiophene bearing an activated methylene group in a tandem nucleophilic reaction (scheme 3.1). The chemistry of acylthiourea seemed to be sufficiently developed (Aly *et al.*, 2007; Saeed *et al.*, 2014), and the precursors of our choice for the synthesis exploration viz; 1-aroyl-3,3-diaminothioureas have a two-fold diversity amplification (contributions from

carbonyl and secondary amine components). So the reaction would lead to thiazole unit with disubstituted amino group on *C2* of the ring and a **D/A** group at the *C4* of thiazole depending on the choice of the reagents. Along similar lines, an electron withdrawing group (EWG) on the thiophene ring may activate the methylene group for condensation with the carbonyl group in the aroylthiourea and subsequently furnish yet another **A**(EWG)-thiophene(**D**) unit. Thus, if the thiazole ring construction proceeds as per envisaged, then we would be successful in constructing a tetrad with **A-D-A-D** configuration having a vast scope of molecular engineering around the core.

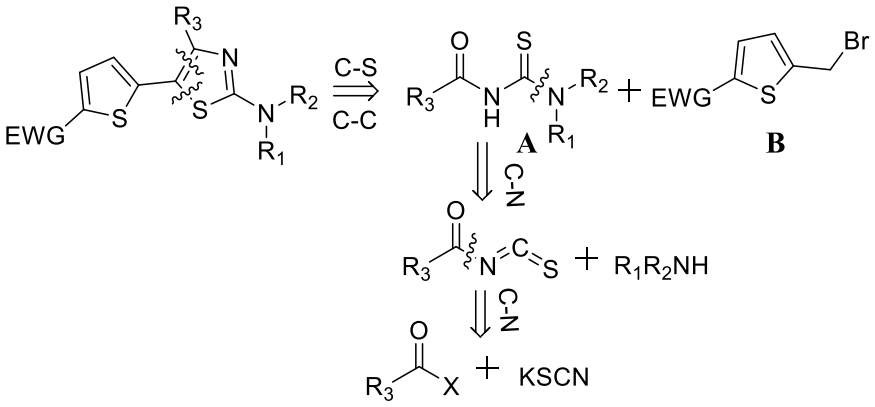

Scheme 3.1: Retrosynthesis of thienylthiazole

3.2.3. [4+1] ring synthesis route to thiazole-het core

To validate the retrosynthetic route, we first synthesized the precursor 1-(acyl/aroyl)-3,3-(disubstituted) thiourea **A** using aroyl/heteroyl chloride, KSCN and secondary amines in a one-pot sequential protocol with due modification in the literature procedure (Arslan *et al.*, 2003; Douglass and Dains, 1934). In order to activate the methylene group for nucleophilic reactions, we choose NO_2 as the EWG on the thiophene ring and the allylic bromination of 2-methyl-5-nitrothiophene (Rinkes, 1932) using NBS afforded 2-(bromomethyl)-5-nitrothiophene **B** (Dullaghan *et al.*, 1952). Now, with both the precursors in hand, we attempted the synthesis of TT by the reaction of **A** and **B** in DMF in the presence

of a base. The mixture was stirred for 30-45 minutes at room temperature or at temperatures below 45°C. This was followed by workup and purification by column chromatography, whereupon we isolated TT molecules in good yield. The products were characterized by spectroscopic and single crystal XRD studies and detailed descriptions are included in the synthesis part.

The mechanism of TT core formation can be explained by two consecutive nucleophilic attacks, wherein the S-alkylisothiourea formed from 1-(acyl/aroyl)-3,3-(disubstituted) thiourea and 2-(bromomethyl)-5-nitrothiophene, following HBr elimination, further undergoes base assisted intramolecular Knoevenagel condensation-cyclization to give the thiazole (scheme 3.2). Thus we prove that NO_2 on the *C5* position of thiophene ring is strong enough to activate methylene group in the S-alkylisothiourea for a Knoevenagel condensation under mild conditions (Radhakrishnan and Sreejalekshmi, 2016a). To best of our knowledge, this is the simplest method for the construction of TT core using readily available reagents and without the use of an expensive metal catalyst. It is to be emphasized that the reaction proceeds with good yield and good atom economy.

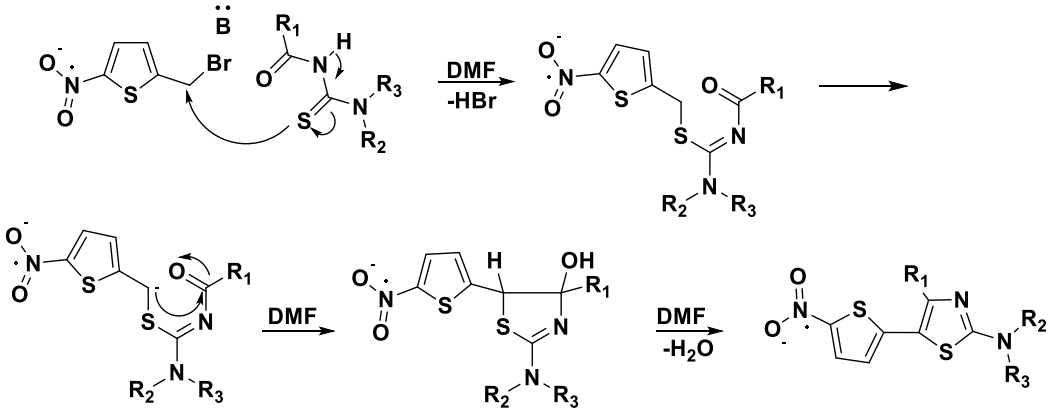

Scheme 3.2. Mechanism of thienylthiazole formation

It's noteworthy that the synthetically achieved TT core has tunable handles at *C2* and *C4* of thiazole ring which are contributions from the carbonyl chloride and secondary amine. Further, the halomethyl reagent utilized in ring construction

step contributed the thiophene unit in the TT core. This would suggest that a heterocycle bearing a halomethyl unit when suitably activated can contribute its heterocycle to the thiazole-heterocycle (thiazole-het) core. The facile synthetic strategy and versatility of the route was successfully established by the synthesis of 22 member library **1a-v**, in a diversity oriented manner utilizing commercially available reagents (Scheme 3.3) (Radhakrishnan and Sreejalekshmi, 2018).

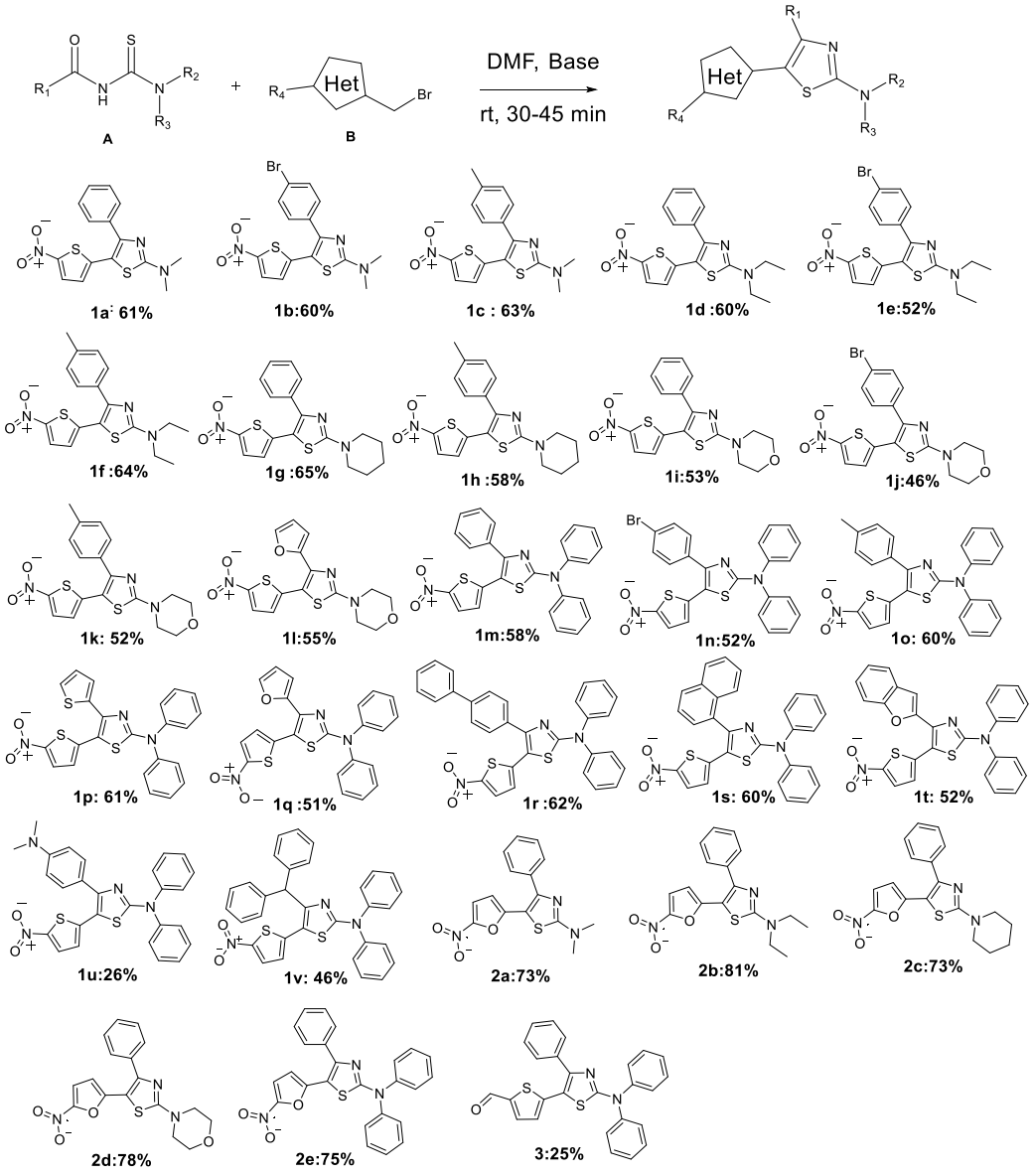

Scheme 3.3: General route for the synthesis thiazole-het core

Using the simple strategy, we could develop different multi-heterocyclic cores with varying number of heterocycles attesting to the wide scope of the synthetic route. For example, **1i**, **1j**, **1k**, **1p**, **1q** and **1t** bear three heterocyclic units whereas, in **1l** four heterocyclic core were incorporated which validated the success of the route for the development of multi-heterocyclic molecules.

The synthetic simplicity, versatility and availability of wide range of starting compounds encouraged us to expand the library to other biheteroyl core. By reacting suitable heterocycle bearing active methylene unit with thioureas would straightway result in novel biheteroyl core as exemplified in the synthesis of a novel class of furanylthiazole (FT) core. By reacting appropriate thioureas with commercially available 2-bromomethyl-5-nitrofuran, we synthesized five members of the FT family by keeping *C4* of thiazole constant and varying *C2* using different secondary amines.

Inspired by the computational studies on the tunable properties of the system, we continued molecular engineering around the core and replaced nitrothiophene unit with thiophene carbaldehyde. This resulted in another family of 5-(thiazol-5-yl)thiophene-2-carbaldehyde, **3** which was successfully synthesized from the corresponding thiourea and bromomethyl derivative. This modification is considered as highly significant since it opens new vistas in achieving diversity oriented fluorophore library by functional group transformation, coupling various acceptor fragments and extension of π-conjugation along the charge transfer direction. Hence using aldehyde **3**, in simple Knoevenagel condensations with malononitrile and 1,3-diethyl-2-thiobarbituric acid, we synthesized **4** and **5** respectively in good yield (Scheme 3.4).

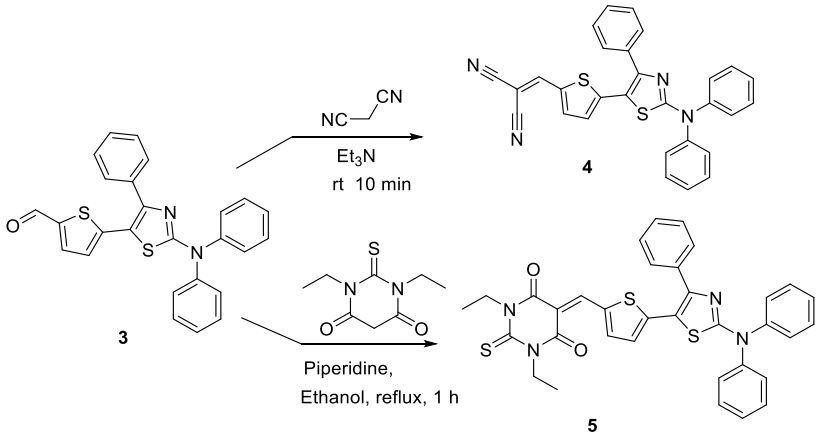

Scheme 3.4: Synthesis of π-extended thiazoles through heterocycle *C5* modification in thiazole-het core

3.2.4. Development of alternate green synthetic procedures

Recently there is a paradigm shift in the chemical industry towards the use of greener technologies for product manufacturing. This has imposed an increased pressure on the researchers to develop sustainable processes in line with green chemistry principles which prefer to utilize renewable raw materials, eliminate waste and side products, and avoid the use of toxic/hazardous reagents and solvents in the manufacturing of chemical products (Sheldon, 2005). The elimination of organic solvents in chemical reactions or use of alternative reaction media such as water or ionic liquids and employment of catalytic methodologies are widely used to tackle these problems. Mechanochemical synthesis uses simple grinding of reactants without/with minimal use of solvents and has gained considerable attention (G-W.Wang, 2013) towards the development of green chemical synthesis methods.

As shown earlier, our synthetic route for the minimal architecture molecules proceeds with minimum energy consumption in a reduced number of steps and under milder reaction conditions. We further attempted developing sustainable chemistry approaches for the synthesis of these thiazoles due to their potential applications in medicinal and materials field. It was exciting to note that

simple grinding of 1-(acyl/aroyl)-3,3-(disubstituted) thiourea with 5-nitro-2-bromomethyl thiophene in the presence of a base using a mortar and pestle for 10 minutes resulted in the formation of thiazole **1a** in around 60% yield and the product was characterized using mass spectrometry. We further verified the versatility of the method for the synthesis FT and 5-(thiazol-5-yl)thiophene-2-carbaldehyde cores. Inspired by these interesting results we further attempted a one-pot sequential protocol for the synthesis of **1a**. A one pot mechanochemical synthesis of **1a** was achieved by sequential grinding of carbonyl chloride and KSCN for 15 minutes followed by the addition of secondary amine and finally bromomethyl thiophene. This finding is highly encouraging since the versatility and the simplicity of the routes are highly amenable for the development of combinatorial libraries of multi-heterocyclic systems for diverse applications.

3.3. Experimental Details

3.3.1. General reagent information

Carbonyl chorides and secondary amines were purchased from either Sigma Aldrich or Merck chemicals. 2-methylthiophene, thiophene-2-cabaldehyde, 2-bromomethyl-5-nitrofuran and malonitrile were purchased from Sigma-chemicals. Potassium thiocyanate was purchased from Finar chemicals. The solvents, DMF and acetone were obtained from Merck chemicals and used after purification following standard procedures.

3.3.2. General analytical information

The purity of the synthesized compounds was assessed by thin layer chromatography (TLC) using silica gel 60 F254 (Merck) plates and fluorescence was visualized using UV lamp of wavelength 365nm. Column chromatography was performed using 60-120 mesh silica gel. Melting points were determined using

DSC (DSC Q20, TA Instruments). Single crystal data were obtained using Bruker Kappa APEXII single crystal X-ray diffractometer. NMR spectra were recorded in Bruker AV III 500MHz FTNMR spectrometer using $CDCl_3$ and DMSO-d_6 as solvents and TMS as an internal standard. Mass spectra were recorded under ESI/HRMS using Thermoscientific Exactive mass spectrometer.

3.4. Synthesis

3.4.1. General procedure for the synthesis of aroylthioureas

Aroylthioureas were prepared by the following general procedure. Aroyl chloride was added slowly to a solution of KSCN (10 mmol) in acetone, refluxed for 30 minutes and then cooled to room temperature. A solution of the secondary amine in acetone was then added slowly and stirred for 2 hours. The reaction mixture was added to crushed ice, precipitated product was filtered, dried and recrystallized from appropriate solvents.

3.4.2. General procedure for the synthesis of thiazoles

To a solution of 2-bromomethyl-5-nitrothiophene or 2-bromomethyl-5-nitrofuran (1mmol) in DMF (2mL), 1-(acyl/aroyl)-3,3-(disubstituted) thiourea (1mmol) was added followed by triethylamine (1.2 mmol) and stirred for 30-45 minutes at room temperature. The reaction mixture was then added slowly to crushed ice with vigorous stirring. The precipitated compound was filtered and dried. (Alternatively, extraction with DCM followed by evaporation of the solvent can be performed). The residue was subjected to silica gel column chromatography to yield the product. Single crystals suitable for XRD analysis were generated by the recrystallization from suitable solvent by slow evaporation method.

3.4.3. Compound characterization details

N, N-dimethyl-5-(5-nitrothiophen-2-yl)-4-phenylthiazol-2-amine (**1a**)

Purified by column chromatography with 1% ethyl acetate: petroleum ether. Yield: 202 mg (61%). Red solid, m.p. 160.1- 161.5 °C. ^{1}H NMR (500 MHz, $CDCl_3$, ppm): δ= 3.11 (s, 6H), 6.60 (d, *J*=4.5 Hz, 1H), 7.35-7.36 (m, 3H), 7.45-7.47 (m, 2H), 7.61(d, *J*=4.5 Hz, 1H); ^{13}C NMR (125 MHz, $CDCl_3$, ppm): δ= 39.1, 111.6, 122.4, 128.0, 128.1, 128.2, 128.3, 133.6, 143.1, 147.1, 152.1, 168.0. HRMS (ESI) calc. $C_{15}H_{14}N_3O_2S_2$ $[M+H]^+$: 332.0524, found: 332.0528.

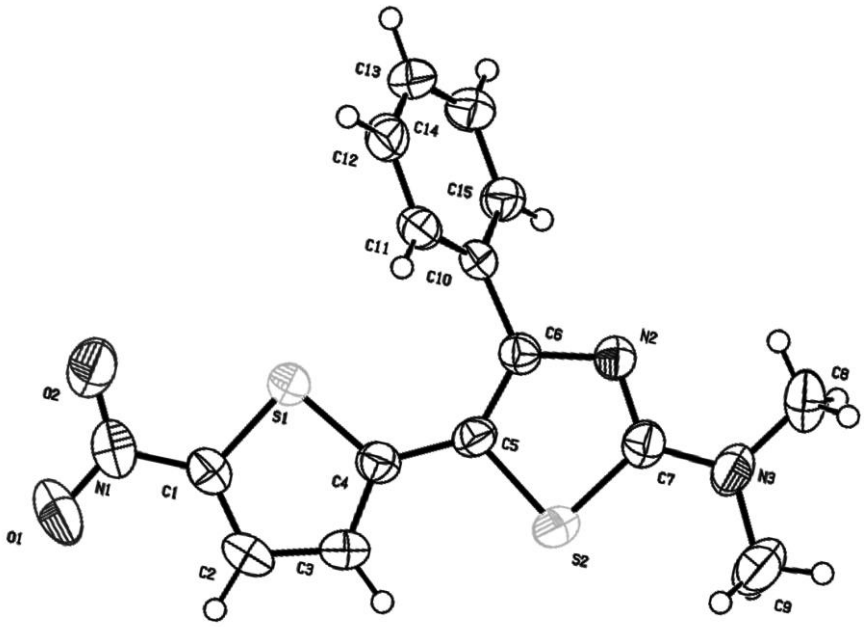

Figure 3.2: Ortep diagram of **1a** (recrystallized from methanol) with 50 % probability ellipsoid (CCDC number: 11424468)

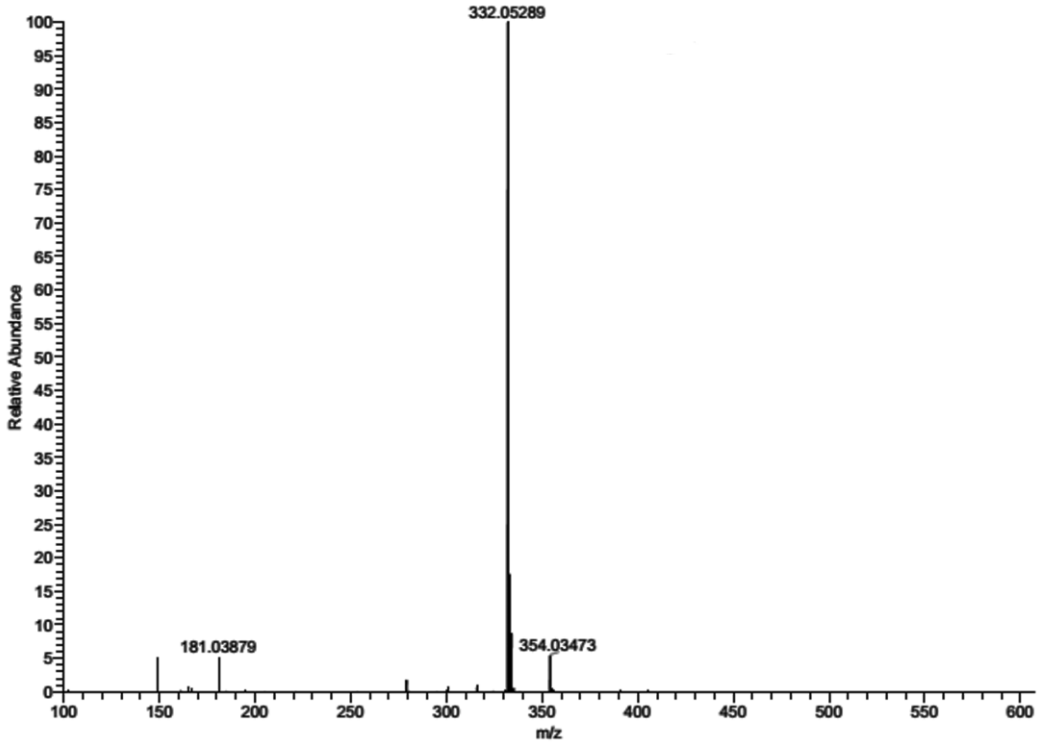

Figure 3.3: HR-MS spectrum of **1a**

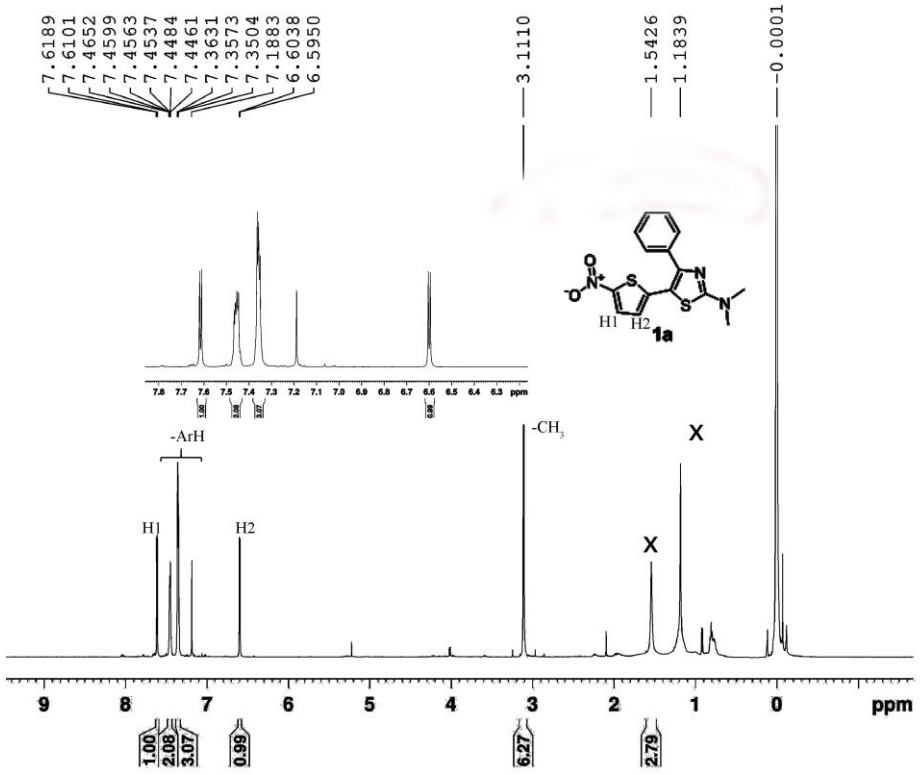

Figure 3.4: ^{1}H NMR spectrum of **1a**

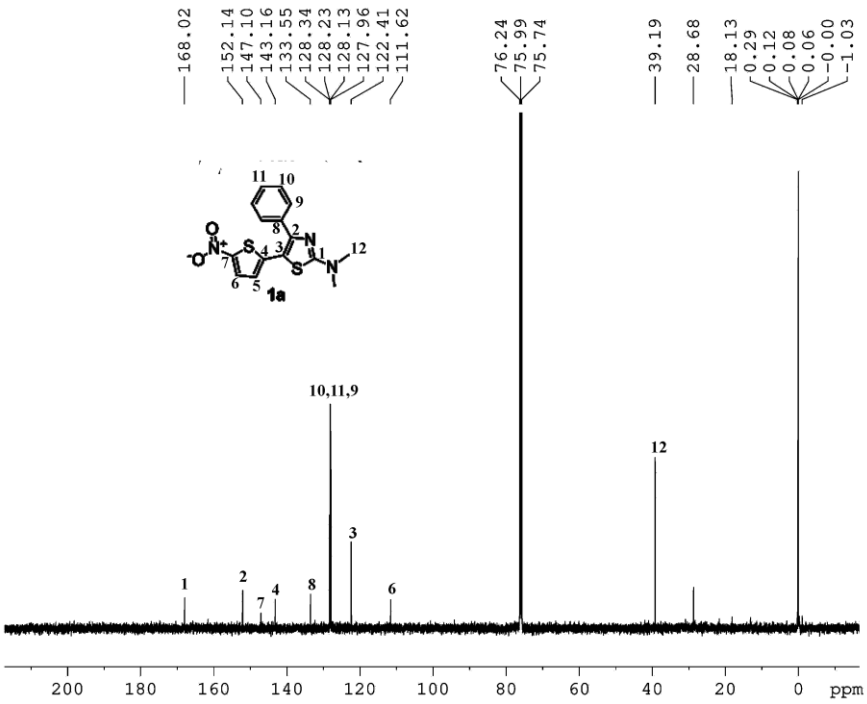

Figure 3.5: ^{13}C NMR spectrum of **1a**

4-(4-bromophenyl)-N,N-dimethyl-5-(5-nitrothiophen-2-yl)thiazol-2-amine (**1b**)

Purified by column chromatography with 1% ethyl acetate: petroleum ether. Yield: 245 mg (60%). Red solid, m.p. 162.7-163.8°C. ^{1}H NMR (500 MHz, $CDCl_3$, ppm): δ= 3.10 (s, 6H), 6.63 (d, J=4.5 Hz, 1H), 7.35-7.36 (m, 2H), 7.47-7.48 (m, 2H), 7.64 (d. *J*=4.5 Hz, 1H); ^{13}C NMR (125 MHz, $CDCl_3$, ppm): δ= 39.1, 111.5, 122.5, 122.9, 128.3, 129.8, 131.0, 132.4, 142.5, 147.5, 150.4, 168.0. HRMS (ESI) calc. $C_{15}H_{13}BrN_3O_2S_2$ $[M+H]^+$: 409.9629, found: 409.9641.

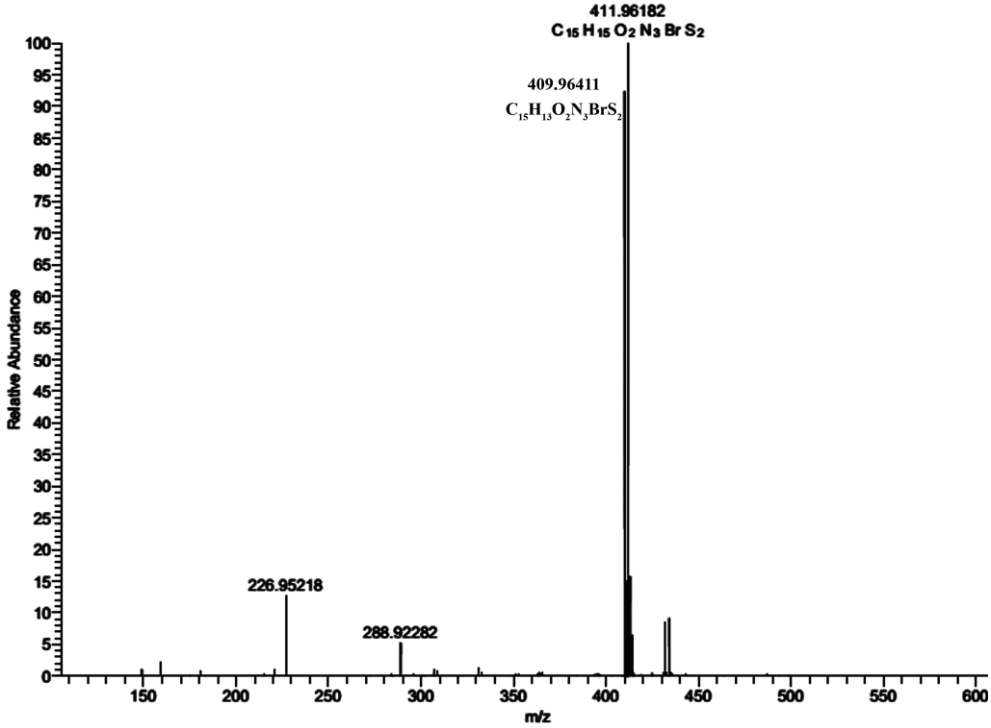

Figure 3.6: HR-MS spectrum of **1b**

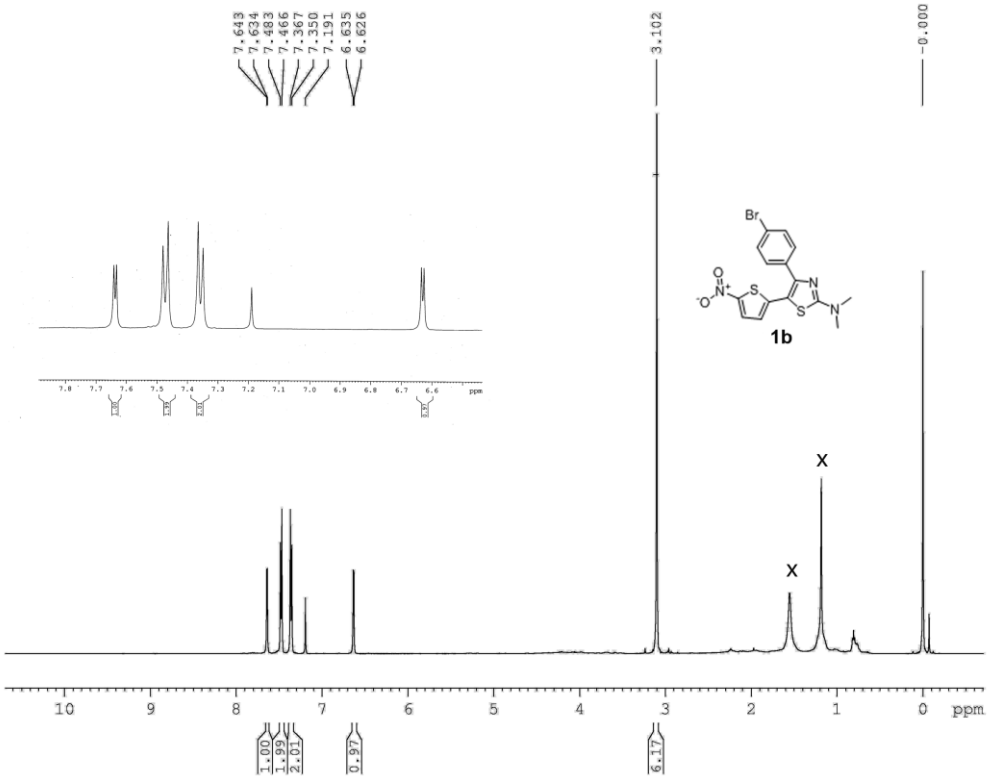

Figure 3.7: ^{1}H NMR spectrum of **1b**

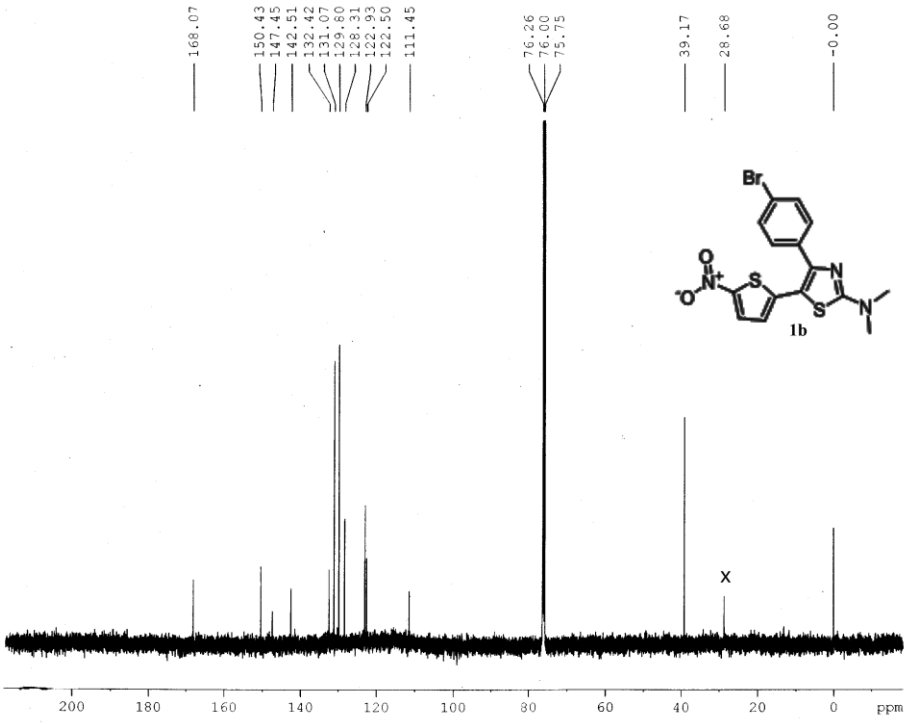

Figure 3.8: ^{13}C NMR spectrum of **1b**

N,N-dimethyl-5-(5-nitrothiophen-2-yl)-4-(p-tolyl)thiazol-2-amine (**1c**)

Purified by column chromatography with 1% ethyl acetate: petroleum ether. Yield: 217 mg (63%). Red solid, m.p. 147.7-148.8 °C. ^{1}H NMR (500 MHz, $CDCl_3$, ppm): δ=2.33 (s, 3H), 3.10 (s, 6H), 6.61 (d, *J*=4.4 Hz, 1H), 7.15-7.19 (m, 2H), 7.34-7.35 (m, 2H), 7.62 (d, *J*=4.5 Hz, 1H); ^{13}C NMR (125 MHz, $CDCl_3$, ppm): δ=21.6, 39.1, 122.2, 127.9, 128.3, 128.7, 130.5, 138.4, 139.0, 143.5, 146.9, 152.4, 167.9. HRMS (ESI) calc. $C_{16}H_{16}N_3O_2S_2$ $[M+H]^+$: 346.0680, found: 346.0683.

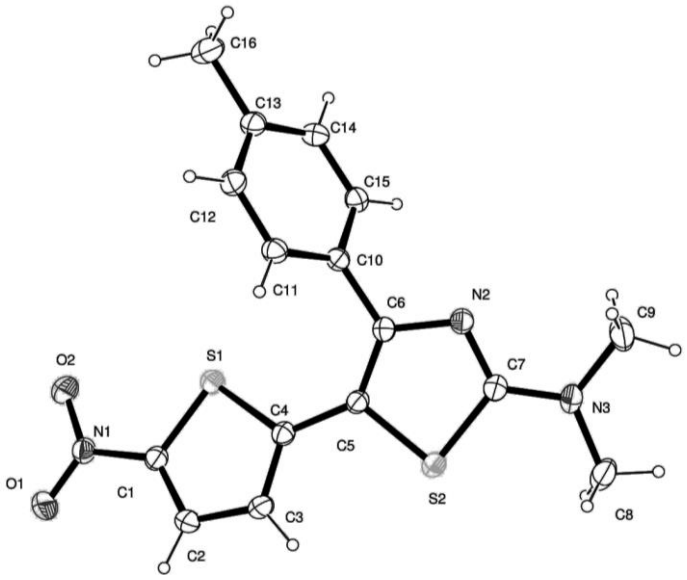

Figure 3.9: Ortep diagram of **1c** (recrystallized from ethanol) with 20 % probability ellipsoid

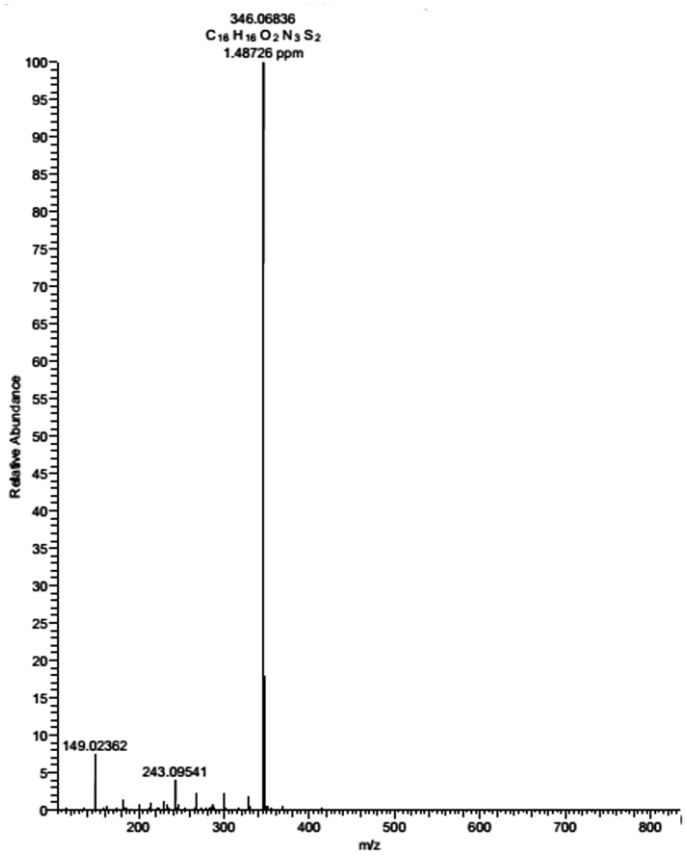

Figure 3.10: HR-MS spectrum of **1c**

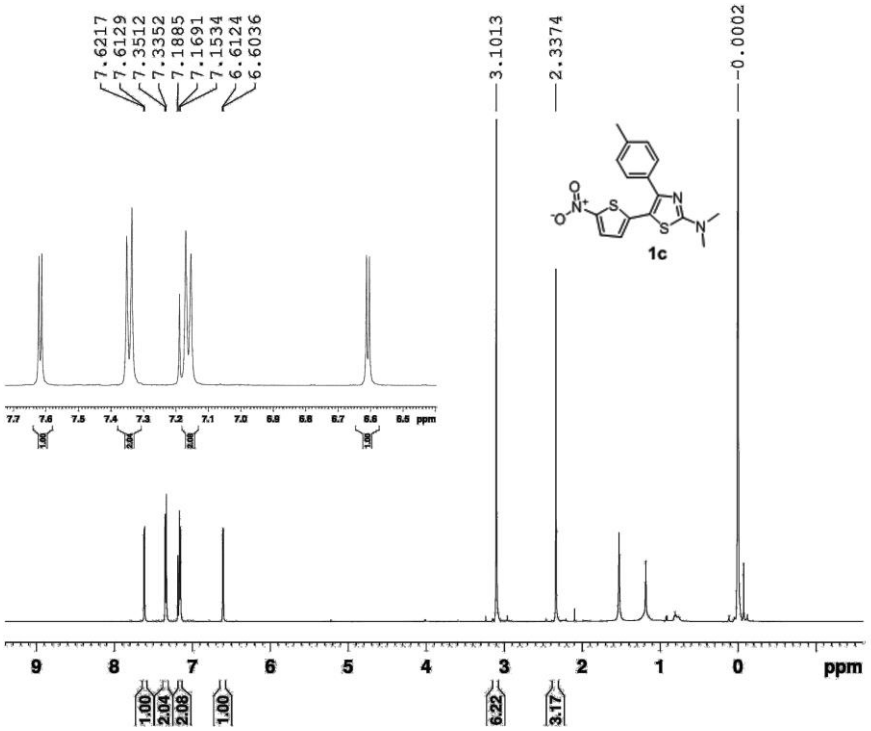

Figure 3.11: 1H NMR spectrum of **1c**

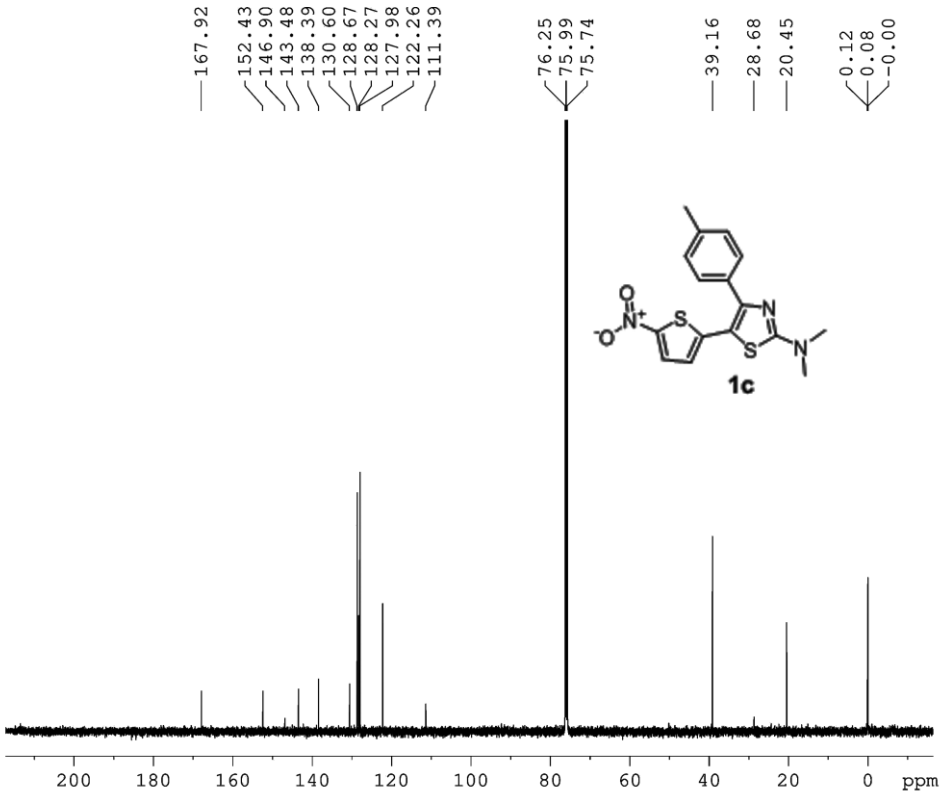

Figure 3.12: ^{13}C NMR spectrum of **1c**

N,N-diethyl-5-(5-nitrothiophen-2-yl)-4-phenylthiazol-2-amine (**1d**)

Purified by column chromatography with 1% ethyl acetate: petroleum ether. Yield: 215 mg (60%). Red waxy solid. ^{1}H NMR (500 MHz, $CDCl_3$, ppm): δ=1.20-1.23 (m, 6H), 3.45-3.50 (m, 4H), 6.58 (d, *J*=4.5 Hz, 1H), 7.34-7.36 (m, 3H), 7.45-7.47 (m, 2H), 7.61 (d, *J*=4.5 Hz, 1H). ^{13}C NMR (125 MHz, $CDCl_3$, ppm): δ=11.6, 44.6, 110.6, 122.2, 127.9, 128.1, 128.3, 128.3, 133.7, 143.5, 147.5, 152, 166.6. HRMS (ESI) calc. $C_{17}H_{18}O_2N_3S_2$ $[M+H]^+$:360.0836, found: 360.0842.

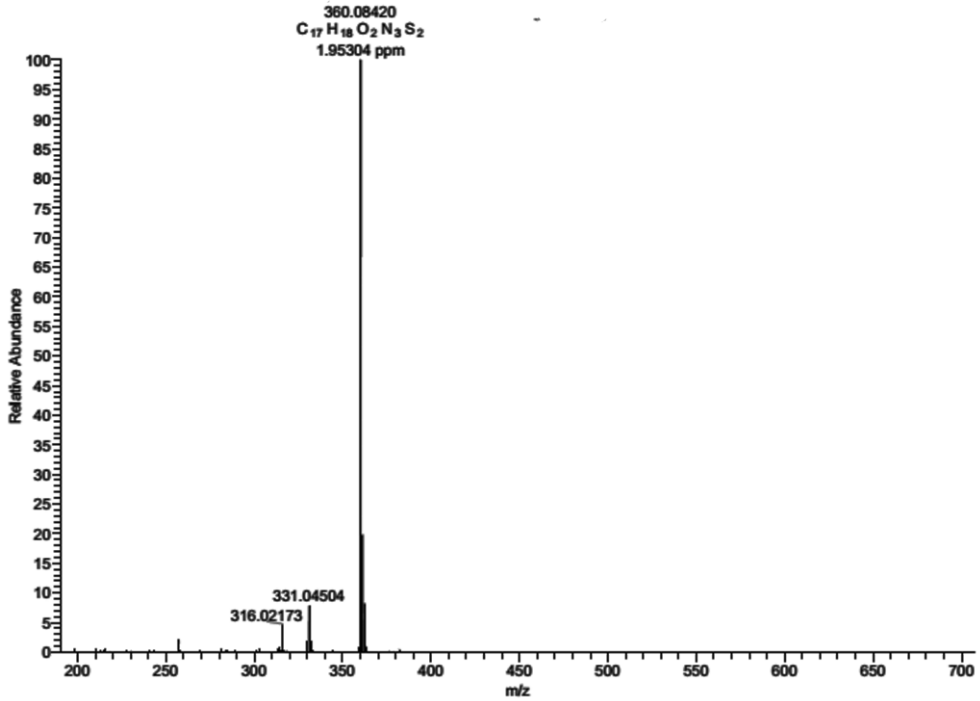

Figure 3.13: HR-MS spectrum of **1d**

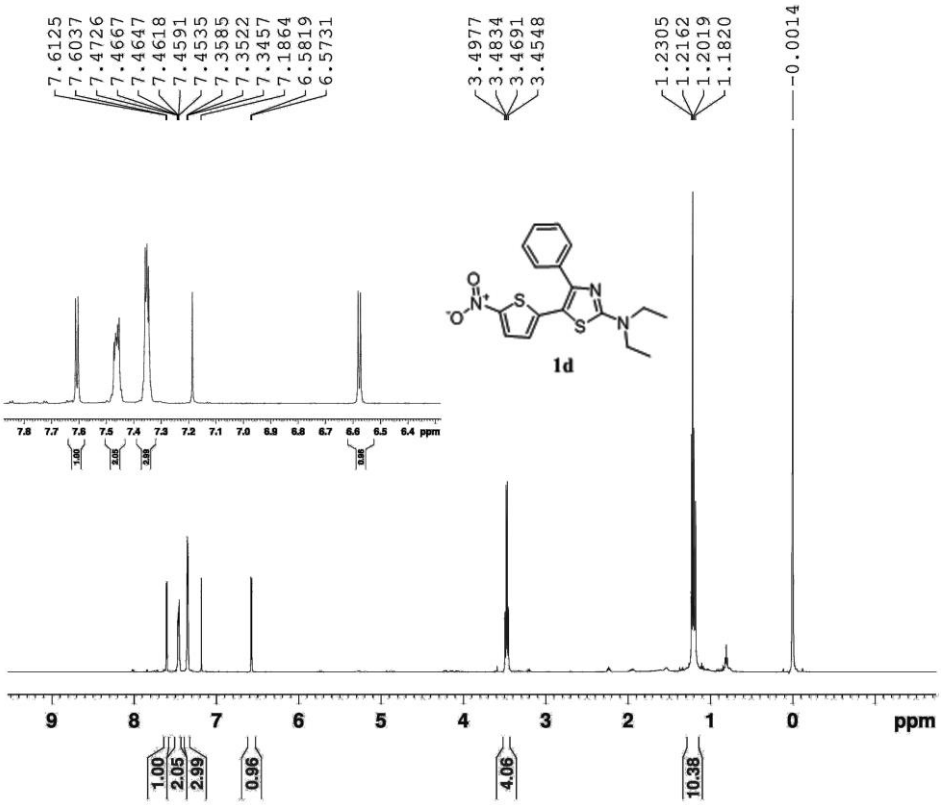

Figure 3.14: [1]H NMR spectrum of **1d**

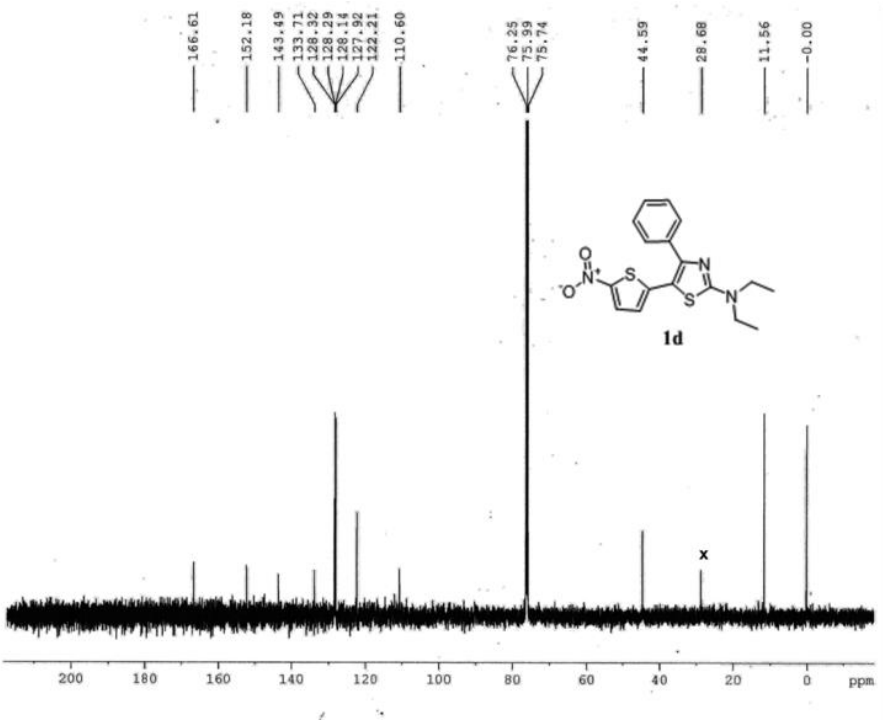

Figure 3.15: [13]C NMR spectrum of **1d**

4-(4-bromophenyl)-N,N-diethyl-5-(5-nitrothiophen-2-yl)thiazol-2-amine (**1e**)

Purified by column chromatography with 2% ethyl acetate: petroleum ether. Yield: 227mg (52%). Red solid, m.p. 94.5-95.0°C. ^{1}H NMR (500 MHz, $CDCl_3$, ppm): δ=1.21(t, *J*=7.0 Hz, 6H), 3.44-3.48 (m, 4H), 6.60 (d, *J*=4.5 Hz, 1H), 7.35-7.37 (m, 2H), 7.46-7.48 (m, 2H), 7.62 (d, *J*=4.5 Hz, 1H); ^{13}C NMR (125 MHz, $CDCl_3$, ppm): δ=11.5, 44.6, 110.4, 122.4, 122.8, 128.4, 129.8, 131.0, 132.6, 142.8, 147.2, 150.4, 166.6. HRMS (ESI) calc. $C_{17}H_{17}N_3O_2S_2Br$ $[M+H]^+$: 437.9940, found: 437.9953.

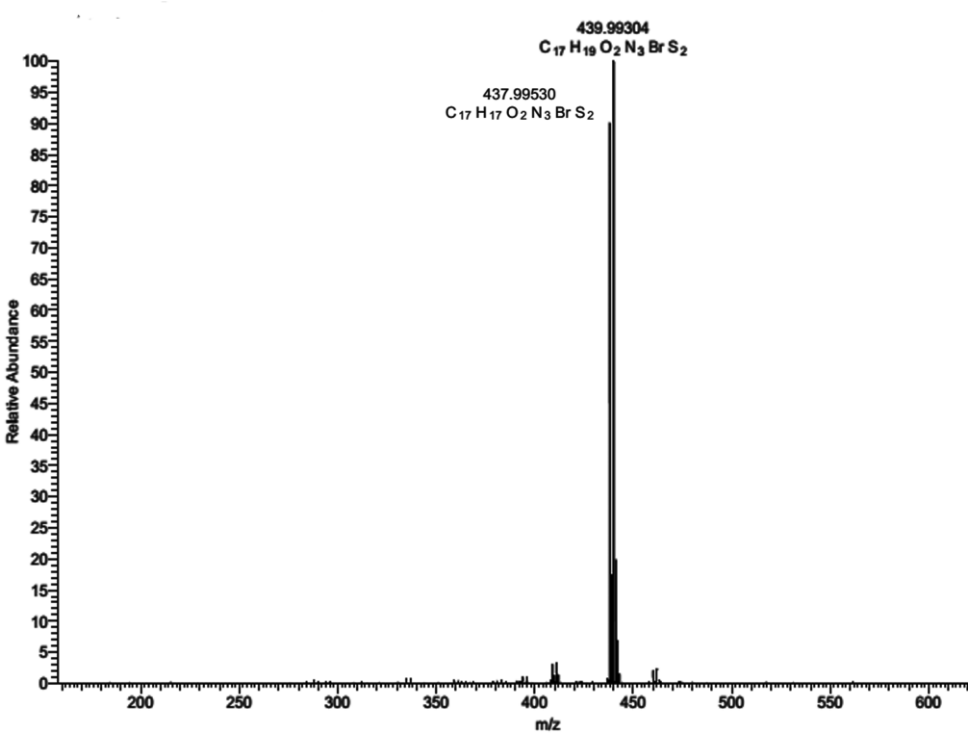

Figure 3.16: HR-MS spectrum of **1e**

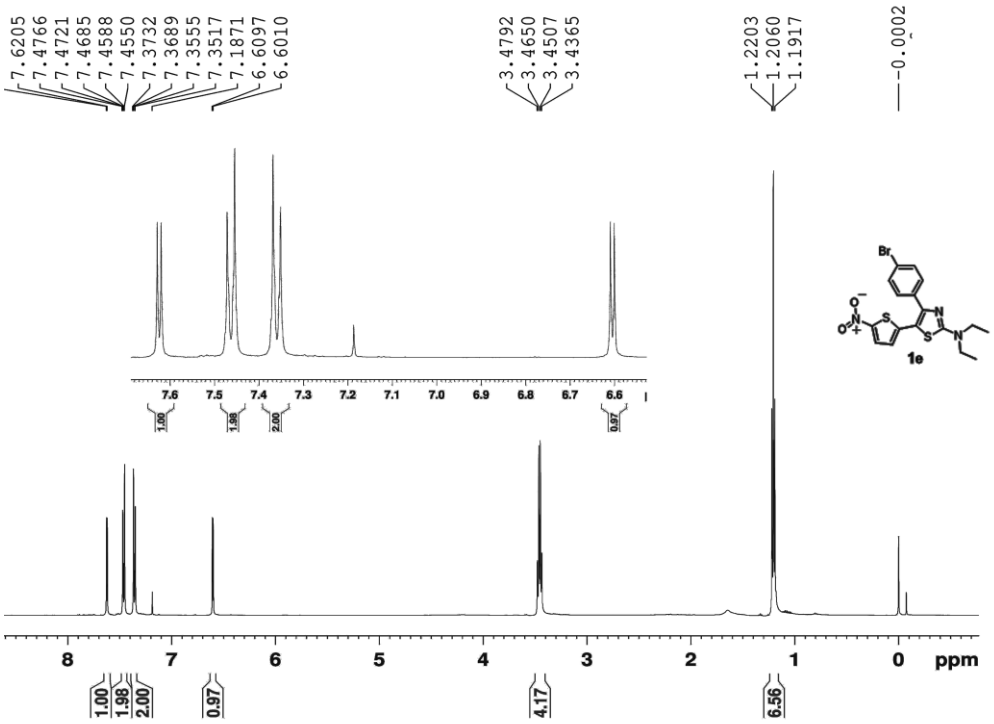

Figure 3.17: [1]H NMR spectrum of **1e**

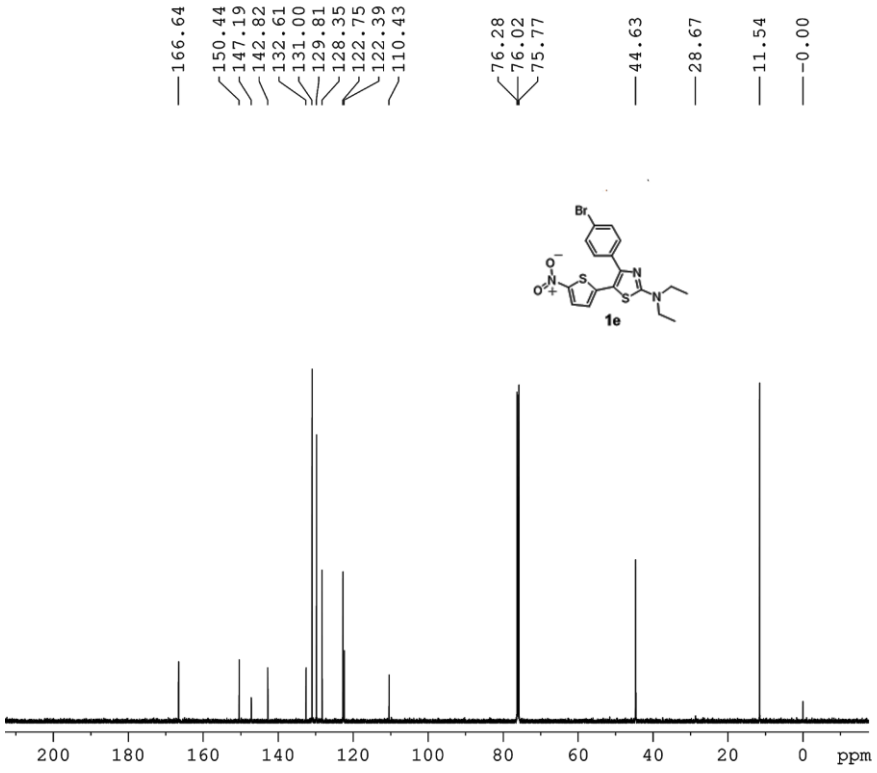

Figure 3.18: [13]C NMR spectrum of **1e**

N,N-diethyl-5-(5-nitrothiophen-2-yl)-4-(p-tolyl)thiazol-2-amine (**1f**)

Purified by column chromatography with 1% ethyl acetate: petroleum ether. Yield: 238 mg (64%). Waxy red solid. ^{1}H NMR (500 MHz, $CDCl_3$, ppm): δ=1.19-1.22 (m, 6H), 3.45-3.49 (m, 4H), 2.33 (s, 3H), 6.57 (d, *J*=4.5 Hz,1H), 7.15-7.19 (m, 2H), 7.34-7.36 (m, 2H), 7.61 (d, *J*=4.5 Hz, 1H); ^{13}C NMR (125 MHz, $CDCl_3$, ppm): δ=11.6, 20.5, 44.6, 99.0, 122.0, 127.8, 128.0, 128.3, 128.6, 138.3, 143.7, 146.5, 152.4, 166.8. HRMS (ESI) calc. $C_{18}H_{20}O_2N_3S_2$ $[M+H]^+$: 374.0992, found: 374.0999.

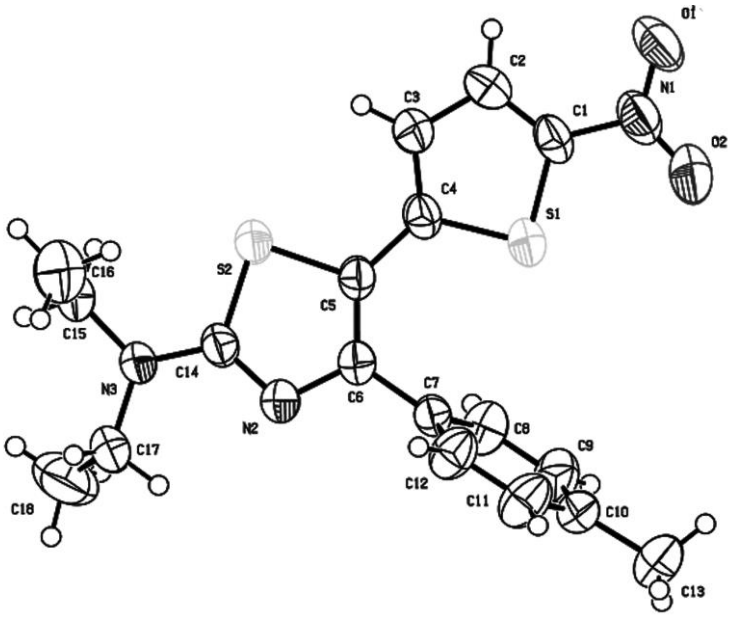

Figure 3.19: Ortep diagram of **1f** (recrystallized from ethanol) with 50 % probability ellipsoid

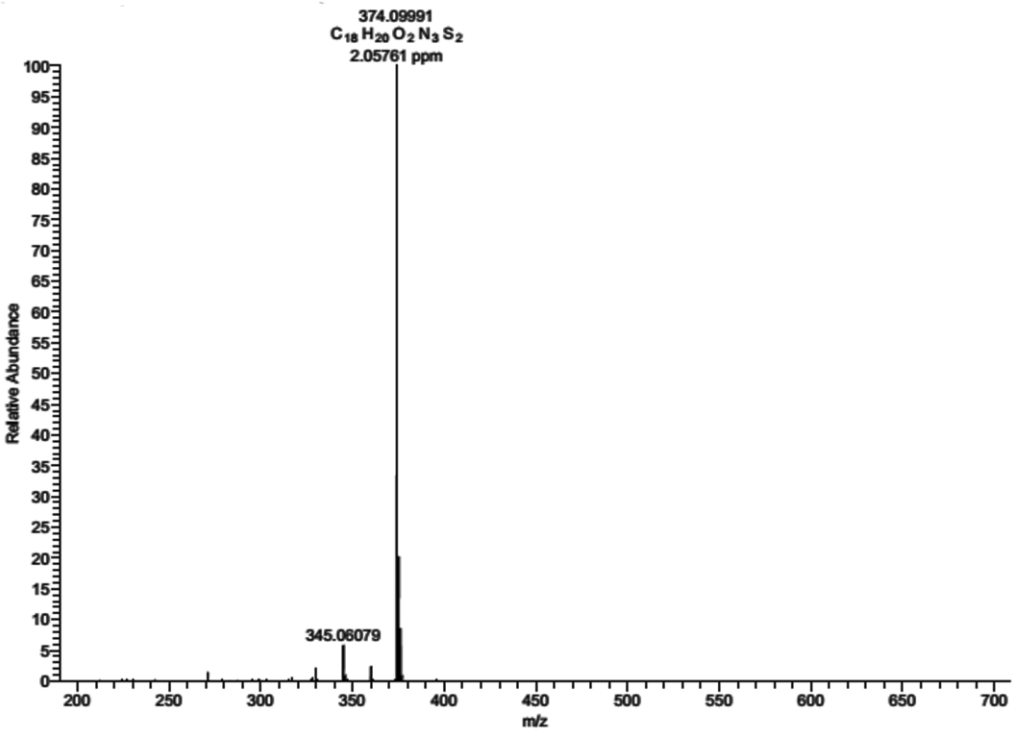

Figure 3.20: HR-MS spectrum of **1f**

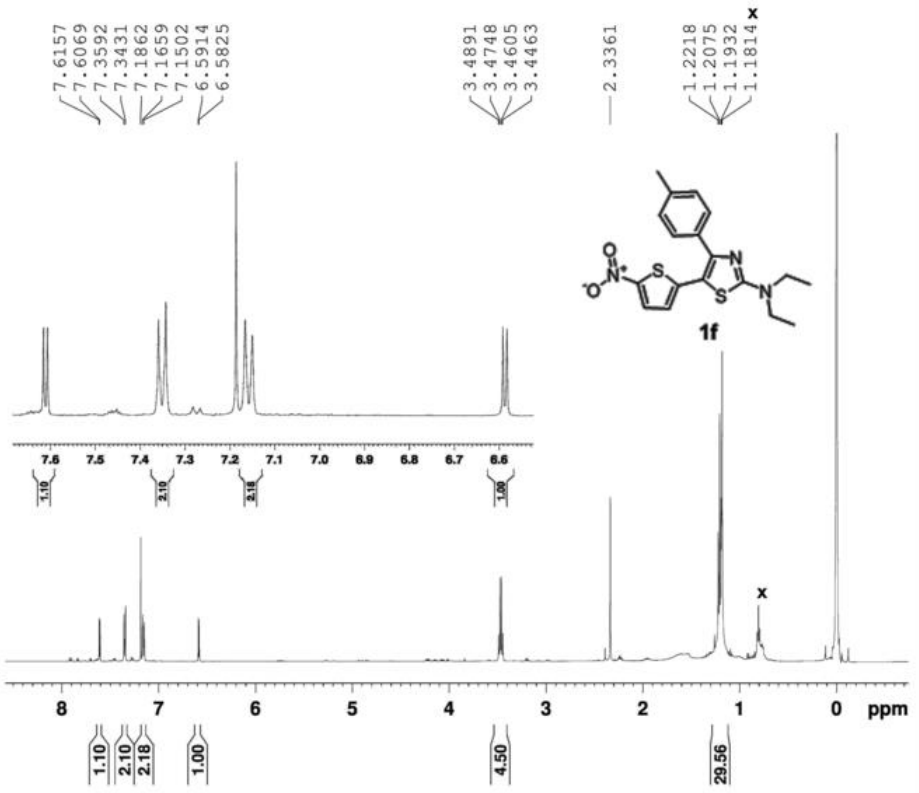

Figure 3.21: ^{1}H NMR spectrum of **1f**

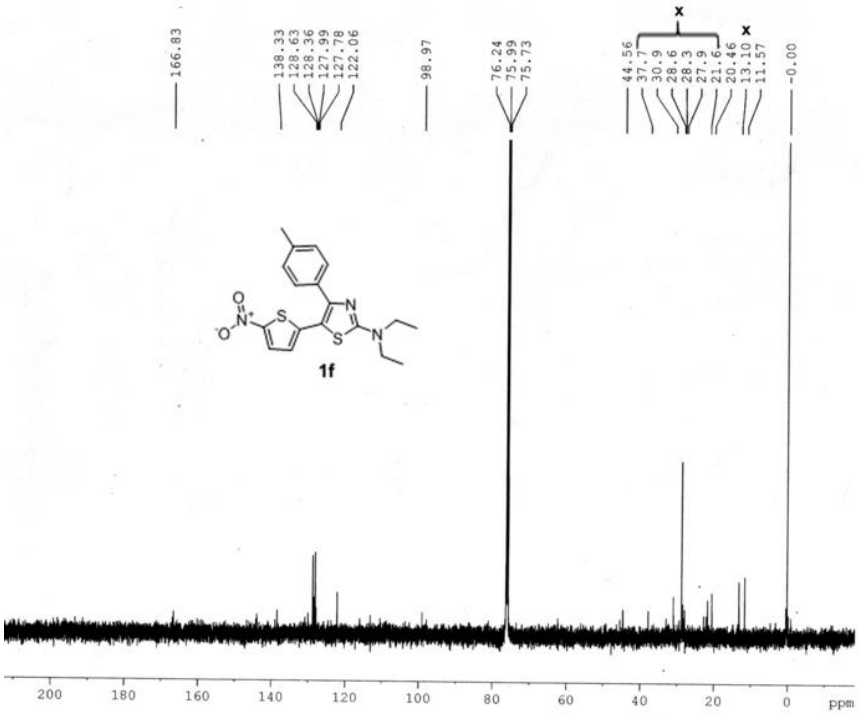

Figure 3.22: ^{13}C NMR spectrum of **1f**

5-(5-nitrothiophen-2-yl)-4-phenyl-2-(piperidin-1-yl)thiazole (**1g**)

Purified by column chromatography with 1% ethyl acetate: petroleum ether. Yield: 241 mg (65%). Red solid, m.p. 177.3-178.6 °C. ^{1}H NMR (500 MHz, $CDCl_3$, ppm): δ=1.57-1.71 (m, 6H), 3.47-3.48 (m, 4H), 6.59 (d, *J*=4.5 Hz, 1H), 7.34-7.36 (m, 3H), 7.44-7.46 (m, 2H), 7.61 (d, *J*=4.5 Hz, 1H); ^{13}C NMR (125 MHz, $CDCl_3$, ppm): δ=23.0, 24.1, 48.5, 111.2, 122.4, 127.9, 128.1, 128.3, 128.3, 133.6, 143.2, 147.1, 151.9, 168.1. HRMS (ESI) calc. $C_{18}H_{18}O_2N_3S_2$ $[M+H]^+$: 372.0836, found: 372.0838.

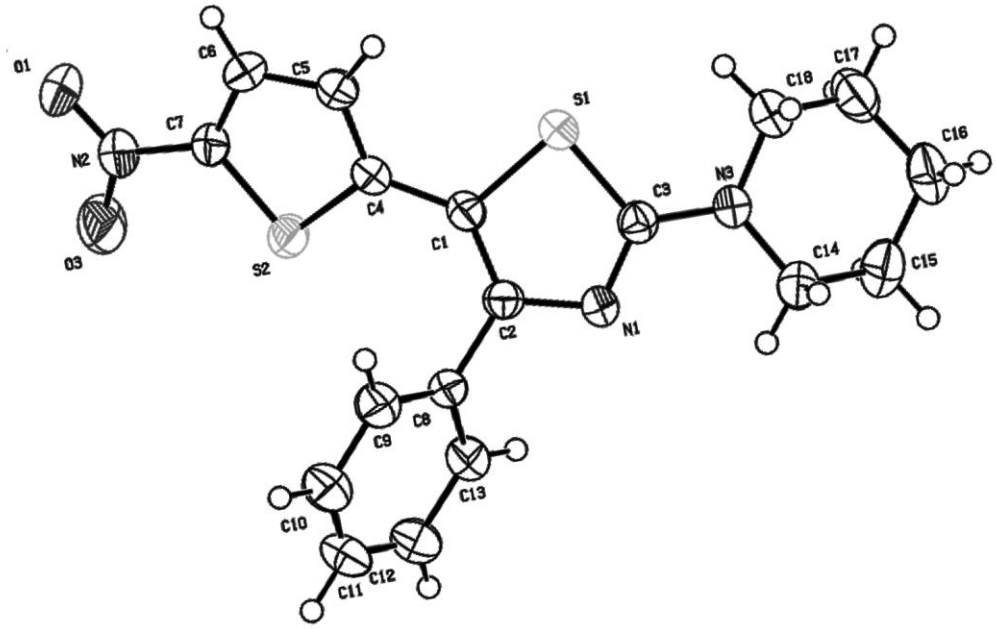

Figure 3.23: Ortep diagram of **1g** (recrystallized from ethanol) with 50 % probability ellipsoid (CCDC number: 1440185)

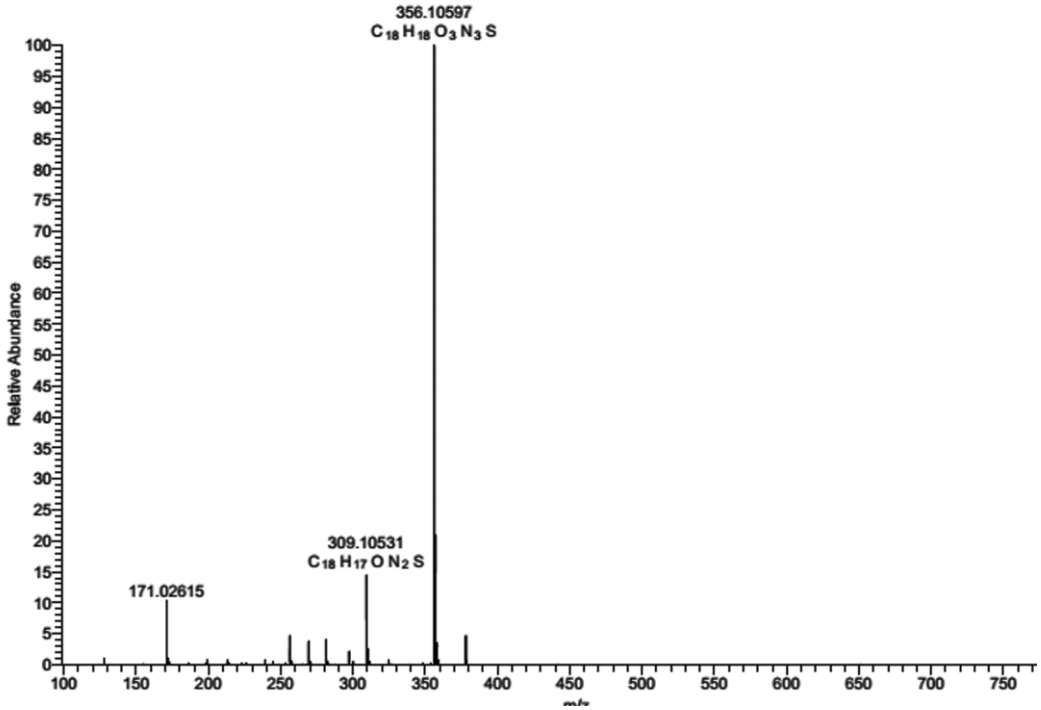

Figure 3.24: HR-MS spectrum of **1g**

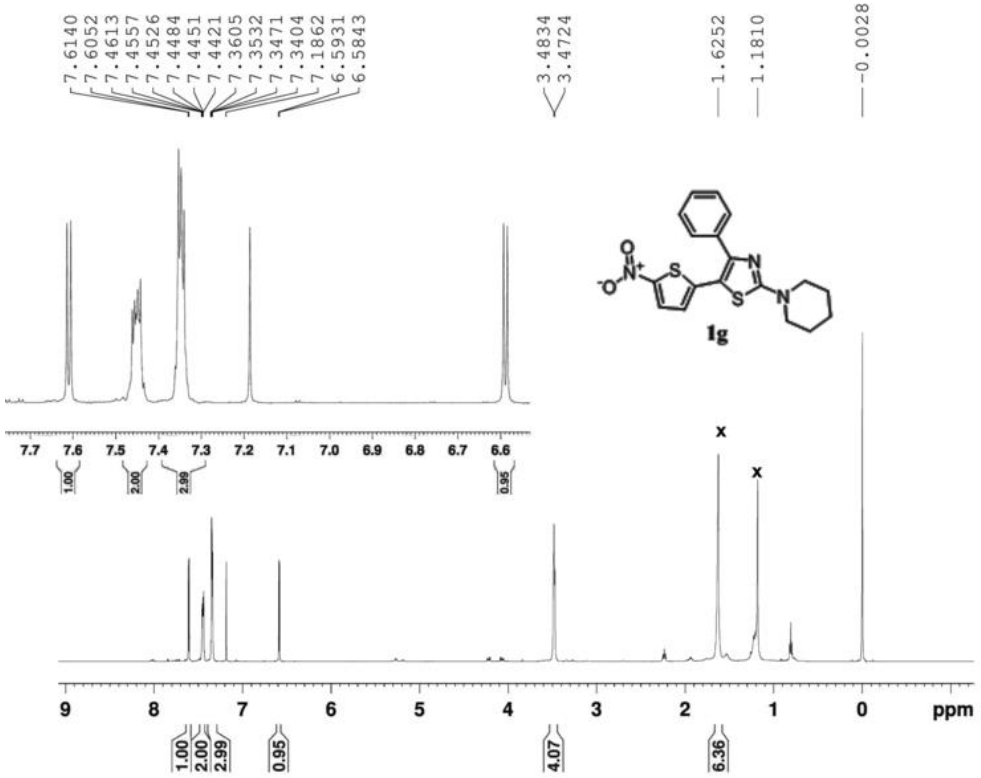

Figure 3.25: [1]H NMR spectrum of **1g**

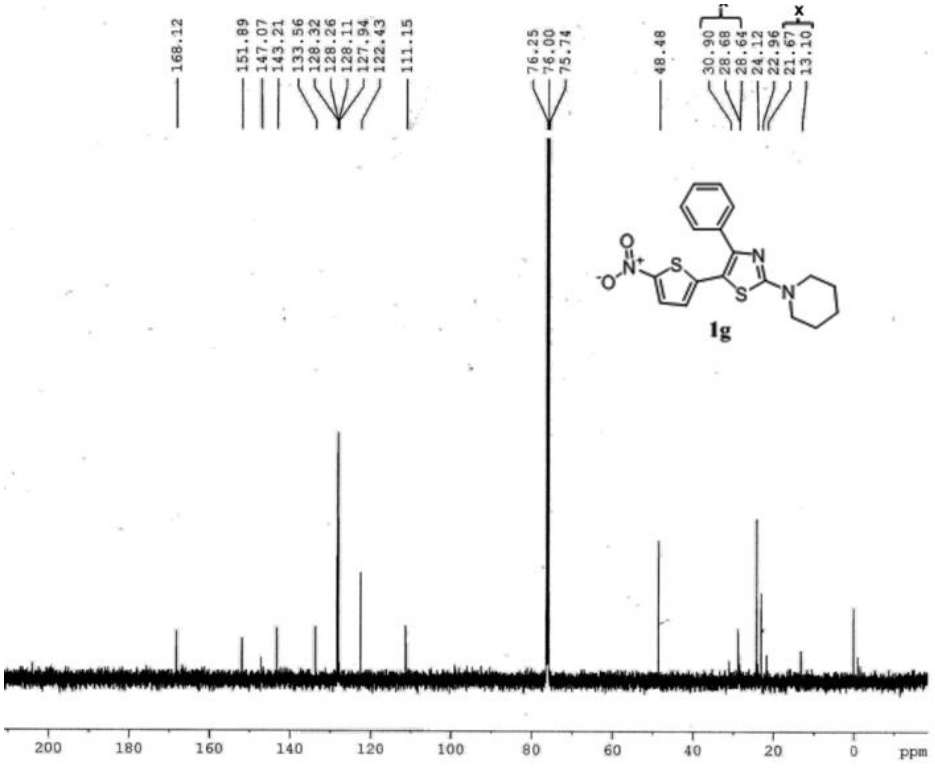

Figure 3.26: [13]C NMR spectrum of **1g**

5-(5-nitrothiophen-2-yl)-2-(piperidin-1-yl)-4-(p-tolyl)thiazole (**1h**)

Purified by column chromatography with 1% ethyl acetate: petroleum ether. Yield: 223 mg (58%). Red solid, m.p. 118.4-119.5 °C. ^{1}H NMR (500 MHz, $CDCl_3$, ppm): δ=1.69-1.73 (m, 6H), 2.40 (s, 3H), 3.54-3.55 (m, 4H), 6.67 (d, *J*=4.5 Hz, 1H), 7.22-7.26 (m, 2H), 7.40-7.42 (m, 2H), 7.67 (d, *J*=4.5 Hz, 1H).^{13}C NMR (125 MHz, $CDCl_3$, ppm): δ=21.5, 24.0, 25.2, 49.5, 112.0, 123.3, 129.0, 129.3, 129.7, 131.6, 139.4, 144.6, 147.6, 153.2, 169.0. HRMS (ESI) calc. $C_{19}H_{20}O_2N_3S_2$ $[M+H]^+$:386.0992, found: 386.0993.

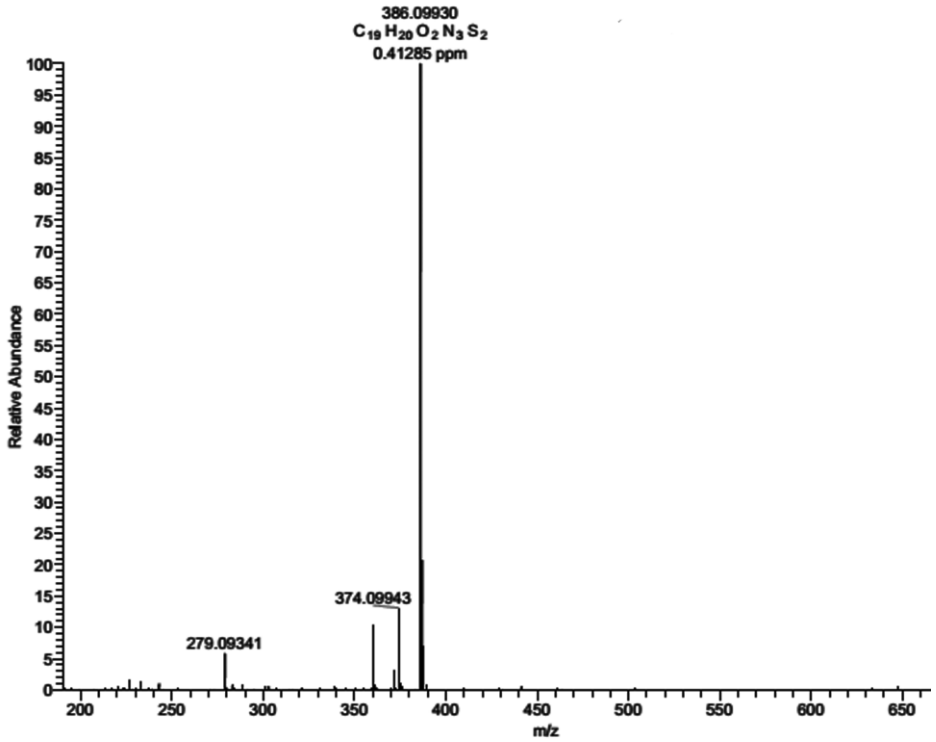

Figure 3.27: HR-MS spectrum of **1h**

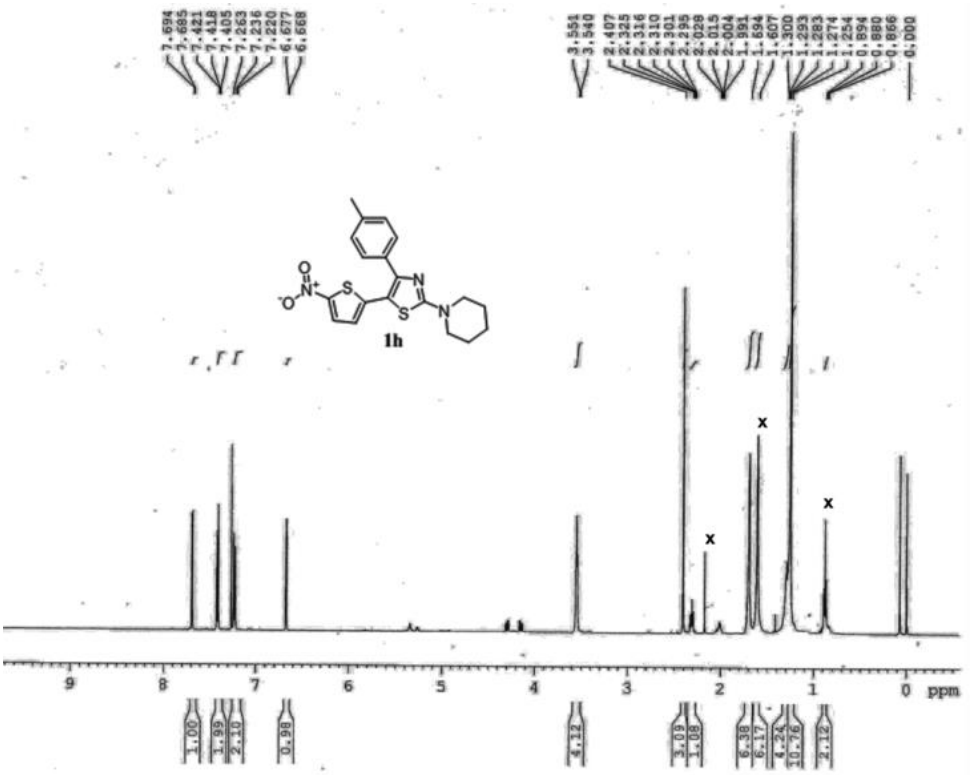

Figure 3.28: ^{1}H NMR spectrum of **1h**

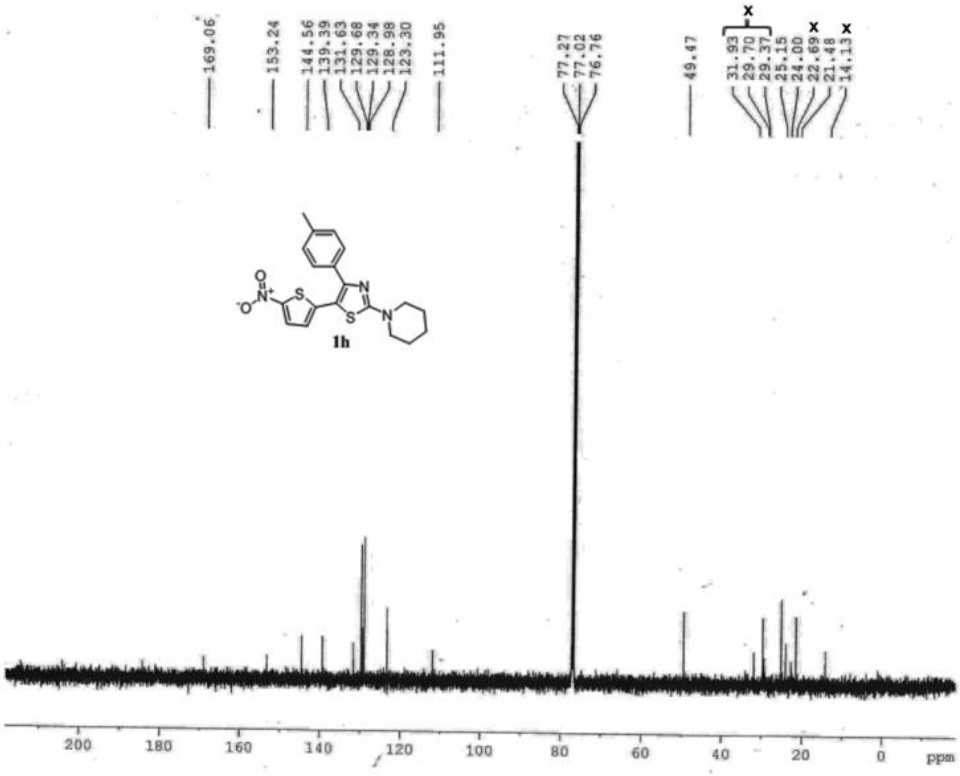

Figure 3.29: ^{13}C NMR spectrum of **1h**

4-(5-(5-nitrothiophen-2-yl)-4-phenylthiazol-2-yl)morpholine (**1i**)

Purified by column chromatography with 5% ethyl acetate: petroleum ether. Yield: 197mg (53%). Red solid, m.p. 193.4-194.1°C. ^{1}H NMR (500 MHz, $CDCl_3$, ppm): δ=3.49-3.51 (m, 4H), 3.75-3.77 (m, 4H), 6.65 (d, *J*=4.0 Hz, 1H), 7.35-7.36 (m, 3H), 7.44-7.46 (m, 2H), 7.63 (d, *J*=4.0 Hz, 1H); ^{13}C NMR (125 MHz, $CDCl_3$, ppm): δ=47.3, 65.0, 112.0, 123.1, 127.9, 128.1, 128.4, 133.2, 137.8, 142.4, 147.8, 151.4, 168.2. HRMS (ESI) calc. $C_{17}H_{16}N_3O_3S_2$ $[M+H]^+$: 374.0628, found: 374.0618.

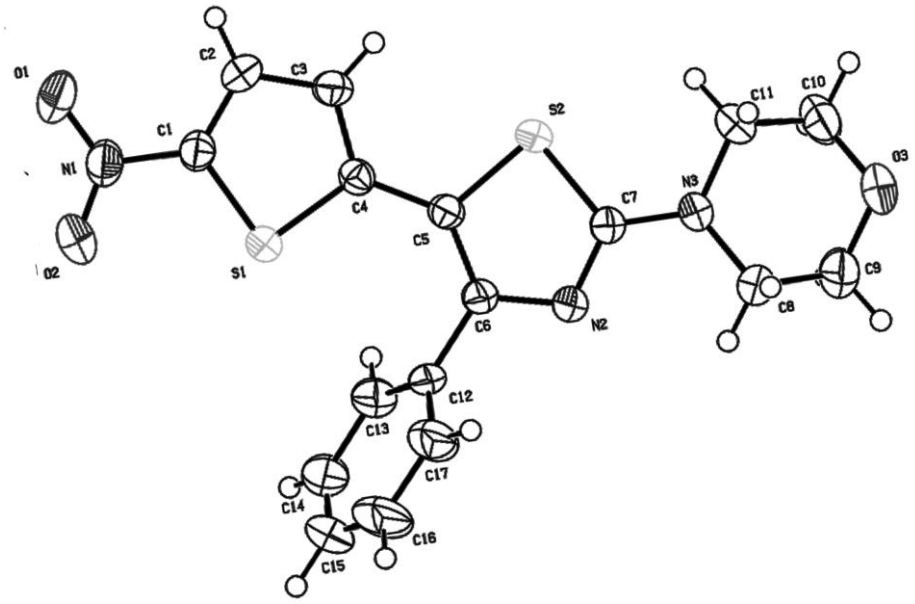

Figure 3.30: Ortep diagram of **1i** (recrystallized from ethanol) with 50 % probability ellipsoid (CCDC number: 1585456)

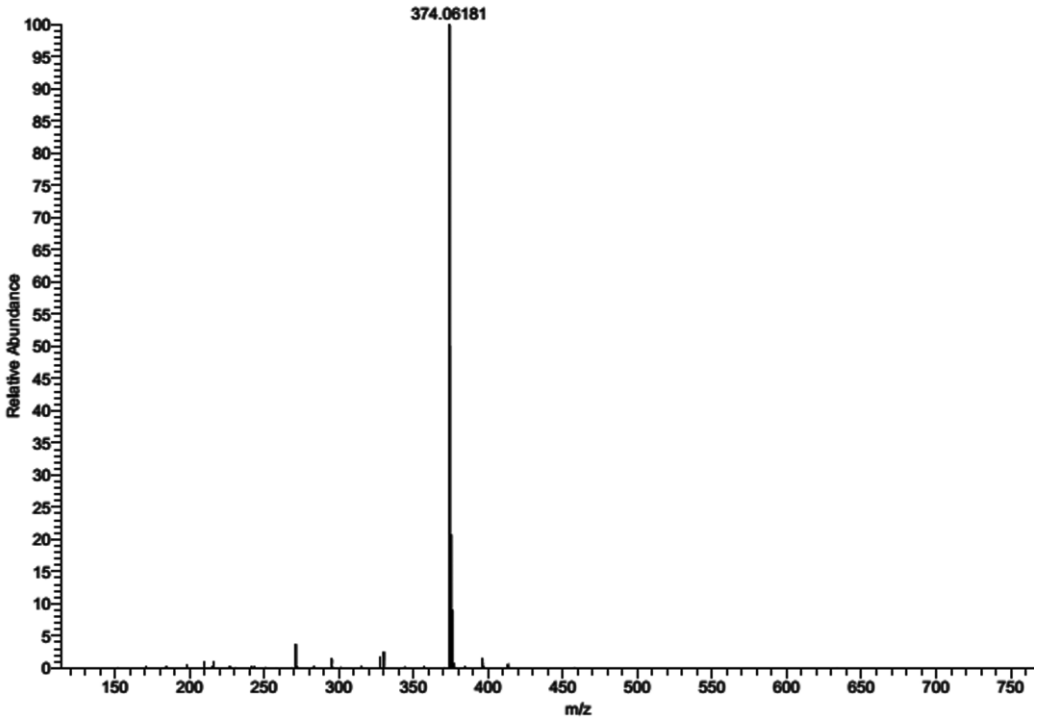

Figure 3.31: HR-MS spectrum of **1i**

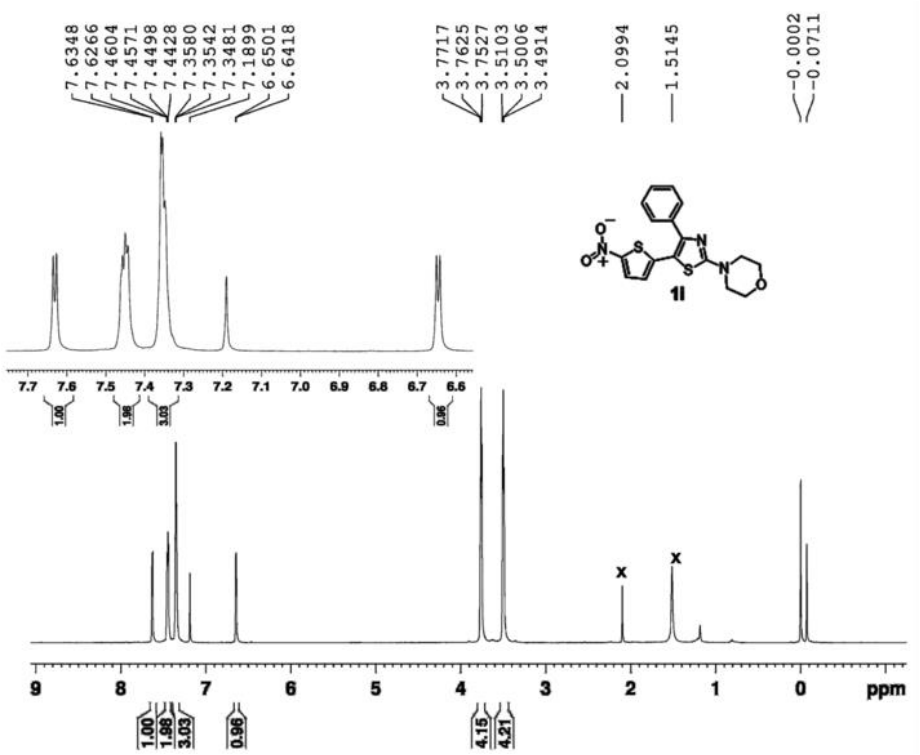

Figure 3.32: ^{1}H NMR spectrum of **1i**

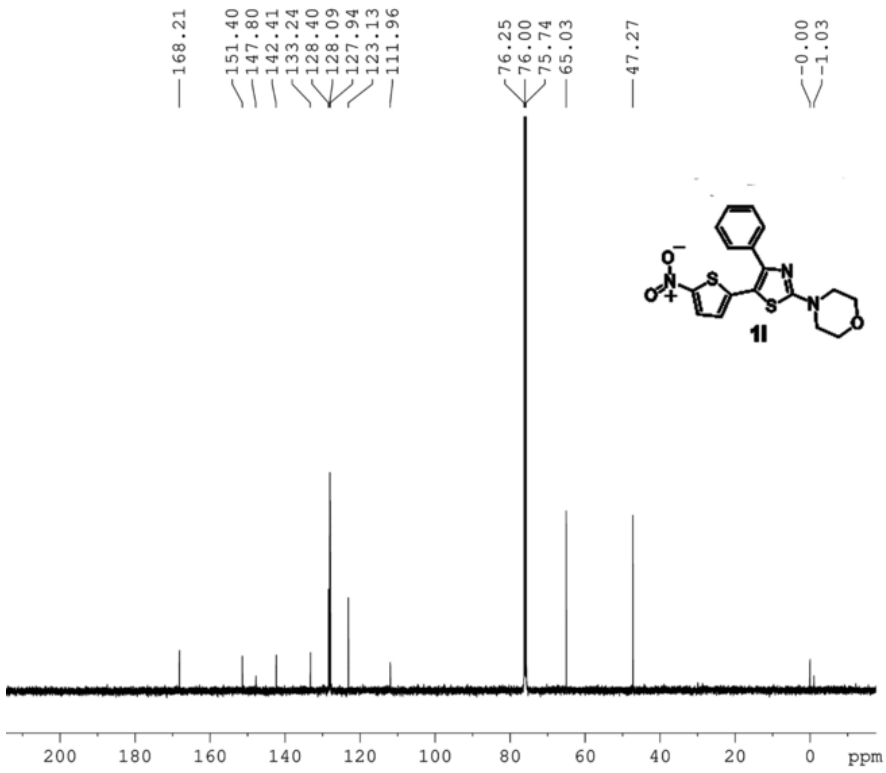

Figure 3.33: ^{13}C NMR spectrum of **1i**

4-(4-(4-bromophenyl)-5-(5-nitrothiophen-2-yl)thiazol-2-yl)morpholine (**1j**)

Purified by column chromatography with 6% ethyl acetate: petroleum ether. Yield: 208 mg (46%). Red solid, m.p. 172.9-173.6°C. ^1H NMR (500 MHz, $CDCl_3$, ppm): δ=3.55-3.57 (m, 4H), 3.82-3.84 (m, 4H), 6.74 (d, *J*=4.5 Hz, 1H), 7.41-7.43 (m, 2H), 7.53-7.55 (m, 2H), 7.72 (d, *J*=4.5 Hz, 1H); ^{13}C NMR (125 MHz, $CDCl_3$, ppm): δ=29.7, 48.3, 66.0, 112.9, 123.6, 124.7, 129.2, 130.8, 132.1, 133.1, 142.8, 149.2, 150.8, 169.3. HRMS (ESI) calc. $C_{17}H_{15}N_3O_3S_2Br$ $[M+H]^+$: 451.9733, found: 451.9730.

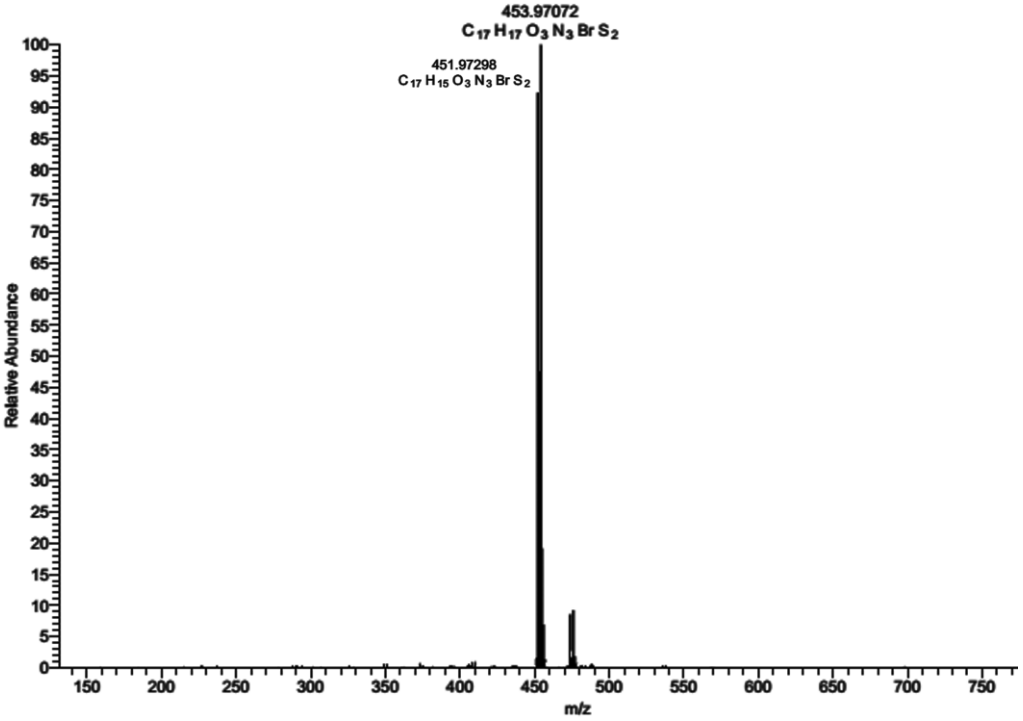

Figure 3.34: HR-MS spectrum of **1j**

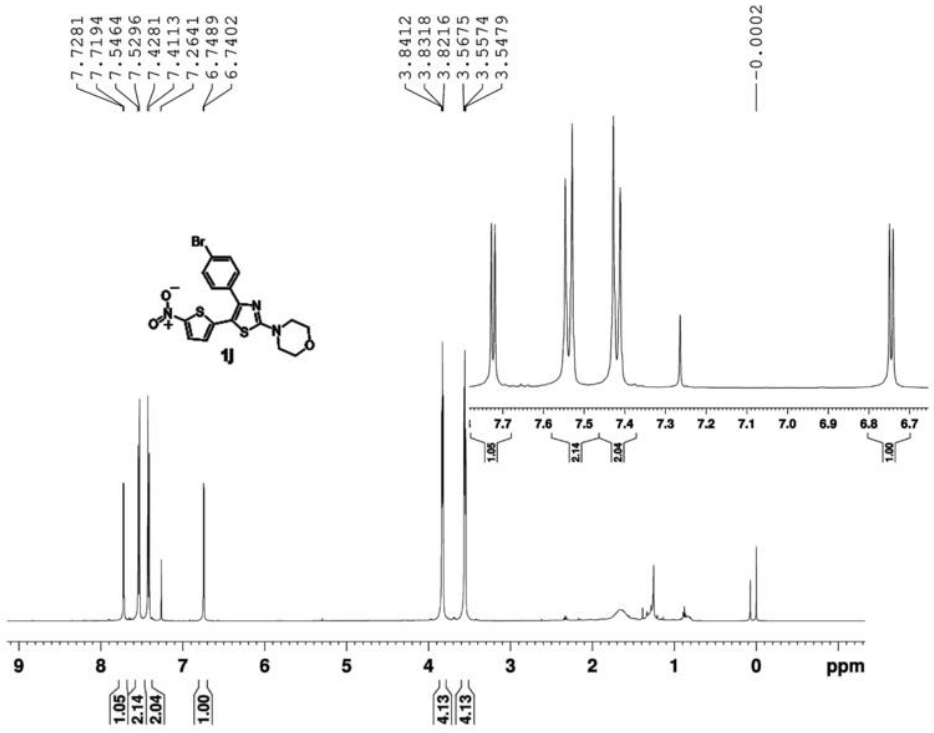

Figure 3.35: ^{1}H NMR spectrum of **1j**

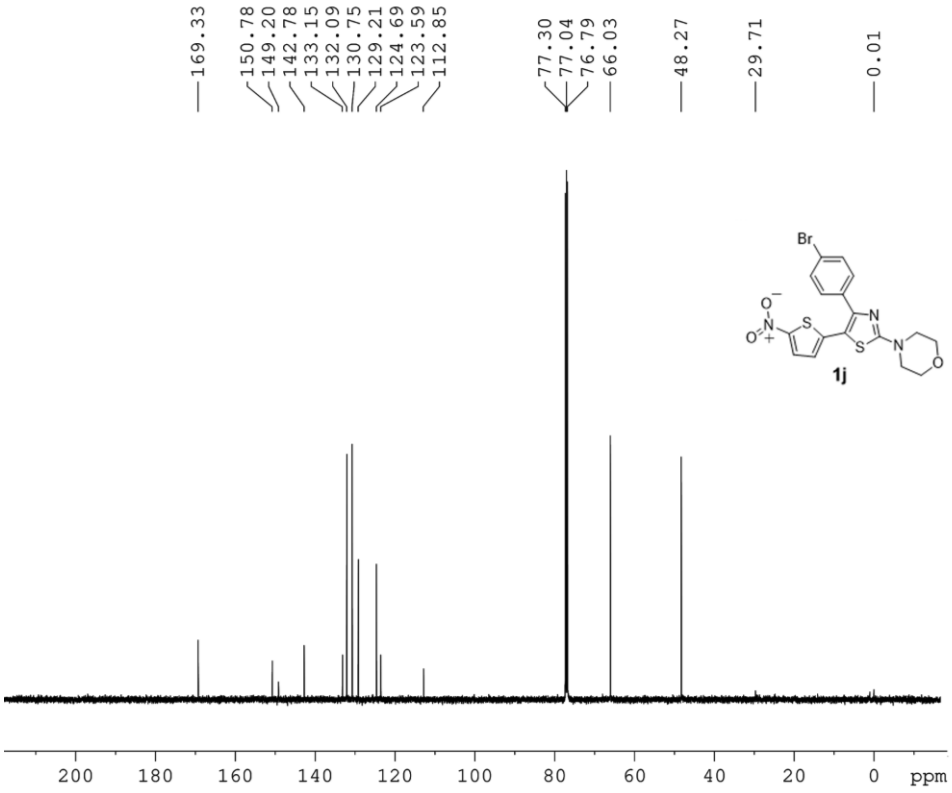

Figure 3.36: ^{13}C NMR spectrum of **1j**

4-(5-(5-nitrothiophen-2-yl)-4-(p-tolyl)thiazol-2-yl)morpholine (**1k**)

Purified by column chromatography with 5% ethyl acetate: petroleum ether. Yield: 194mg (52%). Red solid, m.p.127.2-128.1°C. ^{1}H NMR (500 MHz, $CDCl_3$, ppm): δ=2.33 (s, 3H), 3.48-3.50 (m, 4H), 3.77 (m, 4H), 6.65 (d, *J*=4.0 Hz, 1H), 7.15-7.16 (m, 2H), 7.33-7.35 (m, 2H), 7.63 (d, *J*=4.0 Hz, 1H); ^{13}C NMR (125 MHz, $CDCl_3$, ppm): δ=20.5, 47.3, 65.0, 111.7, 123.0, 128.0, 128.1, 128.7, 130.3, 138.5, 142.7, 147.6, 151.7, 168.1. HRMS (ESI) calc. $C_{18}H_{18}N_3O_3S_2$ $[M+H]^+$: 388.0784, found:388.0776.

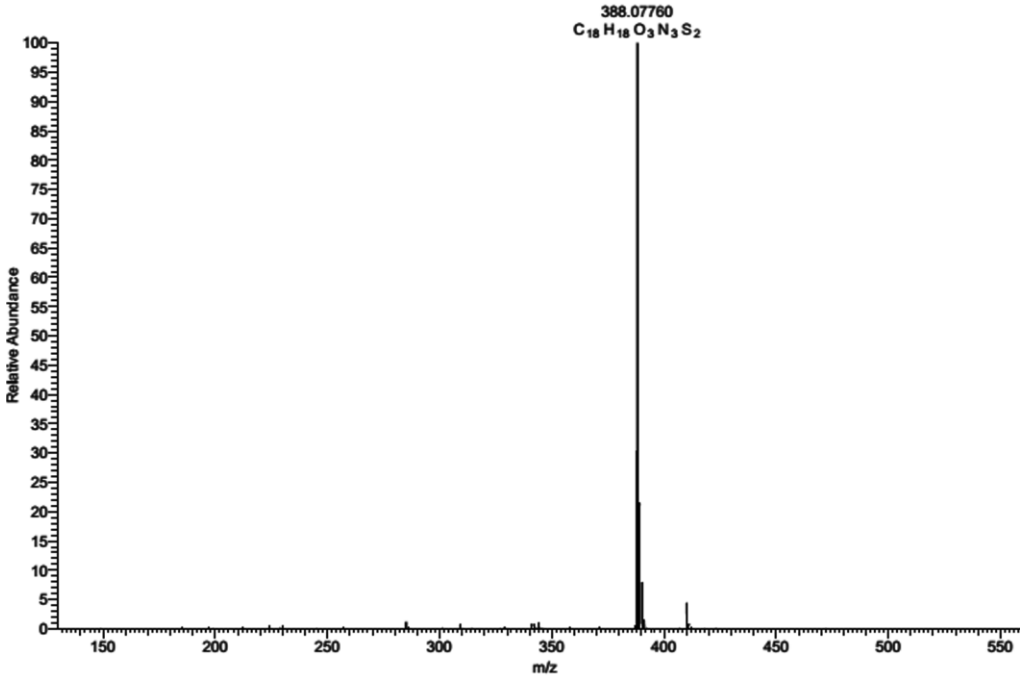

Figure 3.37: HR-MS spectrum of **1k**

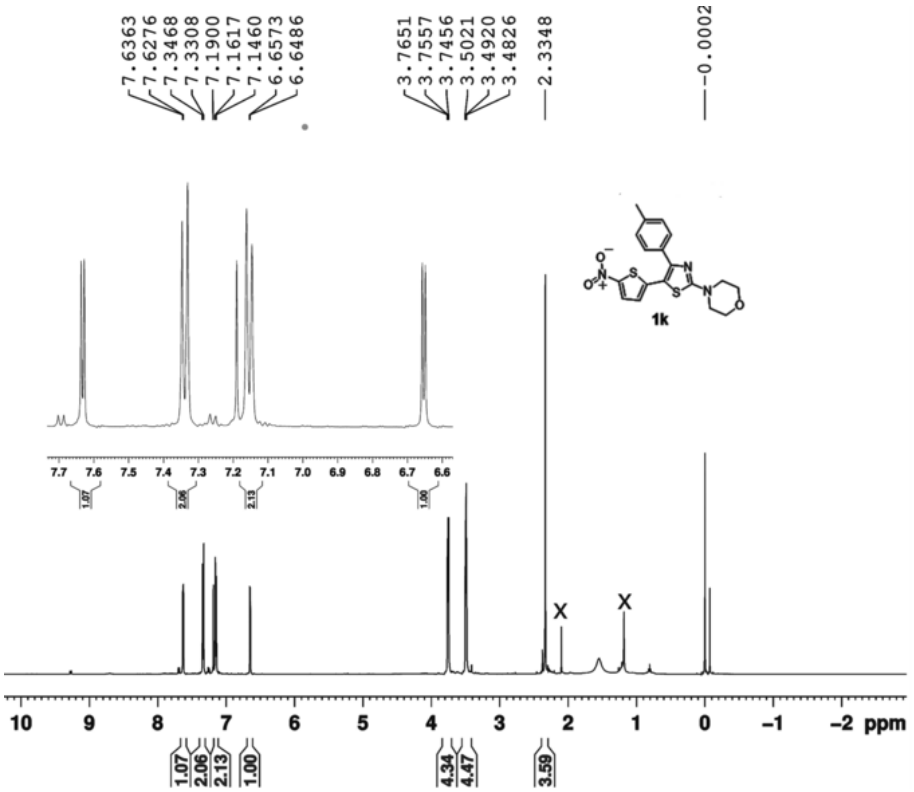

Figure 3.38: ^{1}H NMR spectrum of **1k**

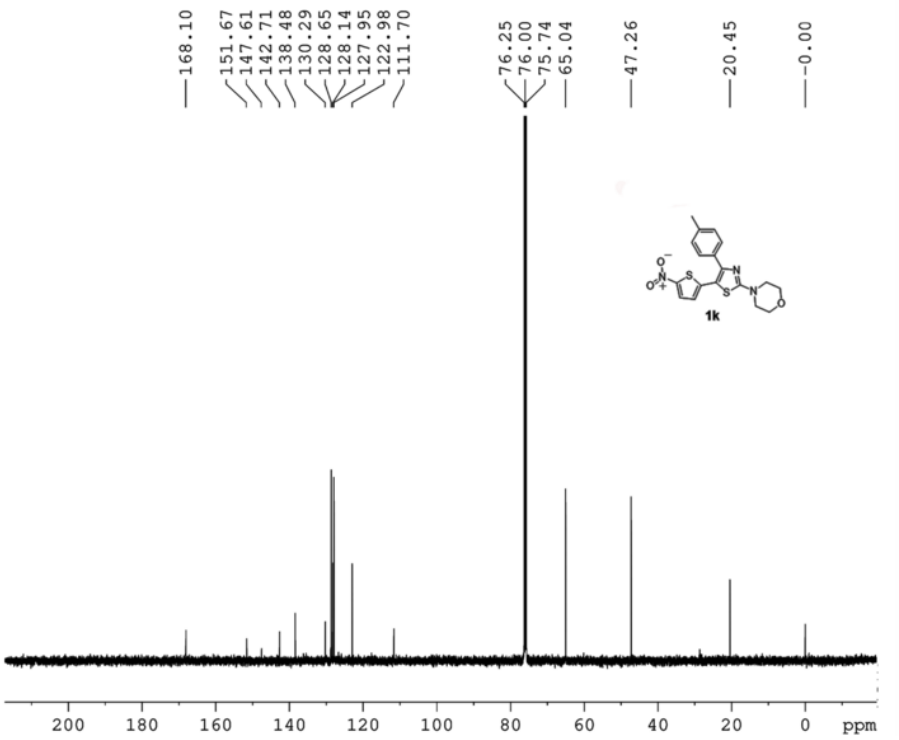

Figure 3.39: ^{13}C NMR spectrum of **1k**

4-(4-(furan-2-yl)-5-(5-nitrothiophen-2-yl)thiazol-2-yl)morpholine (**1l**)

Purified by column chromatography with 10% ethyl acetate: petroleum ether. Yield: 200 mg (55%). Red solid, m.p. 131.2-131.9 °C. ^1H NMR (500 MHz, $CDCl_3$, ppm): δ=3.47-3.49 (m, 4H), 3.75-3.77 (m, 4H), 6.43-6.44 (m, 1H), 6.74 (d, *J*=3.0 Hz, 1H), 6.98 (d, *J*=4.0 Hz, 1H), 7.41 (m, 1H), 7.74 (d, *J*=4.0 Hz, 1H); ^{13}C NMR (125 MHz, $CDCl_3$, ppm): δ=48.2, 111.7, 111.8, 112.3, 125.9, 128.9, 140.7, 142.2, 142.9, 148.9, 149.5, 169.0. HRMS (ESI) calc. $C_{15}H_{14}N_3O_4S_2$ $[M+H]^+$: 364.0420, found: 364.0415.

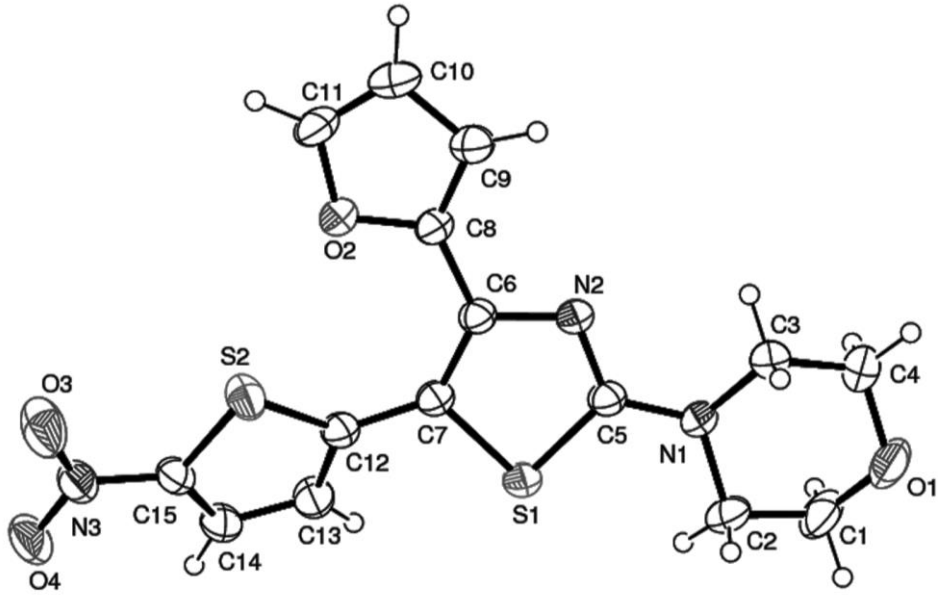

Figure 3.40: Ortep diagram of **1l** (recrystallized from ethanol) with 40 % probability ellipsoid

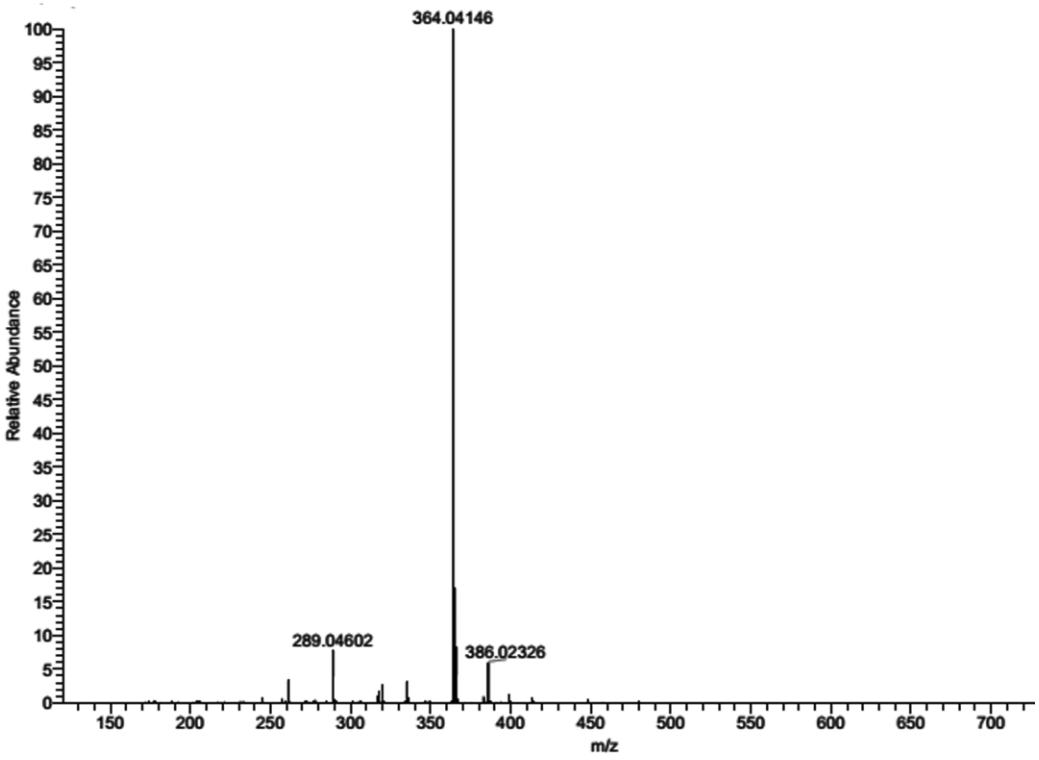

Figure 3.41: HR-MS spectrum of **1l**

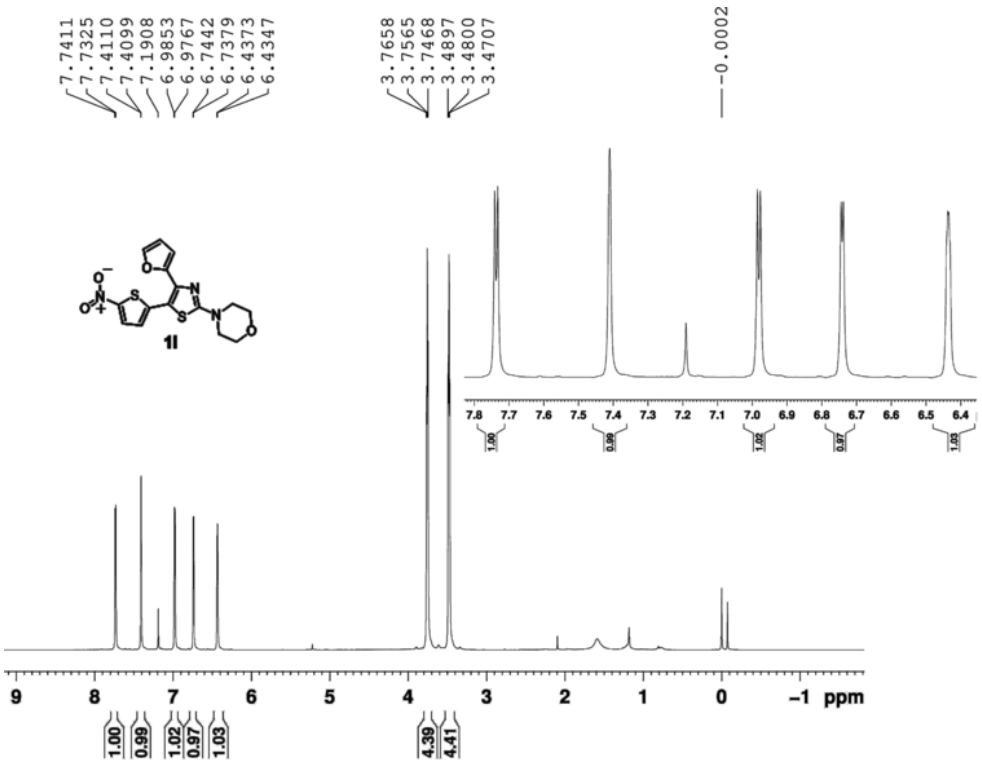

Figure 3.42: ^{1}H NMR spectrum of **1l**

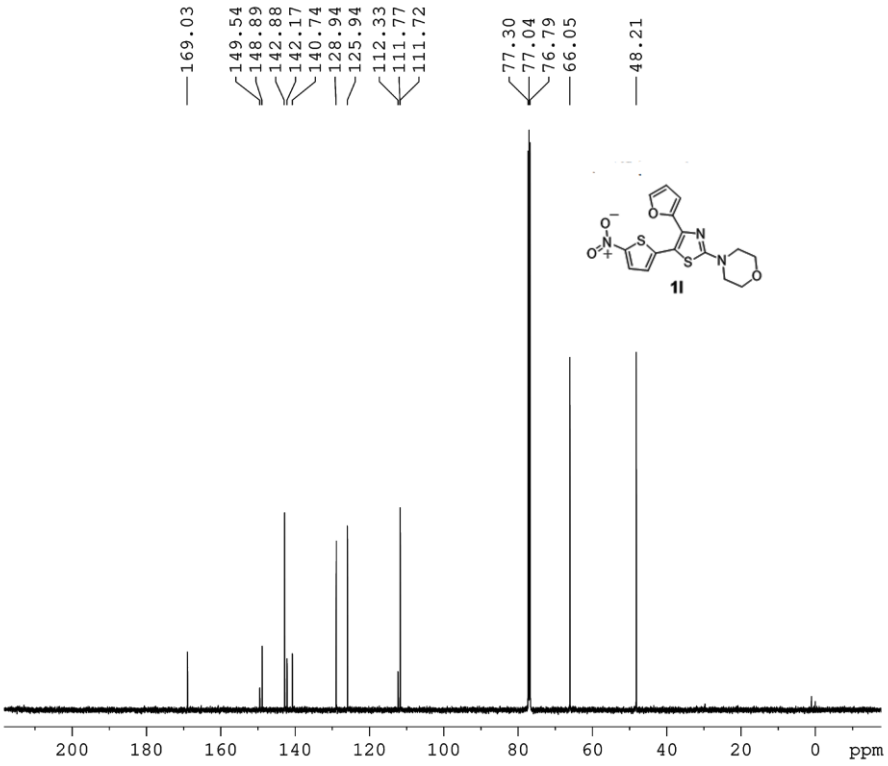

Figure 3.43: ^{13}C NMR spectrum of **1l**

5-(5-nitrothiophen-2-yl)-N,N,4-triphenylthiazol-2-amine (**1m**)

Purified by column chromatography with 2% ethyl acetate: petroleum ether. Yield: 264 mg (58%). Red solid, m.p. 194.6-195.7°C. ^{1}H NMR (500 MHz, $CDCl_3$, ppm): δ=6.63 (d, *J*=4.5 Hz, 1H), 7.18-7.22 (m, 2H), 7.32-7.39 (m, 11H), 7.47-7.49 (m, 2H), 7.59 (d, *J*=4.5 Hz, 1H); ^{13}C NMR (125 MHz, $CDCl_3$, ppm): δ=115.0, 117.8, 121.4, 124.8, 126.0, 126.0, 126.4, 126.4, 126.7, 128.3, 128.8, 129.0, 129.3, 129.3, 129.7, 129.8, 129.9, 134.1, 142.9, 144.3, 149.2, 151.8, 167.6. HRMS (ESI) calc. $C_{25}H_{18}N_3O_2S_2$ $[M+H]^+$: 456.0835, found: 456.0840.

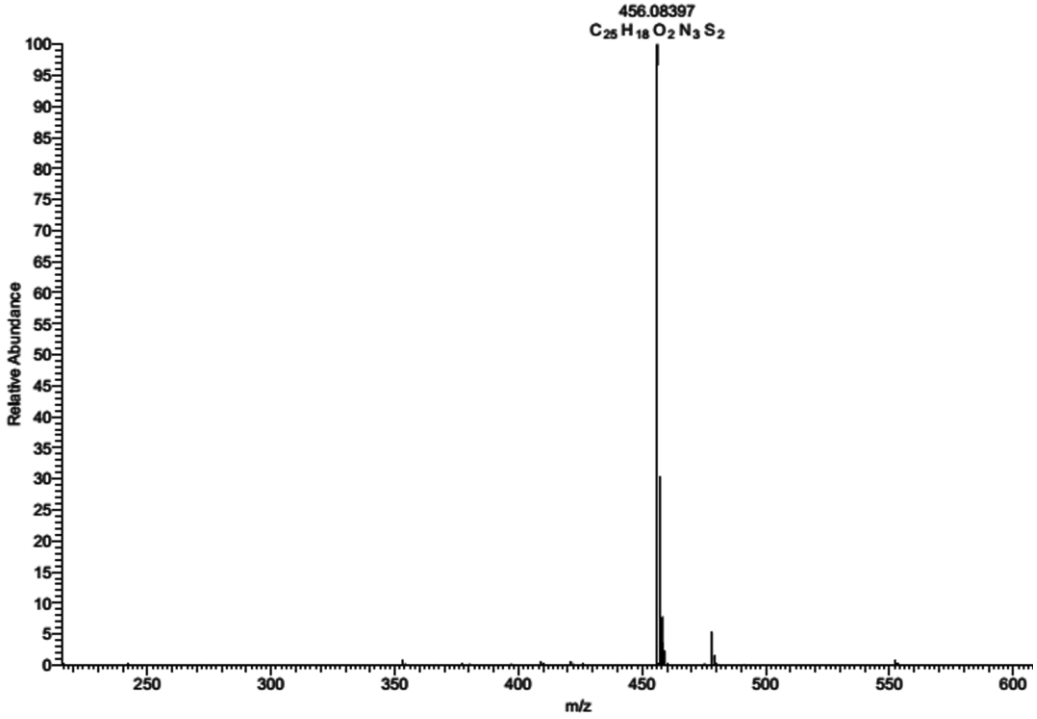

Figure 3.44: HR-MS spectrum of **1m**

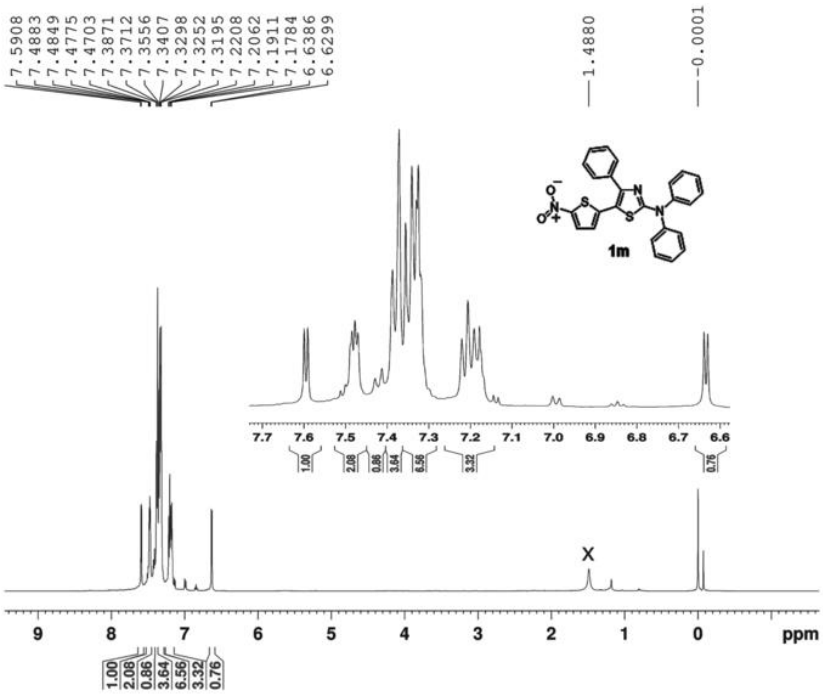

Figure 3.45: ^{1}H NMR spectrum of **1m**

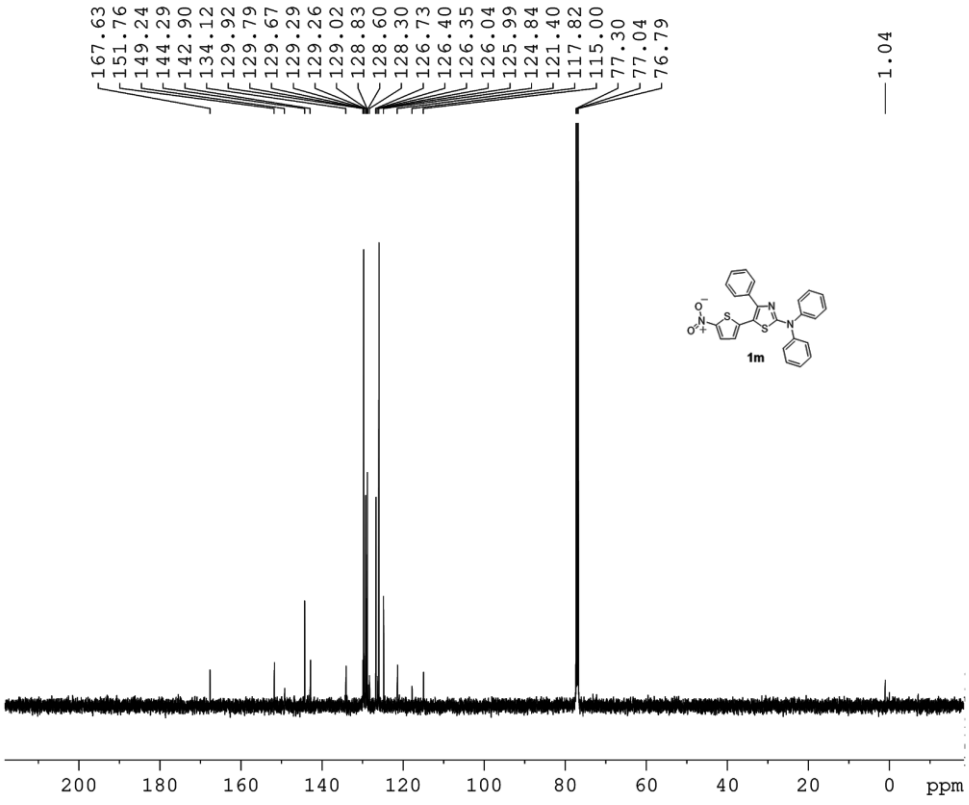

Figure 3.46: ^{13}C NMR spectrum of **1m**

4-(4-bromophenyl)-5-(5-nitrothiophen-2-yl)-N,N-diphenylthiazol-2-amine (**1n**)

Purified by column chromatography with 2% ethyl acetate: petroleum ether. Yield: 277 mg (52%). Red solid, m.p. 186.6-187.5°C. ^{1}H NMR (500 MHz, $CDCl_3$, ppm): δ=7.18-7.25 (m, 3H), 7.29-7.40 (m, 9H), 7.42-7.45 (m, 2H), 7.62 (s, 1H); ^{13}C NMR (125 MHz, $CDCl_3$, ppm): δ=114.8, 123.5, 125.3, 126.0, 126.0, 126.5, 126.8, 129.1, 129.7, 129.8, 130.1, 130.8, 131.5, 132.0, 133.0, 142.2, 144.2, 150.2, 167.8. HRMS (ESI) calc. $C_{25}H_{17}N_3O_2S_2Br$ $[M+H]^+$: 533.9940, found: 533.9942.

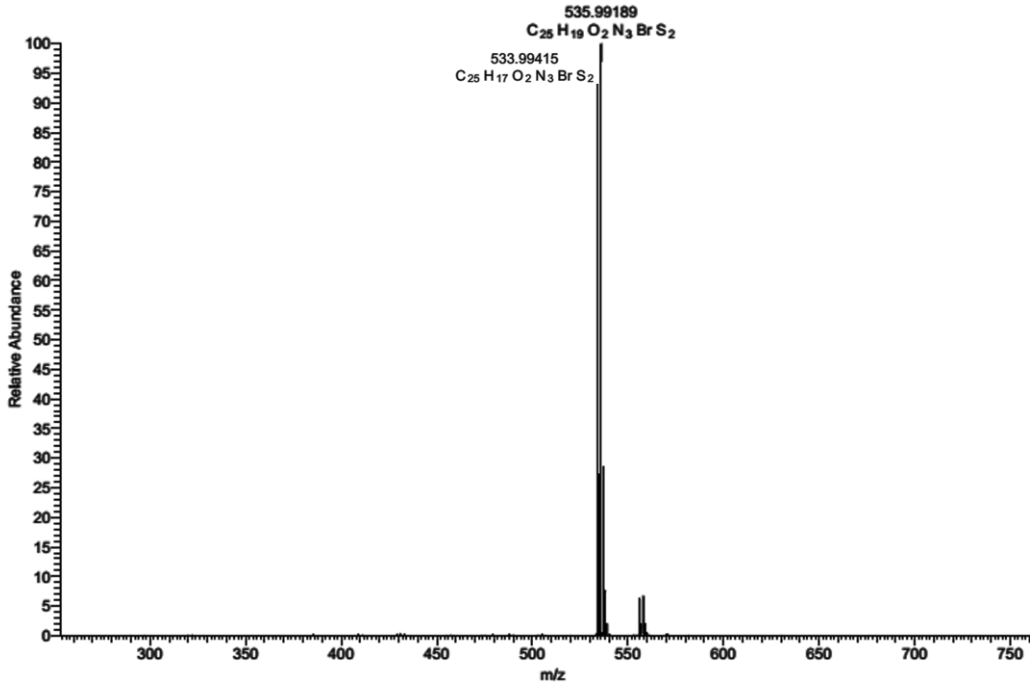

Figure 3.47: HR-MS spectrum of **1n**

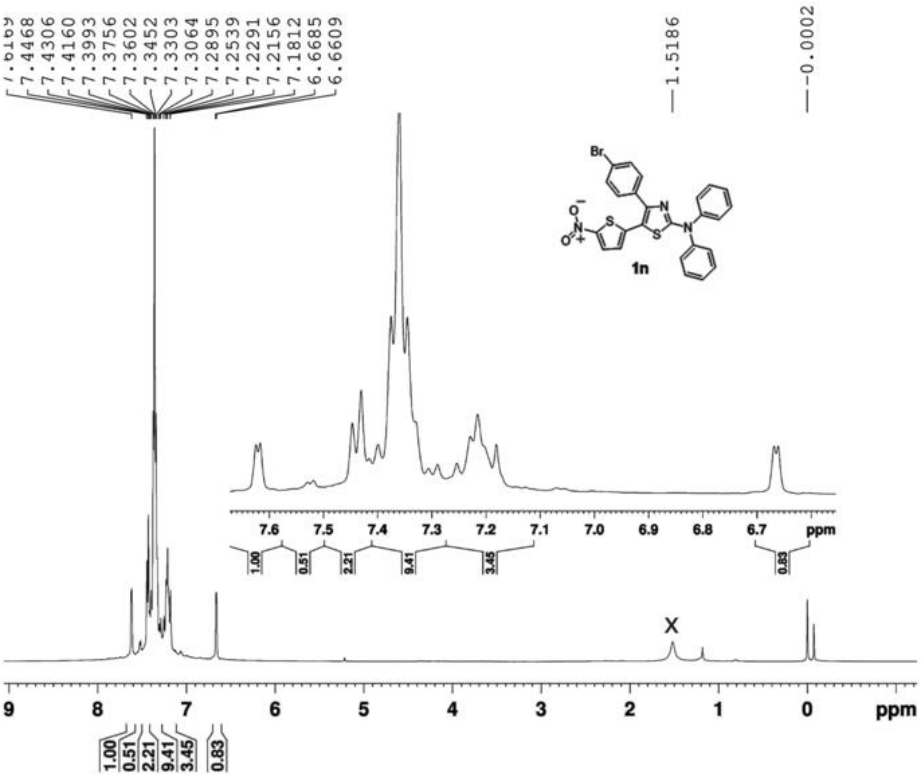

Figure 3.48: [1]H NMR spectrum of **1n**

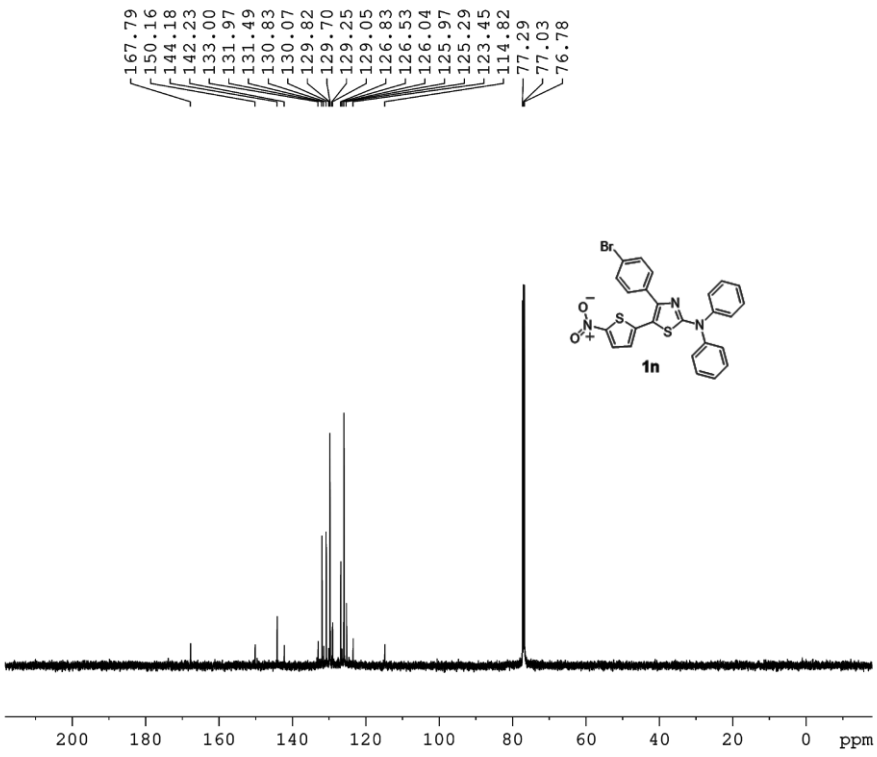

Figure 3.49: [13]C NMR spectrum of **1n**

5-(5-nitrothiophen-2-yl)-N,N-diphenyl-4-(p-tolyl)thiazol-2-amine (**1o**)

Purified by column chromatography with 2% ethyl acetate: petroleum ether. Yield: 281 mg (60%). Red solid, m.p. 174.2-175.1°C. ^{1}H NMR (500 MHz, $CDCl_3$, ppm): δ=2.39 (s, 3H), 6.71 (d, *J*=4.5 Hz, 1H), 7.19-7.21 (m, 2H), 7.25-7.29 (m, 2H), 7.39-7.45 (m, 10H), 7.67 (d, *J*=4.5 Hz, 1H); ^{13}C NMR (125 MHz, $CDCl_3$, ppm): δ=21.5, 114.7, 124.7, 126.0, 126.7, 129.0, 129.1, 129.5, 129.8, 131.2, 139.4, 143.2, 144.3, 149.1, 152.0, 167.5. HRMS (ESI) calc. $C_{26}H_{20}N_3O_2S_2$ $[M+H]^+$: 470.0991, found: 470.0987.

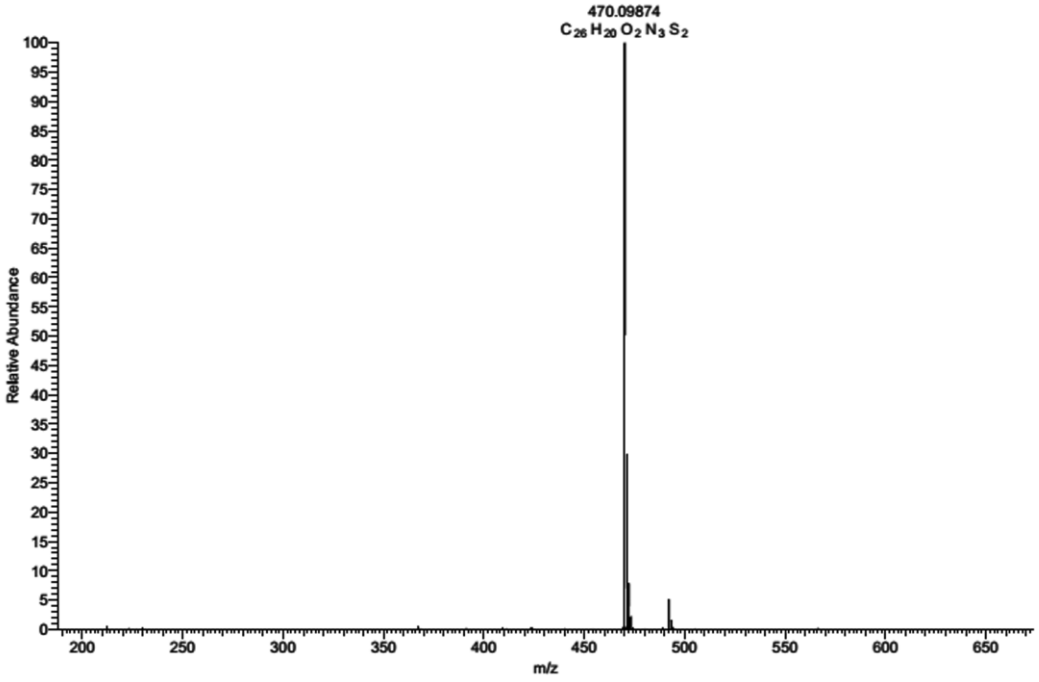

Figure 3.50: HR-MS spectrum of **1o**

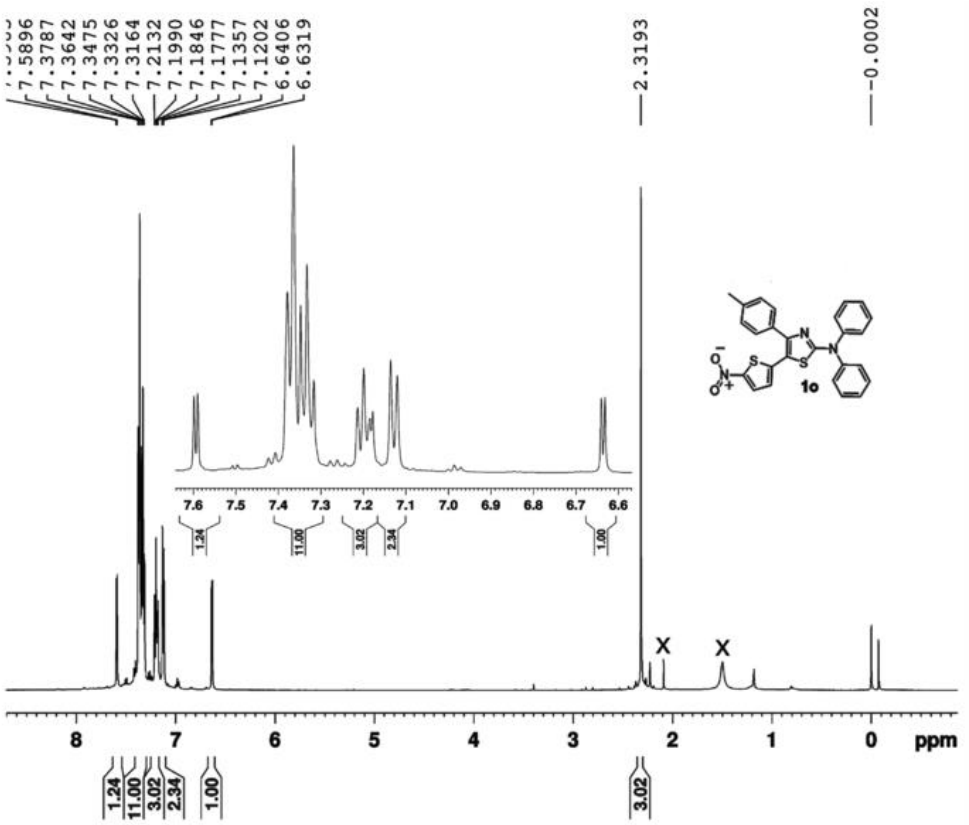

Figure 3.51: [1]H NMR spectrum of **1o**

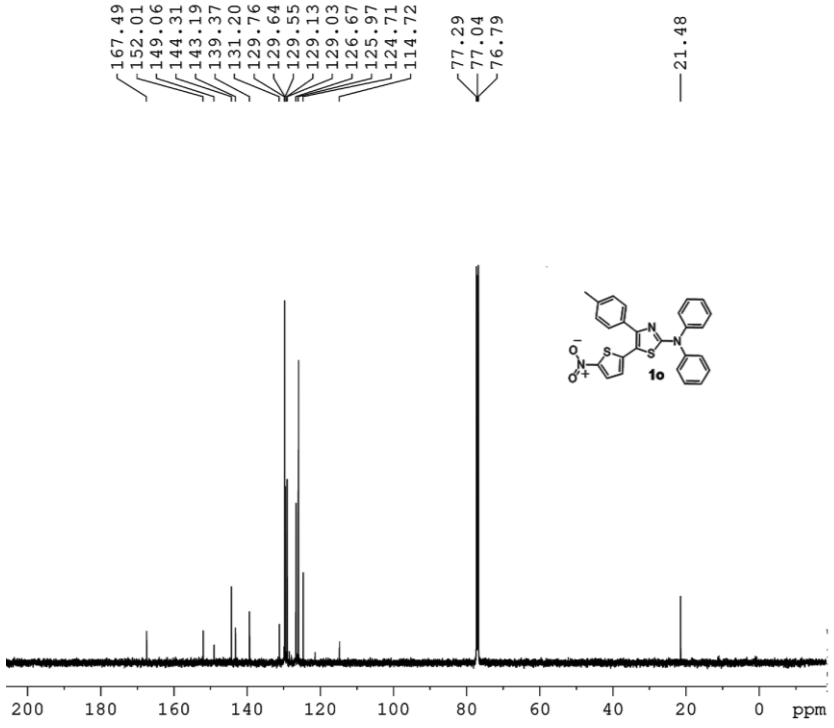

Figure 3.52: [13]C NMR spectrum of **1o**

5-(5-nitrothiophen-2-yl)-N,N-diphenyl-4-(thiophen-2-yl)thiazol-2-amine (**1p**)

Purified by column chromatography with 4% ethyl acetate: petroleum ether. Yield: 281 mg (61%). Red solid, m.p. 138.0-138.8°C. ^{1}H NMR (500 MHz, DMSO-d_6, ppm): δ= 7.12-7.14 (m, 1H), 7.19 (d, *J*=4.5 Hz, 1H), 7.34-7.37 (m, 3H), 7.48-7.54 (m, 8H), 7.70 (d, *J*=5 Hz, 1H), 8.00 (d, *J*=4.5 Hz, 1H); ^{13}C NMR (125 MHz, $CDCl_3$, ppm): δ= 113.3, 121.4, 125.9, 126.4, 126.5, 126.7, 127.5, 127.5, 127.6, 128.9, 129.6, 129.7, 129.9, 136.2, 141.7, 144.1, 144.5, 150.3, 167.3. HRMS (ESI) calc. $C_{23}H_{16}N_3O_2S_3$ $[M+H]^+$: 462.0399, found: 462.0413.

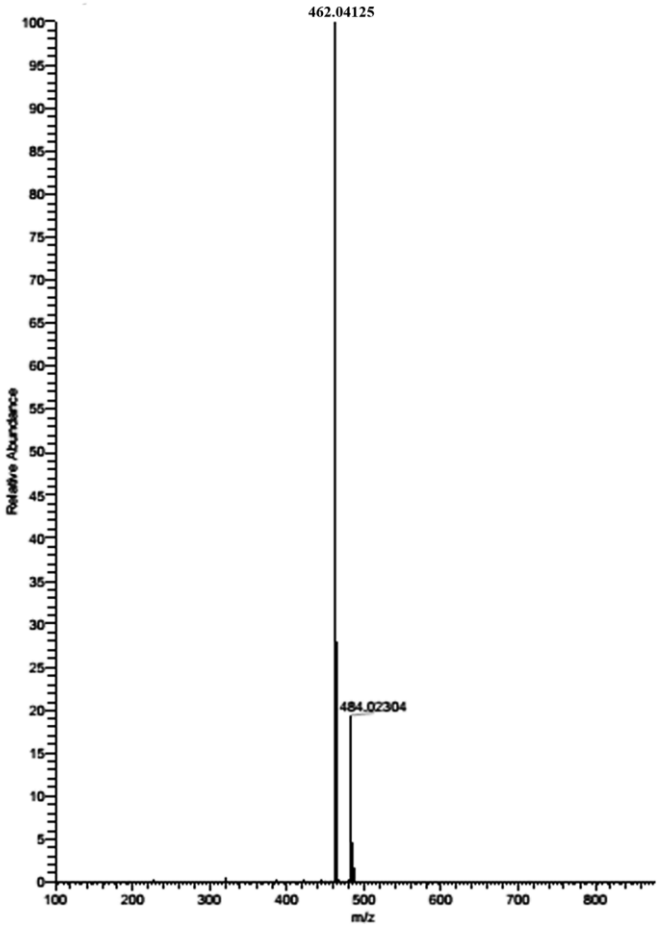

Figure 3.53: HR-MS spectrum of **1p**

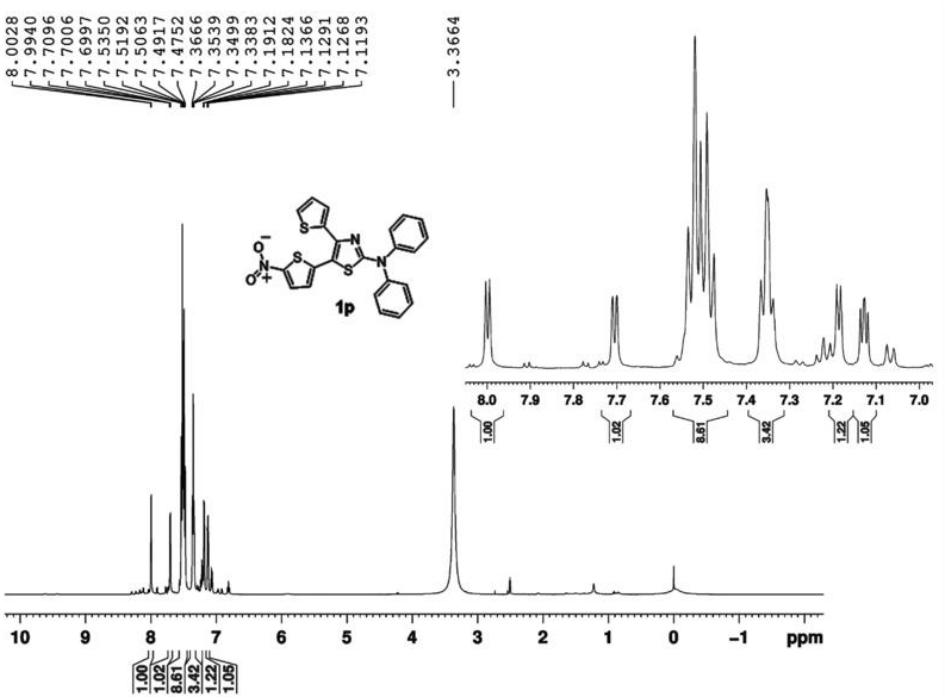

Figure 3.54: [1]H NMR spectrum of **1p**

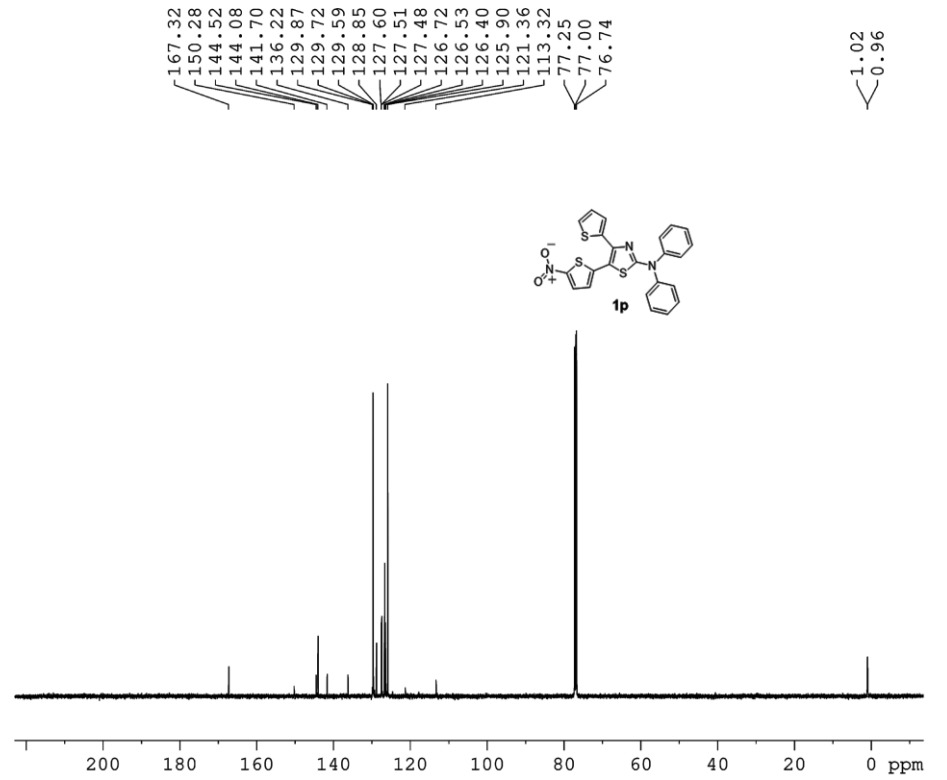

Figure 3.55: [13]C NMR spectrum of **1p**

4-(furan-2-yl)-5-(5-nitrothiophen-2-yl)-N,N-diphenylthiazol-2-amine (**1q**)

Purified by column chromatography with 1% ethyl acetate: petroleum ether. Yield: 227 mg (51%). Red solid, m.p. 154.0-155.3 °C. ^{1}H NMR (500 MHz, $CDCl_3$, ppm): δ=6.42-6.43 (m, 1H), 6.74 (d, *J*=3.5 Hz, 1H), 6.97 (d, *J*=4.5 Hz, 1H), 7.21-7.24 (m, 1H), 7.33-7.40 (m, 10H), 7.71 (d, *J*=4.5 Hz, 1H); ^{13}C NMR (125 MHz, $CDCl_3$, ppm): δ=111.8, 111.9, 114.1, 126.0, 126.3, 126.8, 128.8, 129.8, 140.2, 141.7, 142.8, 144.1, 149.0, 167.4. HRMS (ESI) calc. $C_{23}H_{16}O_3N_3S_2$ $[M+H]^+$: 446.0629, found: 446.0630.

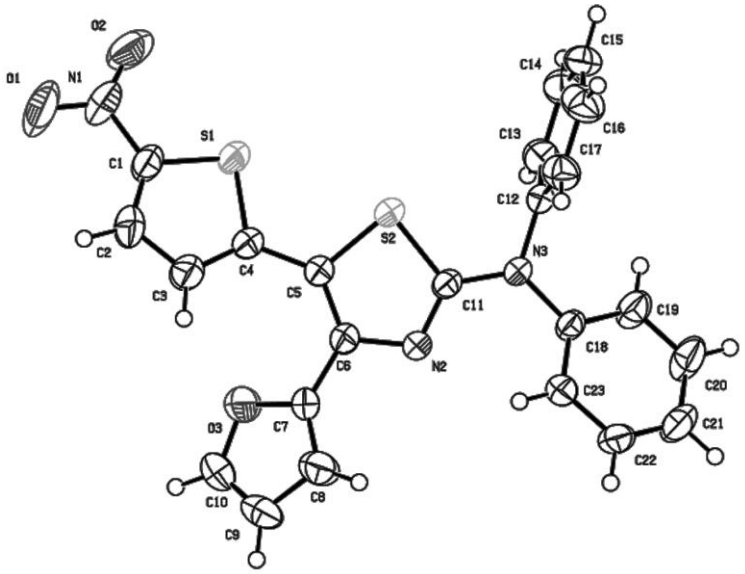

Figure 3.56: Ortep diagram of **1q** (recrystallized from ethanol) with 50 % probability ellipsoid (CCDC number: 1440186)

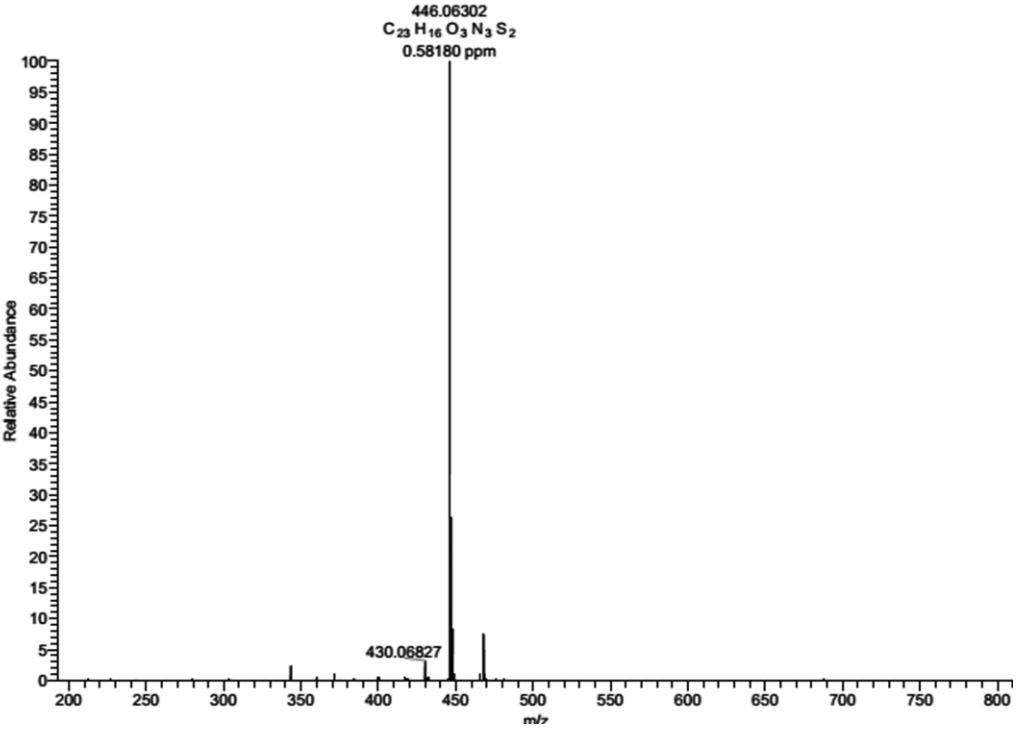

Figure 3.57: HR-MS spectrum of **1q**

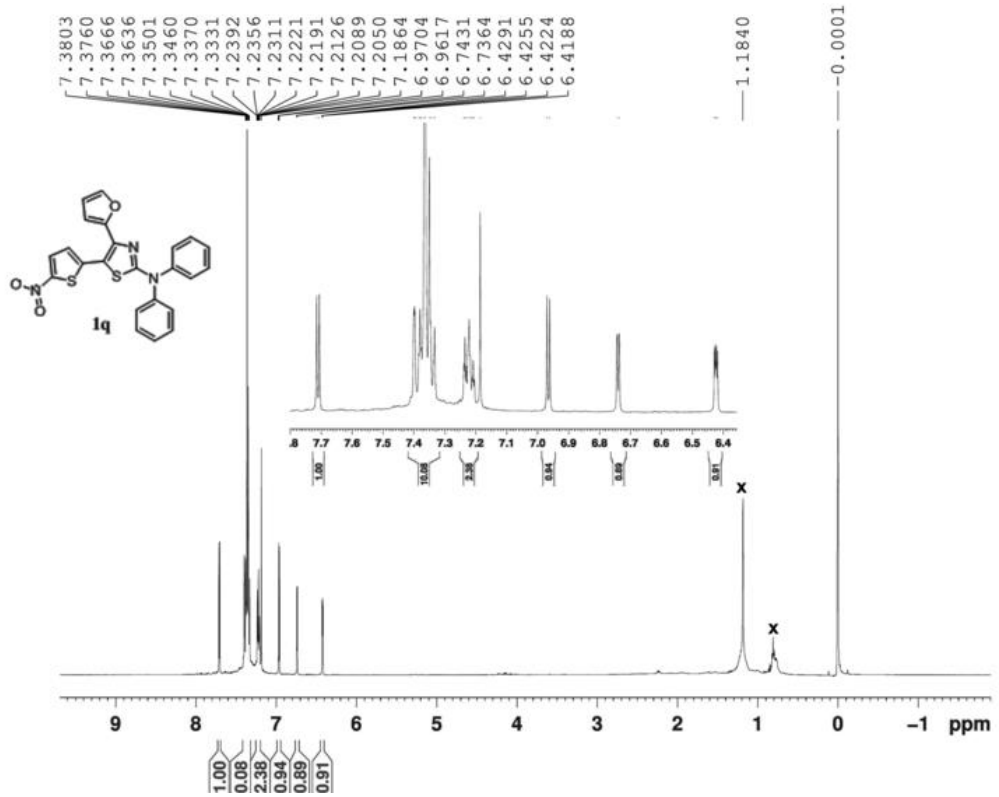

Figure 3.58: [1]H NMR spectrum of **1q**

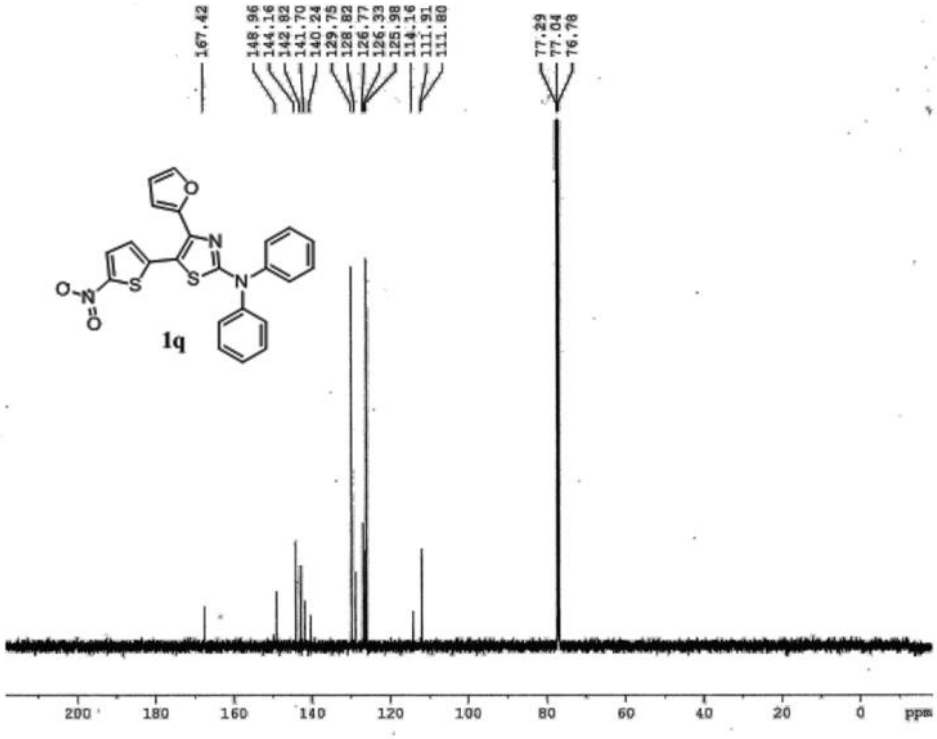

Figure 3.59: ^{13}C NMR spectrum of **1q**

4-([1,1'-biphenyl]-4-yl)-5-(5-nitrothiophen-2-yl)-N,N-diphenylthiazol-2-amine (**1r**)

Purified by column chromatography with 2% ethyl acetate: petroleum ether. Yield: 329 mg (62%). Red solid, m.p. 211.5-212.4°C. ^{1}H NMR (500 MHz, $CDCl_3$, ppm): δ= 6.70 (d, *J*=4.0 Hz, 1H), 7.17-7.22 (m, 2H), 7.28-7.30 (m, 1H), 7.33-7.40 (m, 10H), 7.54-7.58 (m, 6H), 7.62 (d, *J*=4.5 Hz, 1H); ^{13}C NMR (125 MHz, $CDCl_3$, ppm): δ= 114.8, 125.1, 126.0, 126.7, 127.1, 127.4, 127.7, 128.9, 129.1, 129.7, 129.8, 133.0, 140.4, 141.0, 144.3, 142.9, 151.3, 167.7. HRMS (ESI) calc. $C_{31}H_{22}N_3O_2S_2$ $[M+H]^+$: 532.1148, found : 532.1149.

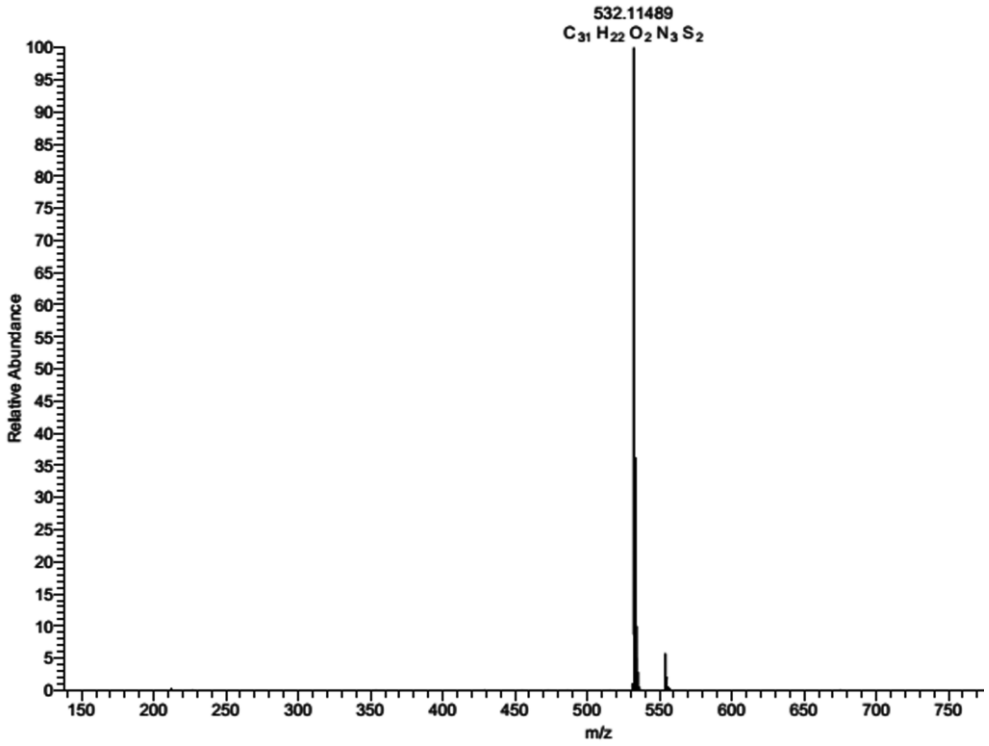

Figure 3.60: HR-MS spectrum of **1r**

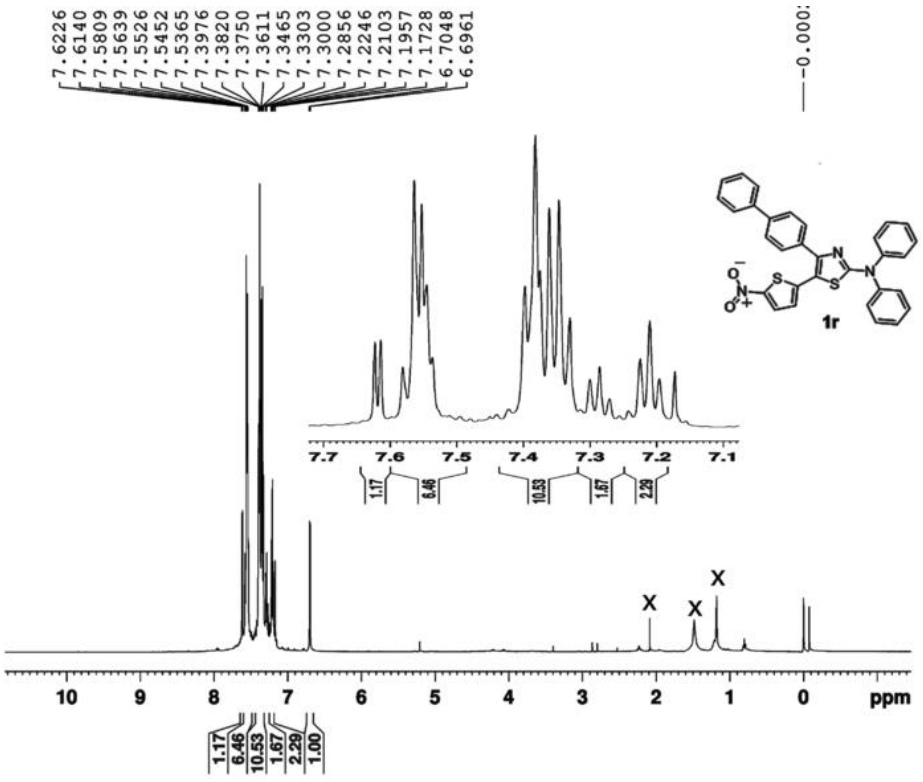

Figure 3.61: ^{1}H NMR spectrum of **1r**

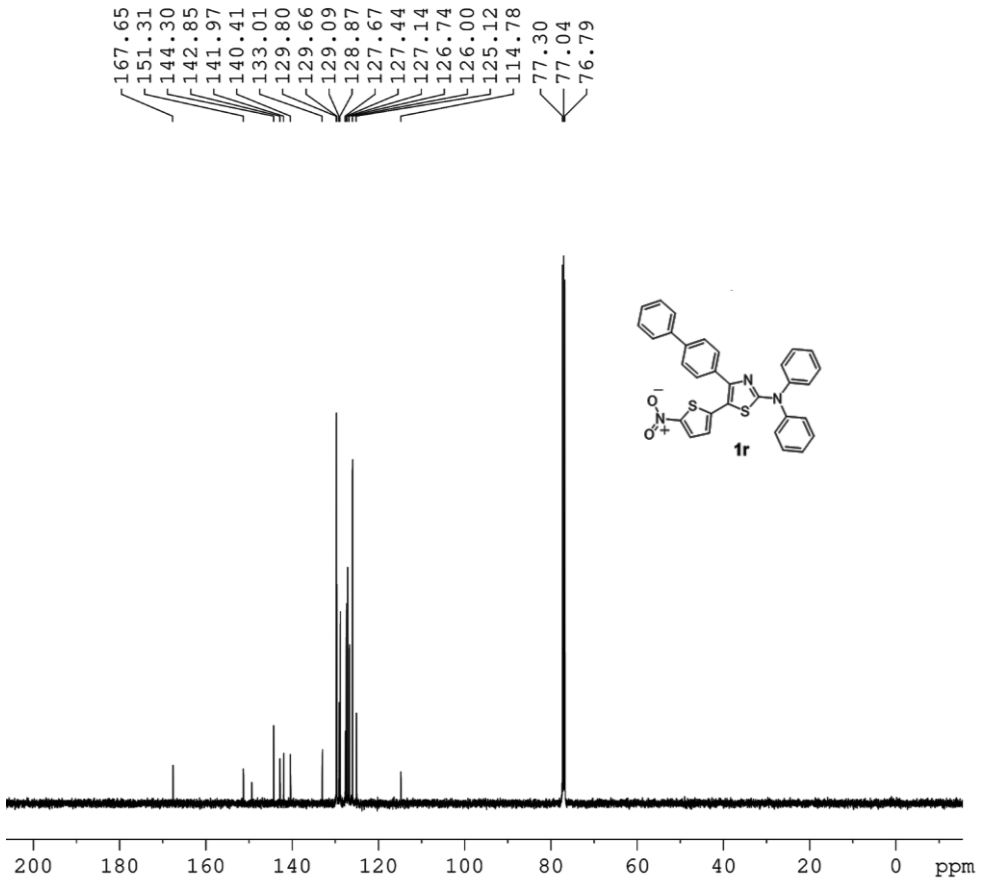

Figure 3.62: ^{13}C NMR spectrum of **1r**

4-(naphthalen-1-yl)-5-(5-nitrothiophen-2-yl)-N,N-diphenylthiazol-2-amine (**1s**)

Purified by column chromatography with 2% ethyl acetate: petroleum ether. Yield: 303 mg (60%). Red solid, m.p. 207.4-208.2°C. ^{1}H NMR (500 MHz, $CDCl_3$, ppm): δ=6.49 (d, *J*=4.5 Hz, 1H), 7.25-7.28 (m, 3H), 7.39-7.42 (m, 4H), 7.47-7.50 (m, 5H), 7.52-7.53 (m, 2H), 7.56-7.59 (m, 2H), 7.79 (d, *J*=8.5 Hz, 1H), 7.92 (d, *J*=8.0 Hz, 1H), 7.99 (d, *J*=8.0 Hz, 1H); ^{13}C NMR (125 MHz, $CDCl_3$, ppm): δ=118.4, 121.4, 123.3, 125.1, 125.7, 126.0, 126.4, 126.8, 126.8, 128.3, 128.6, 128.8, 129.9, 129.9, 130.2, 131.7, 131.8, 134.1, 142.7, 144.3, 148.8, 151.0, 167.6. HRMS (ESI) calc. $C_{29}H_{20}N_3O_2S_2$ $[M+H]^+$: 506.0991, found: 506.0993.

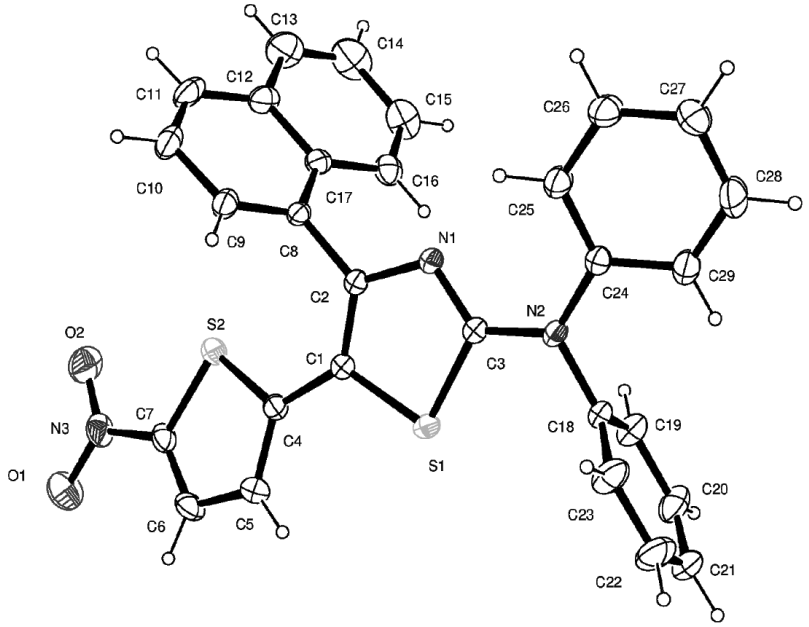

Figure 3.63: Ortep diagram of **1s** (recrystallized from ethanol) with 20 % probability ellipsoid

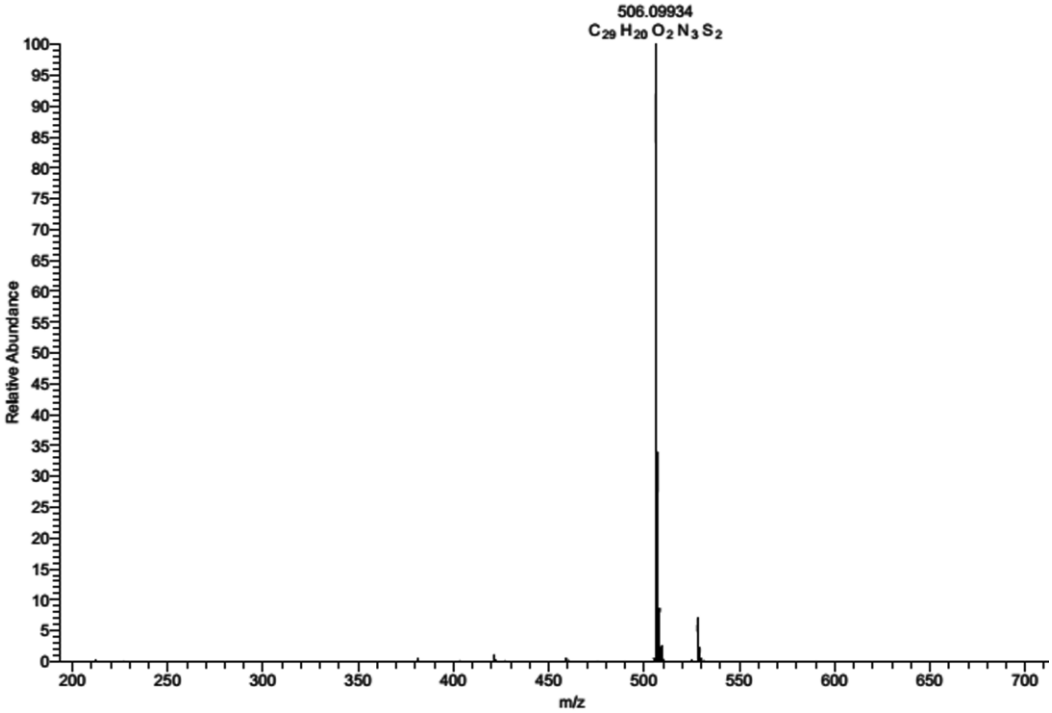

Figure 3.64: HR-MS spectrum of **1s**

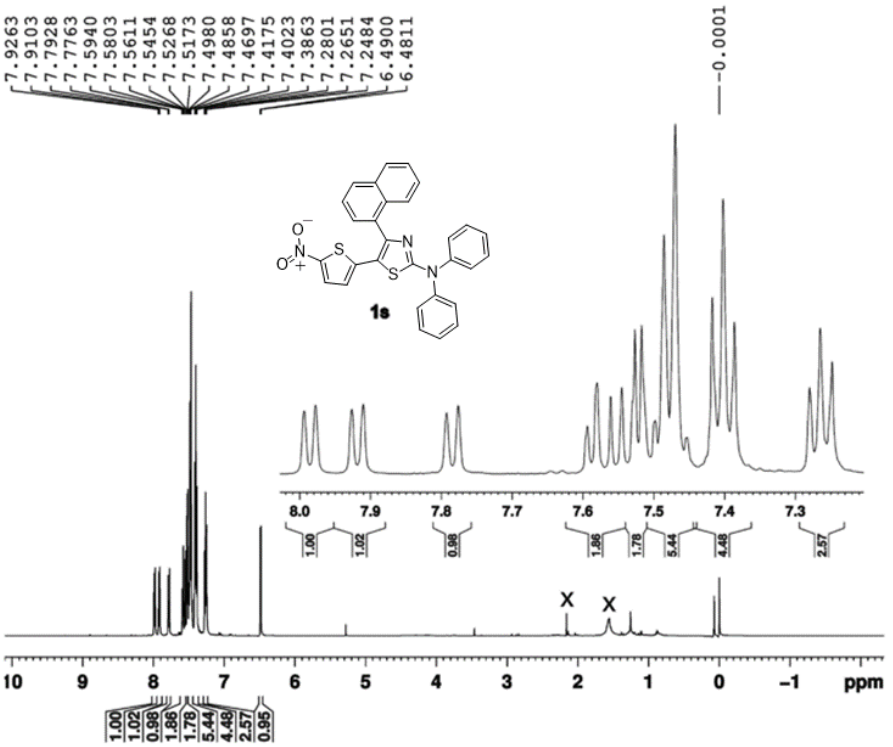

Figure 3.65: ^{1}H NMR spectrum of **1s**

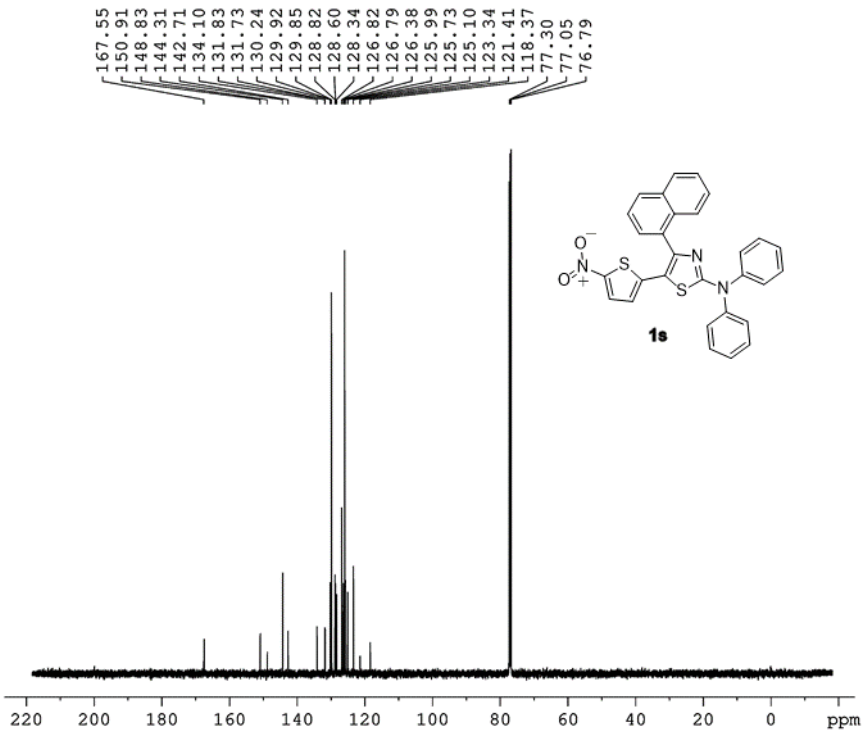

Figure 3.66: ^{13}C NMR spectrum of **1s**

4-(benzofuran-2-yl)-5-(5-nitrothiophen-2-yl)-N,N-diphenylthiazol-2-amine (**1t**)

Purified by column chromatography with 2% ethyl acetate: petroleum ether. Yield: 257 mg (52%). Red solid, m.p. 165.8-166.1°C. ^{1}H NMR (500 MHz, $CDCl_3$, ppm): δ=7.13 (d, *J*=4.5 Hz, 1H), 7.23-7.26 (m, 1H), 7.30-7.33 (m, 3H), 7.43-7.48 (m, 10H), 7.82 (d, *J*=4.5 Hz, 1H); ^{13}C NMR (125 MHz, $CDCl_3$, ppm): δ=107.9, 111.5, 116.1, 121.5, 123.5, 124.8, 125.4, 126.0, 126.1, 126.6, 126.9, 127.0, 128.2, 128.7, 129.7, 129.8, 139.8, 141.2, 144.2, 150.3, 150.7, 154.8, 167.5. HRMS (ESI) calc. $C_{27}H_{18}N_3O_3S_2$ $[M+H]^+$: 496.0784, found: 496.0796.

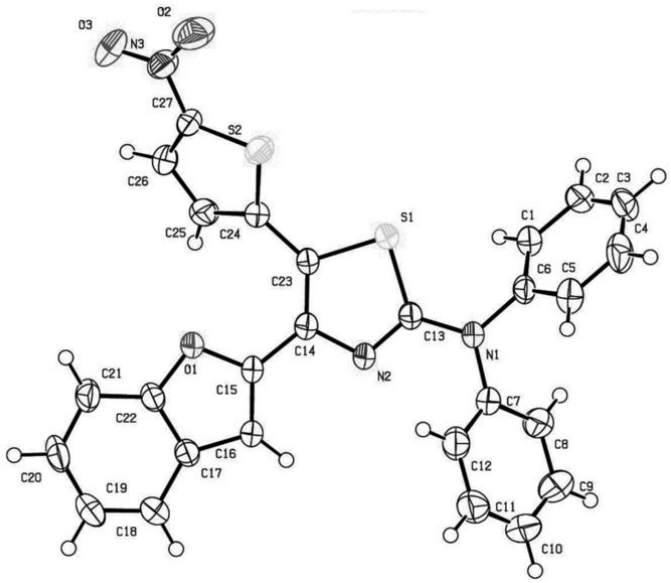

Figure 3.67: Ortep diagram of **1t** (recrystallized from ethanol) with 50 % probability ellipsoid

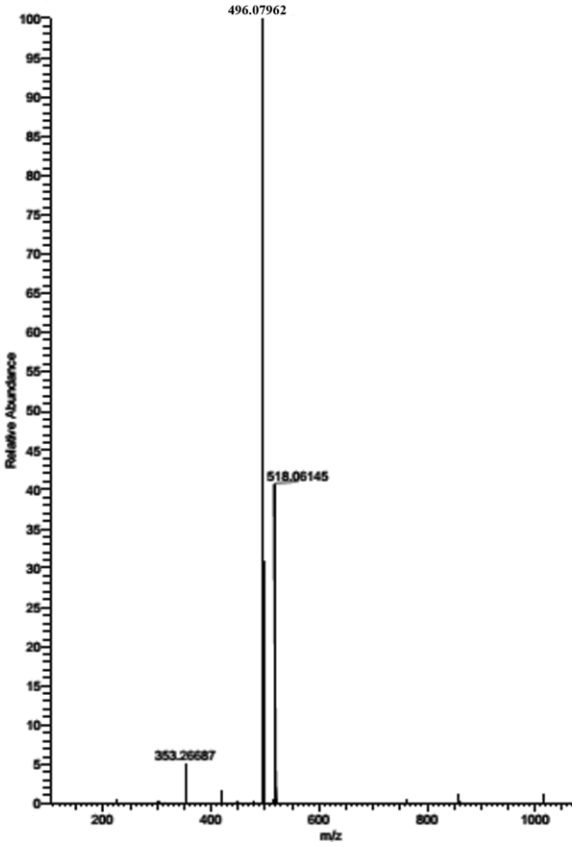

Figure 3.68: HR-MS spectrum of **1t**

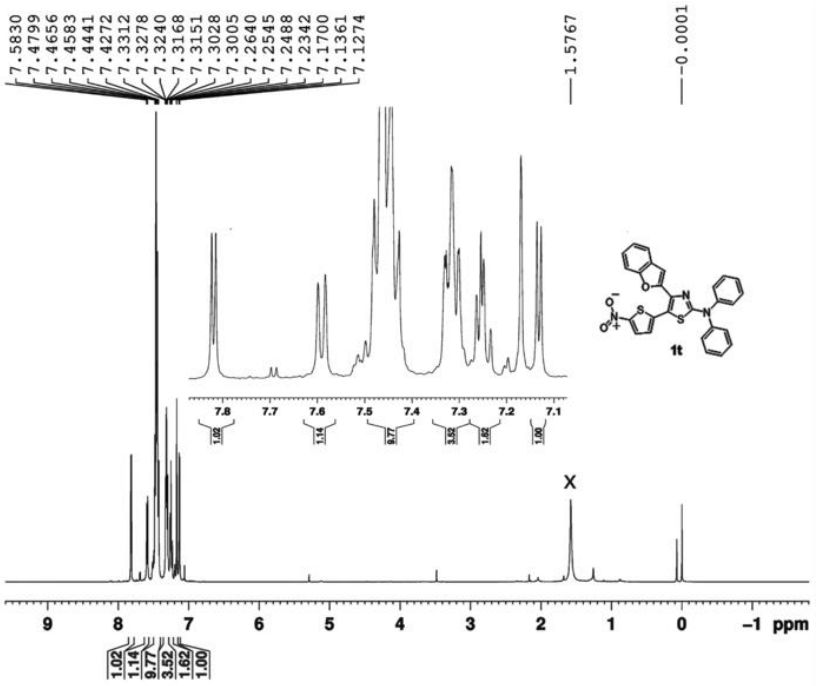

Figure 3.69: ^{1}H NMR spectrum of **1t**

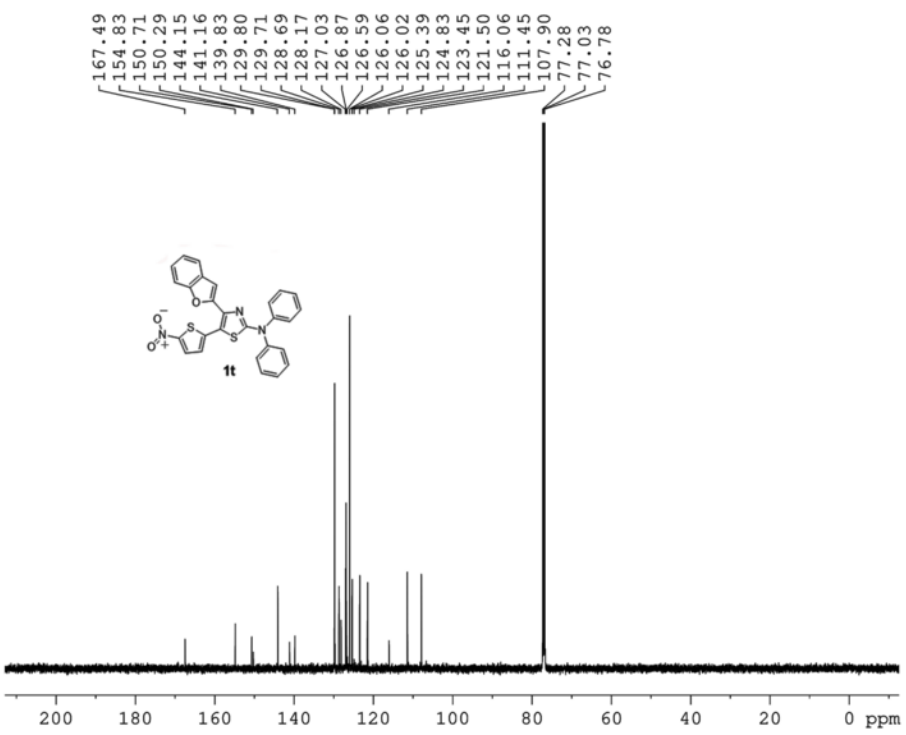

Figure 3.70: ^{13}C NMR spectrum of **1t**

4-(4-(dimethylamino)phenyl)-5-(5-nitrothiophen-2-yl)-N,N-diphenylthiazol-2-amine (**1u**)

Purified by column chromatography with 2% ethyl acetate: petroleum ether. Yield: 130 mg (26%). Red solid, m.p. 133.4-134.7°C. ^{1}H NMR (500 MHz, $CDCl_3$, ppm): δ=3.01 (s, 3H), 6.69 (d, *J*=9 Hz, 2H), 6.74 (d, *J*=4.0 Hz, 1H), 7.25-7.28 (m, 2H), 7.38-7.45 (m, 10H), 7.68 (d, *J*=4.5 Hz, 1H); ^{13}C NMR (125 MHz, $CDCl_3$, ppm): δ=40.3, 112.0, 113.4, 122.4, 124.3, 126.0, 126.6, 129.2, 129.7, 130.3, 144.2, 144.4, 148.4, 151.0, 152.9, 167.2. HRMS (ESI) calc. $C_{27}H_{23}N_4O_2S_2$ $[M+H]^+$: 499.1257, found: 499.1268.

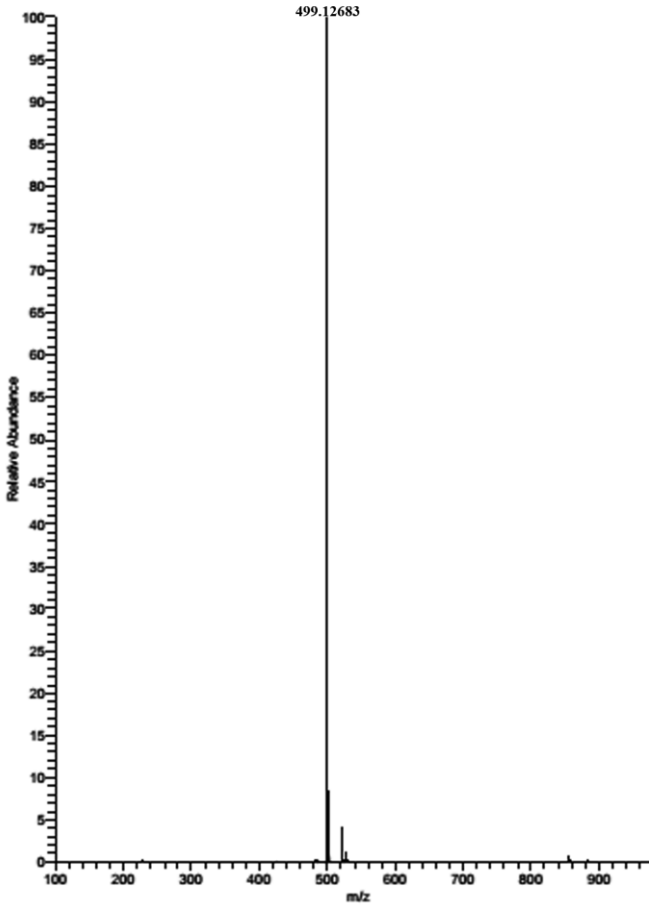

Figure 3.71: HR-MS spectrum of **1u**

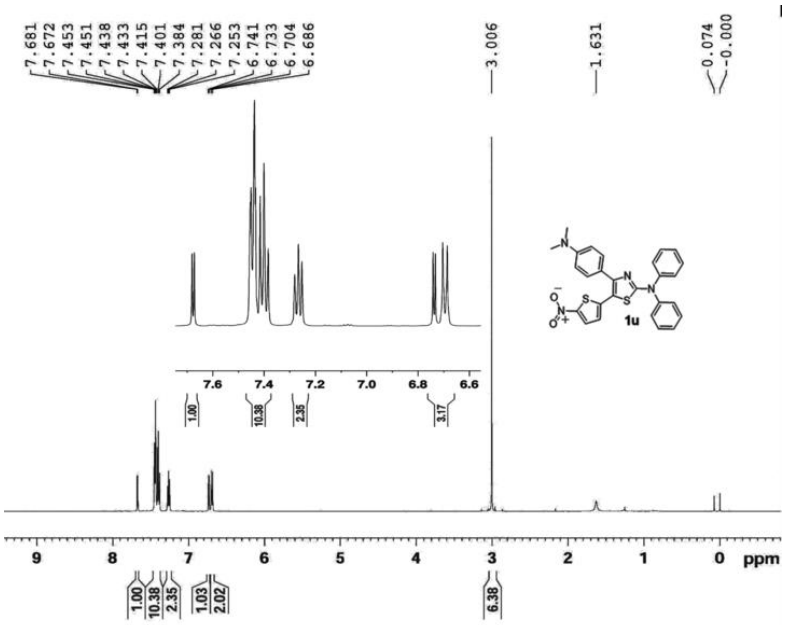

Figure 3.72: ^{1}H NMR spectrum of **1u**

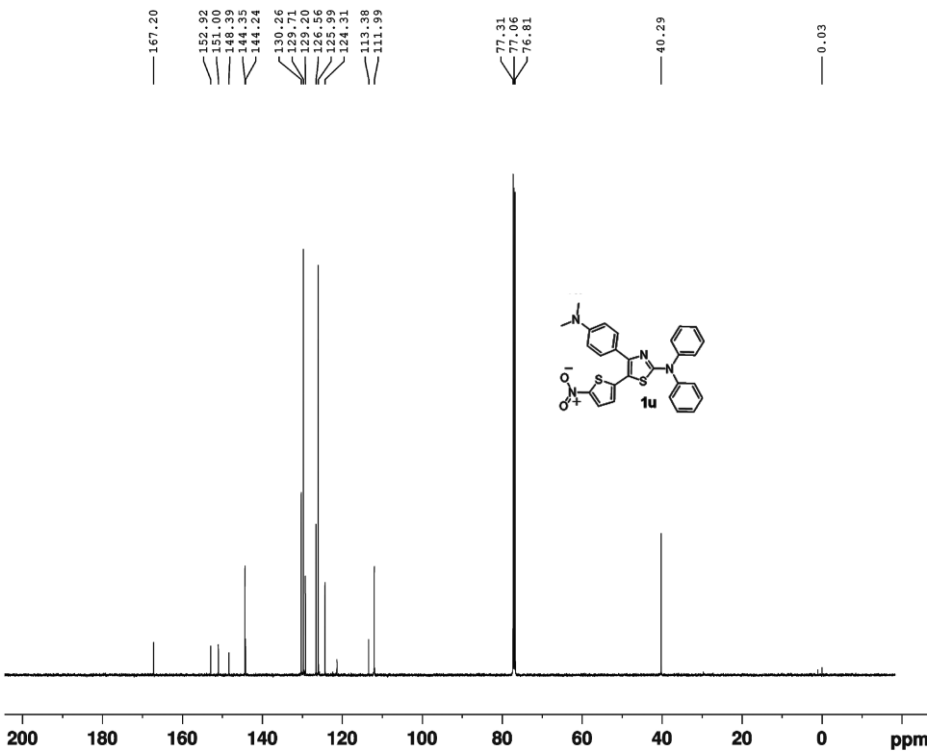

Figure 3.73: ^{13}C NMR spectrum of **1u**

4-benzhydryl-5-(5-nitrothiophen-2-yl)-N,N-diphenylthiazol-2-amine (**1v**)

Purified by column chromatography with 2% ethyl acetate: petroleum ether. Yield: 251 mg (46%). Red solid, m.p. 206.3-207.5°C. ^{1}H NMR (500 MHz, $CDCl_3$, ppm): δ=5.58 (s, 1H), 6.69 (d, *J*=4.5 Hz, 1H), 7.15-7.19 (m, 3H), 7.21-7.31 (m, 17H), 7.69 (d, *J*=4.5 Hz, 1H); ^{13}C NMR (125 MHz, $CDCl_3$, ppm): δ= 51.6, 115.8, 124.6, 125.7, 126.1, 126.5, 126.6, 126.8, 127.6, 128.1, 128.4, 128.5, 129.3, 129.4, 129.5, 129.6, 141.9, 142.3, 143.9, 144.1, 149.5, 153.6, 166.9. HRMS (ESI) calc. $C_{32}H_{24}N_3O_2S_2$ $[M+H]^+$: 546.1304, found: 546.1318.

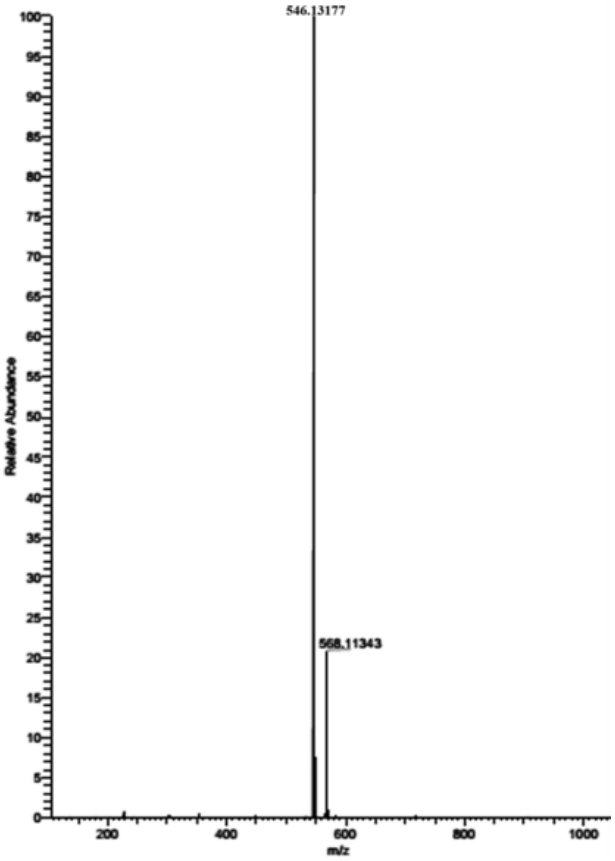

Figure 3.74: HR-MS spectrum of **1v**

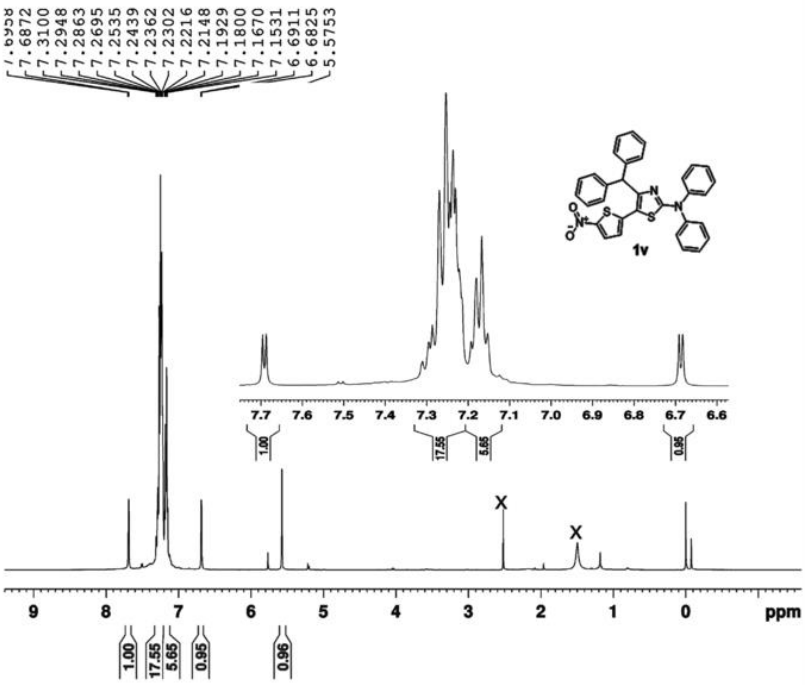

Figure 3.75: ^{1}H NMR spectrum of **1v**

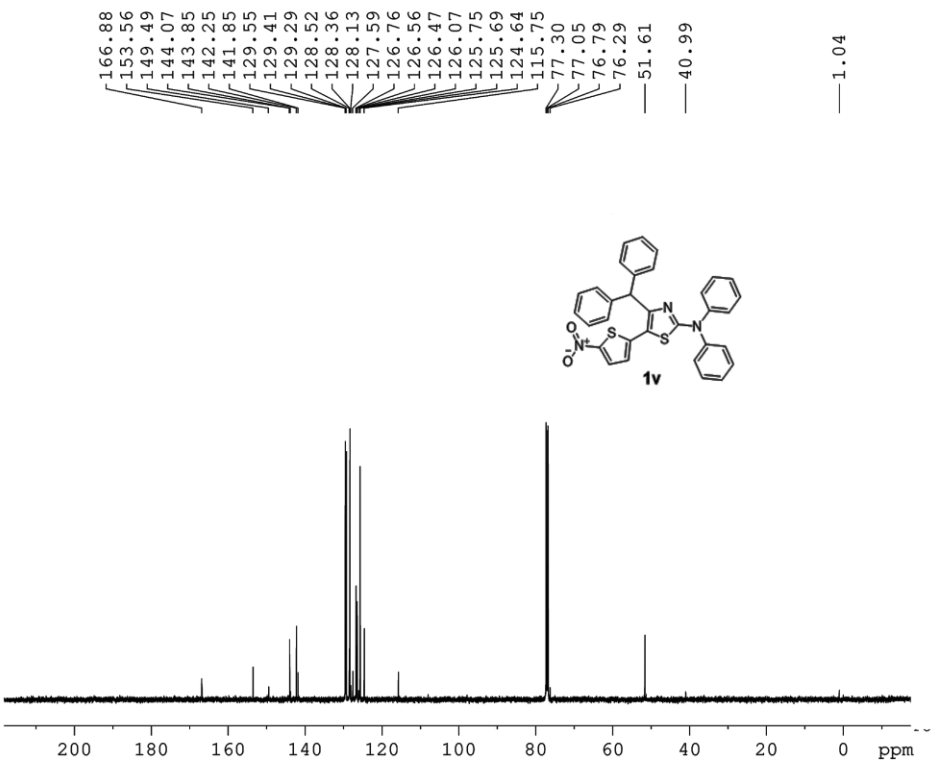

Figure 3.76: ^{13}C NMR spectrum of **1v**

N,N-dimethyl-5-(5-nitrofuran-2-yl)-4-phenylthiazol-2-amine (**2a**)

Purified by column chromatography with 3% ethyl acetate: petroleum ether. Yield: 230 mg (73%). Red solid, m.p. 166.5-166.9°C. ^{1}H NMR (500 MHz, $CDCl_3$, ppm): δ= 3.20 (s, 6H), 6.03 (d, *J*=4.0 Hz, 1H), 7.21 (d, *J*=4.0 Hz, 1H), 7.42-7.44 (m, 3H), 7.58-7.60 (m, 2H); ^{13}C NMR (125 MHz, $CDCl_3$, ppm): δ= 40.3, 107.5, 108.5, 115.0, 128.7, 129.0, 129. 3, 135.0, 150.2, 152.3, 154.7, 170.3. HRMS (ESI) calc. $C_{15}H_{14}N_3O_3S$ $[M+H]^+$: 316.0750, found: 316.0752.

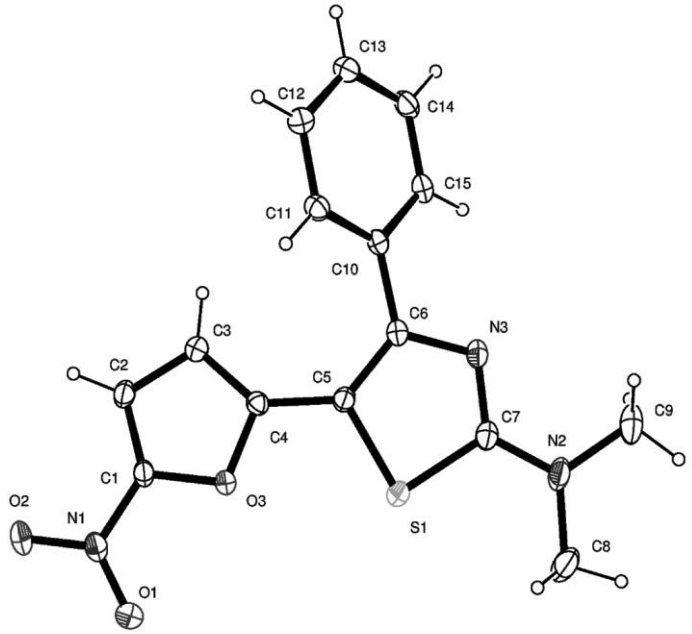

Figure 3.77: Ortep diagram of **2a** (recrystallized from ethanol) with 20 % probability ellipsoid (CCDC number: 1585486)

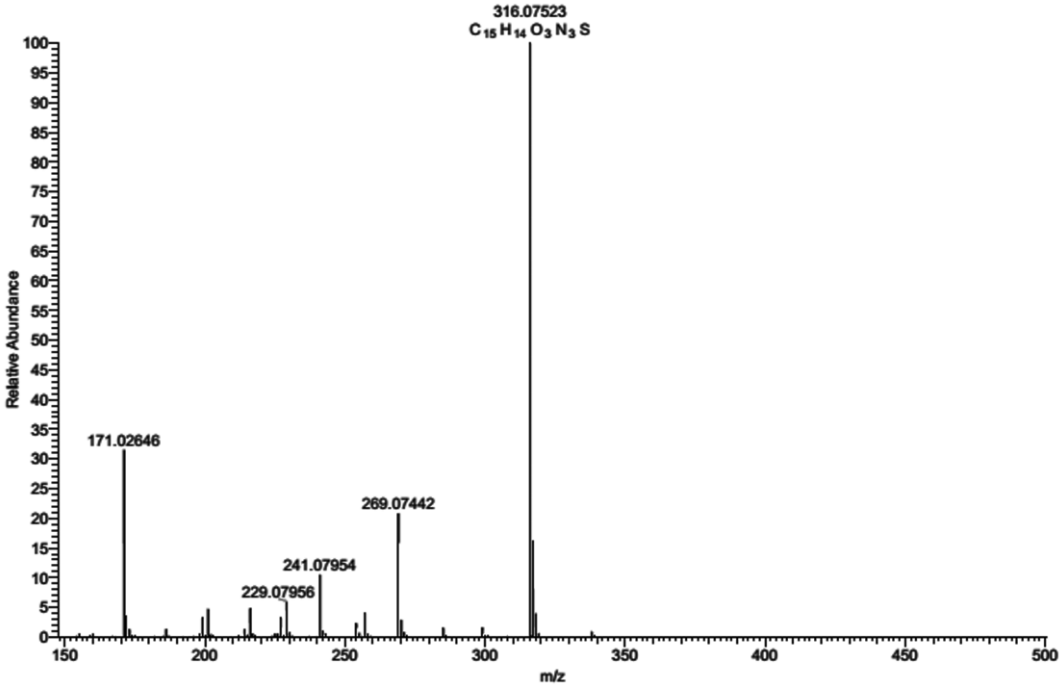

Figure 3.78: HR-MS spectrum of **2a**

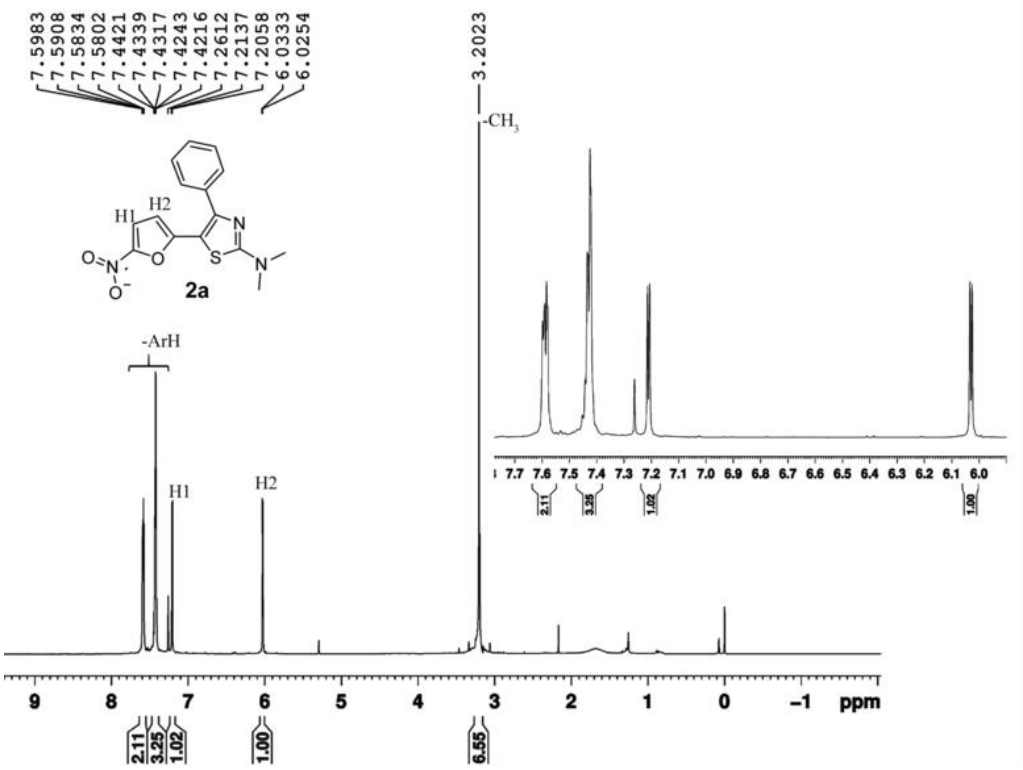

Figure 3.79: [1]H NMR spectrum of **2a**

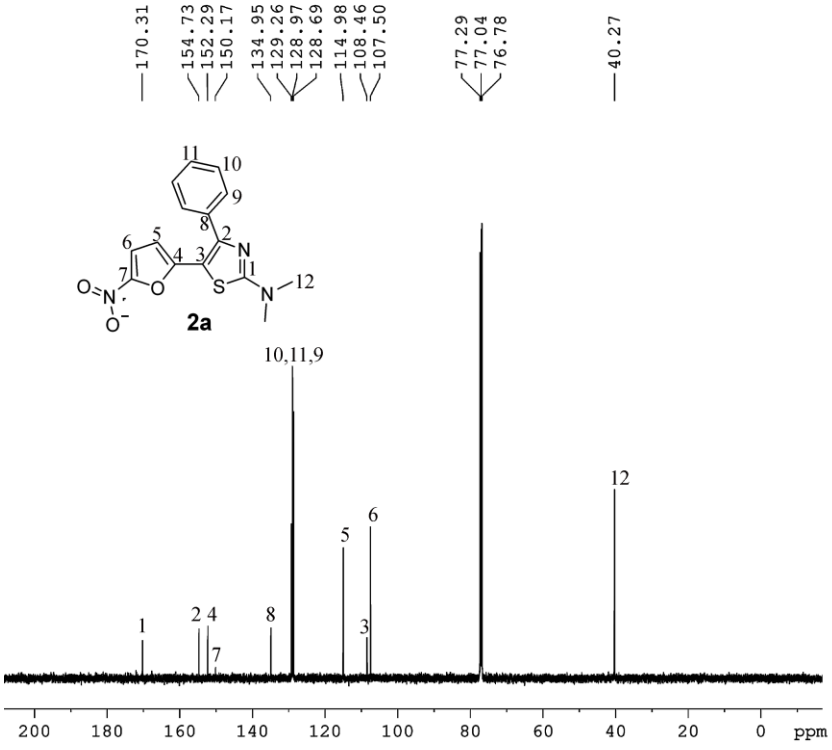

Figure 3.80: [13]C NMR spectrum of **2a**

N,N-diethyl-5-(5-nitrofuran-2-yl)-4-phenylthiazol-2-amine (**2b**)

Purified by column chromatography with 3% ethyl acetate: petroleum ether. Yield: 277 mg (81%). Red solid, m.p. 119.3-120.3°C. ^{1}H NMR (500 MHz, $CDCl_3$, ppm): δ=1.22 (t, *J*=7 Hz, 6H), 3.50 (q, *J*=7 Hz, 4H), 5.95 (d, *J*=4.0 Hz, 1H), 7.14 (d, *J*=4.0 Hz, 1H), 7.35-7.37 (m, 3H), 7.51-7.53 (m, 2H); ^{13}C NMR (125 MHz, $CDCl_3$, ppm): δ=12.6, 45.8, 107.3, 107.4, 115.1, 128.6, 129.0, 129.2, 135.1, 150.5, 152.6, 154.8, 168.9. HRMS (ESI) calc. $C_{17}H_{18}N_3O_3S$ $[M+H]^+$: 344.1063, found: 344.1066.

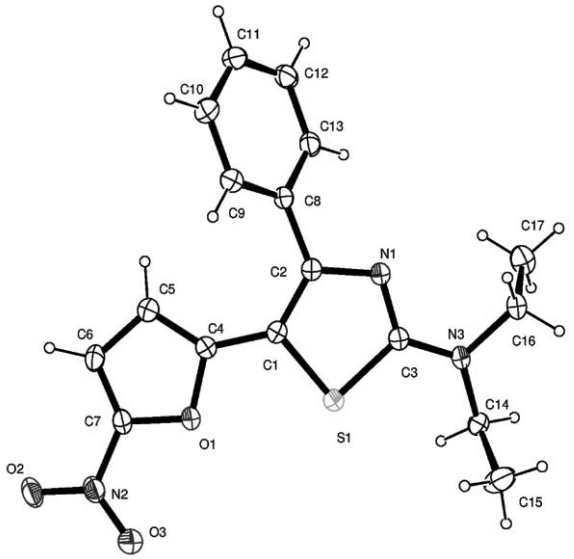

Figure 3.81: Ortep diagram of **2b** (recrystallized from ethanol) with 20 % probability ellipsoid

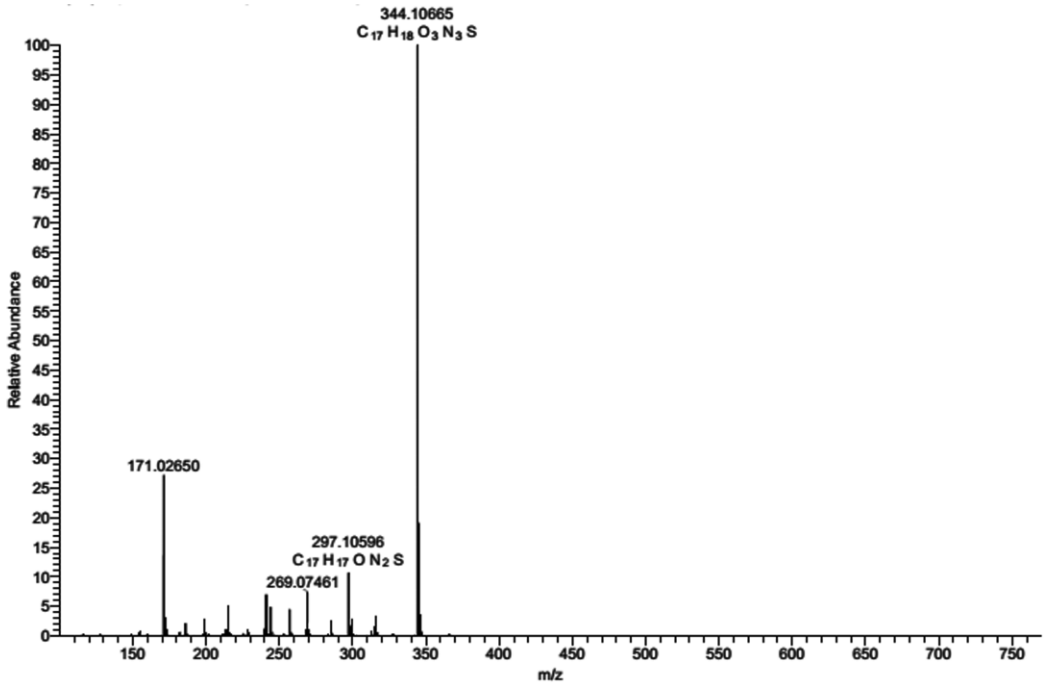

Figure 3.82: HR-MS spectrum of **2b**

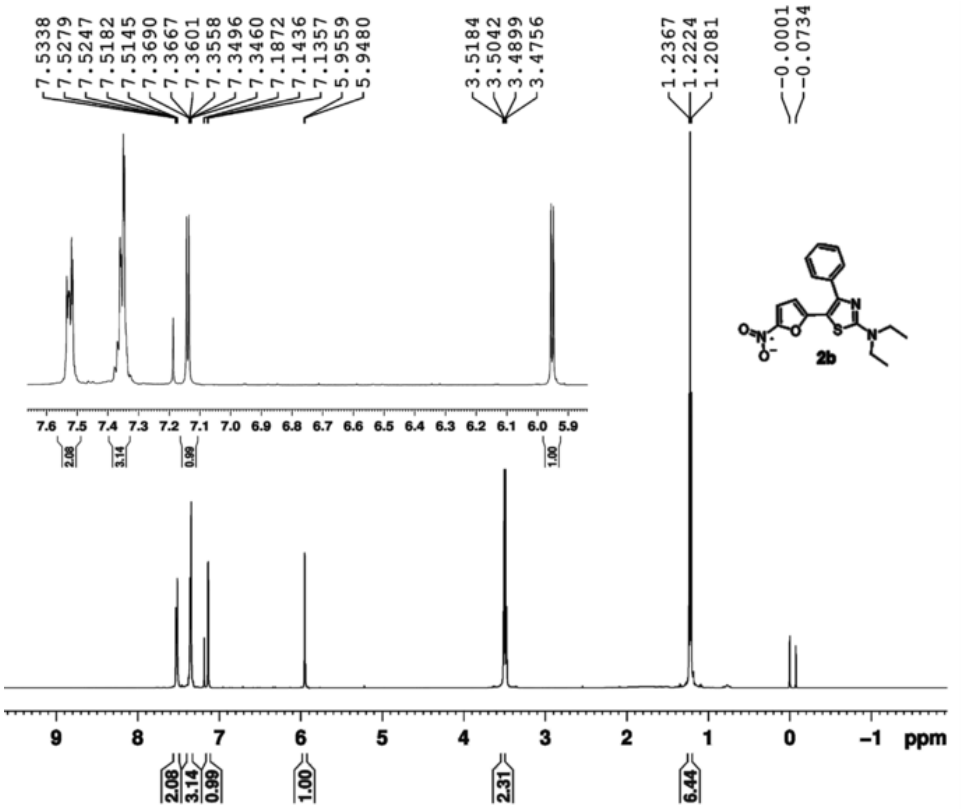

Figure 3.83: [1]H NMR spectrum of **2b**

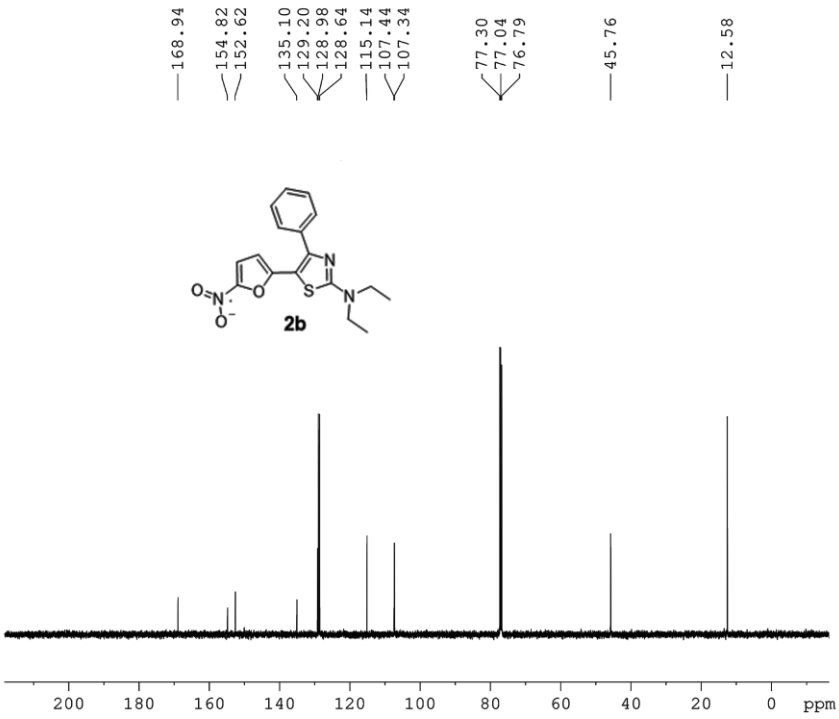

Figure 3.84: ^{13}C NMR spectrum of **2b**

5-(5-nitrofuran-2-yl)-4-phenyl-2-(piperidin-1-yl)thiazole (**2c**)

Purified by column chromatography with 2% ethyl acetate: petroleum ether. Yield: 259 mg (73%). Red solid, m.p. 158.4-158.7°C. ^{1}H NMR (500 MHz, $CDCl_3$, ppm): δ= 1.60-1.80 (m, 6H), 3.57-3.58 (m, 4H), 6.05 (d, *J*=4.0 Hz, 1H), 7.21 (d, *J*=4.0 Hz, 1H), 7.42-7.45 (m, 3H), 7.58 -7.60 (m, 2H); ^{13}C NMR (125 MHz, $CDCl_3$, ppm): δ=24.0, 25.2, 49.6, 108.0, 115.0, 128.6, 129.0, 129.2, 134.5, 150.2, 152.4, 154.6, 170.4. HRMS (ESI) calc. $C_{18}H_{18}N_3O_3S$ $[M+H]^+$: 356.1063, found: 356.1060.

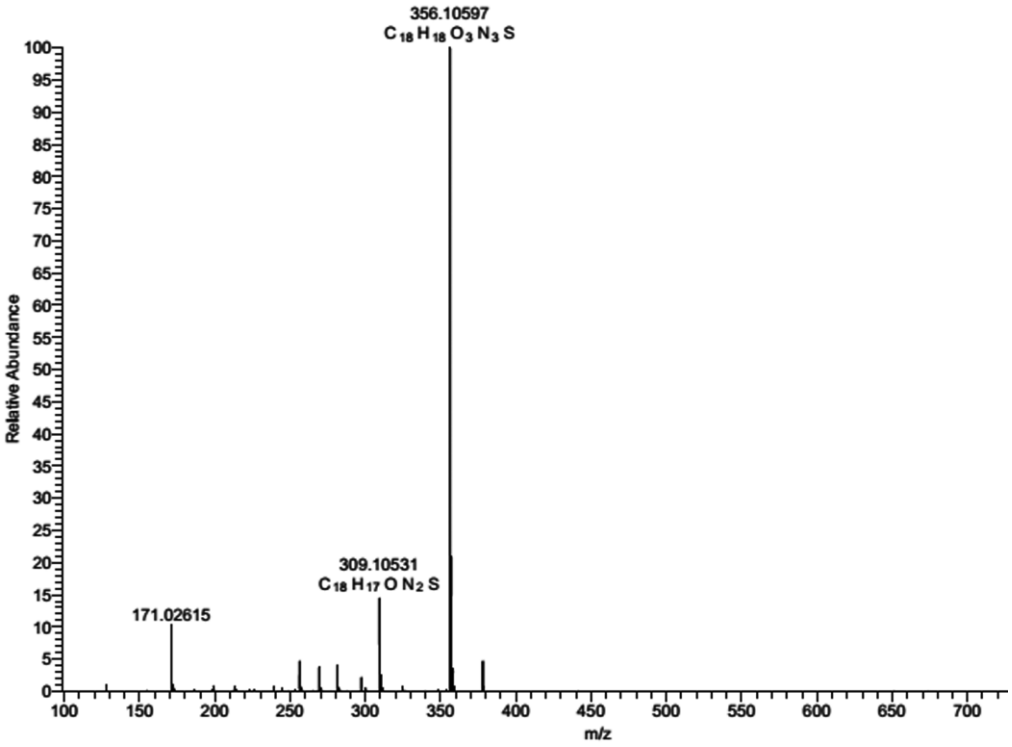

Figure 3.85: HR-MS spectrum of **2c**

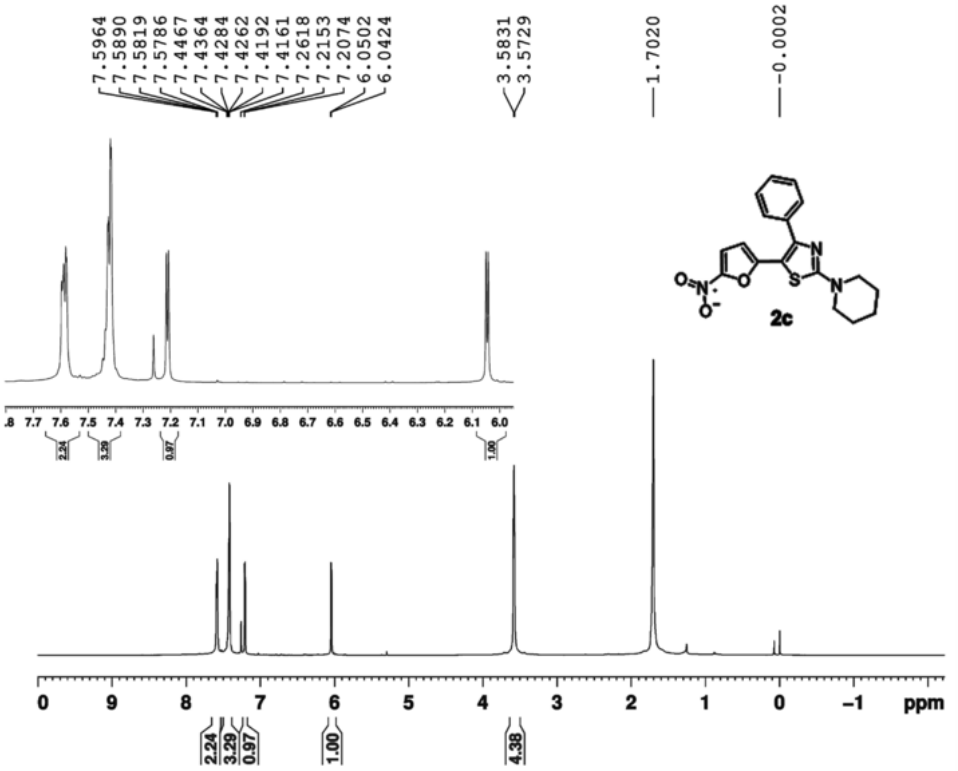

Figure 3.86: ^{1}H NMR spectrum of **2c**

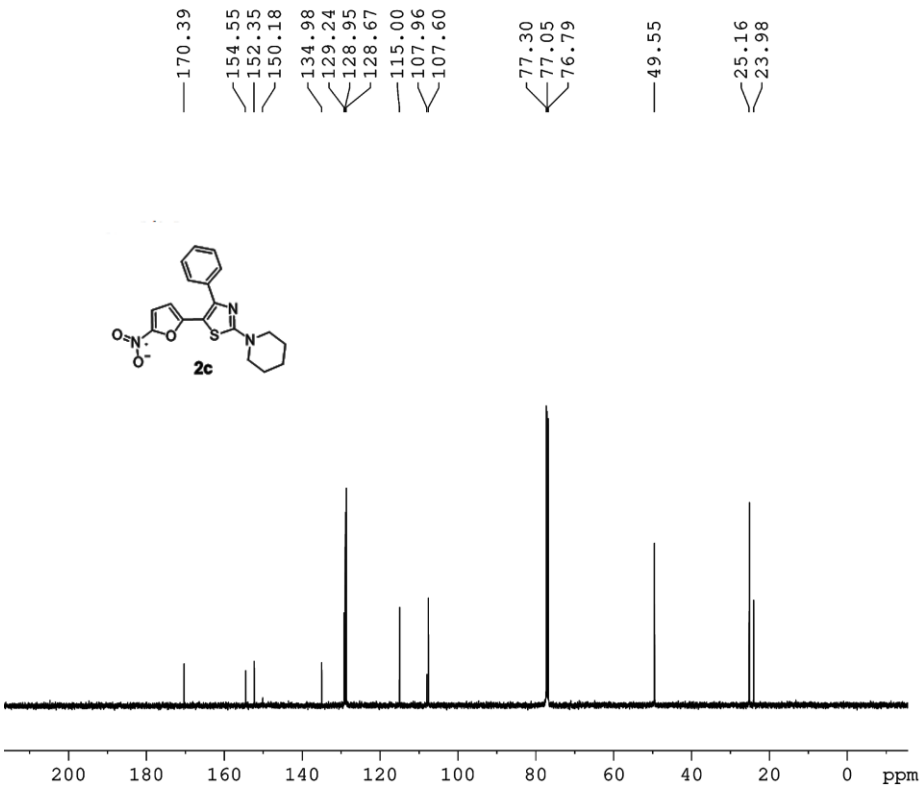

Figure 3.87: ^{13}C NMR spectrum of **2c**

4-(5-(5-nitrofuran-2-yl)-4-phenylthiazol-2-yl)morpholine (**2d**)

Purified by column chromatography with 6% ethyl acetate: petroleum ether. Yield: 292 mg (78%). Red solid, m.p. 200.2-200.5°C. ^{1}H NMR (500 MHz, $CDCl_3$, ppm): δ=3.49-3.51 (m, 4H), 3.75-3.77 (m, 4H), 6.65 (d, *J*=4.0 Hz, 1H), 7.35-7.36 (m, 3H), 7.44-7.46 (m, 2H), 7.63 (d, *J*=4.0 Hz, 1H),); ^{13}C NMR (125 MHz, $CDCl_3$, ppm): δ=47.2, 65.0, 107.1, 108.0, 113.7, 127.7, 127.9, 128.4, 133.6, 149.3, 150.6, 153.0, 169.4. HRMS (ESI) calc. $C_{17}H_{16}N_3O_4S$ $[M+H]^+$: 358.0856, found: 358.0867.

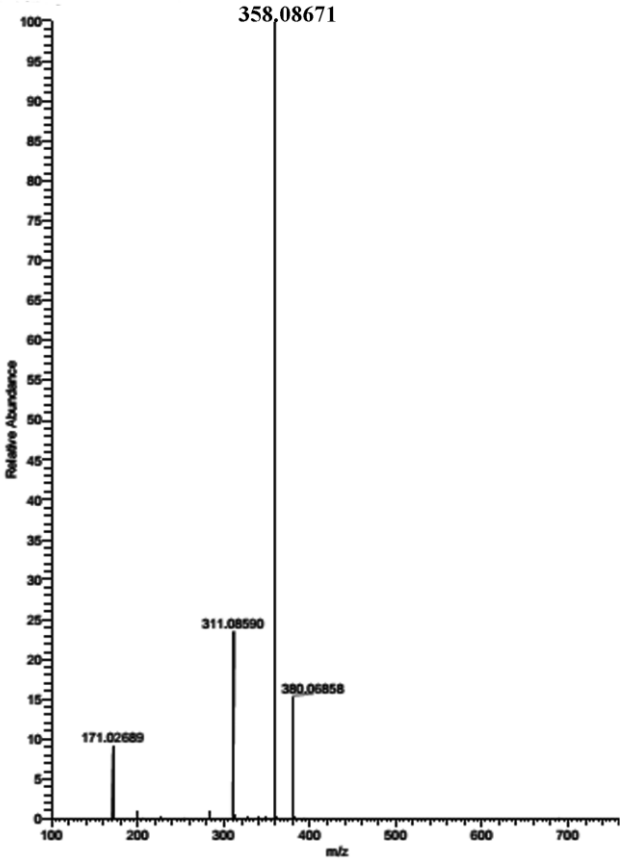

Figure 3.88: HR-MS spectrum of **2d**

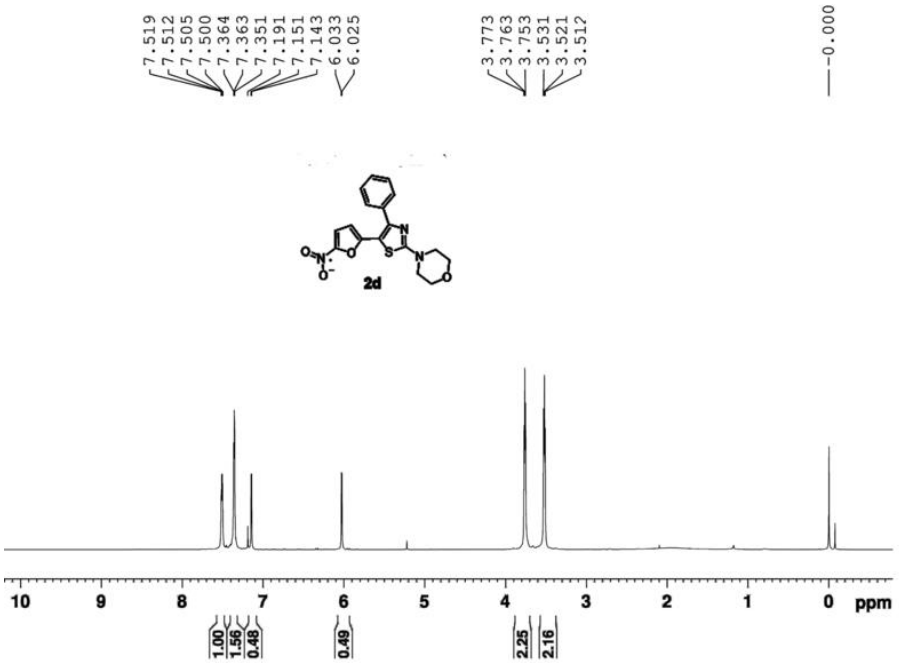

Figure 3.89: ^{1}H NMR spectrum of **2d**

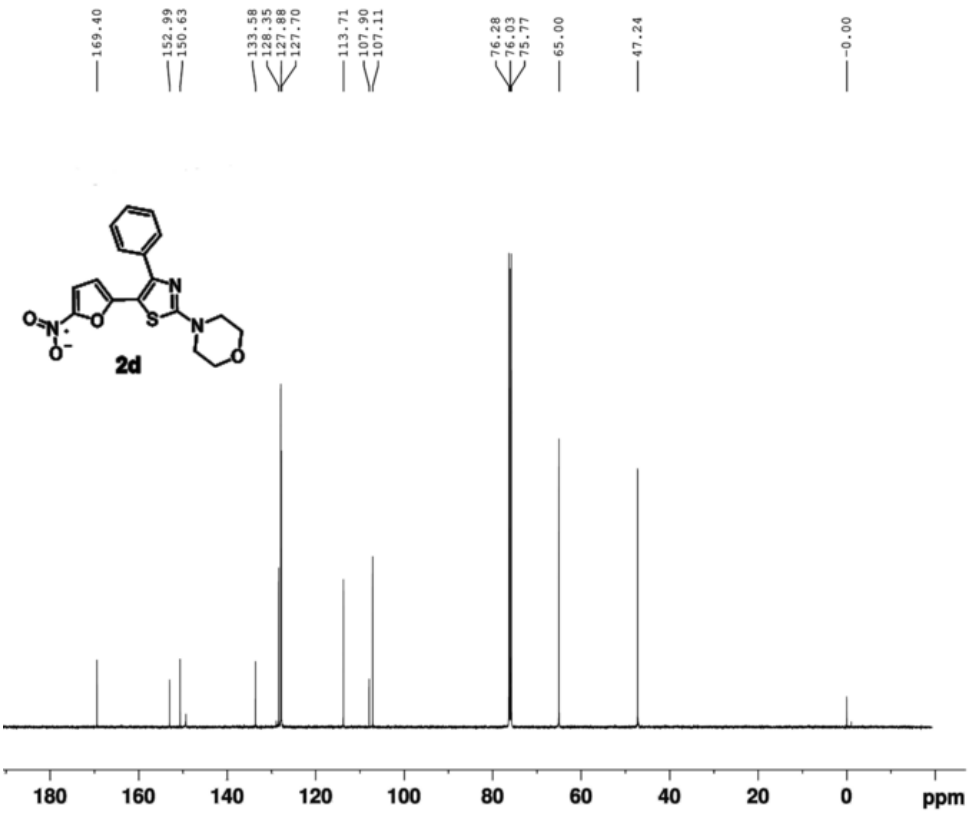

Figure 3.90: ^{13}C NMR spectrum of **2d**

5-(5-nitrofuran-2-yl)-N,N,4-triphenylthiazol-2-amine (**2e**)

Purified by column chromatography with 2% ethyl acetate: petroleum ether. Yield: 329 mg (75%). Yellow brown solid, m.p. 203.4-203.9 °C. ^{1}H NMR (500 MHz, $CDCl_3$, ppm): δ=6.16 (d, *J*=4.0 Hz, 1H), 7.20 (d, *J*=4.0 Hz, 1H), 7.27-7.31 (m, 2H), 7.40-7.47 (m, 11H), 7.60-7.62 (m, 2H); ^{13}C NMR (125 MHz, $CDCl_3$, ppm): δ=108.8, 111.0, 114.5, 126.0, 126.9, 128.6, 129.1, 129.3, 129.8, 134.5, 144.2, 150.5, 151.4, 153.5, 169.0. HRMS (ESI) calc. $C_{25}H_{18}N_3O_3S$ $[M+H]^+$: 440.1063, found: 440.1061.

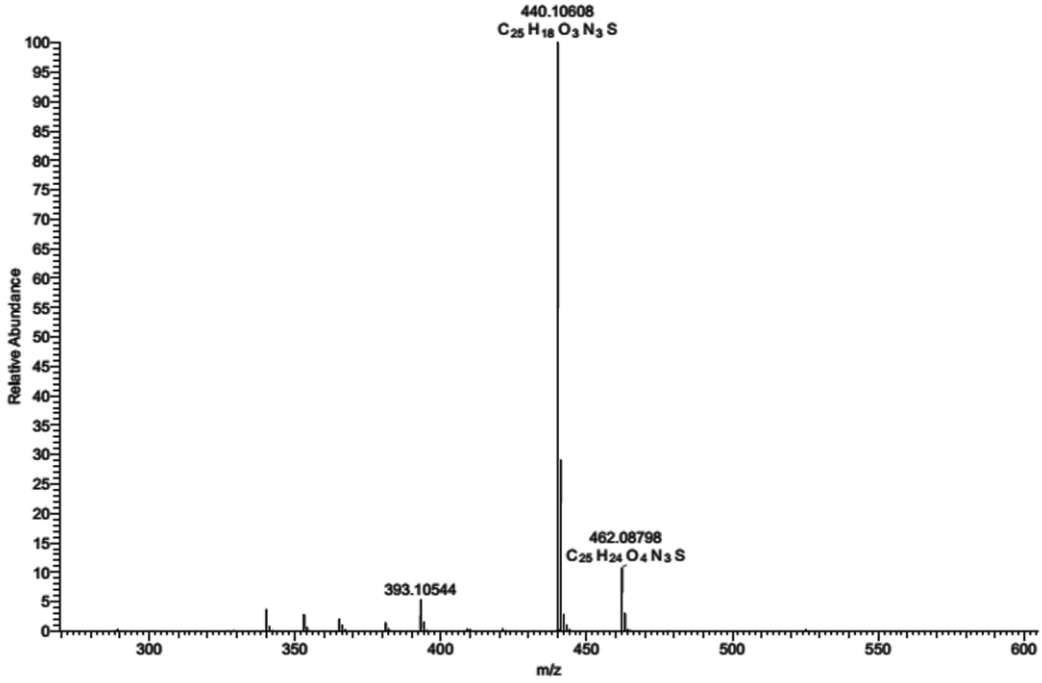

Figure 3.91: HR-MS spectrum of **2e**

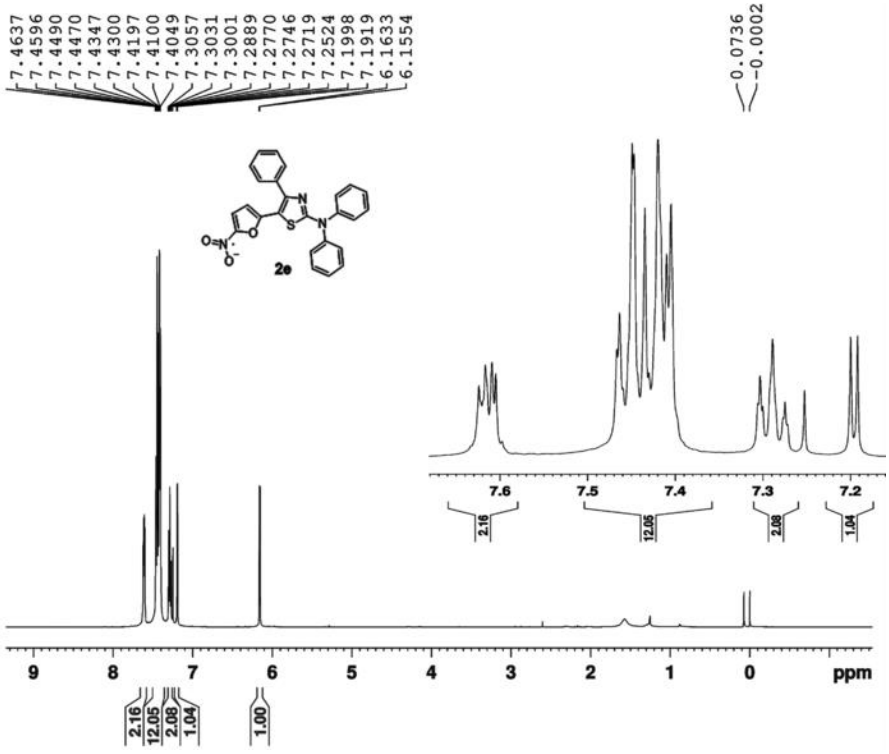

Figure 3.92: ^{1}H NMR spectrum of **2e**

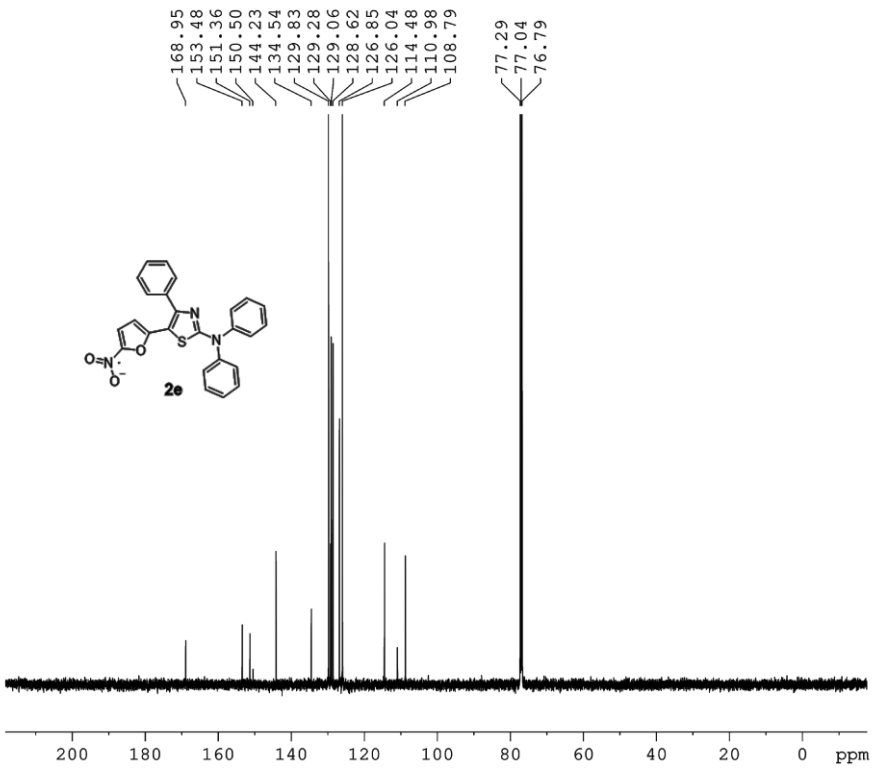

Figure 3.93: ^{13}C NMR spectrum of **2e**

5-(2-(diphenylamino)-4-phenylthiazol-5-yl)thiophene-2-carbaldehyde (**3**)

To the stirred solution of 2-bromomethyl-5-thiophene aldehyde (1mmol) in DMF (3ml), corresponding thioureas were added (1mmol) followed by triethylamine (1.2 mmol) and stirred for 30-45 minutes. The reaction mixture was added to crushed ice, product was filtered, dried and purified by column chromatography with 5% ethyl acetate: petroleum ether Yield: 110 mg (25%). Yellow solid, m.p. 200.6-200.9°C. ^{1}H NMR (500 MHz, $CDCl_3$, ppm): 6.89 (d, *J*=4.0 Hz, 1H), 7.25-7.28 (m, 2H), 7.35-7.36 (m, 3H), 7.39-7.42 (m, 4H), 7.45-7.46 (m, 4H), 7.50 (d, *J*=4.0 Hz, 1H), 7.55-7.57 (m, 2H), 9.74 (s, 1H); ^{13}C NMR (125 MHz, $CDCl_3$, ppm): δ=115.9, 125.9, 126.5, 126.9, 128.6, 128.8, 129.3, 129.7, 134.5, 136.6, 141.9, 144.5, 144.6, 150.5, 167.3, 182.3. HRMS (ESI) calc. $C_{26}H_{19}N_2OS_2$ $[M+H]^+$: 439.0933, found: 439.0940.

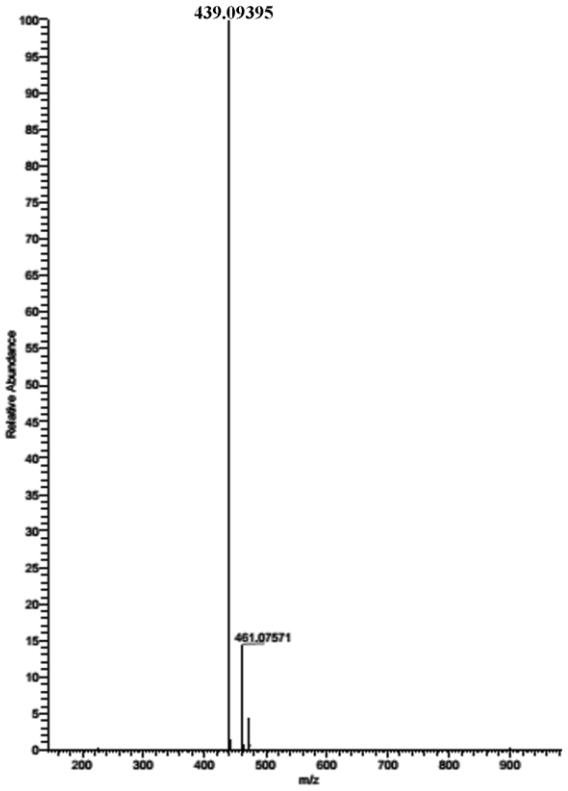

Figure 3.94: HR-MS spectrum of **3**

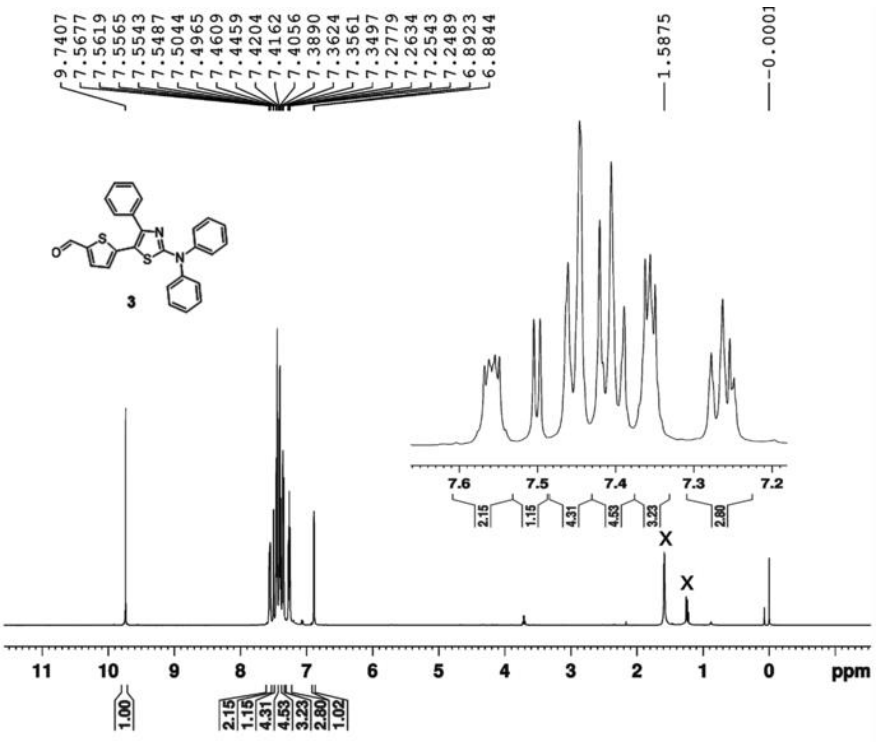

Figure 3.95: ^{1}H NMR spectrum of **3**

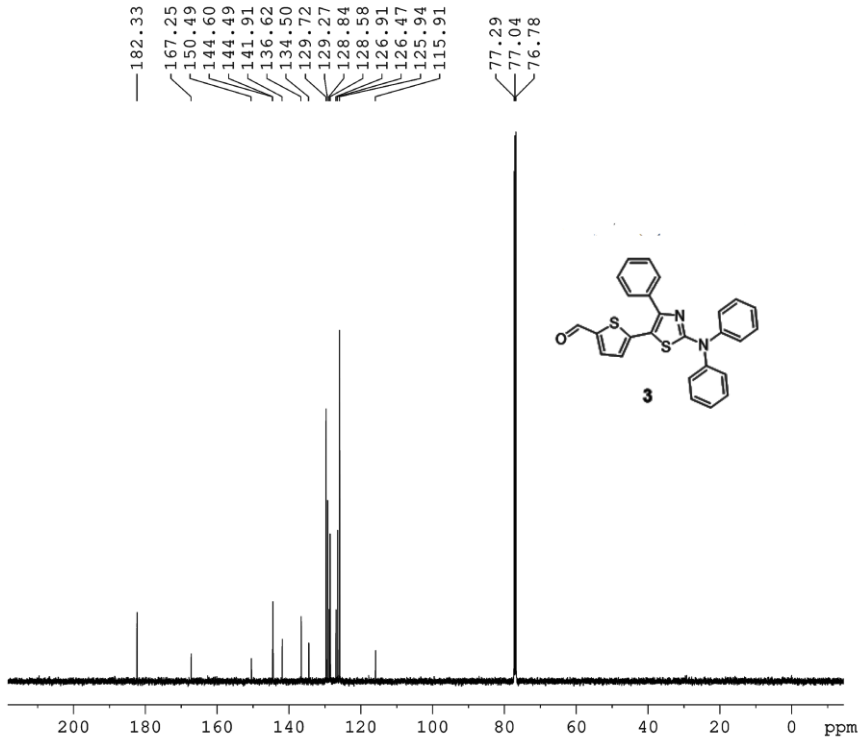

Figure 3.96: ^{13}C NMR spectrum of **3**

2-((5-(2-(diphenylamino)-4-phenylthiazol-5-yl)thiophen-2-yl)methylene)malononitrile (**4**)

To **3** (1mol) in chloroform (10ml), malononitrile (1.2mol) and catalytic amount of triethylamine were added and stirred for one hour. The solvent was evaporated and the compound was purified by column chromatography with 5% ethyl acetate: petroleum ether. Yield: 248 mg (51%). Red solid, m.p. 192.4-192.7 °C. ^1H NMR (500 MHz, $CDCl_3$, ppm): 6.84 (d, *J*=4.5 Hz, 1H), 7.28-7.31 (m, 2H), 7.40-7.48 (m, 12H), 7.55-7.57 (m, 2H) 7.58 (s, 1H); ^{13}C NMR (125 MHz, $CDCl_3$, ppm): δ=74.1, 112.5, 113.5, 114.6, 116.8, 120.0, 125.0, 125.6, 125.8, 127.8, 128.3, 128.3, 128.8, 143.2, 146.3, 148.6, 151.4, 166.9. HRMS (ESI) calc. $C_{29}H_{19}N_4S_2$ $[M+H]^+$: 487.1046, found: 487.1050.

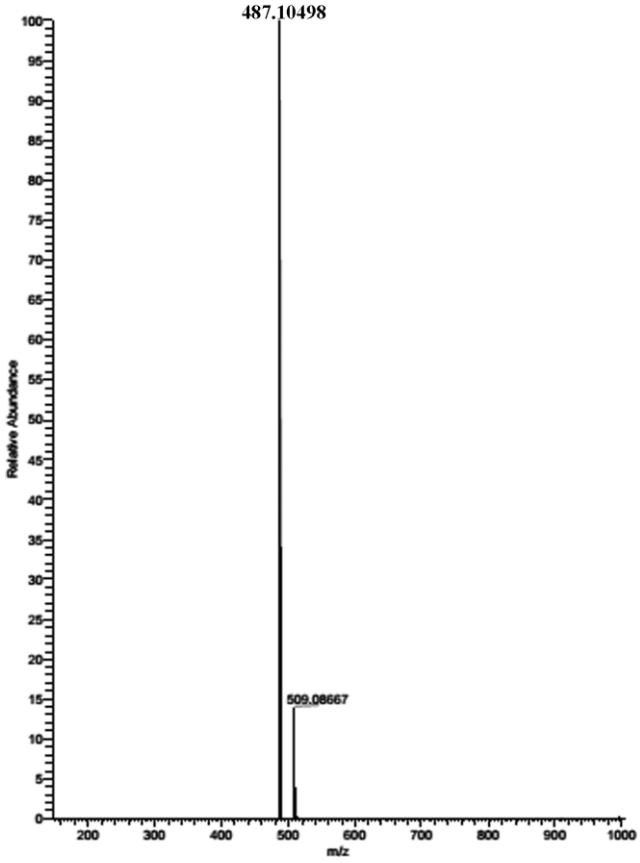

Figure 3.97: HR-MS spectrum of **4**

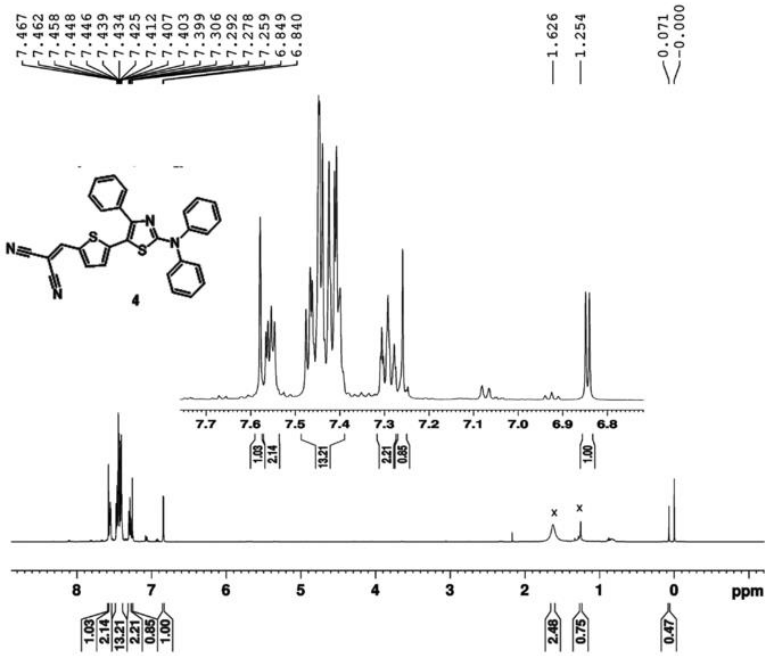

Figure 3.98: ^{1}H NMR spectrum of **4**

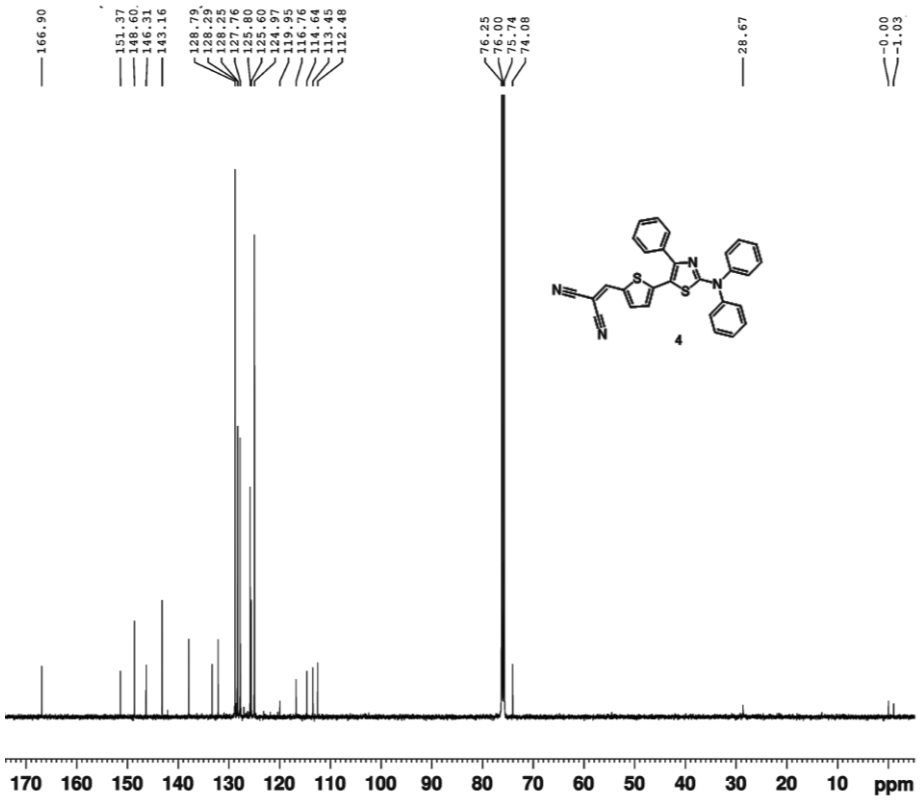

Figure 3.99: ^{13}C NMR spectrum of **4**

5-((5-(2-(diphenylamino)-4-phenylthiazol-5-yl)thiophen-2-yl)methylene)-1,3-diethyl-2-thioxodihydropyrimidine-4,6 (1H,5H)-dione (**5**)

To a solution of **3** in ethanol (10 ml), 1,3-diethyl-2-thiobarbituric acid was added and heated at 50°C for one hour. The resulting mixture was cooled and filtered and the product was purified by column chromatography with 10% ethyl acetate: petroleum ether. Yield: 173 mg (28%). Pink solid, m.p. 275-277°C. ^1H NMR (500 MHz, $CDCl_3$, ppm): 1.14 (m, 6H), 4.46-4.48 (q, 4H), 6.82 (d, *J*=4.5 Hz, 1H), 7.18-7.22 (m, 2H), 7.30-7.33 (m, 3H), 7.35-7.39 (m, 8H), 7.50-7.52 (m, 3H), 8.42 (s, 1H); ^{13}C NMR (125 MHz, $CDCl_3$, ppm): δ=11.3, 11.4, 42.0, 42.9,108.1, 113.0, 114.9, 115.5, 116.8, 119.9, 112.5, 123.0, 125.7, 125.7, 126.3, 127.6, 128.0, 128.3, 128.8, 133.9, 134.7, 138.3, 143.3, 145.9, 147.7, 151.4, 152.1, 158.8, 160.1, 167.1, 177.6. HRMS (ESI) calc. $C_{34}H_{28}N_4O_2S_3$ $[M+Na]^+$: 643.1267, found: 643.1283.

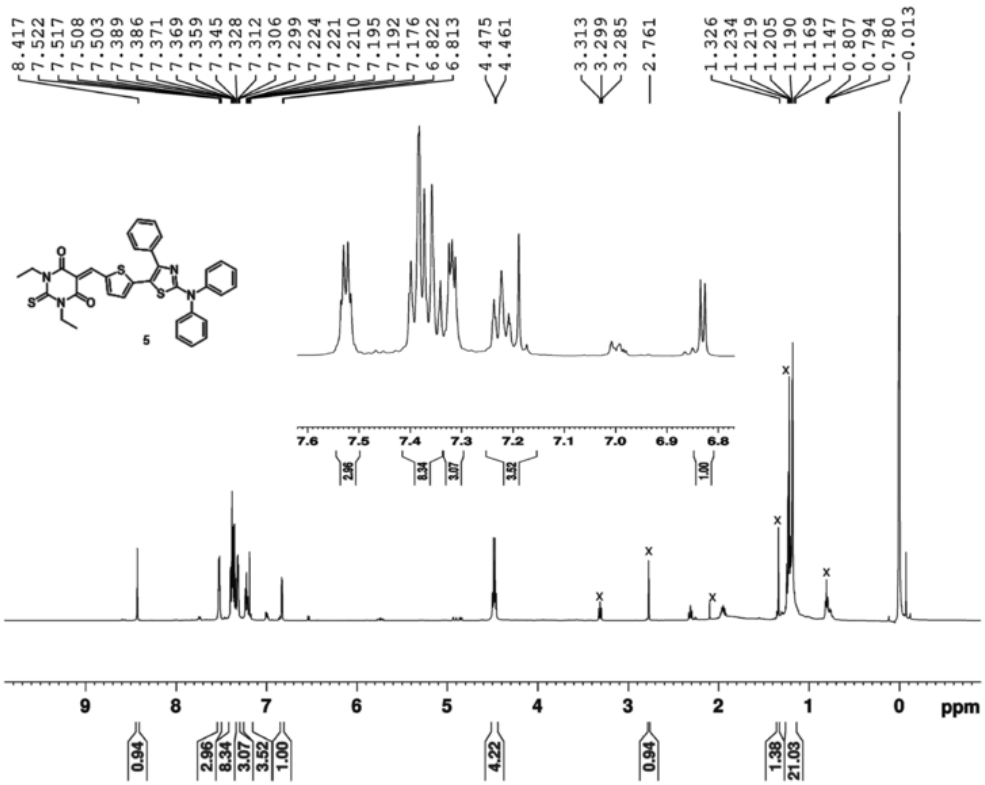

Figure 3.100: ^{1}H NMR spectrum of **5**

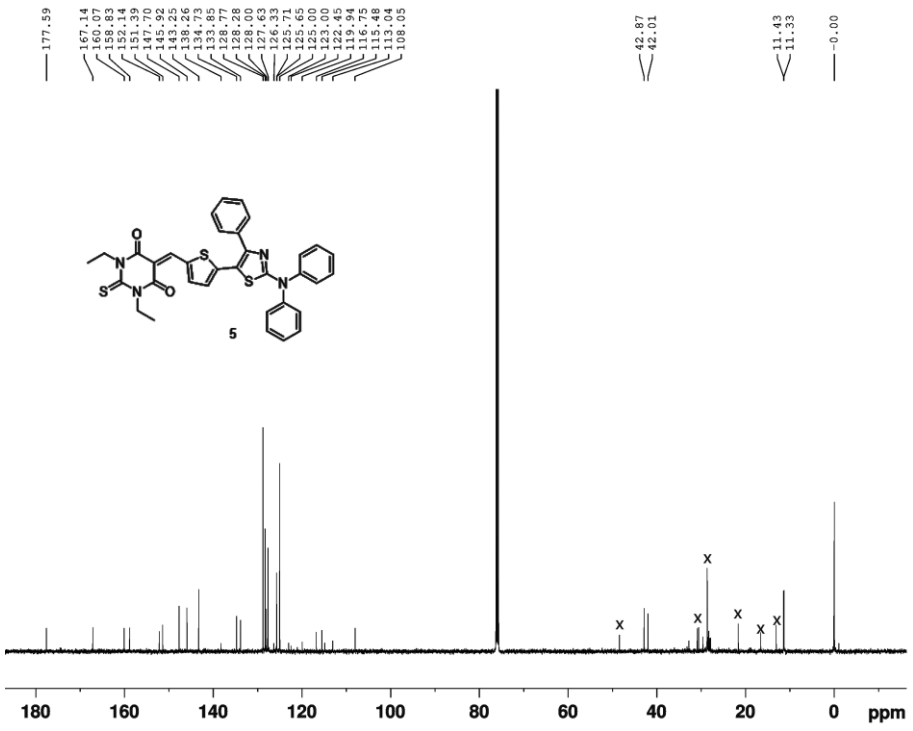

Figure 3.101: ^{13}C NMR spectrum of **5**

3.5. Conclusion

Inspired by the rational design of novel core molecules by computational chemistry tools, we proceeded for the development of synthetic methods to generate the molecules and validate the findings. We explored the untapped potential of classical chemistry and identified [4+1] thiazole ring route where carbonyl compounds, secondary amines and halo methyl heterocycles served as building blocks for the modular synthesis of multi-heterocyclic D-A systems. The synthesis of 5-(thiophen-2-yl)-1,3-thiazole and 5-(furan-2-yl)-1,3-thiazole cores were accomplished by metal free reaction of 1-(acyl/aroyl)-3,3-(disubstituted)thioureas with respective bromomethyl heterocycle. The versatility of developed synthetic method was validated by the synthesis of a diverse class of around 70 member library from which 35 members were fully characterized. We also attempted to adapt our synthetic strategy to suit green chemistry protocols and successfully developed a one pot multi-component mechanochemical method to synthesize these thiazoles. Compared to the existing literature for constructing bi(hetero)aryl core, a majority of which employs highly expensive transition metal catalysts, our method inspired by classical chemistry utilizing readily available starting compounds, is simple, highly versatile, economical, having a high atom economy and amenable to combinatorial synthesis and green synthetic protocols. Our next goal was to experimentally evaluate the photophysical and therapeutic properties of selected molecules from the synthetically accomplished library and the results are now discussed in the successive chapters.

Synthesis Summary			
No	**No of molecules**		**Characterized**
1	Thiourea derivative	Bromo derivative	
	22	4	
2	Thiazole		35
	Thienylthiazole	Furanylthiazole	
	54	16	

CHAPTER 5

INVESTIGATIONS OF THE PHOTOPHYSICAL PROPERTIES OF 5-(HETERO-2-YL)-1,3-THIAZOLES

5.1. Background

The exploration of chemical space of small molecule fluorophores is exciting due to the plethora of properties, finding multitude of applications spanning from biology to materials science (Müller and Bunz, 2007; Wysocki and Lavis, 2011; Yun *et al.*, 2014). With the increasing demand for fluorophores, suitable and efficient scaffolds have to be developed with synthetic flexibility. But the pace in which these new diverse core skeletons developed seems to be rather slower than expected. One reason for this slow pace may be the lack of fundamental understanding of the structure photophysical property relationship (SPPS) to assist in the rational design of novel molecules. The relationship between chemical structure and property will pave the way towards the development of efficient systems with tunable properties. For the development of novel cores, a clear understanding of the fluorophore properties like absorption/emission ranges, molar extinction coefficients, quantum efficiency, and Stokes shifts are necessary (Kim *et al.*, 2015). Despite the deep understanding of the fluorescence phenomena for many years, it was surprising to note that only a few family of fluorophores such as cyanines (Mishra *et al.*, 2000), BODIPY (Boens *et al.*, 2012; Loudet and Burgess, 2007), fluorescein (Kobayashi *et al.*, 2010), coumarin (Schiedel *et al.*, 2001; Takadate *et al.*, 2000) and Seoul-Fluor (Kim *et al.*, 2015) were subjected to the study of fundamental understanding of molecular properties (figure 5.1). For a SPPS to be carried out, a diverse library of the fluorophore scaffold has to be

generated. We believe that the synthetic hurdles in achieving these libraries may be the prime reason for the lack of sufficient studies.

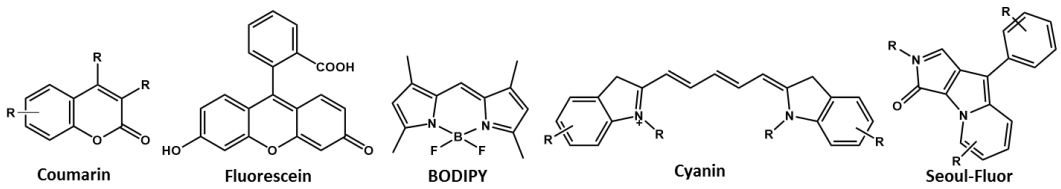

Figure 5.1. Fluorophore scaffolds with SPPS performed

These problems can be tackled to a great extent by the combinatorial chemistry techniques where a series of structural analogues of fluorophores with established chemistries can be synthesized easily and efficiently (Vendrell *et al.*, 2012). Combinatorial chemistry boosts the process of fluorescence probe developments with the help of diversity-oriented libraries where structurally diverse molecules are generated (Yun *et al.*, 2014). The combinatorial methodologies in fluorophore development are still underdeveloped, but its potential in populating the small molecule chemical space is very clear and promising results are already documented in the literature.

Despite these facts, the number of scaffolds possessing emission colour tunability is quite limited (Lavis and Raines, 2008). A rationally designed core can generate wide variety of colours using simple substituents, and it will expand the use of these cores for a variety of applications. Although, solution and solid state emitting full colour tunable scaffolds were reported (Kim and Park, 2009; Shimizu and Hiyama, 2010), a single score skeleton capable of exhibiting both solution and solid state emissions along with full colour tunability is rarely reported.

Recently, the research on D-A systems based on monocyclic 1,3-azoles has attracted considerable attention (Yamaguchi *et al.*, 2015). However, the fluorescent properties of thiazole core were not at all explored until last decade and common thiazole based scaffolds are depicted in figure 5.2. Among these, substituted 4-hydroxy-1,3-thiazoles were the highly explored class and studies were

initiated a decade ago by Beckert's group (Stippich *et al.*, 2009; Täuscher *et al.*, 2010). Although these molecules possessed good solution emission properties, their solid state emissions were not well explored. Very recently, a D-A type series of dyes based on the 4-alkoxythiazoles and azaacenes were reported (Gampe *et al.*, 2017). Yamaguchi *et al.* reported a family of 5-N-arylaminothiazoles having colour tunability from 460-610 nm with good quantum yield (QY) and solvatochromism (Yamaguchi *et al.*, 2015). Subsequent studies reported the different properties of these systems like vapochromism, halochromism and white light emission (Yamaguchi *et al.*, 2016; Yamaguchi *et al.*, 2017). Sekar *et al*. reported another class of styryl dyes containing thiazole core, albeit with low QY values in all the studied solvents (Tayade and Sekar, 2017; Thorat and Sekar, 2017). Recently thiazole fluorophores bearing aryl enamine/aza-enamine side chains were also discovered but with very low QY, below 3% (Lugovik *et al.*, 2017). However, fluorophore cores built on thiazole rings are limited to the above systems, but other well-known systems having thiazole as a substituent or benzothiazole family of fluorophores were widely explored. From these reports, it is evident that the potential of thiazoles as a fluorescence scaffold was largely unrecognized and we hope that future work on it will unravel its hidden potential.

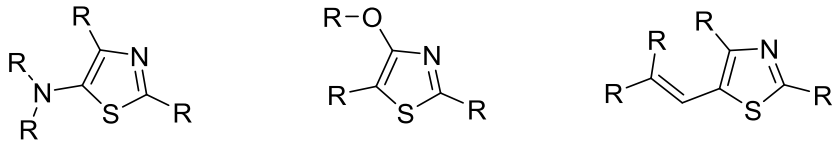

Yamaguchi *et al.* Beckert *et al.* Sekar *et al.*

Figure 5.2. Thiazole based fluorophore scaffolds

5.2. Results and Discussions

5.2.1. Study of structure photophysical properties

With a diverse set of synthesized library of 5-(hetero-2-yl)-1,3-thiazoles in hand, we decided to undertake a detailed study on the photophysical properties of

the molecules. This would help to validate our computational chemistry findings and to understand the chemical structure-photophysical relationship which would facilitate the rational design of new analogues with improved properties. The solution state spectra were recorded in 6 different solvents viz;- n-hexane, toluene, dichloromethane (DCM), tetrahydrofuran (THF), acetonitrile (ACN) and dimethyl sulphoxide (DMSO) and details are listed in Table 5.1 (Radhakrishnan and Sreejalekshmi, 2018).

Table 5.1. Photophysical properties of the studied compounds

Code	Solvent	λ_{abs}[a]/ λ_{em}[b] (nm)	Stokes shift nm (cm^{-1})	QY[c] (%)	Code	λ_{abs}[a]/ λ_{em}[b] (nm)	Stokes shift nm (cm^{-1})	QY[c] (%)
1a	n-hexane	440/533	93 (3965)	11.2	**1b**	436/531	95 (4103)	6.9
	Toluene	468/579	111 (4096)	50.9		464/578	114 (4251)	81.2
	THF	473/614	141 (4855)	2.0		469/507	138 (4847)	9.0
	DCM	483/641	158 (5103)	0.2		479/636	157 (5153)	0.5
	ACN	479/646	167 (5397)	NE		478/642	164 (5344)	0.1
	DMSO	496/646	150 (4681)	NE		494/652	158 (4905)	0.4
1c	n-hexane	443/537	94 (3951)	8.9	**1d**	446/537	91 (3800)	12.6
	Toluene	471/585	114 (4137)	70.0		474/580	106 (3856)	52.5
	THF	476/616	140 (4775)	6.1		479/609	130 (4456)	4.0
	DCM	485/651	166 (5258)	0.4		492/642	150 (4749)	0.2
	ACN	483/659	176 (5529)	0.2		487/646	159 (4958)	0.05
	DMSO	500/658	158 (4802)	0.2		503/654	151 (5243)	0.2
1e	n-hexane	446/538	92 (3800)	9.1	**1f**	452/544	92 (3742)	16.0
	Toluene	471/580	109 (3990)	52.3		477/583	106 (3812)	42.1
	THF	476/612	136 (4669)	7.8		482/617	135 (4539)	3.6
	DCM	488/652	164 (5154)	0.3		494/642	148 (4667)	0.1
	ACN	484/649	165 (5253)	NE		487/647	160 (5078)	NE
	DMSO	500/655	155 (4733)	0.3		504/656	152 (4597)	0.2
1g	n-hexane	445/543	98 (4056)	10.5	**1h**	450/545	95 (3874)	8.2
	Toluene	471/585	114 (4137)	55.5		474/586	112 (4032)	37.7
	THF	476/614	138 (4722)	13.0		477/619	142 (4809)	3.3
	DCM	487/644	157 (5006)	1.2		489/644	155 (4922)	0.1
	ACN	480/640	160 (5208)	NE		483/653	170 (5390)	NE
	DMSO	497/644	147 (4593)	NE		501/652	151 (4623)	0.2
1i	n-hexane	433/532	99 (4298)	3.8	**1j**	432/530	98 (4280)	1.1
	Toluene	457/574	117 (4460)	71.5		456/576	120 (4569)	42.8
	THF	462/611	149 (5278)	7.5		455/608	153 (5531)	12.2
	DCM	470/644	174 (5749)	0.3		464/647	183 (6096)	0.4
	ACN	468/641	173 (5767)	NE		466/645	179 (5955)	NE
	DMSO	483/656	173 (5460)	NE		479/658	179 (5679)	0.1
1k	n-hexane	434/536	102 (4385)	12.0	**1l**	435/527	92 (4013)	53.0
	Toluene	465/581	116 (4294)	45.8		461/578	117 (4391)	55.7

	THF	468/614	146 (5081)	6.1		467/603	136 (4829)	11.1
	DCM	474/638	164 (5423)	0.3		476/633	157 (5211)	0.6
	ACN	468/647	179 (5912)	NE		468/645	177 (5864)	0.3
	DMSO	490/659	169 (5234)	0.1		486/654	168 (5286)	0.1
1m	n-hexane	439/534	95 (4052)	23.9	**1n**	439/534	95 (4052)	10.7
	Toluene	457/577	120 (4551)	69.1		457/578	121 (4581)	75.3
	THF	460/601	141 (5100)	18.6		461/603	142 (5108)	18.7
	DCM	470/653	183 (5963)	1.1		470/652	182 (5939)	1.6
	ACN	463/673	210 (6739)	0.3		464/672	208 (6671)	0.4
	DMSO	483/674	191 (5867)	0.4		474/673	199 (6238)	0.4
1o	n-hexane	446/538	92 (3834)	24.0	**1p**	451/549	98 (3958)	41.6
	Toluene	461/578	117 (4391)	64.2		465/593	128 (4642)	42.3
	THF	466/602	136 (4848)	15.4		466/623	157 (5408)	9.3
	DCM	476/660	184 (5857)	0.9		473/657	184 (5921)	0.3
	ACN	470/660	190 (6125)	0.2		469/654	185 (6031)	NE
	DMSO	485/668	183 (5648)	0.4		480/667	187 (5841)	0.1
1q	n-hexane	446/532	86 (3625)	47.5	**1r**	447/542	95 (3921)	12.3
	Toluene	465/573	108 (4053)	60.9		460/577	117 (4408)	68.3
	THF	472/605	133 (4658)	24.0		468/616	148 (5134)	19.0
	DCM	472/649	177 (5778)	1.2		476/669	193 (6061)	0.9
	ACN	483/641	158 (5103)	NE		467/671	204 (6510)	0.1
	DMSO	481/649	168 (5382)	NE		480/671	191 (5930)	0.3
1s	n-hexane	433/532	99 (4298)	17.3	**1t**	448/533	85 (3560)	6.5
	Toluene	460/560	117 (3882)	40.8		464/575	111 (4160)	71.2
	THF	468/616	148 (5134)	36.8		467/599	132 (4719)	30.2
	DCM	476/669	193 (6061)	12.2		476/652	176 (5671)	4.3
	ACN	467/671	204 (6510)	0.7		465/661	196 (6377)	0.2
	DMSO	480/671	191 (5930)	1.6		478/667	189 (5928)	0.6
1u	n-hexane	470/598	128 (4554)	19.2	**1v**	433/517	95 (3752)	87.1
	Toluene	491/671	180 (5463)	3.0		452/556	104 (4138)	49.7
	THF	493/645	152 (4780)	0.1		457/595	138 (5075)	13.7
	DCM	NM				466/644	178 (5931)	1.5
	ACN	NM				459/654	195 (6496)	0.1
	DMSO	NM				472/665	193 (6149)	0.2
2a	n-hexane	425/507	82 (3806)	5.3	**2b**	431/512	83 (3671)	9.6
	Toluene	457/550	93 (3700)	2.3		459/544	85 (3404)	2.6
	THF	455/572	117 (4496)	1.0		461/575	114 (4301)	2.2
	DCM	469/612	143 (4982)	0.4		477/615	138 (4704)	0.6
	ACN	465/630	165 (5632)	0.4		469/628	159 (5398)	0.1
	DMSO	475/635	159 (5305)	0.2		483/628	145 (4780)	0.3
2c	n-hexane	429/512	83 (3779)	2.7	**2d**	424/505	81 (3783)	4.0
	Toluene	455/551	96 (3829)	2.2		447/543	96 (3955)	4.5
	THF	453/581	128 (4863)	1.6		447/573	126 (4919)	2.8
	DCM	478/624	146 (4895)	0.4		454/609	155 (5606)	0.6
	ACN	469/635	166 (5574)	0.2		452/632	180 (6301)	0.2
	DMSO	474/644	170 (5569)	0.2		464/634	170 (5779)	0.3
2e	n-hexane	426/512	86 (3943)	0.2	**3**	401/493	92 (4654)	3.8
	Toluene	446/547	101 (4140)	5.1		412/511	99 (4702)	8.8
	THF	447/569	122 (4797)	4.2		409/521	112 (5256)	3.3
	DCM	459/628	169 (5863)	1.6		415/532	117 (5299)	6.9
	ACN	443/638	195 (6899)	0.3		408/537	129 (5888)	8.4

	DMSO	459/642	183 (6210)	0.7		416/550	134 (5857)	22.5
4	n-hexane	497/558	61 (2200)	2.6	**5**	554/595	41 (1244)	4.4
	Toluene	499/584	85 (2917)	4.0		560/628	68 (1934)	8.8
	THF	496/620	124 (4032)	8.0		552/657	105 (2895)	21.3
	DCM	506/628	122 (3839)	10.7		566/671	105 (2765)	22.8
	ACN	491/644	153 (4839)	6.0		548/688	140 (3713)	1.9
	DMSO	499/657	158 (4819)	7.4		558/695	135 (3533)	3.5

Photophysical properties measured in solutions of concentration 10^{-5} mol L^{-1}. [a]Longest absorption maxima are only reported. [b]Emission maximum was obtained at excitation maximum. [c]Quantum yields (QY) were measured relative to rhodamine 6G in ethanol (0.92). For the measurements in hexane and for **3**, absolute QY was measured using an integrating sphere. NE- very weakly emissive. NM-Not measured.

The results from the studies revealed that the nature of the core, substituents, and polarity of solvents all have profound influence on absorption and emission spectra. All the molecules absorbed in the visible region which is a favourable attribute to the core structure. In the TT family of molecules **1a-v** bearing NO_2 acceptor at *C5* of thiophene, λ_{abs} wavelength bathochromically shifted from 432 - 470 nm in n-hexane and from 472 - 504 nm in DMSO. However, on moving to FT core, where the thiophene ring was replaced by the less aromatic furan ring, the absorption spectra were blue shifted as evident from the representative examples **2a-e**, where λ_{abs} varied from 424 - 431 nm and from 459 - 483 nm in n-hexane and DMSO respectively. The weaker electronic coupling of furan compared to thiophene would have contributed to the hypsochromic optical absorbance shift (Jahnke *et al.*, 2014). These results were as expected and in line with our computational calculations and signify the choice of heterocycle unit attached to *C5* of thiazole as the first option for tuning the photophysical properties.

The absorption spectra of selected molecules in THF are depicted in figure 5.3. The absorption spectra were characterized by two bands - one high energy band from an n-π^* transition and low energy band contributed by a π-π^* transition. Further, we analysed how the different substituents on thiazole influence the absorption spectra in different solvents. For example, we kept a phenyl group at *C4* and varied the substituent at *C2* of the thiazole using secondary amines viz; dimethylamine, diethylamine, piperidine, morpholine and diphenylamine with pKa values of 10.72, 10.98, 11.22, 8.36, and 0.79 respectively. The donor strength of

amine group at *C2* of thiazole influenced the λ_{abs} and 13 nm and 20 nm shift was observed in nonpolar n-hexane and polar DMSO respectively among the studied compounds. Morpholine substitution at *C2* produced the lowest λ_{abs} in nonpolar solvents probably because of the decreased electron donation ability of morpholine group. Similarly, we studied the substituent effect at *C4* on the λ_{abs} by keeping *C2* as fixed by substituting diphenyl group and varied *C4*. Presence of electron donating groups red shifted the absorption wavelength whereas steric crowding on *C4* blue shifted the absorption wavelength in all studied compounds. We also studied the influence of *C5* of thiazole on absorption tunability. By increasing the acceptor strength, absorption became more red shifted as evident from the representative examples of **3**, **2e**, **1m**, **4**, and **5** where absorption varied from 401 to 554 nm in n-hexane and 416 to 558 in DMSO. On comparing **1m** and **5,** absorption varied from 439 to 483 nm with an increasing solvent polarity from n-hexane to DMSO in **1m** whereas in **5,** no significant variation was observed. These observations suggested the importance of *C5* position in tuning the λ_{abs}.

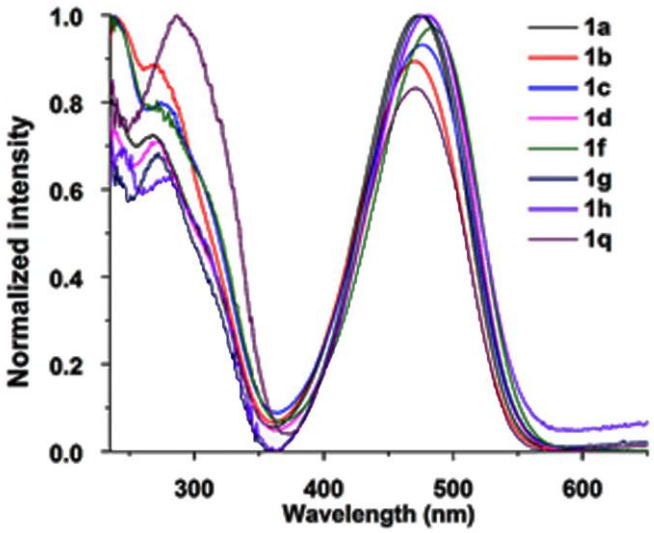

Figure 5.3. Absorption spectra of selected molecules in THF

Another interesting feature about the molecular design was its capability to exhibit multidirectional ICT (MICT) as illustrated by the example of **1u**. The electron donation from both amino groups at *C2* and *C4* to the nitro acceptor on

thiophene had a synergetic effect on the λ_{abs}. It was evident from the FMO analysis that CT direction shifted from to *C4* to *C5* rather than the usual *C2* to *C5* (figure 5.4). Also, the HOMO had a larger electron density from the dimethylaniline fragment than from the diphenylamine group. Further evaluation of the MICT nature of the core will be discussed in chapter 6.

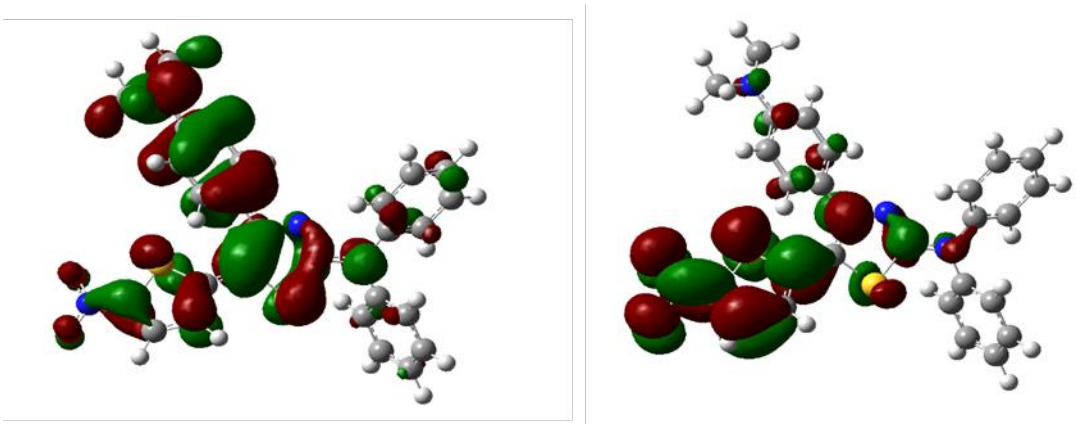

Figure 5.4. HOMO and LUMO of **1u** calculated at PBE0/6-31G(d,p) level of theory to elucidate the MICT

We also conducted a detailed evaluation of the emission properties in various solvents. The emission spectra of selected molecules in n-hexane is depicted in the figure 5.5. Nitro TT derivatives were highly emissive in non polar solvents whereas in polar solvents, emissions broadened and quenched. This is a characteristic behaviour of the majority of the push pull molecules (Rettig, 1986). In non polar solvents, a structured emission was observed with a distinct peak for FT derivatives whereas for TT derivatives a shoulder was observed (figure 5.6). But on increasing the solvent polarity, the locally excited emission converted to an ICT emission with disappearance of the vibrational fine structures accompanied by a red shift in λ_{em}. The calculated dipole moments values indicated that TT derivatives are more polar in the ground state than its furan counterpart and hence in non polar solvents they tend to exhibit a CT state whereas less polarized FT molecules produced a much clear structured emission.

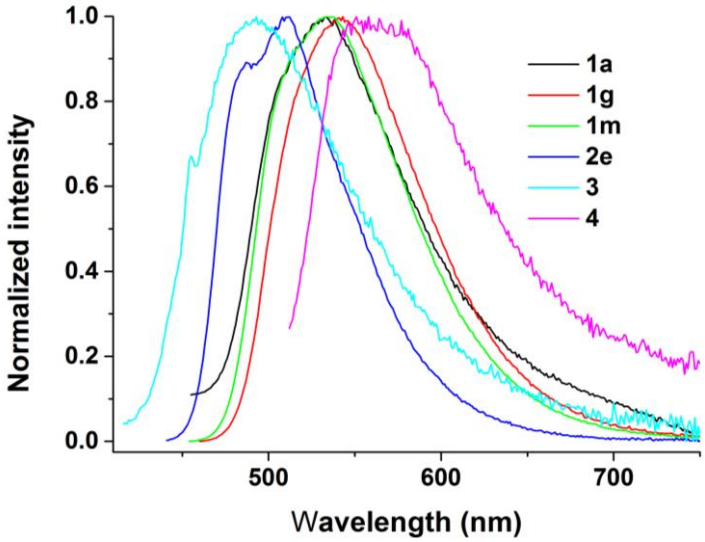

Figure 5.5. Emission spectra of selected compounds in n-hexane

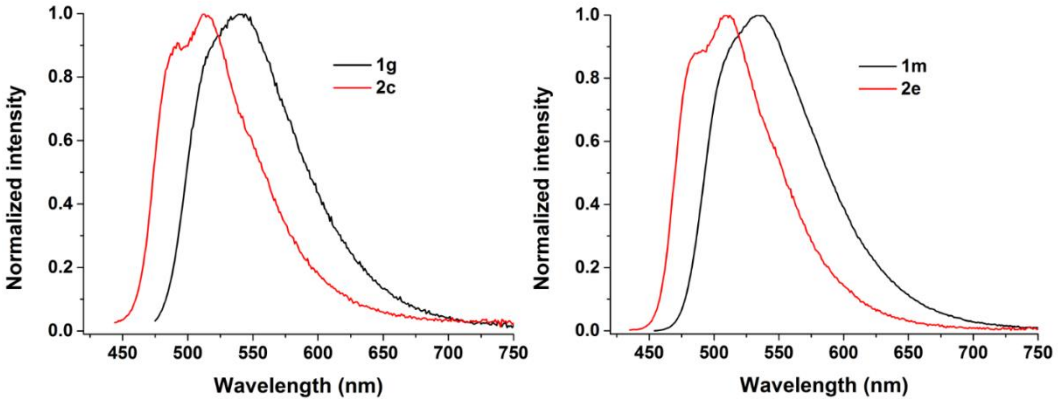

Figure 5.6. Comparison of **e**mission spectra of thiazole-thiophene/furan in n-hexane

All the molecules were characterized by excitation independent emission. The excitation spectra of selected molecules in THF recorded at their emission maxima are depicted in the figure 5.7.

The decrease in emission intensity in the polar solvents can be explained by twisted intramolecular charge transfer (TICT) phenomena, mainly found in many of the molecular rotors. As polarity increased, molecule adopted a twisted structure in the excited state with a shift in the λ_{abs}. A charge separated state was generated which was stabilized by polar solvents and leading to internal conversion and thermal deactivation. In high viscous solvents, the molecular rotation is

kinetically less favourable and enhanced emission is generally observed. To verify this we measured emission intensity in varying fraction of methanol-glycerol. On increasing the glycerol fraction emission intensity increased and in neat glycerol, a 20 fold enhancement in the emission intensity was observed as depicted in the figure 5.8, which confirmed the presence of TICT behaviour.

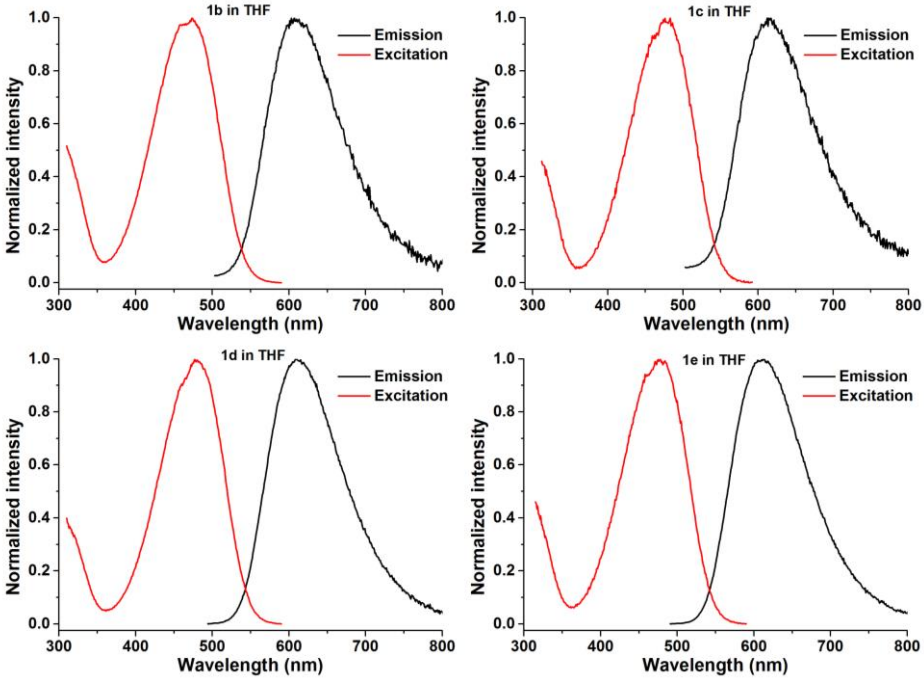

Figure 5.7. Excitation spectra of selected compounds in THF

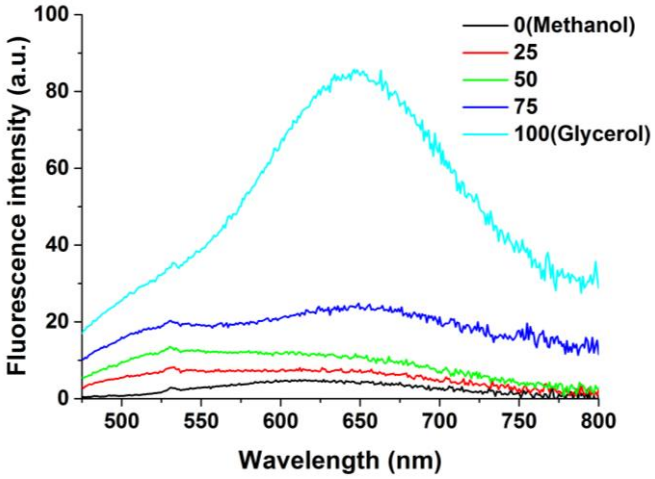

Figure 5.8. Fluorescence spectra of **1o** in the binary mixture of methanol-glycerol

We also evaluated the substituent effects on the emission behaviour (figure 5.9). Derivatives of TT core with NO_2 acceptor on thiophene *C5* were highly emissive in nonpolar solvents (QY upto 87%) whereas emission nearly quenched and broadened with increase in solvent polarity as expected for most of the push pull molecules. Consider **1a**, **1d**, **1g**, **1i** and **1m** where *C4* was fixed by phenyl group and *C2* was varied using different secondary amines. Here, in non polar n-hexane emission spectra were hardly affected (only 9 nm variation) whereas in polar DMSO a 30 nm variation was observed. In non polar solvents, morpholine produced the lowest (532 nm in **1i**) and piperidine substitution produced the highest λ_{em} (543 nm in **1g**) whereas in polar solvents, piperidine afforded the least (644 nm in **1g**) and diphenyl substitution brought the maximum (674 nm in **1m**) in λ_{em}. Similarly, we fixed *C2* by diphenyl group and varied *C4* by different substituents. By changing the substituent from diphenylethyl to dimethylaniline, an 81 nm shift (517 nm for **1v** and 598 nm for **1u)** in λ_{em} was obtained. As observed in the absorption spectra, a MICT emission was also produced by placing a stronger electron donor fragment in *C4*. A 64 nm and 94 nm variations were observed in n-hexane and toluene respectively by varying the substituent from phenyl to dimethyl aniline (for **1m** -534 and 577 nm whereas for **1u** - 598 and 671 nm in n-hexane and toluene respectively). The synergetic influence of two electron donating groups from *C2* and *C4* red shifted the λ_{em}. Likewise, electron rich heteroarenes at *C4* produced a red shifted emission. For example in **1p**, substitution of electron rich heterocycle thiophene at *C4* produced a 15 and 16 nm red shifted emission respectively in n-hexane and toluene compared to **1m**. Steric effects and expansion of π-conjugation at *C4* also strongly influenced the fluorescence behaviour. In n-hexane and DCM, **1s** fluoresce at 532 and 642 nm, **1v** emits at 517 and 644 nm whereas **1r** emits at 542 and 669 nm, which suggested another possibility of tuning the λ_{em} along *C4*. Steric crowding contributed to blue shifted emission whereas increasing conjugation along *C4* red shifted the spectrum. It is also to be noticed that λ_{em} of FT were blue shifted in all studied solvents as compared to their TT analogues.

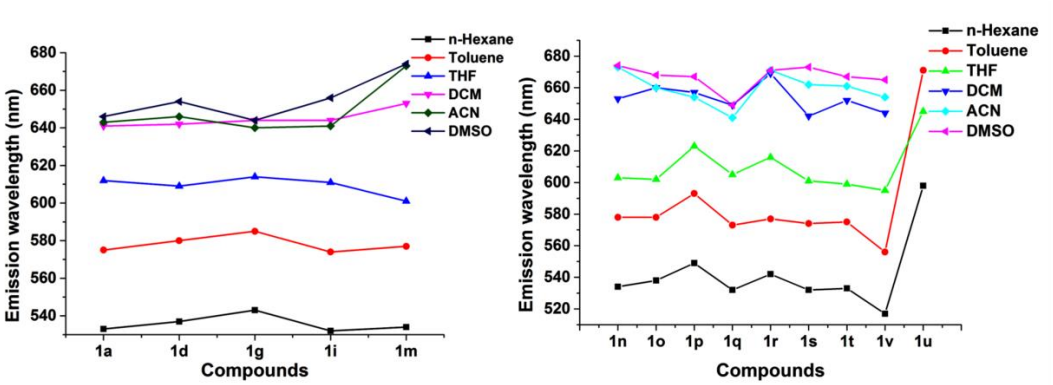

Figure 5.9. Substituent effect at *C2* and *C4* on emission spectra

Further, we evaluated the substituent effect at *C5* of the heterocycle on fluorescence spectrum. Replacing nitro substituent with an aldehyde group, dicyanovinyl or 1,3-diethyl-2-thiobarbituric acid had a dramatic influence on the emission behaviour. In n-hexane, **3**, **4** and **5** emitted at 493, 558, 595 nm whereas in DMSO they emitted at 550, 657 and 695 nm respectively. Colour tunability among the studied compounds in toluene and THF are represented in the figure 5.10.

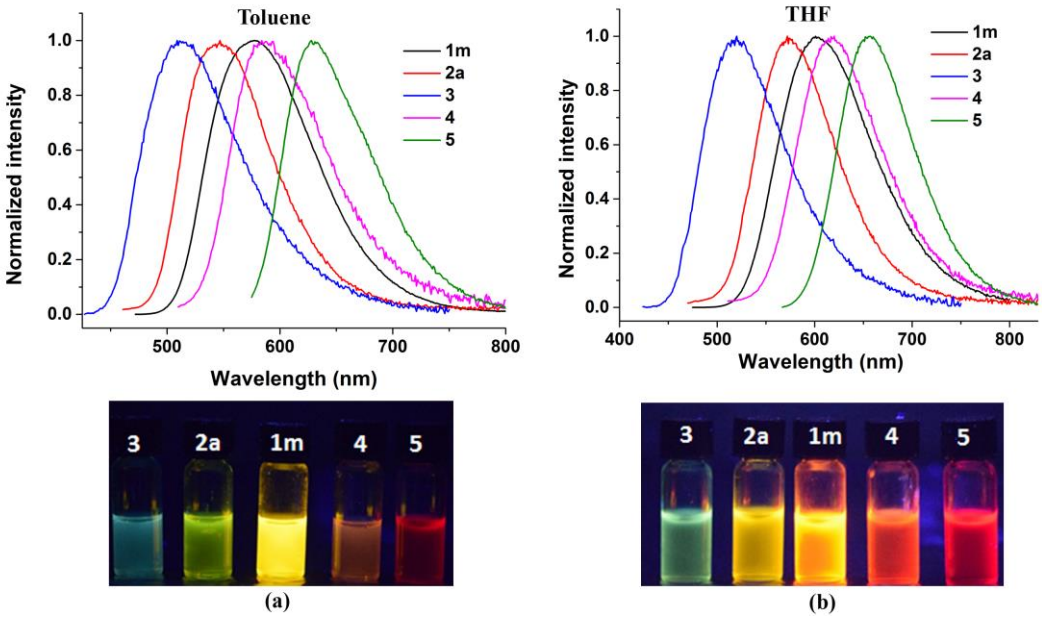

Figure 5.10. Emission colour tunability in toluene and THF

It was interesting to notice that the chemical modification at *C5* is critical in colour tunability of the designed core (figure 5.11). Manipulation of push pull effect and conjugation along *C5* with diverse substituents will give the freedom to design custom made fluorophores with varying properties.

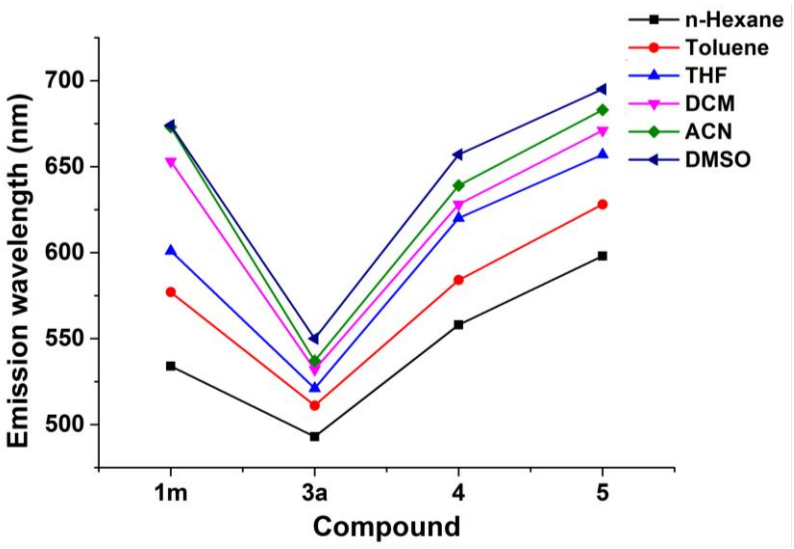

Figure 5.11. Substituent effect at *C5* on emission spectra

Fluorophores with large Stokes shift (SS) values are always demanding especially in bio-imaging where self-quenching and reabsorption can be minimized by the use of such compounds (Lakowicz, 2006). Small organic fluorophore scaffolds with large SS are limited in number. All the nitro and aldehyde substituted compounds of TT and FT showed large SS values whose magnitude was dependent on solvent polarity. In excited state, molecules underwent reorganization where polar solvents stabilized these states better than the non polar ones and hence resulted in larger SS. In the nitro TT **1a**, **1d**, **1g**, **1i** and **1m**, SS varied between 93, 91, 98, 99 and 95 nm in n-hexane whereas in polar DMSO, it varied between 150, 151, 147, 173 and 191 nm respectively. Substituent effect on SS is depicted in figure 5.12. Among *C4* substituents, morpholine and diphenyl units produced the largest SS values in nonpolar and polar solvents respectively. The SS values of FT family were smaller than that for the TT family.

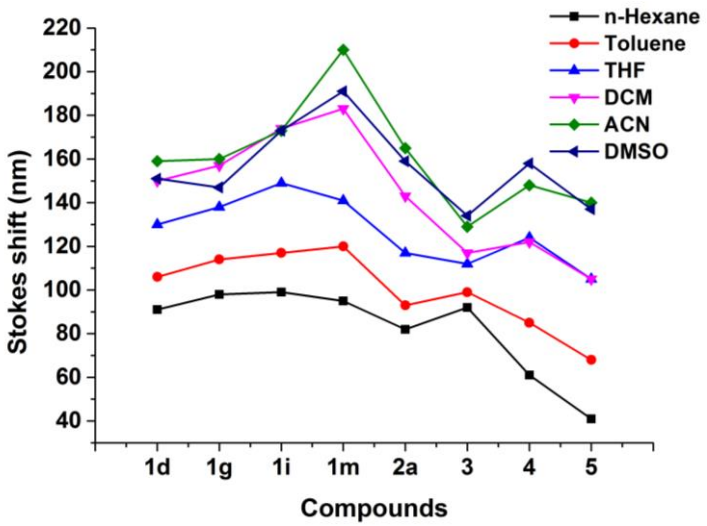

Figure 5.12. Substituent effect on Stokes shift

Next we tried to understand the structure-QY relationship among the studied compounds. Many of the push molecules are highly emissive in nonpolar solvents but they become nonemissive in polar solvents. Similarly, nitro TT were highly emissive in toluene and moderately emissive in THF and n-hexane whereas in polar solvents emissions quenched. This extremely opposite relationship between quantum efficiency and polarity will help in designing environmental sensitive fluorophores that will behave differently in hydrophobic and hydrophilic environments (Vázquez *et al.*, 2005). The substituent effect on the QY variation was not fully understood with the synthesized library of compounds and a further study has to be carried out with a larger set of molecules for a reasonable conclusion about the structure-quantum yield relationship. But the significant results which were obtained (figure 5.13) have to be verified with the expanded set of the library. Diphenyl substituent at *C2* generally produced larger QY values. It was interesting to note that the presence of a bulky group like naphthyl had a profound effect on the QY value. For example, among **1m** and **1s**, QY values decreased in toluene, but there was an 11, 2 and 4 fold increase observed in DCM, THF, and DMSO respectively. Changing the *C5* substituent also had notable effect on the QY with changing solvent polarity. Replacing nitro group by aldehyde group at *C5* brought down the QY in nonpolar solvents, but a 6, 33 and 59 fold increase in QY value

was observed for compound **3** compared to that for **1m** in polar solvents DCM, ACN and DMSO respectively. Similarly low energy emissive molecules **4** and **5** produced considerable increase in QY values in polar solvents. The interesting thing to notice was that FT analogues exhibited much lesser QY values in studied solvents compared to their TT counterparts. For example, there was a 22, 12, 25, 16 and 13 fold decrease in QY observed in toluene for compounds **2a-e** compared to their TT analogues.

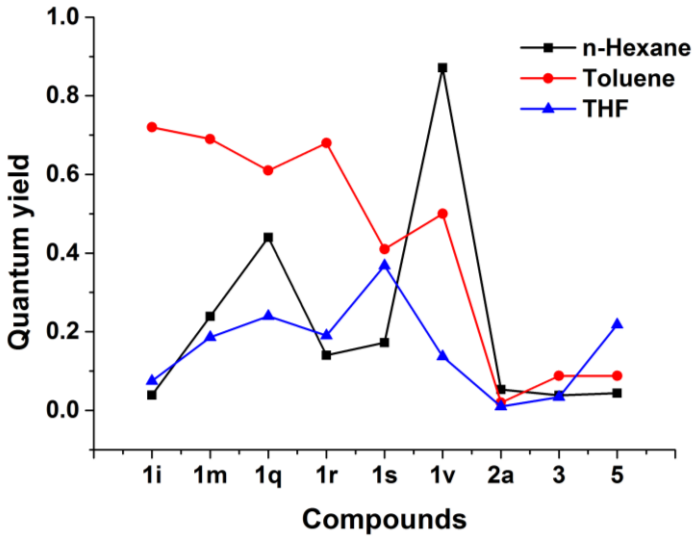

Figure 5.13. Substituent effect on quantum yield

The main findings from the structure photophysical property relationship are now summarised. 1) The nature core and substituents around it have a profound effect in deciding the photophysical properties. 2) Modification of charge transfer directions has a major effect on absorption and emission spectra. 3) *C5* position of heterocycle is crucial in achieving the full colour tunability (figure 5.14). 4) Presence of electron donating groups at *C4* induce red shift in absorption and emission whereas steric substituents blue shift the spectra. 5) Electron donation ability of secondary amine groups at *C2* of thiazole influences the absorption spectrum. 6) Solvents have a vital role in the absorption and emission properties and photophysical properties can be tuned according to the solvents.

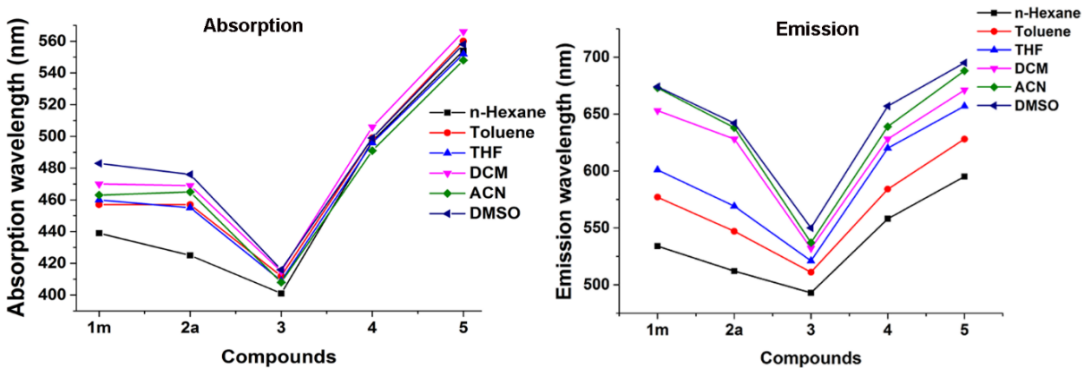

Figure 5.14. Overall variation in absorption and emission wavelengths

5.2.2. Solvatochromism

In line with our expectations, the molecules are sensitive to the perturbations in solvent environment and exhibited positive solvatochromism in absorption and emission spectra. All the 5-(hetero-2-yl)-1,3-thiazoles with nitro and aldehyde substituents at *C5* displayed positive solvatochromism. This feature is expected to allow the design and development of environmental sensitive fluorophores (Yang *et al.*, 2014). The positive solvatochromism can be explained by the difference in ground and excited state geometries and the better stabilization of excited state by more polar solvents. For example, in **1a**, emission shifted from 533 nm to 614 nm in THF and to 647 nm in ACN. The detailed values are in the table 5.2.

Table 5.2: Spectroscopic properties of **1a**

Solvent	**$E_T(30)$**	**Δf**	**λ_{abs} (nm)**	**λ_{em} (nm)**	**Stokes shift (cm^{-1})**
n-Hexane	31.0	0.002	440	533	3965
Toluene	33.9	0.016	468	579	4096
Ethyl acetate	38.1	0.2	469	604	4765
THF	37.4	0.21	473	614	4855
DCM	40.7	0.218	483	641	5103
Acetonitrile	45.6	0.306	479	646	5397

The solvatochromism was better studied using Lippert–Mataga and Reichardt plot and good correlations were observed.

The Lippert−Mataga equation (Lippert, 1955; Mataga *et al.*, 1956) is given by

$$\Delta\vartheta = \vartheta_{abs} - \vartheta_{em} = \frac{2\Delta f}{hca^3}\left(\mu_e - \mu_g\right)^2 + constant$$

$$\Delta f = \frac{(\epsilon - 1)}{(2\epsilon + 1)} - \frac{(n^2 - 1)}{(2n^2 + 1)}$$

where $\Delta\vartheta$ is the Stokes shift –the difference between absorption (ϑ_{abs}) and emission maxima (ϑ_{em}) in wavenumbers, h is Planck's constant, c is the speed of light, a is the Onsager cavity radius, μ_g and μ_e are the ground and excited state dipole moments. Δf is the orientational polarizability which can be calculated using the dielectric constant (ϵ) and refractive index of the solvent (n).

For **1a**, the Onsager radius was 5.25Å, calculated quantum mechanically using B3LYP/6-31g(d,p) level of theory. The plot of orientational polarizability (Δf) against Stokes shift furnished a linear fit with a slope of 4545.06. Using this value, the difference between the ground and excited state dipole moments was calculated and found to be 8.08D. The large difference in the dipole moment between the ground and excited state indicate a strong ICT which accounts for the solvatochromism. The fluorescence solvatochromism and Lippert−Mataga plot are depicted in the figure 5.15.

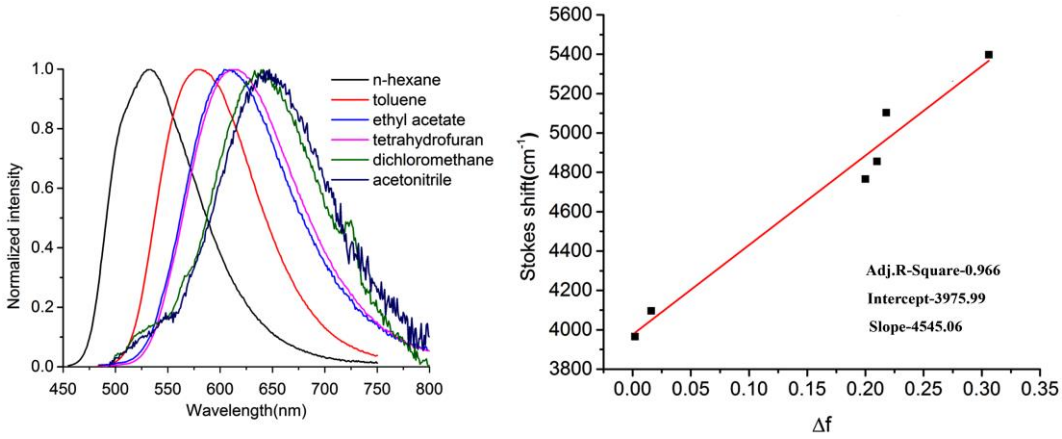

Figure 5.15. Emission spectra (left) and Lippert−Mataga plot of **1a** (right) in various solvents

Similarly, Lippert−Mataga analysis was carried out for **1b**. The calculated Onsager radius was 5.48Å. The plot of orientational polarizability Δf against Stokes shift furnished a linear fit with a slope of 4392.39 (figure 5.16). The dipole moment difference between ground and excited was calculated to be 8.47D, which rationalize the positive solvatochromism.

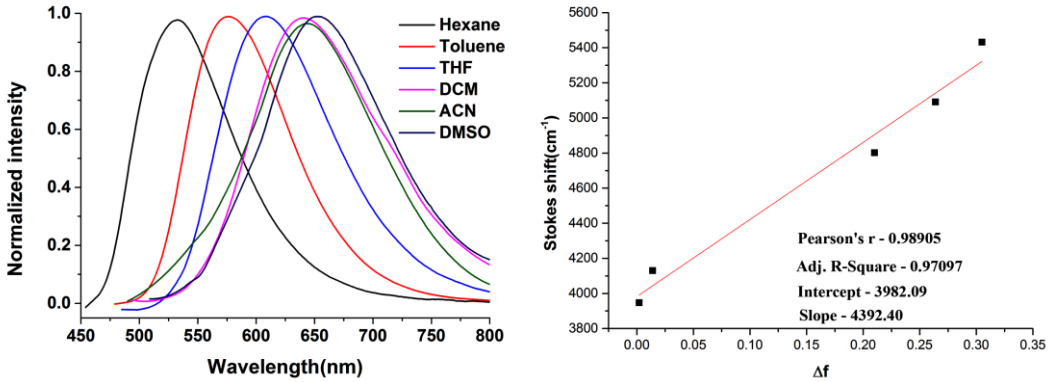

Figure 5.16. Emission spectra (left) and Lippert−Mataga plot of **1b** (right) in various solvents

Solvatochromism was further analyzed with the help of another well-known empirical solvent polarity parameter E_T^N, where its values are correlated with the polarity probe pyridinium N-phenolate betaine (Reichardt, 1994). The change in dipole moment between ground and excited states can be calculated using the equation (Ravi *et al.*, 1995),

$$\Delta\vartheta = 11307.6 \left[\left(\frac{\Delta\mu}{\Delta\mu_D}\right)^2 \left(\frac{a_D}{a}\right)^3\right] E_T^N + constant$$

where $\Delta\vartheta$ is the Stokes shift, a is the Onsager cavity radius, $\Delta\mu$ change in dipole moment and a_D and $\Delta\mu_D$ are that of betaine dye (Reichardt and Welton, 2011) (a_D= 6.2 Å and $\Delta\mu_D$= 9D).

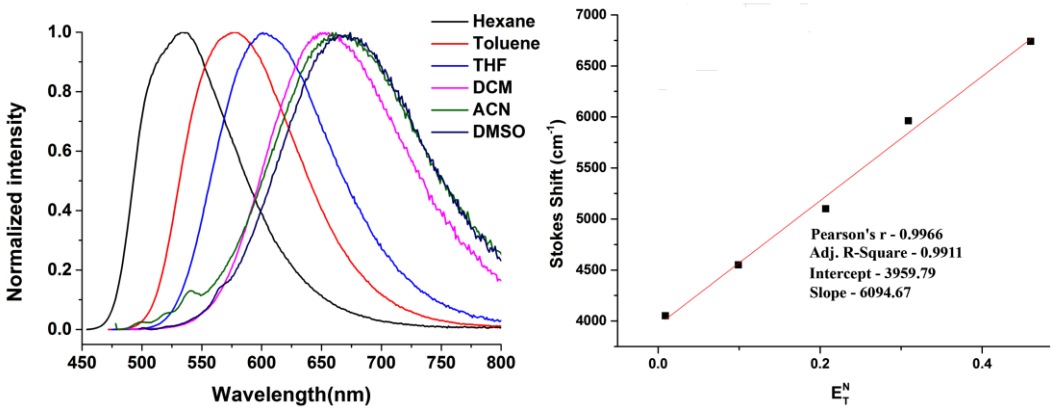

Figure 5.17. Emission spectra of **1m** (left) and the plot of Stokes shift against E_T^N (right) in various solvents

For **1m**, the plot of Stokes shift as a function of E_T^N was correlated by a linear fit (without DMSO) with a slope of 6094.66 (figure 5.17). The change in dipole moment calculated was 7.04D which explains the positive solvatochromism.

5.2.3. Photostability measurements

The photostability of dye molecules are extremely important for their use in practical applications. Hence we measured the photostability of a randomly selected molecule **1m**, in non polar solvent toluene where it was highly emissive. The molecules was irradiated with Xe arc lamp of 150 W continuously for one hour and fluorescence spectra were recorded in every 2 minutes intervals (figure 5.18). It was interesting note that no obvious change in the emission intensity was observed and the molecule was highly stable in toluene. The excellent photostability would give an added advantage to the developed molecules for their technological applications.

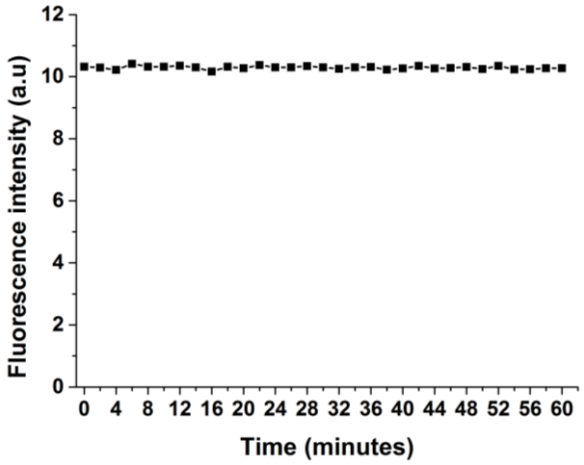

Figure 5.18. Photostability measurements of **1m** in toluene. Excitation wavelength was 470 nm and emission was recorded at 570 nm

5.2.4. Solid state fluorescence

The population of solid state emissive scaffolds are much less in number compared to their solution state counterparts. Majority of the well known highly emissive organic fluorophores are non-emissive in the condensed state due to aggregation caused quenching phenomena (Hong *et al.*, 2011; Mei *et al.*, 2014). Efficient organic solid state emissive materials have widespread applications in OLEDs (Li, 2015b), OFETs (Zaumseil and Sirringhaus, 2007), fluorescent sensors (Thomas *et al.*, 2007) and so on. The high demand of novel scaffolds spurred the research in solid emissive fluorophores and a number of novel cores with blue, green, yellow, orange and red emissions were reported (Shimizu and Hiyama, 2010). Molecules which are highly emissive in the red regions are limited due to aggregation caused fluorescence quenching resulting from the π-π stacking or dipole-dipole interaction owing to donor and acceptor substituents (Shimizu and Hiyama, 2010). Several multicolour emissive scaffolds were also reported with good quantum yields by utilizing the donor and acceptor strengths and thereby tuning the ICT (Anthony, 2012; Lee *et al.*, 2014; Wakamiya *et al.*, 2007; Wang *et al.*, 2013b). Recently minimum architecture organic solid state emitters are gaining

considerable attention due to their simple structural features (Beppu *et al.*, 2015; Cheng *et al.*, 2016).

After the detailed and systematic exploration of solution state emission behaviour of the synthesized library, we next studied the solid state emission properties. Similar to solution state, the solid state emission of thiazole fluorophores were also not much explored in the literature. Solid state emission measurements of a few selected compounds resulted in exciting findings. For example, compounds **1a**, **1b**, **1d**, **1g**, **1i** and **1q** emit at 649, 636, 638, 650, 642, and 622 nm respectively (figure 5.19) and proved to be among the smallest family of organic solid red emissive fluorophores reported so far as represented by **1a** having a formula weight (FW) of 331 and with emission at 649 nm. Along the same time, Cheng *et al.* reported a novel molecule of Indazo-Fluor with FW of 274 having an emission at 725 nm (Cheng *et al.*, 2016).

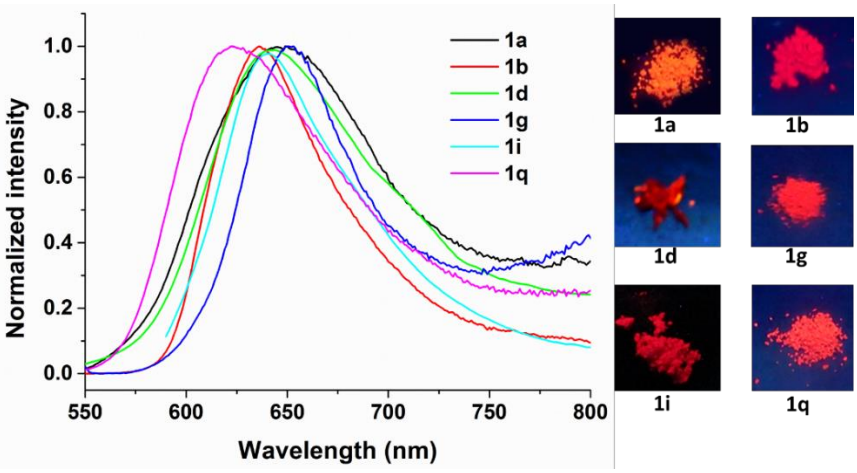

Figure 5.19. Solid state emission spectra (left) and photographs of solid samples under UV lamp of 365 nm (right)

In order to rationalize the observed solid state emission, we examined the solid state landscapes of these systems by single crystal X-ray diffraction (figure 5.20).

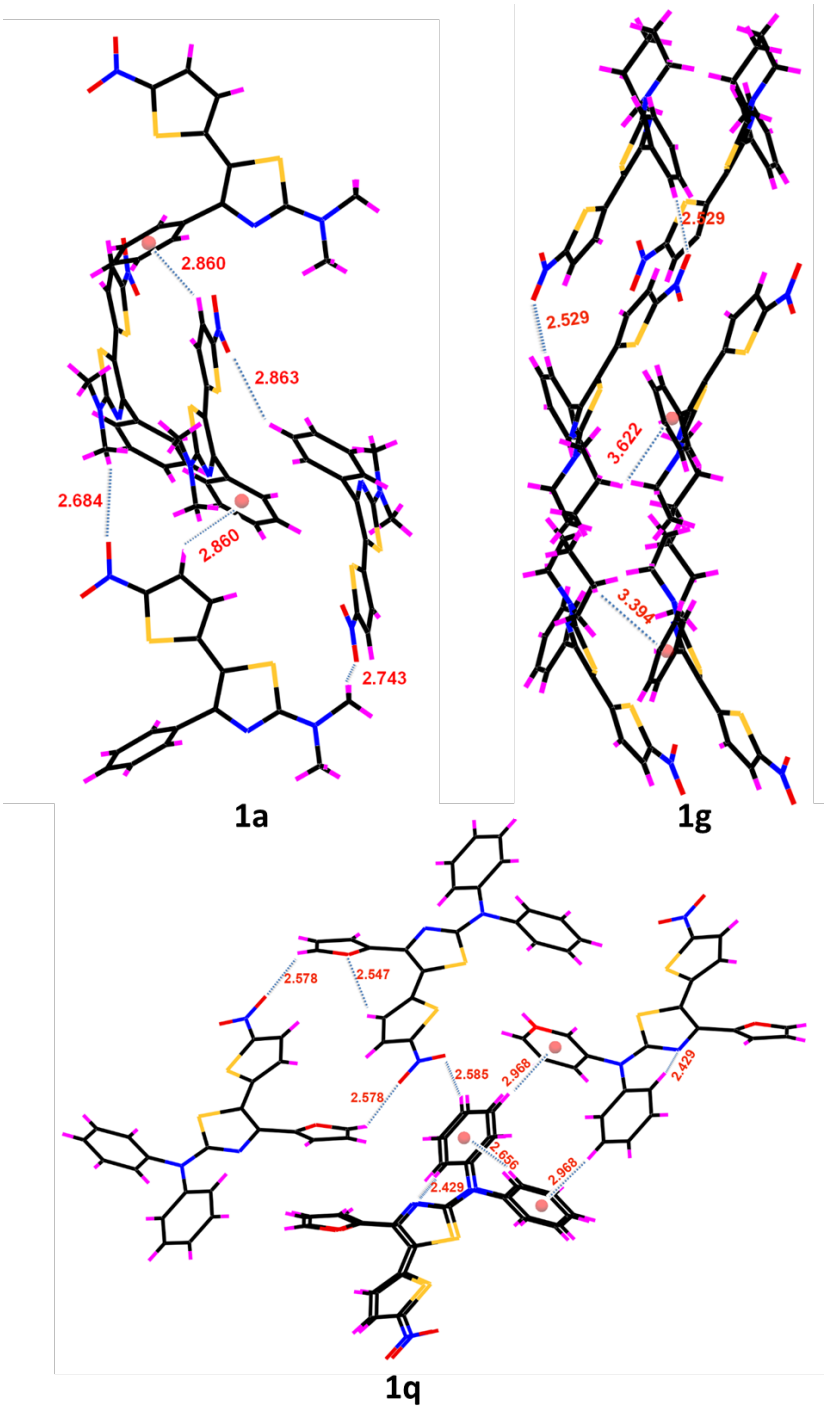

Figure 5.20. Solid state crystal packings in **1a**, **1g** and **1q**

In **1a**, thiazole and thiophene rings aligned *trans* to each other with a dihedral angle of 177.49° and the phenyl ring on *C4* of thiazole ring made a torsional angle of 62.11° with thiazole plane which imparted non-planarity to the

molecular system and prevented the π-π stacking. Thiazole and thiophene on the adjacent layers were separated by a distance of 3.89Å. The strong C-H···π interactions (*C4*-$H_{thiophene}$…$\pi_{benzene}$) with distances of 2.86Å provided structural rigidity to the molecular system which blocked non radiative channel and hence led to solid state emission. Similarly for **1g** and **1q**, the *C4* substituent played a vital role in the non-planarity of the system and analysis of supramolecular structures revealed the presence of multiple short range interactions (C-H···π interaction, H-bonding). All these would have contributed to the structural rigidity and hence minimized the non radiative decay which further signifies the success of our core design strategy and relative positioning of substituents.

5.2.5. Evaluation of theranostic potential

Theranostics is a new treatment modality where therapeutics and diagnostics components are integrated into to a single platform. Recently the idea of '*trackable therapeutics'* emerged where a single molecule can be used for both imaging and therapeutic applications (Bertrand *et al.*, 2016). Although a few number of reports are available (Langdon-Jones *et al.*, 2017), the potential of this novel concept is clear, and significant improvements are needed for transferring it from lab to clinic.

We initiated a preliminary study to evaluate the theranostic potential of the synthesized family of 5-(hetero-2-yl)-1,3-thiazole. The theranostic potential of the molecule **3** was studied against cancer cell line HeLa and normal cell line L929. Cellular uptake was studied after one-day growth. In normal cell line, cellular uptake was observed with bright green fluorescence without affecting the cell morphology (figure 5.21). In HeLa cell line, a bright green emission was observed along with majority of dyes localized in cytoplasm (figure 5.22). Membrane blebbing and a small nuclear fragmentation leading to cell apoptosis and cellular fragmentation was observed. These results clearly indicate that **3** is cytotoxic to cancer cell line HeLa, where as it is noncytotoxic to L929 within the studied

concentrations. These results are promising that a single molecule can act as a therapeutic as well as imaging agent. Since we already established the therapeutic potential of the 5-(hetero-2-yl)-1,3-thiazole using the molecular modelling studies and fluorescence fine tuning by structure photophysical studies, a further detailed study by the judicial selection substituents by incorporating both these aspects is expected to result in the successful development of theranostic platforms.

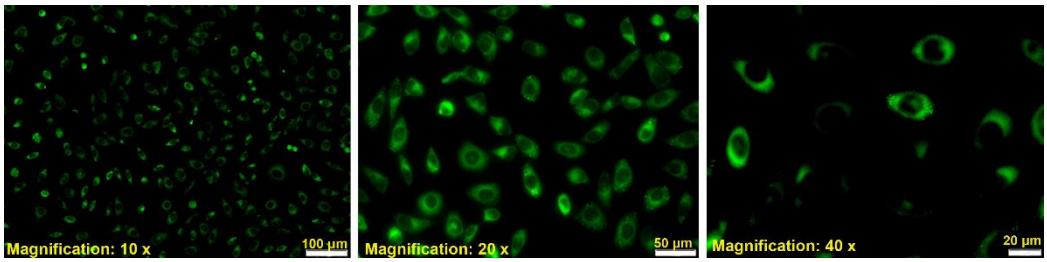

Figure 5.21. Fluorescence image of **3** in L929 cell lines under different magnification

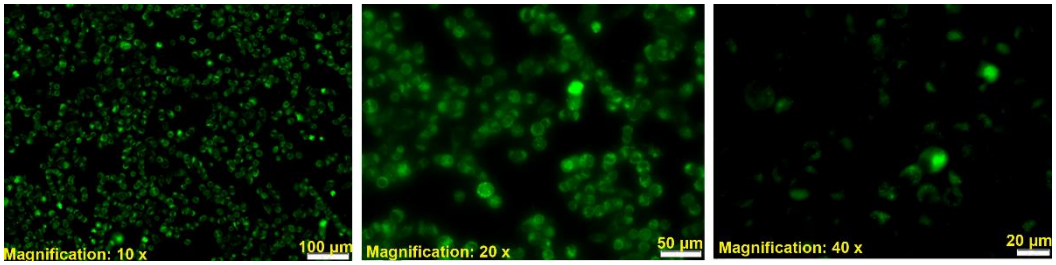

Figure 5.22. Fluorescence image of **3** in HeLa cell lines under different magnifications

5.3. Experimental Details

5.3.1. UV-Visible absorption studies

Spectroscopic/hplc grade solvents from Merck Chemicals/ Spectrochem were used for all spectral measurements without further purification. Varian Cary 100 Bio UV-Vis spectrophotometer was used for UV-Vis spectroscopy measurements. All the measurements were performed with 10^{-6} M concentration of the compounds.

5.3.2. Fluorescence studies

Fluorescence spectra were recorded using Horiba Jobin Yvon Fluoromax-4 spectrometer and molecules were excited at their absorption maximum. Sample concentrations were kept at 10^{-6} M. A UV lamp of wavelength 365nm was used for visualization and fluorescence imaging. Absolute QYs of the samples were recorded on Horiba Fluoromax Quanta-φ with a calibrated integrating sphere system under laboratory conditions. The relative QYs were calculated using Rhodamine 6G in ethanol as standard (QY=0.94) (Brouwer, 2011) at an excitation wavelength of 488nm using the equation

$$\emptyset = \emptyset_R \frac{I \times OD_R \times n^2}{I_R \times OD \times n_R^2}$$

where $\emptyset$ and $\emptyset_R$ are fluorescence QY of sample and reference, I and I_R are integrated area of sample and reference, OD and OD_R are optical density of sample and reference, and n and n_R are the refractive indices of sample and reference respectively.

5.4. Conclusion

We have studied the photophysical properties of a 30 member library in six solvents. Molecular engineering around the thiazole core led to interesting photophysical properties. For absorption, 173, 169, 163, 172, 159, 161 nm and for emission, 158, 192, 189, 191, 184, 186 nm variations were obtained in n-hexane, toluene, THF, DCM, ACN and DMSO by simply modifying the substituents on thiazole. SPPR study revealed some interesting facts about the tunable sites. The *C5* of thiazole proved crucial in attaining colour tunability of the system and can be modified with acceptor fragments of varying strengths. Electron donating groups at *C4* of thiazole imparted a red shift to both the absorption and emission spectra, whereas bulky substituents blue shifted the spectra. Photophysical properties of the

molecules were solvent dependent and all the derivatives with nitro and aldehyde substituents at *C5* show positive solvatochromism in both absorption and emission. Most of the molecules were characterized by large SS values in all the studied solvents. High QY values were obtained with non polar solvents. The solid state emission studies on selected molecules indicated that they are emissive in condensed state and crystal structure analysis hinted the role of molecular rigidity attained by multiple short interactions to be responsible for the solid state emission. Finally, evaluation of theranostic property identified that these molecules are potential candidates for the development of theranostic platforms. Computational chemistry calculations were used to rationalize the experimentally observed properties and will be discussed in the next chapter.

Photophysical studies- Summary			
No	**No of molecules studied**		**Solvents**
1	Thienylthiazole	Furanylthiazole	n-Hexane, Toluene, THF DCM, ACN and DMSO
	25	5	
2	Solid state fluorescence		
	6		

CHAPTER 8

CONCLUSION AND FUTURE PERSPECTIVES

8.1. Conclusion

Inspired by the vast possibilities and opportunities in theranostics research, we attempted to contribute to this growing field by the development of a novel family of molecules based on 1,3-thiazole core. The journey undertaken during the design and development of the multiheterocyclic core and its property evaluation using both computational and experimental methods for trackable therapeutics is summarized in the following sections.

We explored the hidden potential of computational chemistry tools in the development of novel scaffolds for theranostics. We have selected 1,3-thiazole as our central core due to its pharmacophoric potential and by coupling diverse heterocycles with it, designed a novel 5-(hetero-2-yl)-1,3-thiazole core. Fluorescence property was imparted to the newly designed core by a D-A strategy using the ICT phenomena through a CAFD approach assisting the selection of D and A units. Utilizing the inherent three site tunability around the core, a combinatorial library of fluorophore was designed and preliminary structure photophysical properties were evaluated with the aid of QM calculations.

Followed by the rational design of novel scaffolds, we attempted the synthetic feasibility of these cores. Inspired by the untapped potential of classical synthetic chemistry methods, we developed a simple and economical [4+1] thiazole ring construction route for the synthesis of multiheterocyclic D-A systems using carbonyl compounds, secondary amines and halomethyl heterocycles by avoiding highly expensive transition metals. The versatility of the developed method was validated by the synthesis 70 member library consisting of 5-(thiophene-2-yl)-1,3-

thiazole and 5-(furan-2-yl)-1,3-thiazole core, and out of which 35 members were fully characterized. The synthesis of 5-(thiazole-5-yl)thiophene-2–carbaldehyde opened new vistas enabling the functional group transformation and extending the π-conjugation. We also transformed our synthetic methodology to green synthetic protocols and developed a one-pot multicomponent mechanochemical method.

Further, the therapeutical potential of the core was evaluated by both *in vitro* and *in silico* methods. The preliminary cytotoxic studies of selected molecules against cancer cell lines showed **1a** to be active towards HL-60 and promising results were obtained in MCF-7 cell lines. A virtual library was built using commercially available building blocks having diverse substituents for *in silico* analysis. From the ADME property prediction, it was found that 97.5% molecules of the in house library had properties that fall within the range of that for known drug molecules. *In silico* binding analysis was performed in three different family proteins viz- human estrogen receptor, aurora kinase and cyclin dependant kinase to explore the potential of designed molecules for multitargeted drug design. Furanylthiazole core was found to have better binding affinity in the active site of proteins and 3-pyridyl, 2-substituted quinoxalines and pyrazines played vital roles in ATP competitive binding in aurora kinase proteins.

After identifying the therapeutical potential of the core molecules, we explored the photophysical properties in both solution and solid state. A structure photophysical property relationship was established using a 30 member library in six different solvents of varying polarity. The study revealed the importance of different substituents at the periphery of the core in imparting the wide range of photophysical properties. The *C5* of the heterocycle was found to play a vital role in the full colour tunability of the system. *C4* of the thiazole have the potential to behave as an orthogonal handle and also can be used for the design of MICT molecules. The photophysical properties of the molecules were solvent dependent and they exhibited positive solvatochromism in both absorption and emission. The nitro and aldehyde substituted TT/FT derivatives were characterized by large

Stokes shift and all the TT derivatives showed high quantum yield values up to 87% in non polar solvents. The solid state fluorescence property revealed the potential of the molecules to develop into one of the rare class of full colour tunable emissive molecules both in solution and solid state. The fluorescence imaging in HeLa and L929 cell lines indicated that these molecules are potential candidates for theranostic platforms.

Detailed QM calculations were performed to understand the fundamental nature of the core. Twelve different functionals were evaluated for the accurate prediction of vertical excitation energies and PBE0 was found to be the best among them with MAE less than 0.3 eV. The solvent effect on the absorption wavelength was studied using PCM calculations. The ICT and MICT nature was confirmed by the percentage contribution of fragments to HOMO and LUMO using PDOS calculations. Computational chemistry calculations further helped to identify the existence of charge separated quinoid state in polar solvents and conformational preferences within the crystal structure.

In order to expand the thiazole chemistry from drug discovery to materials chemistry, we explored the multifunctional properties of the 5-(hetero-2-yl)-1,3-thiazoles. Static and dynamic functional molecules were found within the developed library. The molecules were capable of exhibiting AIE phenomena and further, the aggregate formation was studied using MD simulations. The prototype of naked eye sensor for acid vapours was developed. Derivatives with aldehyde substitution at *C5* of thiophene exhibited mechanoresponsive fluorescence phenomena, which would open a new avenue for the use of these novel class molecules for multifunctional molecular materials.

In summary, we have successfully designed a novel multiheterocyclic core, the 5-(hetero-2-yl)-1,3-thiazole by molecular hybridisation for theranostics applications. A simple and highly versatile synthetic strategy was developed using readily available building blocks and a combinatorial library of molecules was

designed and synthesized. Therapeutic properties of the designed molecules were studied using *in vitro* and *in silico* analyses. A SPPR was established by the in depth photophysical study using the fluorophore library. The potential of the system for theranostics was confirmed by the imaging capabilities and cytotoxicity studies on normal and cancer cell lines. Computational chemistry calculation was used to understand the fundamental nature of the core and to rationalize the observed phenomena. And finally, the potential of the developed molecules for multifunctional applications was evaluated.

8.2. Future Perspectives

We believe that this work is a small but significant step towards our long term journey for the development of multifunctional materials from organic heterocyclic molecules. We anticipate that the complete potential applications of these newly designed cores are yet to emerge and we continuing to improve the design by resolving the shortcomings and expanding the chemical space around the core. Using the diversity oriented synthetic strategy, the library can be expanded by integrating various heterocycle fragments for the development of multiheterocyclics. Due to the versatility and simplicity of the synthetic methods, we have already initiated the development of designer systems such as dendritic architecture using thiazole-heterocycle hybrids. Further optimizations needed for the development of theranostic platforms are in progress. By utilizing the advantage of the design strategy based on D-π-A, the systems have the potential to be developed as multifunctional materials. Further detailed study has to be carried out for design and property optimizations to explore their prospective applications in optoelectronics, nonlinear optics and similar fields to tap the full potential of these molecular materials.

REFERENCES

1. Adamo, C., and Barone, V. (1998). Exchange functionals with improved long-range behavior and adiabatic connection methods without adjustable parameters: The m PW and m PW1PW models. *The Journal of Chemical Physics*, 108(2): 664-675.

2. Adamo, C., and Barone, V. (1999). Toward reliable density functional methods without adjustable parameters: The PBE0 model. *The Journal of Chemical Physics*, 110(13): 6158-6170.

3. Adamo, C., and Jacquemin, D. (2013). The calculations of excited-state properties with time-dependent density functional theory. *Chemical Society Reviews*, 42(3): 845-856.

4. Adamo, C., Scuseria, G. E., and Barone, V. (1999). Accurate excitation energies from time-dependent density functional theory: Assessing the PBE0 model. *The Journal of Chemical Physics*, 111(7): 2889-2899.

5. Afzal, O., Kumar, S., Haider, M. R., Ali, M. R., Kumar, R., Jaggi, M., et al. (2015). A review on anticancer potential of bioactive heterocycle quinoline. *European Journal of Medicinal Chemistry*, 97: 871-910.

6. Albert, I. D., Marks, T. J., and Ratner, M. A. (1997). Large molecular hyperpolarizabilities. Quantitative analysis of aromaticity and auxiliary donor-acceptor effects. *Journal of the American Chemical Society*, 119(28): 6575-6582.

7. Alberto, M. E., Iuga, C., Quartarolo, A. D., and Russo, N. (2013). Bisanthracene bis (dicarboxylic imide)s as potential photosensitizers in photodynamic therapy: a theoretical investigation. *Journal of Chemical Information and Modeling*, 53(9): 2334-2340.

8. Ali, I., Nadeem Lone, M., A Al-Othman, Z., Al-Warthan, A., and Marsin Sanagi, M. (2015). Heterocyclic scaffolds: centrality in anticancer drug development. *Current Drug Targets*, 16(7): 711-734.

9. Aly, A. A., Ahmed, E. K., El-Mokadem, K. M., and Hegazy, M. E.-A. F. (2007). Update survey on aroyl substituted thioureas and their applications. *Journal of Sulfur Chemistry*, 28(1): 73-93.

10. Amir-Aslani, A., and Mangematin, V. (2010). The future of drug discovery and development: shifting emphasis towards personalized medicine. *Technological Forecasting and Social Change*, 77(2): 203-217.

11. Andersson, K., Malmqvist, P. Å., and Roos, B. O. (1992). Second-order perturbation theory with a complete active space self-consistent field reference function. *The Journal of Chemical Physics*, 96(2): 1218-1226.

12. Anthony, S. P. (2012). Organic solid-state fluorescence: strategies for generating switchable and tunable fluorescent materials. *ChemPlusChem*, 77(7): 518-531.

13. Arslan, H., Külcü, N., and Flörke, U. (2003). Synthesis and characterization of copper (II), nickel (II) and cobalt (II) complexes with novel thiourea derivatives. *Transition Metal Chemistry*, 28(7): 816-819.

14. Bai, Z., and Gust, R. (2009). Breast cancer, estrogen receptor and ligands. *Archiv der Pharmazie*, 342(3): 133-149.

15. Balkenhohl, F., von dem Bussche-Hünnefeld, C., Lansky, A., and Zechel, C. (1996). Combinatorial synthesis of small organic molecules. *Angewandte Chemie International Edition*, 35(20): 2288-2337.

16. Bardhan, R., Chen, W., Perez-Torres, C., Bartels, M., Huschka, R. M., Zhao, L. L., et al. (2009). Nanoshells with targeted simultaneous enhancement of magnetic and optical imaging and photothermal therapeutic response. *Advanced Functional Materials*, 19(24): 3901-3909.

17. Bardhan, R., Lal, S., Joshi, A., and Halas, N. J. (2011). Theranostic nanoshells: from probe design to imaging and treatment of cancer. *Accounts of Chemical Research*, 44(10): 936-946.

18. Barone, V. (2011). *Computational strategies for spectroscopy: from small molecules to nano systems*: John Wiley & Sons, New Jersey.

19. Barone, V., Bellina, F., Biczysko, M., Bloino, J., Fornaro, T., Latouche, C., et al. (2015). Toward the design of alkynylimidazole fluorophores: computational and experimental characterization of spectroscopic features in solution and in poly (methyl methacrylate). *Physical Chemistry Chemical Physics*, 17(40): 26710-26723.

20. Bartlett, R. (1997). *Modern ideas in coupled-cluster methods*: World Scientific, Singapore.

21. Becke, A. D. (1993). Density functional thermochemistry. III. The role of exact exchange. *The Journal of Chemical Physics*, 98: 5648-5652.

22. Beno, B. R., Yeung, K.-S., Bartberger, M. D., Pennington, L. D., and Meanwell, N. A. (2015). A survey of the role of noncovalent sulfur interactions in drug design. *Journal of Medicinal Chemistry*, 58(11): 4383-4438.

23. Beppu, T., Tomiguchi, K., Masuhara, A., Pu, Y. J., and Katagiri, H. (2015). Single benzene green fluorophore: solid-state emissive, water-soluble, and solvent-and pH-independent fluorescence with large stokes shifts. *Angewandte Chemie International Edition*, 54(25): 7332-7335.

24. Bertrand, B., Doulain, P.-E., Goze, C., and Bodio, E. (2016). Development of trackable metal-based drugs: new generation of therapeutic agents. *Dalton Transactions*, 45(33): 13005-13011.

25. Beverina, L., and Salice, P. (2010). Squaraine compounds: tailored design and synthesis towards a variety of material science applications. *European Journal of Organic Chemistry*, 2010(7): 1207-1225.

26. Birks, J. B. (1970). *Photophysics of aromatic molecules*: Wiley London.

27. Bochkov, A. Y., Akchurin, I. O., Dyachenko, O. A., and Traven, V. F. (2013). NIR-fluorescent coumarin-fused BODIPY dyes with large Stokes shifts. *Chemical Communications*, 49(99): 11653-11655.

28. Boens, N., Leen, V., and Dehaen, W. (2012). Fluorescent indicators based on BODIPY. *Chemical Society Reviews*, 41(3): 1130-1172.

29. Boese, A. D., and Handy, N. C. (2001). A new parametrization of exchange–correlation generalized gradient approximation functionals. *The Journal of Chemical Physics*, 114(13): 5497-5503.

30. Bousquet, D., Fukuda, R., Maitarad, P., Jacquemin, D., Adamo, C., Ehara, M., et al. Excited-state geometries of heteroaromatic compounds : a comparative TD-DFT and SAC-CI study Contents. *Journal of Chemical Theory and Computation*, 9(5): 2368-2379.

31. Bräse, S. (2015). *Privileged scaffolds in medicinal chemistry: design, synthesis, evaluation*: Royal Society of Chemistry, UK.

32. Bratsos, I., Jedner, S., Gianferrara, T., and Alessio, E. (2007). Ruthenium anticancer compounds: challenges and expectations. *CHIMIA International Journal for Chemistry*, 61(11): 692-697.

33. Breitung, E. M., Shu, C.-F., and McMahon, R. J. (2000). Thiazole and thiophene analogues of donor-acceptor stilbenes: molecular hyperpolarizabilities and structure-property relationships. *Journal of the American Chemical Society*, 122(6): 1154-1160.

34. Brouwer, A. M. (2011). Standards for photoluminescence quantum yield measurements in solution (IUPAC Technical Report). *Pure and Applied Chemistry*, 83(12): 2213-2228.

35. Bruning, J. B., Parent, A. A., Gil, G., Zhao, M., Nowak, J., Pace, M. C., et al. (2010). Coupling of receptor conformation and ligand orientation determine graded activity. *Nature Chemical Biology*, 6(11): 837-843.

36. Buenker, R. J., and Peyerimhoff, S. D. (1968). CI method for the study of general molecular potentials. *Theoretical Chemistry Accounts: Theory, Computation, and Modeling (Theoretica Chimica Acta)*, 12(3): 183-199.

37. Bugaj, A. M. (2011). Targeted photodynamic therapy–a promising strategy of tumor treatment. *Photochemical and Photobiological Sciences*, 10(7): 1097-1109.

38. Bürckstümmer, H., Tulyakova, E. V., Deppisch, M., Lenze, M. R., Kronenberg, N. M., Gsänger, M., et al. (2011). Efficient solution-processed bulk heterojunction solar cells by antiparallel supramolecular arrangement of dipolar donor–acceptor dyes. *Angewandte Chemie*, 123(49): 11832-11836.

39. Bureš, F. (2014). Fundamental aspects of property tuning in push–pull molecules. *RSC Advances*, 4(102): 58826-58851.

40. Burke, M. D., and Schreiber, S. L. (2004). A planning strategy for diversity-oriented synthesis. *Angewandte Chemie International Edition*, 43(1): 46-58.

41. Butler, M. S., Robertson, A. A., and Cooper, M. A. (2014). Natural product and "natural product derived drugs in clinical trials. *Natural Product Reports*, 31(11): 1612-1661.

42. Cances, E., Mennucci, B., and Tomasi, J. (1997). A new integral equation formalism for the polarizable continuum model: Theoretical background and applications to isotropic and anisotropic dielectrics. *The Journal of Chemical Physics*, 107(8): 3032-3041.

43. Cardoso, C. R., Lima, M. r. V., Cheleski, J., Peterson, E. J., Venâncio, T., Farrell, N. P., et al. (2014). Luminescent ruthenium complexes for theranostic applications. *Journal of Medicinal Chemistry*, 57(11): 4906-4915.

44. Caricato, M., Mennucci, B., and Tomasi, J. (2004). Solvent effects on the electronic spectra: An extension of the polarizable continuum model to the zindo method. *The Journal of Physical Chemistry A*, 108(29): 6248-6256.

45. Caricato, M., Trucks, G. W., Frisch, M. J., and Wiberg, K. B. (2010). Electronic transition energies: a study of the performance of a large range of single reference density functional and wave function methods on valence and Rydberg states compared to experiment. *Journal of Chemical Theory and Computation*, 6(2): 370-383.

46. Carraro, F., Pucci, A., Naldini, A., Schenone, S., Bruno, O., Ranise, A., et al. (2004). Pyrazolo [3, 4-d] pyrimidines endowed with antiproliferative activity on ductal infiltrating carcinoma cells. *Journal of Medicinal Chemistry*, 47(7): 1595-1598.

47. Carvajal, R. D., Tse, A., and Schwartz, G. K. (2006). Aurora kinases: new targets for cancer therapy. *Clinical Cancer Research*, 12(23): 6869-6875.

48. Celli, J. P., Spring, B. Q., Rizvi, I., Evans, C. L., Samkoe, K. S., Verma, S., et al. (2010). Imaging and photodynamic therapy: mechanisms, monitoring, and optimization. *Chemical Reviews*, 110(5): 2795-2838.

49. Chai, J.-D., and Head-Gordon, M. (2008a). Long-range corrected hybrid density functionals with damped atom–atom dispersion corrections. *Physical Chemistry Chemical Physics*, 10(44): 6615-6620.

50. Chai, J.-D., and Head-Gordon, M. (2008b). Systematic optimization of long-range corrected hybrid density functionals. *The Journal of Chemical Physics*, 128(8): 084106.

51. Charaf-Eddin, A., Planchat, A., Mennucci, B., Adamo, C., and Jacquemin, D. (2013). Choosing a functional for computing absorption and fluorescence band shapes with TD-DFT. *Journal of Chemical Theory and Computation*, 9(6): 2749-2760.

52. Chemla, D. S. (2012). *Nonlinear optical properties of organic molecules and crystals* (Vol. 1): Elsevier.

53. Chen, F., Hong, H., Goel, S., Graves, S. A., Orbay, H., Ehlerding, E. B., et al. (2015a). In vivo tumor vasculature targeting of CuS@ MSN based theranostic nanomedicine. *ACS Nano*, 9(4): 3926-3934.

54. Chen, G. S., and Chern, J.-W. (2007). *Computer-aided drug design*: Wiley, NY, USA.

55. Chen, S., Li, L., Zhao, H., and Li, B. (2013). $Ce(OTf)_3$-catalyzed multicomponent domino cyclization–aromatization of ferrocenylacetylene, aldehydes, and amines: a straightforward synthesis of ferrocene-containing quinolines. *Tetrahedron*, 69(30): 6223-6229.

56. Chen, X., Gambhir, S. S., and Cheon, J. (2011). Guest Editorial- Theranostic nanomedicine. *Accounts of Chemical Research*, 44(10): 841-841.

57. Chen, X., Huang, X., He, Q., Xie, Y., and Yang, C. (2014). Palladium-catalyzed oxidative C–H/C–H cross-coupling of benzothiazoles with thiophenes and thiazoles. *Chemical Communications*, 50(30): 3996-3999.

58. Chen, Y., Zhu, Q., Tian, Y., Tang, W., Pan, F., Xiong, R., et al. (2015b). Supramolecular aggregates from polyacrylates and Gd (III)-containing cationic surfactants as high-relaxivity MRI contrast agents. *Polymer Chemistry*, 6(9): 1521-1526.

59. Cheng, Y., Li, G., Liu, Y., Shi, Y., Gao, G., Wu, D., et al. (2016). Unparalleled ease of access to a library of biheteroaryl fluorophores via oxidative cross-coupling reactions: discovery of photostable NIR probe for mitochondria. *Journal of the American Chemical Society*, 138(14): 4730-4738.

60. Cherniawski, B. P., Lopez, S. A., Burnett, E. K., Yavuz, I., Zhang, L., Parkin, S. R., et al. (2017). The effect of hexyl side chains on molecular conformations, crystal packing, and charge transport of oligothiophenes. *Journal of Materials Chemistry C*, 5(3): 582-588.

61. Chi, Z., Zhang, X., Xu, B., Zhou, X., Ma, C., Zhang, Y., et al. (2012). Recent advances in organic mechanofluorochromic materials. *Chemical Society Reviews*, 41(10): 3878-3896.

62. Cicenas, J., Kalyan, K., Sorokinas, A., Jatulyte, A., Valiunas, D., Kaupinis, A., et al. (2014). Highlights of the latest advances in research on CDK inhibitors. *Cancers*, 6(4): 2224-2242.

63. Cj, O. C., Beckmann, H. S., and Spring, D. R. (2012). Diversity-oriented synthesis: producing chemical tools for dissecting biology. *Chemical Society Reviews*, 41(12): 4444-4456.

64. Cohen, P., and Alessi, D. R. (2012). Kinase drug discovery–what's next in the field? *ACS Chemical Biology*, 8(1): 96-104.

65. Conde, J., Bao, C., Cui, D., Baptista, P. V., and Tian, F. (2014). Antibody–drug gold nanoantennas with Raman spectroscopic fingerprints for in vivo tumour theranostics. *Journal of Controlled Release*, 183: 87-93.

66. Cook, J. J., Bednar, B., Lynch, J. J., Gould, R. J., Egbertson, M. S., Halczenko, W., et al. (1999). Tirofiban (Aggrastat®). *Cardiovascular Therapeutics,* 17(3): 199-224.

67. Cossi, M., and Barone, V. (2001). Time-dependent density functional theory for molecules in liquid solutions. *The Journal of Chemical Physics*, 115(10): 4708-4717.

68. Cramer, C. J. (2002). *Essentials of computational chemistry: theories and models*: John Wiley & Sons.

69. Crawley, N., Thompson, M., and Romaschin, A. (2014). Theranostics in the growing field of personalized medicine: An analytical chemistry perspective. *Analytical Chemistry*, 86(1): 130-160.

70. Dar, A. A., Goff, L. W., Majid, S., Berlin, J., and El-Rifai, W. (2010). Aurora kinase inhibitors-rising stars in cancer therapeutics? *Molecular Cancer Therapeutics*, 9(2): 268-278.

71. Das, M., Duan, W., and Sahoo, S. K. (2015). Multifunctional nanoparticle–EpCAM aptamer bioconjugates: A paradigm for targeted drug delivery and imaging in cancer therapy. *Nanomedicine: Nanotechnology, Biology and Medicine*, 11(2): 379-389.

72. De Moliner, F., Kielland, N., Lavilla, R., and Vendrell, M. (2017). Modern synthetic avenues for the preparation of functional fluorophores. *Angewandte Chemie International Edition*, 56(14): 3758-3769.

73. de Souza, M. V. N. (2005). Synthesis and biological activity of natural thiazoles: An important class of heterocyclic compounds. *Journal of Sulfur Chemistry*, 26(4-5): 429-449.

74. Deng, Z.-L., Du, C.-X., Li, X., Hu, B., Kuang, Z.-K., Wang, R., et al. (2013). Exploring the biologically relevant chemical space for drug discovery. *Journal of Chemical Information and Modeling*, 53(11): 2820-2828.

75. Ding, X., Liu, J., Li, J., Wang, F., Wang, Y., Song, S., et al. (2016). Polydopamine coated manganese oxide nanoparticles with ultrahigh relaxivity as nanotheranostic agents for magnetic resonance imaging guided synergetic chemo-/photothermal therapy. *Chemical Science*, 7(11): 6695-6700.

76. Doane, T. L., and Burda, C. (2012). The unique role of nanoparticles in nanomedicine: imaging, drug delivery and therapy. *Chemical Society Reviews*, 41(7): 2885-2911.

77. Dolmans, D. E., Fukumura, D., and Jain, R. K. (2003). Photodynamic therapy for cancer. *Nature Reviews Cancer*, 3(5): 380-387.

78. Douglass, I. B., and Dains, F. (1934). Some derivatives of benzoyl and furoyl isothiocyanates and their use in synthesizing heterocyclic compounds. *Journal of the American Chemical Society*, 56(3): 719-721.

79. Duan, C., Huang, F., and Cao, Y. (2012). Recent development of push–pull conjugated polymers for bulk-heterojunction photovoltaics: rational design and fine tailoring of molecular structures. *Journal of Materials Chemistry*, 22(21): 10416-10434.

80. Dullaghan, M. E., Owen, L. J., and Nord, F. (1952). 5-Nitro-2-thenaldehyde. *Journal of the American Chemical Society*, 74(10): 2676-2677.

81. Dykstra, C., Frenking, G., Kim, K., and Scuseria, G. (2011). *Theory and applications of computational chemistry: the first forty years*: Elsevier.

82. El-Shishtawy, R. M., Borbone, F., Al-Amshany, Z. M., Tuzi, A., Barsella, A., Asiri, A. M., et al. (2013). Thiazole azo dyes with lateral donor branch: Synthesis, structure and second order NLO properties. *Dyes and Pigments*, 96(1): 45-51.

83. Ernzerhof, M., and Scuseria, G. E. (1999). Assessment of the Perdew–Burke–Ernzerhof exchange-correlation functional. *The Journal of Chemical Physics*, 110(11): 5029-5036.

84. Ethirajan, M., Chen, Y., Joshi, P., and Pandey, R. K. (2011). The role of porphyrin chemistry in tumor imaging and photodynamic therapy. *Chemical Society Reviews*, 40(1): 340-362.

85. Evers, A., and Klabunde, T. (2005). Structure-based drug discovery using GPCR homology modeling: successful virtual screening for antagonists of the alpha1A adrenergic receptor. *Journal of Medicinal Chemistry*, 48(4): 1088-1097.

86. Fabian, J. (2001). Electronic excitation of sulfur-organic compounds–performance of time-dependent density functional theory. *Theoretical Chemistry Accounts*, 106(3): 199-217.

87. Fabian, J. (2010). TDDFT-calculations of Vis/NIR absorbing compounds. *Dyes and Pigments*, 84(1): 36-53.

88. Fan, W., Shen, B., Bu, W., Chen, F., He, Q., Zhao, K., et al. (2014). A smart upconversion-based mesoporous silica nanotheranostic system for synergetic chemo-/radio-/photodynamic therapy and simultaneous MR/UCL imaging. *Biomaterials*, 35(32): 8992-9002.

89. Fang, J., Liao, L., Yin, H., Nakamura, H., Subr, V., Ulbrich, K., et al. (2015). Photodynamic therapy and imaging based on tumor-targeted nanoprobe, polymer-conjugated zinc protoporphyrin. *Future Science OA*, 1(3).

90. Fisher, B., Costantino, J. P., Wickerham, D. L., Redmond, C. K., Kavanah, M., Cronin, W. M., et al. (1998). Tamoxifen for prevention of breast cancer: report of the national surgical adjuvant breast and bowel project p-1 study. *JNCI: Journal of the National Cancer Institute*, 90(18): 1371-1388.

91. Foresman, J. B., Head-Gordon, M., Pople, J. A., and Frisch, M. J. (1992). Toward a systematic molecular orbital theory for excited states. *The Journal of Physical Chemistry*, 96(1): 135-149.

92. França, T. C. C. (2015). Homology modeling: an important tool for the drug discovery. *Journal of Biomolecular Structure and Dynamics*, 33(8): 1780-1793.

93. Frangioni, J. V. (2003). In vivo near-infrared fluorescence imaging. *Current Opinion in Chemical Biology*, 7(5): 626-634.

94. Funkhouser, J. (2002). Reinventing pharma: the theranostic revolution. *Current Drug Discovery*, 2: 17-19.

95. Galloway, W. R., Isidro-Llobet, A., and Spring, D. R. (2010). Diversity-oriented synthesis as a tool for the discovery of novel biologically active small molecules. *Nature Communications*, 1: 80.

96. Gampe, D. M., Hänsch, V. G., Schramm, S., Menzel, R., Weiss, D., and Beckert, R. (2017). Mixing chromophores: donor–acceptor dyes with low-lying LUMOs and narrow band gaps by connecting 4-alkoxythiazoles and azaacenes. *European Journal of Organic Chemistry*, 2017(10): 1369-1379.

97. Gao, M., Yu, F., Lv, C., Choo, J., and Chen, L. (2017). Fluorescent chemical probes for accurate tumor diagnosis and targeting therapy. *Chemical Society Reviews*, 46(8): 2237-2271.

98. Gholap, S. S. (2016). Pyrrole: An emerging scaffold for construction of valuable therapeutic agents. *European Journal of Medicinal Chemistry*, 110:13-31.

99. Global, G. (2015). regional, and national age-sex specific all-cause and cause-specific mortality for 240 causes of death, 1990-2013: a systematic analysis for the global burden of disease study 2013. *Lancet*, 385(9963): 117-171.

100. Gold, L., Polisky, B., Uhlenbeck, O., and Yarus, M. (1995). Diversity of oligonucleotide functions. *Annual Rreview of Biochemistry*, 64(1): 763-797.

101. Gridelli, C., Maione, P., Del Gaizo, F., Colantuoni, G., Guerriero, C., Ferrara, C., et al. (2007). Sorafenib and sunitinib in the treatment of advanced non-small cell lung cancer. *The Oncologist*, 12(2): 191-200.

102. Griffiths, J. (1982). Practical aspects of colour prediction of organic dye molecules. *Dyes and Pigments*, 3(2-3): 211-233.

103. Guillaumont, D., and Nakamura, S. (2000). Calculation of the absorption wavelength of dyes using time-dependent density-functional theory (TD-DFT). *Dyes and Pigments*, 46(2): 85-92.

104. Gund, P. (1977). Three-dimensional pharmacophoric pattern searching. *Progress in molecular and subcellular biology* (pp. 117-143): Springer.

105. Gupton, J. T. (2006). Pyrrole natural products with antitumor properties. *Heterocyclic Antitumor Antibiotics* (pp. 53-92): Springer.

106. Hagfeldt, A., Boschloo, G., Sun, L., Kloo, L., and Pettersson, H. (2010). Dye-sensitized solar cells. *Chemical Reviews*, 110(11): 6595-6663.

107. Hansch, C., Leo, A., and Taft, R. W. (1991). A survey of Hammett substituent constants and resonance and field parameters. *Chemical Reviews*, 91(2): 165-195.

108. Hartman, G. D., Egbertson, M. S., Halczenko, W., Laswell, W. L., Duggan, M. E., Smith, R. L., et al. (1992). Non-peptide fibrinogen receptor antagonists. 1. Discovery and design of exosite inhibitors. *Journal of Medicinal Chemistry*, 35(24): 4640-4642.

109. Hartwell, L. H., and Kastan, M. B. (1994). Cell cycle control and cancer. *Science-AAAS-Weekly Paper Edition*, 266(5192): 1821-1828.

110. He, G. S., Tan, L.-S., Zheng, Q., and Prasad, P. N. (2008). Multiphoton absorbing materials: molecular designs, characterizations, and applications. *Chemical Reviews*, 108(4): 1245-1330.

111. Hegarty, D., and Robb, M. A. (1979). Application of unitary group methods to configuration interaction calculations. *Molecular Physics*, 38(6): 1795-1812.

112. Henary, M., Pannu, V., Owens, E. A., and Aneja, R. (2012). Near infrared active heptacyanine dyes with unique cancer-imaging and cytotoxic properties. *Bioorganic and Medicinal Chemistry Letters*, 22(2): 1242-1246.

113. Hoeben, F. J., Jonkheijm, P., Meijer, E., and Schenning, A. P. (2005). About supramolecular assemblies of π-conjugated systems. *Chemical Reviews*, 105(4): 1491-1546.

114. Hong, Y., Lam, J. W., and Tang, B. Z. (2009). Aggregation-induced emission: phenomenon, mechanism and applications. *Chemical Communications,* (29): 4332-4353.

115. Hong, Y., Lam, J. W., and Tang, B. Z. (2011). Aggregation-induced emission. *Chemical Society Reviews*, 40(11): 5361-5388.

116. Horiuchi, D., Huskey, N. E., Kusdra, L., Wohlbold, L., Merrick, K. A., Zhang, C., et al. (2012). Chemical-genetic analysis of cyclin dependent kinase 2 function reveals an important role in cellular transformation by multiple oncogenic pathways. *Proceedings of the National Academy of Sciences*, 109(17): E1019-E1027.

117. Hrobarik, P., Zahradnik, P., and Fabian, W. M. (2004). Computational design of benzothiazole-derived push–pull dyes with high molecular quadratic hyperpolarizabilities. *Physical Chemistry Chemical Physics*, 6(3): 495-502.

118. Hrobáriková, V., Hrobárik, P., Gajdoš, P., Fitilis, I., Fakis, M., Persephonis, P., et al. (2010). Benzothiazole-based fluorophores of donor-π-acceptor-π-donor type displaying high two-photon absorption. *The Journal of Organic Chemistry*, 75(9): 3053-3068.

119. Huang, M., Shen, A., Ding, J., and Geng, M. (2014). Molecularly targeted cancer therapy: some lessons from the past decade. *Trends in Pharmacological Sciences*, 35(1): 41-50.

120. Huang, Y., Hemmer, E., Rosei, F., and Vetrone, F. (2016). Multifunctional liposome nanocarriers combining upconverting nanoparticles and anticancer drugs. *The Journal of Physical Chemistry B*, 120(22): 4992-5001.

121. Improta, R. (2011). UV-visible absorption and emission energies in condensed phase by PCM/TD-DFT methods. *Computational Strategies for Spectroscopy: From Small Molecules to Nano Systems*: 37-75.

122. Ioakimidis, L., Thoukydidis, L., Mirza, A., Naeem, S., and Reynisson, J. (2008). Benchmarking the reliability of QikProp. Correlation between experimental and predicted values. *Molecular Informatics*, 27(4): 445-456.

123. Isegawa, M., Peverati, R., and Truhlar, D. G. (2012). Performance of recent and high-performance approximate density functionals for time-dependent density functional theory calculations of valence and Rydberg electronic transition energies. *The Journal of Chemical Physics*, 137(24): 244104.

124. Jacquemin, D., Assfeld, X., Preat, J., and Perpète, E. A. (2007). Comparison of theoretical approaches for predicting the UV/Vis spectra of anthraquinones. *Molecular Physics*, 105(2-3): 325-331.

125. Jacquemin, D., Perpete, E. A., Ciofini, I., and Adamo, C. (2008a). Accurate simulation of optical properties in dyes. *Accounts of Chemical Research*, 42(2): 326-334.

126. Jacquemin, D., Perpète, E. a., Ciofini, I., and Adamo, C. (2009). Accurate simulation of optical properties in dyes. *Accounts of Chemical Research*, 42: 326-334.

127. Jacquemin, D., Perpète, E. A., Scalmani, G., Frisch, M. J., Assfeld, X., Ciofini, I., et al. (2006a). Time-dependent density functional theory investigation of the absorption, fluorescence, and phosphorescence spectra of solvated coumarins. *The Journal of Chemical Physics*, 125(16): 164324.

128. Jacquemin, D., Perpete, E. A., Scuseria, G. E., Ciofini, I., and Adamo, C. (2008b). TD-DFT performance for the visible absorption spectra of organic dyes: conventional versus long-range hybrids. *Journal of Chemical Theory and Computation*, 4(1): 123-135.

129. Jacquemin, D., Planchat, A., Adamo, C., and Mennucci, B. (2012). TD-DFT assessment of functionals for optical 0–0 transitions in solvated dyes. *Journal of Chemical Theory and Computation*, 8(7): 2359-2372.

130. Jacquemin, D., Preat, J., Wathelet, V., and Perpète, E. A. (2006b). Substitution and chemical environment effects on the absorption spectrum of indigo. *The Journal of Chemical Physics*, 124(7): 074104.

131. Jahnke, A. C., Spulber, M., Neuburger, M., Palivan, C. G., and Wenger, O. S. (2014). Electronic coupling mediated by furan, thiophene, selenophene and tellurophene in a homologous series of organic mixed valence compounds. *Chemical Communications*, 50(74): 10883-10886.

132. Jenkins, I. H., and Pickup, P. G. (1993). Electronically conducting polymers containing conjugated bithiazole moieties from bis (thienyl) bithiazoles. *Macromolecules*, 26(17): 4450-4456.

133. Jiao, C., Huang, K.-W., and Wu, J. (2011). Perylene-fused BODIPY dye with near-IR absorption/emission and high photostability. *Organic Letters*, 13(4): 632-635.

134. Jo, S. D., Ku, S. H., Won, Y.-Y., Kim, S. H., and Kwon, I. C. (2016). Targeted nanotheranostics for future personalized medicine: recent progress in cancer therapy. *Theranostics*, 6(9): 1362.

135. Josefsen, L. B., and Boyle, R. W. (2012). Unique diagnostic and therapeutic roles of porphyrins and phthalocyanines in photodynamic therapy, imaging and theranostics. *Theranostics*, 2(9): 916.

136. Joule, J. A., and Mills, K. (2010). *Heterocyclic Chemistry* (5th ed.): John Wiley & Sons, Ltd., UK.

137. Kamal, A., Dastagiri, D., Ramaiah, M. J., Reddy, J. S., Bharathi, E. V., Reddy, M. K., et al. (2011). Synthesis and apoptosis inducing ability of new anilino substituted pyrimidine sulfonamides as potential anticancer agents. *European Journal of Medicinal Chemistry*, 46(12): 5817-5824.

138. Kashyap, S. J., Garg, V. K., Sharma, P. K., Kumar, N., Dudhe, R., and Gupta, J. K. (2012). Thiazoles: having diverse biological activities. *Medicinal Chemistry Research*, 21(8): 2123-2132.

139. Katori, A., Azuma, E., Ishimura, H., Kuramochi, K., and Tsubaki, K. (2015). Fluorescent dyes with directly connected xanthone and xanthene units. *The Journal of Organic Chemistry*, 80(9): 4603-4610.

140. Keen, N., and Taylor, S. (2004). Aurora-kinase inhibitors as anticancer agents. *Nature Reviews Cancer*, 4(12): 927-936.

141. Kelkar, S. S., and Reineke, T. M. (2011). Theranostics: Combining imaging and therapy. *Bioconjugate Chemistry*, 22(10): 1879-1903.

142. Kim, E., Koh, M., Ryu, J., and Park, S. B. (2008). Combinatorial discovery of full-color-tunable emissive fluorescent probes using a single core skeleton, 1, 2-dihydropyrrolo[3,4-β]indolizin-3-one. *Journal of the American Chemical Society*, 130(37): 12206-12207.

143. Kim, E., Lee, Y., Lee, S., and Park, S. B. (2015). Discovery, understanding, and bioapplication of organic fluorophore: a case study with an indolizine-based novel fluorophore, Seoul-Fluor. *Accounts of Chemical Research*, 48(3): 538-547.

144. Kim, E., and Park, S. B. (2009). Chemistry as a prism: a review of light-emitting materials having tunable emission wavelengths. *Chemistry–An Asian Journal*, 4(11): 1646-1658.

145. Kim, J., Kim, H., and Park, S. B. (2014). Privileged structures: efficient chemical "Navigators" toward unexplored biologically relevant chemical spaces. *Journal of the American Chemical Society*, 136(42): 14629-14638.

146. Kivala, M., and Diederich, F. (2008). Acetylene-derived strong organic acceptors for planar and nonplanar push-pull chromophores. *Accounts of Chemical Research*, 42(2): 235-248.

147. Kobayashi, H., Ogawa, M., Alford, R., Choyke, P. L., and Urano, Y. (2010). New strategies for fluorescent probe design in medical diagnostic imaging. *Chemical Reviews*, 110(5): 2620.

148. Koinuma, H., and Takeuchi, I. (2004). Combinatorial solid-state chemistry of inorganic materials. *Nature Materials*, 3(7): 429-438.

149. Kollareddy, M., Zheleva, D., Dzubak, P., Brahmkshatriya, P. S., Lepsik, M., and Hajduch, M. (2012). Aurora kinase inhibitors: progress towards the clinic. *Investigational New Drugs*, 30(6): 2411-2432.

150. Kowada, T., Maeda, H., and Kikuchi, K. (2015). BODIPY-based probes for the fluorescence imaging of biomolecules in living cells. *Chemical Society Reviews*, 44(14): 4953-4972.

151. Kumar, S. V., Parameshwarappa, G., and Ila, H. (2013). Synthesis of 2, 4, 5-trisubstituted thiazoles via Lawesson's reagent-mediated chemoselective thionation–cyclization of functionalized enamides. *The Journal of Organic Chemistry*, 78(14): 7362-7369.

152. Lace, B., and Prandi, C. (2016). Shaping small bioactive molecules to untangle their biological function: a focus on fluorescent plant hormones. *Molecular Plant*, 9(8): 1099-1118.

153. Lakowicz, J. R. (2006). *Principles of fluorescence spectroscopy* (Vol.3): Springer, Boston, MA.

154. Landry, Y., and Gies, J. P. (2008). Drugs and their molecular targets: an updated overview. *Fundamental & Clinical Pharmacology*, 22(1): 1-18.

155. Langdon-Jones, E. E., Jones, A. B., Williams, C. F., Hayes, A. J., Lloyd, D., Mottram, H. J., et al. (2017). Anticancer, azonafide-inspired fluorescent ligands and their rhenium (i) complexes for cellular imaging. *European Journal of Inorganic Chemistry*, 2017(3): 759-766.

156. Laurent, A. D., Adamo, C., and Jacquemin, D. (2014). Dye chemistry with time-dependent density functional theory. *Physical Chemistry Chemical Physics*, 16(28): 14334-14356.

157. Laurent, A. D., and Jacquemin, D. (2013). TD-DFT benchmarks: A review. *International Journal of Quantum Chemistry*, 113(17): 2019-2039.

158. Lavis, L. D., and Raines, R. T. (2008). Bright ideas for chemical biology. *ACS Chemical Biology*, 3(3): 142-155.

159. Le Guennic, B., and Jacquemin, D. (2015). Taking up the cyanine challenge with quantum tools. *Accounts of Chemical Research*, 48(3): 530-537.

160. Le Guennic, B., Maury, O., and Jacquemin, D. (2012). Aza-boron-dipyrromethene dyes: TD-DFT benchmarks, spectral analysis and design of original near-IR structures. *Physical Chemistry Chemical Physics*, 14(1): 157-164.

161. Leang, S. S., Zahariev, F., and Gordon, M. S. (2012). Benchmarking the performance of time-dependent density functional methods. *The Journal of Chemical Physics*, 136(10): 104101.

162. Lee, H., Akers, W., Bhushan, K., Bloch, S., Sudlow, G., Tang, R., et al. (2011). Near-infrared pH-activatable fluorescent probes for imaging primary and metastatic breast tumors. *Bioconjugate Chemistry*, 22(4): 777-784.

163. Lee, S. Y., Yasuda, T., Yang, Y. S., Zhang, Q., and Adachi, C. (2014). Luminous butterflies: efficient exciton harvesting by benzophenone derivatives for full-color delayed fluorescence OLEDs. *Angewandte Chemie*, 126(25): 6520-6524.

164. Levi, L., and Müller, T. J. (2016). Multicomponent syntheses of functional chromophores. *Chemical Society Reviews*, 45(10): 2825-2846.

165. Lewars, E. G. (2016). *Computational chemistry: introduction to the theory and applications of molecular and quantum mechanics*: Springer., Switzerland.

166. Li, X., Gao, X., Shi, W., and Ma, H. (2013). Design strategies for water-soluble small molecular chromogenic and fluorogenic probes. *Chemical Reviews*, 114(1): 590-659.

167. Li, Y., Chen, H., Xu, J., Yadav, N. N., Chan, K. W., Luo, L., et al. (2016). CEST theranostics: label-free MR imaging of anticancer drugs. *Oncotarget*, 7(6): 6369.

168. Li, Y., Tan, C.-P., Zhang, W., He, L., Ji, L.-N., and Mao, Z.-W. (2015a). Phosphorescent iridium (III)-bis-N-heterocyclic carbene complexes as mitochondria-targeted theranostic and photodynamic anticancer agents. *Biomaterials*, 39: 95-104.

169. Li, Z. R. (2015b). *Organic light-emitting materials and devices*: CRC press, NewYork.

170. Liao, J. J.-L. (2007). Molecular recognition of protein kinase binding pockets for design of potent and selective kinase inhibitors. *Journal of Medicinal Chemistry*, 50(3): 409-424.

171. Lim, E.-K., Kim, T., Paik, S., Haam, S., Huh, Y.-M., and Lee, K. (2014). Nanomaterials for theranostics: recent advances and future challenges. *Chemical Reviews*, 115(1): 327-394.

172. Lim, E. K., Huh, Y. M., Yang, J., Lee, K., Suh, J. S., and Haam, S. (2011). pH-triggered drug-releasing magnetic nanoparticles for cancer therapy guided by molecular imaging by MRI. *Advanced Materials*, 23(21): 2436-2442.

173. Lin, J. B., Jin, Y., Lopez, S. A., Druckerman, N., Wheeler, S. E., and Houk, K. N. (2017). Torsional barriers to rotation and planarization in heterocyclic oligomers of value in organic electronics. *Journal of Chemical Theory and Computation*, 13(11): 5624-5638.

174. Lipinski, C. A. (2004). Lead-and drug-like compounds: the rule-of-five revolution. *Drug Discovery Today: Technologies*, 1(4): 337-341.

175. Lippert, E. (1955). Dipolmoment und elektronenstruktur von angeregten molekülen. *Zeitschrift für Naturforschung A*, 10(7): 541-545.

176. Liu, G.-N., Zhang, M.-J., Liu, W.-Q., Sun, H., Li, X.-Y., Li, K., et al. (2015). Structures and multiple properties of two polar metal–organic frameworks based on achiral N, O-coordinated ligands: toward multifunctional materials. *Dalton Transactions*, 44(43): 18882-18892.

177. Liu, J., Han, J., Kang, Z., Golamaully, R., Xu, N., Li, H., et al. (2014). In vivo near-infrared photothermal therapy and computed tomography imaging of cancer cells using novel tungsten-based theranostic probe. *Nanoscale*, 6(11): 5770-5776.

178. Liu, X., Xu, Z., and Cole, J. M. (2013). Molecular design of UV–vis absorption and emission properties in organic fluorophores: toward larger bathochromic shifts, enhanced molar extinction coefficients, and greater Stokes shifts. *The Journal of Physical Chemistry C*, 117(32): 16584-16595.

179. Lopez-Rodriguez, V., Gaspar-Carcamo, R., Pedraza-Lopez, M., Rojas-Calderon, E., de Murphy, C. A., Ferro-Flores, G., et al. (2015). Preparation and preclinical evaluation of 66 Ga-DOTA-E (c(RGDfK))$_2$ as a potential theranostic radiopharmaceutical. *Nuclear Medicine and Biology*, 42(2): 109-114.

180. Loudet, A., and Burgess, K. (2007). BODIPY dyes and their derivatives: syntheses and spectroscopic properties. *Chemical Reviews*, 107(11): 4891-4932.

181. Lu, B., and Atala, A. (2016). Small molecules: controlling cell fate and function. *In Situ Tissue Regeneration*, 87-110.

182. Lu, Y., and Mahato, R. I. (2009). *Pharmaceutical perspectives of cancer therapeutics*: Springer Science & Business Media, Heidelberg-London-New York.

183. Lugovik, K. I., Popova, A. V., Eltyshev, A. K., Benassi, E., and Belskaya, N. P. (2017). Synthesis of thiazoles bearing aryl enamine/aza-enamine side chains: effect of the π-conjugated spacer structure and hydrogen bonding on photophysical properties. *European Journal of Organic Chemistry*, 2017(28): 4175-4187.

184. Luo, J., Xie, Z., Lam, J. W., Cheng, L., Chen, H., Qiu, C., et al. (2001). Aggregation-induced emission of 1-methyl-1,2,3,4,5-pentaphenylsilole. *Chemical Communications*(18): 1740-1741.

185. Luo, S., Tan, X., Qi, Q., Guo, Q., Ran, X., Zhang, L., et al. (2013). A multifunctional heptamethine near-infrared dye for cancer theranostics. *Biomaterials*, 34(9): 2244-2251.

186. Luo, Z., Yuan, X., Yu, Y., Zhang, Q., Leong, D. T., Lee, J. Y., et al. (2012). From aggregation-induced emission of Au (I)–thiolate complexes to ultrabright

Au (0)@ Au (I)–thiolate core–shell nanoclusters. *Journal of the American Chemical Society*, 134(40): 16662-16670.

187. Lv, P.-C., Li, H.-Q., Sun, J., Zhou, Y., and Zhu, H.-L. (2010). Synthesis and biological evaluation of pyrazole derivatives containing thiourea skeleton as anticancer agents. *Bioorganic and Medicinal Chemistry*, 18(13): 4606-4614.

188. Lv, R., Yang, P., He, F., Gai, S., Yang, G., Dai, Y., et al. (2015). An imaging-guided platform for synergistic photodynamic/photothermal/chemo-therapy with pH/temperature-responsive drug release. *Biomaterials*, 63: 115-127.

189. Lyu, Y., Chen, G., Shangguan, D., Zhang, L., Wan, S., Wu, Y., et al. (2016). Generating cell targeting aptamers for nanotheranostics using cell-SELEX. *Theranostics*, 6(9): 1440.

190. Frisch, M. J.; Trucks, G. W.; Schlegel, H. B.; Scuseria, G. E.; Robb, M. A.; Cheeseman, et al. *Gaussian 09*, Gaussian, Inc.: Wallingford, CT, USA, 2009.

191. Ma, Y., Huang, J., Song, S., Chen, H., and Zhang, Z. (2016). Cancer-targeted nanotheranostics: recent advances and perspectives. *Small*, 12(36): 4936-4954.

192. Maeng, J. H., Lee, D.-H., Jung, K. H., Bae, Y.-H., Park, I.-S., Jeong, S., et al. (2010). Multifunctional doxorubicin loaded superparamagnetic iron oxide nanoparticles for chemotherapy and magnetic resonance imaging in liver cancer. *Biomaterials*, 31(18): 4995-5006.

193. Malumbres, M. (2014). Cyclin-dependent kinases. *Genome Biology*, 15(6): 122.

194. Marder, S. R., Kippelen, B., Jen, A. K.-Y., and Peyghambarian, N. (1997). Design and synthesis of chromophores and polymers for electro-optic and photorefractive applications. *Nature*, 388(6645): 845-851.

195. Marenich, A. V., Cramer, C. J., Truhlar, D. G., Guido, C. A., Mennucci, B., Scalmani, G., et al. (2011). Practical computation of electronic excitation in solution: vertical excitation model. *Chemical Science*, 2(11): 2143-2161.

196. Mariaule, G., and Belmont, P. (2014). Cyclin-dependent kinase inhibitors as marketed anticancer drugs: where are we now? A short survey. *Molecules*, 19(9): 14366-14382.

197. Martins, P., Jesus, J., Santos, S., Raposo, L. R., Roma-Rodrigues, C., Baptista, P. V., et al. (2015). Heterocyclic anticancer compounds: recent advances and the paradigm shift towards the use of nanomedicine's tool box. *Molecules*, 20(9): 16852-16891.

198. Mataga, N., Kaifu, Y., and Koizumi, M. (1956). Solvent effects upon fluorescence spectra and the dipolemoments of excited molecules. *Bulletin of the Chemical Society of Japan*, 29(4): 465-470.

199. Matsuura, A., Sato, H., Sotoyama, W., Takahashi, A., and Sakurai, M. (2008). AM1, PM3, and PM5 calculations of the absorption maxima of basic organic dyes. *Journal of Molecular Structure: Theochem*, 860(1): 119-127.

200. Mei, J., Hong, Y., Lam, J. W., Qin, A., Tang, Y., and Tang, B. Z. (2014). Aggregation-induced emission: The whole is more brilliant than the parts. *Advanced Materials*, 26(31): 5429-5479.

201. Mei, J., Leung, N. L., Kwok, R. T., Lam, J. W., and Tang, B. Z. (2015). Aggregation-induced emission: together we shine, united we soar! *Chemical review,* 115(21): 11718-11940.

202. Meng, S., and Ma, J. (2008). Solvatochromic shift of donor− acceptor substituted bithiophene in solvents of different polarity: quantum chemical and molecular dynamics simulations. *The Journal of Physical Chemistry B*, 112(14): 4313-4322.

203. Mennucci, B., and Tomasi, J. (1997). Continuum solvation models: A new approach to the problem of solute's charge distribution and cavity boundaries. *The Journal of Chemical Physics*, 106(12): 5151-5158.

204. Miertuš, S., Scrocco, E., and Tomasi, J. (1981). Electrostatic interaction of a solute with a continuum. A direct utilizaion of AB initio molecular potentials for the prevision of solvent effects. *Chemical Physics*, 55(1): 117-129.

205. Min, K. H., Min, H. S., Lee, H. J., Park, D. J., Yhee, J. Y., Kim, K., et al. (2015). pH-controlled gas-generating mineralized nanoparticles: a theranostic agent for ultrasound imaging and therapy of cancers. *ACS Nano*, 9(1): 134-145.

206. Mishra, A., and Bäuerle, P. (2012). Small molecule organic semiconductors on the move: promises for future solar energy technology. *Angewandte Chemie International Edition*, 51(9): 2020-2067.

207. Mishra, A., Behera, R. K., Behera, P. K., Mishra, B. K., and Behera, G. B. (2000). Cyanines during the 1990s: a review. *Chemical Reviews*, 100(6): 1973-2012.

208. Mishra, A., Fischer, M. K., and Bäuerle, P. (2009). Metal-free organic dyes for dye-sensitized solar cells: From structure: Property relationships to design rules. *Angewandte Chemie International Edition*, 48(14): 2474-2499.

209. Modjtahedi, H., and Dean, C. (1994). The receptor for EGF and its ligands-expression, prognostic value and target for therapy in cancer. *International Journal of Oncology*, 4(2): 277-296.

210. Moss, G. (1996). Basic terminology of stereochemistry (IUPAC Recommendations 1996). *Pure and Applied Chemistry*, 68(12): 2193-2222.

211. Mountzios, G., Terpos, E., and Dimopoulos, M.-A. (2008). Aurora kinases as targets for cancer therapy. *Cancer Treatment Reviews*, 34(2): 175-182.

212. Muller, C. D., Falcou, A., Reckefuss, N., and Rojahn, M. (2003). Multi-colour organic light-emitting displays by solution processing. *Nature*, 421(6925): 829.

213. Müller, T. J., and Bunz, U. H. (2007). *Functional organic materials: syntheses, strategies and applications*: John Wiley and Sons, Weinheim.

214. Mura, S., and Couvreur, P. (2012). Nanotheranostics for personalized medicine. *Advanced Drug Delivery Reviews*, 64(13): 1394-1416.

215. Muthu, M. S., Kutty, R. V., Luo, Z., Xie, J., and Feng, S.-S. (2015). Theranostic vitamin E TPGS micelles of transferrin conjugation for targeted co-delivery of docetaxel and ultra bright gold nanoclusters. *Biomaterials*, 39: 234-248.

216. Narang, A. S., and Varia, S. (2011). Role of tumor vascular architecture in drug delivery. *Advanced Drug Delivery Reviews*, 63(8): 640-658.

217. Naumov, P. e., Ozawa, Y., Ohkubo, K., and Fukuzumi, S. (2009). Structure and spectroscopy of oxyluciferin, the light emitter of the firefly bioluminescence. *Journal of the American Chemical Society*, 131(32): 11590-11605.

218. Nikonova, A. S., Astsaturov, I., Serebriiskii, I. G., Dunbrack, R. L., and Golemis, E. A. (2013). Aurora A kinase (AURKA) in normal and pathological cell division. *Cellular and Molecular Life Sciences*, 70(4): 661-687.

219. Nishihara, Y. (2012). *Applied cross-coupling reactions* (Vol. 80): Springer Science & Business Media, Heidelberg.

220. O'boyle, N. M., Tenderholt, A. L., and Langner, K. M. (2008). Cclib: a library for package-independent computational chemistry algorithms. *Journal of Computational Chemistry*, 29(5): 839-845.

221. O'Neill, M., and Kelly, S. M. (2011). Ordered materials for organic electronics and photonics. *Advanced Materials*, 23(5): 566-584.

222. Overington, J. P., Al-Lazikani, B., and Hopkins, A. L. (2006). How many drug targets are there? *Nature Reviews Drug discovery*, 5(12): 993-996.

223. Ozturk, T., Ertas, E., and Mert, O. (2007). Use of Lawesson's reagent in organic syntheses. *Chemical Reviews*, 107(11): 5210-5278.

224. Pammolli, F., Magazzini, L., and Riccaboni, M. (2011). The productivity crisis in pharmaceutical R&D. *Nature Reviews Drug discovery*, 10(6): 428-438.

225. Panja, S., Dey, G., Bharti, R., Kumari, K., Maiti, T., Mandal, M., et al. (2016). Tailor-made temperature-sensitive micelle for targeted and on-demand release of anticancer drugs. *ACS Applied Materials & Interfaces*, 8(19): 12063-12074.

226. Pavlopoulos, T. (1973). Prediction of laser action properties of organic dyes from their structure and the polarization characteristics of their electronic transitions. *IEEE Journal of Quantum Electronics*, 9(5): 510-516.

227. Perdew, J. P., Burke, K., and Ernzerhof, M. (1996). Generalized gradient approximation made simple. *Physical Review Letters*, 77(18): 3865.

228. Pinilla, C., Appel, J., Blondelle, S., Dooley, C., Dörner, B., Eichler, J., et al. (1995). A review of the utility of soluble peptide combinatorial libraries. *Biopolymers*, 37(3): 221-240.

229. Prampolini, G., Bellina, F., Biczysko, M., Cappelli, C., Carta, L., Lessi, M., et al. (2013). Computational design, synthesis, and mechanochromic properties of new thiophene-based π-conjugated chromophores. *Chemistry-A European Journal*, 19(6): 1996-2004.

230. Quartarolo, A. D., Lanzo, I., Sicilia, E., and Russo, N. (2009). Can phthalocyanines and their substituted α-para-(methoxy) phenyl derivatives act as photosensitizers in photodynamic therapy? A TD-DFT study. *Physical Chemistry Chemical Physics*, 11(22): 4586-4592.

231. Radhakrishnan, R., and Sreejalekshmi, K. G. (2016a). Expanding the donor–acceptor toolbox with a minimal 5-(thiophen-2-yl)-1,3-thiazole core: transition metal-free synthesis and molecular design for HOMO–LUMO energy modulations. *New Journal of Chemistry*, 40(4): 3036-3039.

232. Radhakrishnan, R., and Sreejalekshmi, K. G. (2016b). Fluorophores based on a minimal thienylthiazole core: towards multifunctional materials with solid state red emissions, solvatochromism and AIE behaviour. *RSC Advances*, 6(39): 32705-32709.

233. Radhakrishnan, R., and Sreejalekshmi, K. G. (2018). Computational design, synthesis and structure property evaluation of 1, 3-thiazole based colour tunable multi-heterocyclic small organic fluorophores as multi-functional molecular materials. *The Journal of Organic Chemistry,* 83(7):3453-3466

234. Radi, M., Dreassi, E., Brullo, C., Crespan, E., Tintori, C., Bernardo, V., et al. (2011). Design, synthesis, biological activity, and ADME properties of pyrazolo [3, 4-d] pyrimidines active in hypoxic human leukemia cells: a lead optimization study. *Journal of Medicinal Chemistry*, 54(8): 2610-2626.

235. Rai, P., Mallidi, S., Zheng, X., Rahmanzadeh, R., Mir, Y., Elrington, S., et al. (2010). Development and applications of photo-triggered theranostic agents. *Advanced Drug Delivery Reviews*, 62(11): 1094-1124.

236. Rajappa, S., Nair, M. D., Advani, B. G., Sreenivasan, R., and Desai, J. A. (1979). A general synthesis of thiazoles. Part 3. Comparative evaluation of different functionalised thioureas as precursors. *Journal of the Chemical Society, Perkin Transactions 1*: 1762-1764.

237. Rajappa, S., Sudarsanam, V., and Yadav, V. (1982). A general synthesis of thiazoles. Part 6. Synthesis of 2-amino-5-heterylthiazoles. *Journal of Chemical Sciences*, 91(5): 451-455.

238. Rajasekharan, K., Nair, K., and Jenardanan, G. (1986). Studies on the synthesis of 5-acyl-2,4-diaminothiazoles from amidinothioureas. *Synthesis*, 1986(05): 353-355.

239. Ravi, M., Soujanya, T., Samanta, A., and Radhakrishnan, T. (1995). Excited-state dipole moments of some coumarin dyes from a solvatochromic method using the solvent polarity parameter, ENT. *Journal of the Chemical Society, Faraday Transactions*, 91(17): 2739-2742.

240. Rawlins, M. D. (2004). Cutting the cost of drug development? *Nature Reviews Drug discovery*, 3(4): 360-364.

241. Reichardt, C. (1994). Solvatochromic dyes as solvent polarity indicators. *Chemical Reviews*, 94: 2319-2358.

242. Reichardt, C., and Welton, T. (2011). *Solvents and solvent effects in organic chemistry*: John Wiley & Sons, Weinheim.

243. Rettig, W. (1986). Charge separation in excited states of decoupled systems-TICT compounds and implications regarding the development of new laser dyes and the primary process of vision and photosynthesis. *Angewandte Chemie International Edition*, 25(11): 971-988.

244. Ried, W., and Kaiser, L. (1976). Neuartige synthese substituierter 2-morpholino- und 2-athoxythiazole. *Justus Liebigs Annalen der Chemie*, 1976(3): 395-399.

245. Rinkes, I. (1932). Researches on thiophen derivatives.(1st. Communication). *Recueil des Travaux Chimiques des Pays-Bas*, 51(12): 1134-1142.

246. Roncali, J., Leriche, P., and Blanchard, P. (2014). Molecular materials for organic photovoltaics: small is beautiful. *Advanced Materials*, 26(23): 3821-3838.

247. Roos, B. O. (1999). Theoretical studies of electronically excited states of molecular systems using multiconfigurational perturbation theory. *Accounts of Chemical Research*, 32(2): 137-144.

248. Rosenthal, E. L., Warram, J. M., de Boer, E., Chung, T. K., Korb, M. L., Brandwein-Gensler, M., et al. (2015). Safety and tumor specificity of cetuximab-IRDye800 for surgical navigation in head and neck cancer. *Clinical Cancer Research*, 21(16): 3658-3666.

249. Runge, E., and Gross, E. K. (1984). Density-functional theory for time-dependent systems. *Physical Review Letters*, 52(12): 997.

250. Saeed, A., Flörke, U., and Erben, M. F. (2014). A review on the chemistry, coordination, structure and biological properties of 1-(acyl/aroyl)-3-(substituted) thioureas. *Journal of Sulfur Chemistry*, 35(3): 318-355.

251. Sagara, Y., and Kato, T. (2009). Mechanically induced luminescence changes in molecular assemblies. *Nature Chemistry*, 1(8): 605-610.

252. Sagara, Y., Yamane, S., Mitani, M., Weder, C., and Kato, T. (2016). Mechanoresponsive luminescent molecular assemblies: an emerging class of materials. *Advanced Materials*, 28(6): 1073-1095.

253. Scarberry, K. E., Dickerson, E. B., McDonald, J. F., and Zhang, Z. J. (2008). Magnetic nanoparticle-peptide conjugates for in vitro and in vivo targeting and extraction of cancer cells. *Journal of the American Chemical Society*, 130(31): 10258-10262.

254. Schärfer, C., Schulz-Gasch, T., Ehrlich, H.-C., Guba, W., Rarey, M., and Stahl, M. (2013). Torsion angle preferences in druglike chemical space: a comprehensive guide. *Journal of Medicinal Chemistry*, 56(5): 2016-2028.

255. Schiedel, M. S., Briehn, C. A., and Bäuerle, P. (2001). Single-compound libraries of organic materials: Parallel synthesis and screening of fluorescent dyes. *Angewandte Chemie International Edition*, 40(24): 4677-4680.

256. Schreiber, S. L. (2000). Target-oriented and diversity-oriented organic synthesis in drug discovery. *Science*, 287(5460): 1964-1969.

257. Schrödinger Release 2017-2, Schrödinger, LLC. (2017). New York, NY, 2017.

258. Shang, Y. (2006). Molecular mechanisms of oestrogen and SERMs in endometrial carcinogenesis. *Nature Reviews Cancer*, 6(5): 360-368.

259. Sheldon, R. A. (2005). Green solvents for sustainable organic synthesis: state of the art. *Green Chemistry*, 7(5): 267-278.

260. Shiau, A. K., Barstad, D., Loria, P. M., Cheng, L., Kushner, P. J., Agard, D. A., et al. (1998). The structural basis of estrogen receptor/coactivator recognition and the antagonism of this interaction by tamoxifen. *Cell*, 95(7): 927-937.

261. Shiau, C.-W., and Chen, K.-F. (2013). Aryl amine substituted pyrimidine and quinazoline and their use as anticaner drugs: Google Patents.

262. Shimizu, M., and Hiyama, T. (2010). Organic fluorophores exhibiting highly efficient photoluminescence in the solid state. *Chemistry–An Asian Journal*, 5(7): 1516-1531.

263. Shoichet, B. K., McGovern, S. L., Wei, B., and Irwin, J. J. (2002). Lead discovery using molecular docking. *Current Opinion in Chemical Biology*, 6(4): 439-446.

264. Siegel, R. L., Miller, K. D., and Jemal, A. (2016). Cancer statistics, 2016. *CA: A Cancer Journal for Clinicians*, 66(1): 7-30.

265. Singh, C., Murru, S., Kavala, V., and Patel, B. K. (2006). It is "thiazolidene-2-imine" and not imidazole-2-thione as the reaction product of 1-benzoyl-3-phenylthiourea with Br_2/enolizable ketone. *Organic Letters*, 8(23): 5397-5399.

266. Singh, S., Aggarwal, A., Bhupathiraju, N. D. K., Arianna, G., Tiwari, K., and Drain, C. M. (2015). Glycosylated porphyrins, phthalocyanines, and other porphyrinoids for diagnostics and therapeutics. *Chemical Reviews*, 115(18): 10261-10306.

267. Singh Sidhu, J., Singla, R., and Jaitak, V. (2016). Indole derivatives as anticancer agents for breast cancer therapy: a review. *Anti-Cancer Agents in Medicinal Chemistry (Formerly Current Medicinal Chemistry-Anti-Cancer Agents)*, 16(2): 160-173.

268. Skehan, P., Storeng, R., Scudiero, D., Monks, A., McMahon, J., Vistica, D., et al. (1990). New colorimetric cytotoxicity assay for anticancer-drug screening. *JNCI: Journal of the National Cancer Institute*, 82(13): 1107-1112.

269. Song, G., Liang, C., Gong, H., Li, M., Zheng, X., Cheng, L., et al. (2015). Core–shell MnSe@Bi_2Se_3 fabricated via a cation exchange method as novel nanotheranostics for multimodal imaging and synergistic thermoradiotherapy. *Advanced Materials*, 27(40): 6110-6117.

270. Song, Y., Zong, H., Trivedi, E. R., Vesper, B. J., Waters, E. A., Barrett, A. G., et al. (2010). Synthesis and characterization of new porphyrazine-Gd (III) conjugates as multimodal MR contrast agents. *Bioconjugate Chemistry*, 21(12): 2267-2275.

271. Sreejalekshmi, K. G., Devi, S. K., and Rajasekharan, K. N. (2006). An efficient protocol for solid phase aminothiazole synthesis. *Tetrahedron Letters*, 47(35): 6179-6182.

272. Stanton, J. F., and Bartlett, R. J. (1993). The equation of motion coupled-cluster method. A systematic biorthogonal approach to molecular excitation energies, transition probabilities, and excited state properties. *The Journal of Chemical Physics*, 98(9): 7029-7039.

273. Staroverov, V. N., Scuseria, G. E., Tao, J., and Perdew, J. P. (2003). Comparative assessment of a new nonempirical density functional: Molecules and hydrogen-bonded complexes. *The Journal of Chemical Physics*, 119(23): 12129-12137.

274. Stephens, P., Devlin, F., Chabalowski, C., and Frisch, M. J. (1994). Ab initio calculation of vibrational absorption and circular dichroism spectra using density functional force fields. *The Journal of Physical Chemistry*, 98(45): 11623-11627.

275. Stippich, K., Weiss, D., Guether, A., Görls, H., and Beckert, R. (2009). Novel luminescence dyes and ligands based on 4-hydroxythiazole. *Journal of Sulfur Chemistry*, 30(2): 109-118.

276. Suggitt, M., and Bibby, M. C. (2005). 50 years of preclinical anticancer drug screening: empirical to target-driven approaches. *Clinical Cancer Research*, 11(3): 971-981.

277. Sun, C.-L., and Shi, Z.-J. (2014). Transition-metal-free coupling reactions. *Chemical Reviews*, 114(18): 9219-9280.

278. Sun, G., Zhao, Y., and Liang, W. (2015). Aggregation-induced emission mechanism of dimethoxy-tetraphenylethylene in water solution: molecular dynamics and QM/MM investigations. *Journal of Chemical Theory and Computation*, 11(5): 2257-2267.

279. Sun, Y., Qu, C., Chen, H., He, M., Tang, C., Shou, K., et al. (2016). Novel benzo-bis (1,2,5-thiadiazole) fluorophores for in vivo NIR-II imaging of cancer. *Chemical Science*, 7(9): 6203-6207.

280. Takadate, A., Masuda, T., Murata, C., Shibuya, M., and Isobe, A. (2000). Structuarl features for fluorescing present in methoxycoumarin derivatives. *Chemical and Pharmaceutical Bulletin*, 48(2): 256-260.

281. Takeuchi, I., Lauterbach, J., and Fasolka, M. J. (2005). Combinatorial materials synthesis. *Materials Today*, 8(10): 18-26.

282. Tan, X., Luo, S., Long, L., Wang, Y., Wang, D., Fang, S., et al. (2017). Structure-guided design and synthesis of a mitochondria-targeting near-infrared fluorophore with multimodal therapeutic activities. *Advanced Materials*, 29(43):1704196.

283. Tan, X., Luo, S., Wang, D., Su, Y., Cheng, T., and Shi, C. (2012). A NIR heptamethine dye with intrinsic cancer targeting, imaging and photosensitizing properties. *Biomaterials*, 33(7): 2230-2239.

284. Tao, T., Peng, Y.-X., Huang, W., and You, X.-Z. (2013). Coplanar bithiazole-centered heterocyclic aromatic fluorescent compounds having different donor/acceptor terminal groups. *The Journal of Organic Chemistry*, 78(6): 2472-2481.

285. Täuscher, E., Weiss, D., Beckert, R., and Görls, H. (2010). Synthesis and characterization of new 4-hydroxy-1, 3-thiazoles. *Synthesis*, 2010(10): 1603-1608.

286. Tayade, R. P., and Sekar, N. (2017). Novel thiazole based styryl dyes with benzimidazole unit-synthesis, photophysical and TD-DFT studies. *Journal of Fluorescence*, 27(1): 167-180.

287. Terai, T., and Nagano, T. (2013). Small-molecule fluorophores and fluorescent probes for bioimaging. *Pflügers Archiv-European Journal of Physiology*, 465(3): 347-359.

288. Thomas, S. W., Joly, G. D., and Swager, T. M. (2007). Chemical sensors based on amplifying fluorescent conjugated polymers. *Chemical Reviews*, 107(4): 1339-1386.

289. Thompson, L. A., and Ellman, J. A. (1996). Synthesis and applications of small molecule libraries. *Chemical Reviews*, 96(1): 555-600.

290. Thorat, K. G., and Sekar, N. (2017). Pyrrole-thiazole based push-pull chromophores: An experimental and theoretical approach to structural, spectroscopic and NLO properties of the novel styryl dyes. *Journal of Photochemistry and Photobiology A: Chemistry*, 333: 1-17.

291. Titus, S. (2016). "Structure based design and development of kinase inhibitors and dendrimeric nanoprobe based on 2-aminothiazole template*"*. Doctor of Philosophy, Indian Institute of Space Science and Technology, Thiruvananthapuram.

292. Titus, S., and Sreejalekshmi, K. G. (2014). One-pot four-component synthesis of 4-hydrazinothiazoles: novel scaffolds for drug discovery. *Tetrahedron Letters*, 55(40): 5465-5467.

293. Titus, S., and Sreejalekshmi, K. G. (2015). Propeller-shaped molecules with a thiazole hub: structural landscape and hydrazone cap mediated tunable host behavior in 4-hydrazino-1,3-thiazoles. *CrystEngComm*, 17(31): 5978-5986.

294. Titus, S., and Sreejalekshmi, K. G. (2017). Enriching biologically relevant chemical space around 2-aminothiazole template for anticancer drug development. *Medicinal Chemistry Research*, 27(1): 23-34.

295. Tomasi, J., Mennucci, B., and Cammi, R. (2005). Quantum mechanical continuum solvation models. *Chemical Reviews*, 105(8): 2999-3094.

296. Tretiak, S. (2001). Random phase approximation/semiempirical computations of electronic structure of extended organic molecules. *Recent Research Developments in Physical Chemistry*, 5: 721-745.

297. Trivedi, E. R., Harney, A. S., Olive, M. B., Podgorski, I., Moin, K., Sloane, B. F., et al. (2010a). Chiral porphyrazine near-IR optical imaging agent exhibiting preferential tumor accumulation. *Proceedings of the National Academy of Sciences*, 107(4): 1284-1288.

298. Trivedi, E. R., Lee, S., Zong, H., Blumenfeld, C. M., Barrett, A. G., and Hoffman, B. M. (2010b). Synthesis of heteroatom substituted naphthoporphyrazine derivatives with near-infrared absorption and emission. *The Journal of Organic Chemistry*, 75(5): 1799-1802.

299. Tunbridge, G. A., Oram, J., and Caggiano, L. (2013). Design, synthesis and antiproliferative activity of indole analogues of indanocine. *Medicinal Chemistry Communications*, 4(11): 1452-1456.

300. Ueda, M. (2012). Chemical biology of natural products on the basis of identification of target proteins. *Chemistry Letters*, 41(7): 658-666.

301. Vázquez, M. E., Blanco, J. B., and Imperiali, B. (2005). Photophysics and biological applications of the environment-sensitive fluorophore 6-N,N-dimethylamino-2, 3-naphthalimide. *Journal of the American Chemical Society*, 127(4): 1300-1306.

302. Veber, D. F., Johnson, S. R., Cheng, H.-Y., Smith, B. R., Ward, K. W., and Kopple, K. D. (2002). Molecular properties that influence the oral bioavailability of drug candidates. *Journal of Medicinal Chemistry*, 45(12): 2615-2623.

303. Vendrell, M., Zhai, D., Er, J. C., and Chang, Y. T. (2012). Combinatorial strategies in fluorescent probe development. *Chemical Reviews*, 112(8): 4391-4420.

304. Vichai, V., and Kirtikara, K. (2006). Sulforhodamine B colorimetric assay for cytotoxicity screening. *Nature Protocols*, 1(3): 1112-1116.

305. Vijayan, R., He, P., Modi, V., Duong-Ly, K. C., Ma, H., Peterson, J. R., et al. (2014). Conformational analysis of the DFG-out kinase motif and biochemical profiling of structurally validated type II inhibitors. *Journal of Medicinal Chemistry*, 58(1): 466-479.

306. Vitaku, E., Smith, D. T., and Njardarson, J. T. (2014). Analysis of the structural diversity, substitution patterns, and frequency of nitrogen heterocycles among US FDA approved pharmaceuticals: miniperspective. *Journal of Medicinal Chemistry*, 57(24): 10257-10274.

307. Vogelstein, B., and Kinzler, K. W. (2004). Cancer genes and the pathways they control. *Nature Medicine*, 10(8): 789-799.

308. Wakamiya, A., Mori, K., and Yamaguchi, S. (2007). 3-Boryl-2,2′-bithiophene as a versatile core skeleton for full-color highly emissive organic solids. *Angewandte Chemie International Edition*, 46(23): 4273-4276.

309. Wakamiya, A., Taniguchi, T., and Yamaguchi, S. (2006). Intramolecular B–N coordination as a scaffold for electron-transporting materials: synthesis and properties of boryl-substituted thienylthiazoles. *Angewandte Chemie International Edition*, 45(19): 3170-3173.

310. Wang, G.-W. (2013a). Mechanochemical organic synthesis. *Chemical Society Reviews*, 42(18): 7668-7700.

311. Wang, K., Huang, S., Zhang, Y., Zhao, S., Zhang, H., and Wang, Y. (2013b). Multicolor fluorescence and electroluminescence of an ICT-type organic solid

tuned by modulating the accepting nature of the central core. *Chemical Science*, 4(8): 3288-3293.

312. Wang, X., Chen, H., Zhang, K., Ma, M., Li, F., Zeng, D., et al. (2014). An intelligent nanotheranostic agent for targeting, redox-responsive ultrasound imaging, and imaging-guided high-intensity focused ultrasound synergistic therapy. *Small*, 10(7): 1403-1411.

313. Welch, G. C., Bakus, R. C., Teat, S. J., and Bazan, G. C. (2013). Impact of regiochemistry and isoelectronic bridgehead substitution on the molecular shape and bulk organization of narrow bandgap chromophores. *Journal of the American Chemical Society*, 135(6): 2298-2305.

314. Wencel-Delord, J., and Glorius, F. (2013). CH bond activation enables the rapid construction and late-stage diversification of functional molecules. *Nature Chemistry*, 5(5): 369-375.

315. WHO. (2015). WHO fact sheet;The top 10 causes of death.

316. Wu, X., Sun, X., Guo, Z., Tang, J., Shen, Y., James, T. D., et al. (2014). In vivo and in situ tracking cancer chemotherapy by highly photostable NIR fluorescent theranostic prodrug. *Journal of the American Chemical Society*, 136(9): 3579-3588.

317. Wu, Y., and Zhu, W. (2013). Organic sensitizers from D–π–A to D–A–π–A: effect of the internal electron-withdrawing units on molecular absorption, energy levels and photovoltaic performances. *Chemical Society Reviews*, 42(5): 2039-2058.

318. Wysocki, L. M., and Lavis, L. D. (2011). Advances in the chemistry of small molecule fluorescent probes. *Current Opinion in Chemical Biology*, 15(6): 752-759.

319. Xiang, M., Cao, Y., Fan, W., Chen, L., and Mo, Y. (2012). Computer-aided drug design: lead discovery and optimization. *Combinatorial Chemistry & High Throughput Screening*, 15(4): 328-337.

320. Xue, P., Ding, J., Wang, P., and Lu, R. (2016). Recent progress in the mechanochromism of phosphorescent organic molecules and metal complexes. *Journal of Materials Chemistry C*, 4(28): 6688-6706.

321. Yamaguchi, K., Murai, T., Guo, J.-D., Sasamori, T., and Tokitoh, N. (2016). Acid-responsive absorption and emission of 5-N-arylaminothiazoles: emission of white light from a single fluorescent dye and a lewis acid. *ChemistryOpen*, 5(5): 434-438.

322. Yamaguchi, K., Murai, T., Hasegawa, S., Miwa, Y., Kutsumizu, S., Maruyama, T., et al. (2015). 5-N-arylaminothiazoles as highly twisted fluorescent monocyclic heterocycles: synthesis and characterization. *Journal of Organic Chemistry*, 80(21): 10742-10756.

323. Yamaguchi, K., Murai, T., Tsuchiya, Y., Miwa, Y., Kutsumizu, S., Sasamori, T., et al. (2017). Pyridinium 5-aminothiazoles: specific photophysical properties and vapochromism in halogenated solvents. *RSC Advances.*, 7(29): 18132-18135.

324. Yanai, T., Tew, D. P., and Handy, N. C. (2004). A new hybrid exchange–correlation functional using the Coulomb-attenuating method (CAM-B3LYP). *Chemical Physics Letters*, 393(1): 51-57.

325. Yang, J., Lee, C. H., Ko, H. J., Suh, J. S., Yoon, H. G., Lee, K., et al. (2007). Multifunctional magneto-polymeric nanohybrids for targeted detection and synergistic therapeutic effects on breast cancer. *Angewandte Chemie*, 119(46): 8992-8995.

326. Yang, Q., Ma, Z., Wang, H., Zhou, B., Zhu, S., Zhong, Y., et al. (2017a). Rational design of molecular fluorophores for biological imaging in the NIR-II window. *Advanced Materials*, 29(12): 1605497.

327. Yang, Y., Lan, J., and You, J. (2017b). Oxidative C–H/C–H coupling reactions between two (hetero) arenes. *Chemical Reviews*, 117(13): 8787-8863.

328. Yang, Z., Cao, J., He, Y., Yang, J. H., Kim, T., Peng, X., et al. (2014). Macro-/micro-environment-sensitive chemosensing and biological imaging. *Chemical Society Reviews*, 43(13): 4563-4601.

329. Ye, D., Shuhendler, A. J., Cui, L., Tong, L., Tee, S. S., Tikhomirov, G., et al. (2014). Bioorthogonal cyclization-mediated in situ self-assembly of small-molecule probes for imaging caspase activity in vivo. *Nature Chemistry*, 6(6): 519-526.

330. Yu, M. K., Kim, D., Lee, I. H., So, J. S., Jeong, Y. Y., and Jon, S. (2011). Image-guided prostate cancer therapy using aptamer-functionalized thermally cross-linked superparamagnetic iron oxide nanoparticles. *Small*, 7(15): 2241-2249.

331. Yuan, L., Lin, W., Yang, Y., and Chen, H. (2012). A unique class of near-infrared functional fluorescent dyes with carboxylic-acid-modulated fluorescence ON/OFF switching: rational design, synthesis, optical properties, theoretical calculations, and applications for fluorescence imaging in living animals. *Journal of the American Chemical Society*, 134(2): 1200-1211.

332. Yuan, Z., Fu, B., Thomas, S., Zhang, S., DeLuca, G., Chang, R., et al. (2016). Unipolar electron transport polymers: A thiazole based all-electron acceptor approach. *Chemistry of Materials*, 28(17): 6045-6049.

333. Yun, S.-W., Kang, N.-Y., Park, S.-J., Ha, H.-H., Kim, Y. K., Lee, J.-S., et al. (2014). Diversity oriented fluorescence library approach (DOFLA) for live cell imaging probe development. *Accounts of Chemical Research*, 47(4): 1277-1286.

334. Yuriev, E., and Ramsland, P. A. (2013). Latest developments in molecular docking: 2010–2011 in review. *Journal of Molecular Recognition*, 26(5): 215-239.

335. Zaumseil, J., and Sirringhaus, H. (2007). Electron and ambipolar transport in organic field-effect transistors. *Chemical Reviews*, 107(4): 1296-1323.

336. Zeng, R.-S., Zou, J.-P., Zhi, S.-J., Chen, J., and Shen, Q. (2003). Novel synthesis of 1-aroyl-3-aryl-4-substituted imidazole-2-thiones. *Organic Letters*, 5(10): 1657-1659.

337. Zhang, B., Wang, J., Yu, J., Fang, X., Wang, X., and Shi, D. (2017). Site-specific biomimetic precision chemistry of bimodal contrast agent with modular peptides for tumor-targeted imaging. *Bioconjugate Chemistry*, 28(2): 330-335.

338. Zhang, L., Lei, K., Zhang, J., Song, W., Zheng, Y., Tan, S., et al. (2016). One small molecule as a theranostic agent: naphthalimide dye for subcellular fluorescence localization and photodynamic therapy in vivo. *Medicinal Chemistry Communications*, 7(6): 1171-1175.

339. Zhang, L. E., Zeng, L., Pan, Y., Luo, S., Ren, W., Gong, A., et al. (2015). Inorganic photosensitizer coupled Gd-based upconversion luminescent nanocomposites for in vivo magnetic resonance imaging and near-infrared-responsive photodynamic therapy in cancers. *Biomaterials*, 44: 82-90.

340. Zhang, R. R., Schroeder, A. B., Grudzinski, J. J., Rosenthal, E. L., Warram, J. M., Pinchuk, A. N., et al. (2017). Beyond the margins: real-time detection of cancer using targeted fluorophores. *Nature Reviews Clinical Oncology*, 14(6): 347-364.

341. Zhang, Y., Lv, T., Zhang, H., Xie, X., Li, Z., Chen, H., et al. (2017). Folate and heptamethine cyanine modified chitosan-based nanotheranostics for tumor targeted near-infrared fluorescence imaging and photodynamic therapy. *Biomacromolecules*, 18(7): 2146-2160.

342. Zhao, Y., and Truhlar, D. G. (2008). The M06 suite of density functionals for main group thermochemistry, thermochemical kinetics, noncovalent interactions, excited states, and transition elements: two new functionals and systematic testing of four M06-class functionals and 12 other functionals. *Theoretical Chemistry Accounts: Theory, Computation, and Modeling (Theoretica Chimica Acta)*, 120(1): 215-241.

343. Zheng, M., Zhao, P., Luo, Z., Gong, P., Zheng, C., Zhang, P., et al. (2014). Robust ICG theranostic nanoparticles for folate targeted cancer imaging and highly effective photothermal therapy. *ACS Applied Materials & Interfaces*, 6(9): 6709-6716.

344. Zheng, X., Peng, Q., Zhu, L., Xie, Y., Huang, X., and Shuai, Z. (2016). Unraveling the aggregation effect on amorphous phase AIE luminogens: a computational study. *Nanoscale*, 8(33): 15173-15180.

345. Zhou, Y., Liu, W.-J., Ma, Y., Wang, H., Qi, L., Cao, Y., et al. (2007). Single microwire transistors of oligoarenes by direct solution process. *Journal of the American Chemical Society*, 129(41): 12386-12387.

LIST OF PUBLICATIONS BASED ON THE THESIS

PUBLICATIONS

1. Radhakrishnan, R., and Sreejalekshmi, K. G. (2018). Computational design, synthesis and structure property evaluation of 1, 3-thiazole based colour tunable multi-heterocyclic small organic fluorophores as multi-functional molecular materials. *The Journal of Organic Chemistry*, 83(7): 3453-3466. (**Cover page**)

2. Radhakrishnan, R., and Sreejalekshmi, K. G. (2016). Fluorophores based on a minimal thienylthiazole core: towards multifunctional materials with solid state red emissions, solvatochromism and AIE behaviour. *RSC Advances*, 6(39): 32705-32709.

3. Radhakrishnan, R., and Sreejalekshmi, K. G. (2016). Expanding the donor–acceptor toolbox with a minimal 5-(thiophen-2-yl)-1,3-thiazole core: transition metal-free synthesis and molecular design for HOMO–LUMO energy modulations. *New Journal of Chemistry*, 40(4): 3036-3039.

PRESENTATIONS IN CONFERENCES OR SEMINARS

Oral presentations

1. Rakesh R and K. G. Sreejalekshmi., Development of 1,3-thiazole-based colour-tunable fluorophores towards multifunctional materials. *MRSI-ATM meeting, IISER Thiruvananthapuram, India, (2018).* **Best paper award.**

2. Rakesh R and K. G. Sreejalekshmi., Design and development of colour tunable multiheterocyclic small organic fluorophores as multifunctional molecular materials. *8th East Asia Symposium on Functional Dyes and Advanced Materials, CSIR-NIIST, Thiruvananthapuram, India, (2017).*

3. Rakesh R and K. G. Sreejalekshmi., Thienylthiazole: a promising core for theranostics**.** *National Seminar on Current Trends in Chemistry (CTriC 2017), Cochin University of Science and Technology, Kochi, India., (2017).*

Poster presentations

1. Rakesh R and K. G. Sreejalekshmi., Design and development of colour tunable multiheterocyclic small organic fluorophores as multifunctional molecular materials. *8th East Asia Symposium on Functional Dyes and Advanced Materials, CSIR-NIIST, Thiruvananthapuram, India, (2017).*

2. Rakesh R, Manjinder Singh, Mrudul C, Lakshmi S, Parvathy V.S, and K.G. Sreejalekshmi., Organic small molecule mechanofluorochromic dyes: synthesis, optical responses in varying macromolecular environments and prospective application in flexible sensors. *8th East Asia Symposium on Functional Dyes and Advanced Materials, CSIR-NIIST, Thiruvananthapuram, India, (2017).*

3. Rakesh R and K. G. Sreejalekshmi, Diversity-oriented design and synthesis of multi-heterocyclic donor acceptor hybrid cores based on 1,3-thiazole. *21st International Conference on Organic Synthesis (ICOS 21), IIT Mumbai, India, (2016).*

4. Rakesh R and K. G. Sreejalekshmi., Exceptional large stokes shift fluorophores: design, synthesis and rationalization of photophysical properties of novel heterocyclic dyes. *CRSI-2015, NCL, Pune, India, (2015).*

5. Rakesh R and K. G. Sreejalekshmi, Synthesis, crystal structure and electronic properties of a thienylthiazole hybrid – a combined experimental and theoretical approach, *8th Asian Photochemistry Conference (APC-2014), Thiruvananthapuram, India, (2014).*

6. Rakesh R, Sarah Titus, and Sreejalekshmi K. G., Electronic structures and spectroscopic properties of benzopyranone derivative: a DFT study. *Research Scholars day, IIST, Thiruvananthapuram, India, (2012).*